Study of the blood-brain interface and glial cells during sepsis-associated encephalopathy : from imaging to histology

Ibtihel Dhaya

THÈSE EN COTUTELLE PRÉSENTÉE

POUR OBTENIR LE GRADE DE

DOCTEUR DE L'UNIVERSITÉ DE BORDEAUX ET DE L'UNIVERSITÉ DE TUNIS EL MANAR

ÉCOLE DOCTORALE SCIENCES DE LA VIE ET DE SANTÉ

ÉCOLE DOCTORALE SCIENCES ET TECHNOLOGIES DU VIVANT ET SCIENCES DE LA TERRE

SPÉCIALITÉ NEUROSCIENCES

Par **Ibtihel DHAYA**

Study of the blood-brain interface and glial cells during sepsis-associated encephalopathy: from imaging to histology

Sous la direction de Jan-Pieter KONSMAN

et de Mohamed AMRI

Soutenue le 20 Décembre 2017

Membres du jury:

M. KONSMAN, Jan Pieter	Docteur, ADT	Université de Bordeaux	Directeur de thèse
M. AMRI, Mohamed	Professeur	Université de Tunis El Manar	Directeur de thèse
M. SHARSHAR, Tarek	Professeur	Université de Versailles	Rapporteur
M. FATTOUCH, Sami	Professeur	Université de Carthage	Rapporteur
M. LIMAM, Farid	Professeur	Université de Carthage	Examinateur
Mme. DARNAUDERY, Muriel	Professeur	Université de Bordeaux	Examinatrice (Présidente)

Titre: Etude de l'interface sang-cerveau et des cellules gliales au cours de l'encéphalopathie associée au sepsis: de l'imagerie à l'histologie

Résumé

L'encéphalopathie associée au sepsis (EAS) est définie comme un dysfonctionnement cérébral diffus induit par une réponse systémique à une infection. Chez les patients septiques, l'imagerie par résonance magnétique (IRM) a indiqué à la fois des anomalies de la substance grise (SG) et blanche (SB) associées à des troubles cognitifs graves, y compris le *delirium*. Pour améliorer notre compréhension des changements hémodynamiques, métaboliques et structuraux associés au sepsis, différentes séquences d'IRM ont été réalisées chez des rats ayant subi une injection ip de solution saline ou de lipopolysaccharide bactérien (LPS) 2,5h plus tôt ou une ligature et ponction caecale 24h plus tôt.

Après ip LPS, l'IRM de contraste de phase a été réalisée pour étudier le flux des artères cérébrales antérieures et moyennes et le marquage des spins artériels (ASL) pour étudier la perfusion des structures cérébrales de la SB et SG. Des séquences d'imagerie par diffusion pondérée (DWI) ont été utilisées pour évaluer les changements structurels. Après la chirurgie CLP, ASL a été utilisé pour étudier les changements de la microcirculation. L'imagerie pondérée en T2, l'imagerie du tenseur de diffusion (DTI) et les statistiques spatiales basées sur les faisceaux (TBSS) ont été réalisées pour caractériser les événements structurels dans différentes structures cérébrales. Après imagerie, les animaux ont été sacrifiés et leur cerveau a été traité pour l'histologie afin de détecter l'enzyme synthétisant les prostaglandines vasoactives cyclooxygénase-2 (COX-2) et le canal hydrique astrocytaire aquaporin-4 (AQP4) dont l'expression peut être régulée à la hausse, évaluer la présence d'immunoglobulines périvasculaires (Ig) indiquant une rupture de la barrière hémato-encéphalique (BHE) et étudier la morphologie des glies puisque la microglie et l'astroglie changent de morphologie lors des conditions inflammatoires.

L'IRM n'a indiqué aucun changement hémodynamique dans la substance grise après l'administration de ip LPS, alors qu'une perfusion cérébrale accrue a été montrée au niveau du corps calleux comme indiqué par l'ASL. DTI a indiqué une augmentation de la diffusion des molécules d'eau parallèlement aux fibres du corps calleux. Ces changements étaient accompagnés d'une dégradation de BHE dans la SB ainsi que la substance grise corticale et striatale adjacente tel est indiqué par la présence périvasculaire d'IgG, sans aucun changement majeur de COX-2 vasculaire ou de morphologie des glies du coprs calleux.

Le dysfonctionnement du SNC induit par le sepsis a résulté en une augmentation du contraste pondéré en T2 dans le cortex, le striatum et la base du cerveau, une diminution de la perfusion sanguine dans le cortex et une augmentation de la diffusion hydrique du corps calleux et du striatum ventral. Ces changements ont été associés dans la SB à des modifications de la morphologie des glies et dans la substance grise à une expression constitutive de COX-2 et AQP4 plus faible dans le cortex cérébral.

La comparaison entre CLP ayant subit ou non une IRM sous anesthésie à l'isoflurane a montré une réponse inflammatoire réduite tel est indiqué par l'expression de COX-2, une activation réduite des glies ainsi qu'une lésion réduite de la BHE dans le CLP subissant une IRM sous anesthésie.
Collectivement, nos résultats suggèrent que des changements hémodynamiques peuvent survenir en l'absence de flux altéré dans les artères irriguant le cerveau antérieur. Ensuite, l'altération de la structure de la SB est une étape précoce de la pathogenèse de l'EAS qui peut résulter soit de la dégradation de la BHE, soit de l'activation des glies. Cette étude sous-tend l'effet délétère d'une seule exposition à l'anesthésie à l'isoflurane qui peut être atténuée par une seconde exposition chez les rats ayant subi une laparotomie ainsi que les effets de l'inflammation systémique induite par le CLP sur les glies pouvant être atténués par imagerie sous anesthésie à l'isoflurane.

Mots clés: Barrière hémato-encéphalique, diffusion hydrique, flux sanguin cérébral, glie, imagerie de diffusion par réonance magnétique, ligature et ponction de cecum, marquage des spins artériels**,** sepsis.

Title: Study of the blood-brain interface and glial cells during sepsis-associated encephalopathy: from imaging to histology

Abstract

Sepsis-associated encephalopathy (SAE) refers to central nervous system dysfunction during the systemic inflammatory response to infection. In septic patients with encephalopathy MRI has indicated both gray and white matter abnormalities that were associated with worse cognitive outcome including delirium. To improve our understanding of sepsis-associated hemodynamic, metabolic, and structural changes, different MRI sequences were performed in rats that either underwent an i.p injection of saline or bacterial lipopolysaccharide (LPS) 2.5h earlier or cecal ligation and puncture (CLP) 24h earlier.
After ip LPS, phase contrast MRI was performed to study anterior and middle cerebral arteries flow and Arterial Spin Labeling (ASL) to study perfusion of white and grey matter brain structures. Diffusion Weighted Imaging (DWI) sequences was used to assess structural changes. After CLP surgery, ASL was used to study microcirculation changes. T2-Weighted Imaging, Diffusion Tensor Imaging (DTI) and tract-based spatial statistics (TBSS) were performed to characterize structural events in different brain structures. After imaging, animals were sacrificed and their brains processed for histology to detect the vasoactive prostaglandin-synthesizing enzyme cyclooxygenase-2 (COX-2) and the astrocytic aquaporin-4 water channel (AQP4) the expression of which can be upregulated during inflammation, to assess the presence of perivascular immunoglobulins (Ig) indicating blood-brain barrier (BBB) leakage and

to study glia cell morphology as both microglia and astrocytes are known to change their morphology in inflammatory conditions.
Magnetic resonance rat brain imaging indicated no hemodynamic changes in the grey matter after ip LPS administration while an increased CBF was shown in corpus callosum white matter as indicated by ASL. DTI indicated increased water diffusion parallel to fibers of the corpus callosum white matter. These changes were accompanied by BBB breakdown in the white matter and adjacent cortical and striatal grey matter as indicated by the perivascular presence of IgG, but no major changes in vascular COX-2 or white matter glia cell morphology.
CLP induced sepsis-associated CNS dysfunction resulted in higher T2-weighted contrast intensities in the cortex, striatum and base of the brain, decreased blood perfusion distribution to the cortex and increased water diffusion in the corpus callosum and ventral striatum compared to sham surgery. These changes were associated in the white matter with modifications in glia cells morphology and in the grey matter with lower expression of constitutive COX-2 expression and AQP4 in the cerebral cortex.
The comparison between CLP that underwent or not MRI under isoflurane anesthesia indicated reduced inflammatory response as indicated by COX-2 expression, reduced glia activation and reduced BBB damage in CLP that underwent MRI under isoflurane anesthesia.
Collectively, our results suggest that hemodynamic changes may occur in the absence of altered flow in forebrain irrigating arteries. Then, altered white matter structure is an early step in SAE pathogenesis that may result either from BBB breakdown or glial cells activation. This study underlies the deleterious effects of a single exposure to isoflurane anesthesia that may be mitigated by a second exposure in sham-operated rats and the effects of CLP-induced systemic inflammation on glial cells that can be attenuated by imaging under isoflurane anesthesia.

Keywords:

Arterial spin labeling, blood-brain barrier, cecal ligation and puncture, cerebral blood flow, diffusion magnetic resonance imaging, glia, sepsis.

Laboratoire de Neurophysiologie Fonctionnelle et Pathologies, UR/11ES09, Tunis, Tunisie.

Institut de Neurosciences Cognitives et Intégratives d'Aquitaine (INCIA), UMR 5287, Bordeaux, France.

Dédicaces

Je dédie ce mémoire :

A mon père et ma mère,

A mes chers frères Iheb et Ayoub,

A ma petite sœur Chaima,

Et enfin à mes deux chers amis qui m'ont énormément soutenu Nesrine Frifita & Ahmed Chaambi.

Je vous aime tous..

Ibtihel

Remerciements

Au terme de ce travail, je tiens à exprimer toutes mes gratitudes et reconnaissances envers toute personne ayant participé de près ou de loin à l'accomplissement de cette thèse.

Je remercie vivement mes deux directeurs de thèse M. Mohamed Amri Professeur à l'université de Tunis El Manar et M. Jan Pieter Konsman Docteur et chargé de recherche à l'université de Bordeaux. Je leur remercie d'abord pour la confiance qu'ils m'ont accordé et de m'avoir accepté pour réaliser cette thèse, pour leur soutien aussi bien administratif que scientifique ainsi que pour leur persévérance de suivi et pour leurs conseils précieux.

Je suis aussi reconnaissante pour les membres du laboratoire de centre de Résonance Magnétique des Systèmes Biologiques (RMSB), de l'Institut de Neurosciences Cognitives et Intégratives d'Aquitaine (INCIA) ainsi que l'équipe de l'Imagerie Moléculaire et Thérapies Innovantes en Oncologie (IMOTION) qui m'ont chaleureusement accueilli.

Je tiens à remercier M. Girard Raffard qui m'a guidé pendant mes premiers pas dans l'analyse d'imagerie et qui était toujours à l'aide avec un grand sourire. Je remercie également M. Bassem Hiba, qui a été toujours prêt pour répondre à nos questions pour nous guider ainsi que pour éclaircir les ambiguïtés et les différentes notions de l'analyse et l'interprétation de l'imagerie IRM. Je remercie également Mme Marion Griton qui a contribué la réalisation d'une grande partie de ce travail sans oublier M. Renaud Nicolas

pour son aide et ses conseils et Véronique Bouchaud qui était toujours à l'écoute et m'a toujours soutenu.

Mes vifs remerciements vont également à madame Muriel Darnaudery Professeur à l'université de Bordeaux, pour l'honneur qu'elle m'a fait de présider le jury de ma thèse de doctorat.

Je remercie profondément monsieur Tarek Sharshar Professeur à l'université de Versailles d'avoir accepté rapporter mon travail, je profite de cette occasion pour lui témoigner mes sincères considérations. Je remercie également, monsieur Sami Fattouch, Professeur à l'université de Carthage d'avoir accepté rapporter ce travail ainsi que monsieur Ferid Limam Professeur à l'université de Carthage d'avoir accepté examiner mon travail.

À toutes ces personnes ainsi que tous ceux que j'ai oublié de mentionner, je tiens à vous remercier sincèrement

Contents

Liste of tables and figures

Chapter 2

Chapter 5

Abbreviations used:

ADC : apparent diffusion coefficient;
AP : area postrema;
AQP4: aquaporin 4;
ASL: aterial spin labeling;
BBB: blood-brain barrier;
CBF: cerebral blood flow;
CE-MRA: contrast-enhanced MRA;
CLP: cecal ligation and puncture;
CMR: cerebral metabolic rate;
$CMRO_2$: cerebral metabolic rate of oxygen;
CNPase: 2',3'-cyclic nucleotide 3'-phosphodiesterase;
CNS: central nervous system;
COX-2: cyclooxygenase-2;
CT: computed tomography;
CVO: circumventricular organs;
DTI: diffusion-tensor imaging;
DWI: diffusion-weighted imaging;
EEG: electroencephalography;
FA: fractional anisotropy;
FAIR: Flow-sensitive Alternating Inversion Recovery;
FLAIR: FLuid-Attenuated Inversion Recovery;
fMRI: functional magnetic resonance imaging;
GFAP: glial fibrillary acidic protein;
i.c.v: intracerebroventricular;
i.p: intraperitoneal;
i.v: intraveneous;
Iba-1: ionized calcium-binding adaptor molecule;
IFN : interferon;
IgG: immunoglobulin G;
IL-1β: interleukin-1β;
IL-6 : interleukin 6;
iNOS : inducible nitric oxide synthase ;
LPS: lipopolysaccharide;
MAP : mean arterial pressure ;
MCAv : middle cerebral arterial blood flow velocity;
MMP: matrix metalloproteinases;
MRA: magnetic resonance angiography;
MRI : magnetic resonance imaging;
NF-κb: Nuclear Factor-kappa B;
NIRS: Near-infrared spectroscopy;
NK: natural killer;
NO: nitric oxide;
Nox2: NADPH oxidase 2;
OVLT: organum vasculosum of the lamina terminalis;
PaC O_2: arterial partial pressure of CO_2
PC: phase contrast;
PET: positron emission tomography;
PRES: posterior reversible encephalopathy syndrome;
REM: rapid eye movements;
SAE: sepsis-associated encephalopathy;
SEP: somatosensoriel evoked potentials
SFO: subfornical organ;
StO2: tissue oxygen saturation;
SWS: slow-wave sleep;

TCD: transcranial doppler;

TLR: Toll-Like Receptor;

TNF: tumor necrosis factor;

TOF: time of flight.

Chapter 1

General introduction

Preface

The human being is so complex that in the 21st century there are still many unresolved enigmas and phenomena despite important advances in science and medicine. We have come far in exploring the human body responses to its environment. But despite scientific research and numerous therapeutic strategies, human health is still threatened by infectious microorganisms and the complications of the diseases they cause.

Man is susceptible to be affected by bacteria present in his environment, including those in the gut lumen. Body tissue invasion by bacteria alerts the innate immune system, which may result in a systemic inflammatory response syndrome to infection called sepsis. In sepsis, the immune, endocrine and nervous systems interact to bring about the so-called non-specific disease symptoms, such as fever, reduced food intake and activity, sleep and altered mental state and cognition. Some of these responses, including fever, sleep and reduced food intake, are now considered adaptive and to contribute to elimination of the infectious organism or to protect the host tissues against free radical stress generated by the innate immune system. Since body temperature, sleep-wake cycles and food intake are controlled by the brain, the occurrence of fever, sleep and reduced food intake in response to infection implies activation of central nervous systems (CNS) pathways. However, these adaptive responses that strengthen immune defenses and eliminate the invading organism may be complicated by the advent of neuroinflammation. Indeed, even though the brain that has been long known as an immune-privileged structure, its proper functioning can be affected during infection-associated inflammation and give rise to sepsis-associated encephalopathy that can manifest itself as *delirium* and lead to long-term cognitive impairment.

If the inflammatory responses and the roles of peripheral and central pro-inflammatory cytokine action and those of prostaglandin production at the blood-brain interface in uncomplicated sepsis-associated fever and reduced activity and food intake have to a large extent been described, the pathophysiological mechanisms underlying brain dysfunction during severe sepsis and septic shock are not well understood. Among the hypotheses that have been proposed to explain sepsis-associated brain dysfunction or encephalopathy are decreased cerebral blood flow, blood flow autoregulation failure, microcirculatory

dysfunction, blood-brain barrier (BBB) breakdown and edema-related changes in white matter integrity.

Magnetic resonance imaging (MRI) has been used to address these different hypotheses in patients and because it allows to assess hemodynamic, metabolic, and structural features of the CNS. Indeed, several MRI studies have been performed in septic patients with signs of brain dysfunction. Although the comparison between studies and patients is far from straightforward because of differences in time of imaging after sepsis onset and individual differences in pre-sepsis conditions and sepsis-associated complications, a few consistent findings have emerged that include signs of vasospasm in the brain-irrigating arteries as well as edema (Bartynski, Boardman, Zeigler, Shadduck, & Lister, 2006; Dhar & Diringer, 2008; Straver et al., 1996; Yoshimoto, Tanaka, & Hoya, 2001).

Even though *in vivo* imaging is indispensable to describe hemodynamic and metabolic modifications during sepsis, structural changes have been traditionally addressed by histological approaches, which today are the gold standard to describe changes in tissue organization. Several studies have employed *post mortem* histological techniques to study nervous tissue disorganization-associated with sepsis in patients and have shown increased perivascular spaces in the white matter as well as signs of hemorrhage in the grey matter (Finelli & Uphoff, 2004; T Sharshar et al., 2004; Tarek Sharshar et al., 2007). However, such approaches only reveal changes that occurred long after sepsis onset and can only be employed on those cases of sepsis leading to death. In animal models of sepsis, the time of sacrifice is controlled and can thus yield more relevant structural and neurochemical *post mortem* finding during early phases of sepsis. These studies have shown upregulation of inflammatory mediators including Nuclear Factor-kappa B (NF-κB), Cyclooxygenase-2 (COX-2), Interleukin-1β (IL-1β) at the blood-brain interface, disruption of the blood-brain barrier (BBB) and glia cell activation.

Brain imaging approaches and histological techniques have allowed to obtain both convergent and divergent findings between clinical sepsis and experimental sepsis models consisting of the systemic administration of bacterial lipopolysaccharides (LPS) in human volunteers or animals and of cecal ligation and puncture (CLP) in animals. MRI changes indicating edema formation and higher brain volume, such as increased T2-weighted contrast and Apparent Diffusion Coefficient (ADC) have been described both in septic patients and experimental sepsis in animals. However, when it comes to monitoring changes in cerebral blood flow during sepsis the results of studies have been much more divergent between human and

animals as well as among animal studies. This may be due to several reasons including the use of different animal species, time point of measurement and to technical limits of approaches, which makes it hard to reach a general conclusion.

But although many brain imaging approaches have been validated for small laboratory animals, virtually no study has employed these in combination with subsequent histology in animal models of sepsis to establish temporal and spatial relationships between CNS hemodynamic, metabolic and structural changes indicated by imaging and histological approaches on brain sections of the same animals.

Part 1: Bacterial infection and sepsis: adaptive CNS-mediated responses

Sickness physiology (fever) and sickness behavior (reduced activity and food intake) are important for survival from bacterial infection

Fever

Although high fever and reduced food intake have long been considered as detrimental for host tissues and potentially life-threatening, moderate fever and anorexia are adaptive physiological responses during systemic inflammation to bacterial infection that contribute to host survival and tissue integrity. Indeed, fever has a crucial role in the enhancement of host defenses and effectiveness of immune responses while inhibiting bacterial growth. Indeed, febrile temperatures influence neutrophil and monocyte motility and migration, phagocytosis, oxygen radical production by phagocytes, and interferon (IFN) production (Harden, Kent, Pittman, & Roth, 2015). IFN-γ is a type 1 cytokine that plays a key role in the regulation of both innate and acquired antimicrobial immunity. After LPS challenge, Natural Killer (NK) cells are the most abundant IFN-γ-producing cells. As reviewed by Mackowiak (1981), fever also inhibits multiplication of potentially pathogenic microorganisms as it affects growth of bacteria, reduces their motility, induces bacterial RNA degradation and mitigates the toxicity of bacterial endotoxin (P. A. Mackowiak, 1981). These different mechanisms may underlie numerous phenomena observed in the history of medicine and science. For example, Louis Pasteur showed that reducing chickens' body temperature by immersing it in cold water reduced native immunity to anthrax (Vallery-Radot, 1923). Another famous example is the quinine-controlled fever therapy proposed by Wagner-Jauregg to treat neurosyphilis (Wagner-Jauregg, 1965). Moreover, it has been shown that increased mortality in septic patients was associated with the failure to mount a fever response (Bryant, Hood, Hood, & Al, 1971; P. Mackowiak, Browne, Southern, & Smith, 1980; Weinstein, Iannini, Stratton, & Eickhoff, 1978). Conversely, moderate rises in body temperature are associated with increased host survival in reptiles (M. Kluger, Ringler, & Anver, 1975) and mammals (rabbits) (J. Kluger & Vaughn, 1978) inoculated with bacteria. Finally, prevention of fever by use of an antipyretic drug increases mortality rate from bacterial infection in reptiles (Bernheim & Kluger, 1976). Collectively, these findings suggest that fever is an adaptive response to bacterial infection and contributes to host survival. However, it is important to keep in mind that many

antipyretic drugs, do not only reduce fever, but have also more general anti-inflammatory and other effects. In fact, antipyretics attenuate LPS-induced endothelial damage (Turek, Templeton, Bottoms, & JF., 1985) and modulate inflammatory processes involved in sepsis via the production of nitric oxide (NO) and the inhibition of COX and NF-κB (Toner, Mcauley, & Shyamsundar, 2015). This may explain why some of these drugs have been found to decrease mortality rate from bacterial infection in rabbits without reducing fever (J. Kluger & Vaughn, 1978). It has been proposed that death, when it occurred in febrile animals is caused by collateral damage from host defenses while death in afebrile animals came as a result of overwhelming bacterial infection (Blatteis, 2003). This may also explain why clinical trials test the beneficial effects of low doses of aspirin on bacterial sepsis are ongoing (Eisen et al., 2017), even though recent trials have shown that aspirin increased morbidity, and in particular severe sepsis, in ICU patients (Harbi, Tamim, Al-dorzi, Sadat, & Arabi, 2016).
Importantly, it has been shown that aspirin does not have any anti-inflammatory effects in human volunteers after administration of low doses of LPS (Jilma et al., 1999) and does not modify survival rate after injection of higher doses of LPS in animals (Ulu, Iskit, Sökmensüer, & Güç, 2015). This may be explained by the fact that aspirin delayed the onset of fever by 1 h but it did not decrease the maximal increase in temperature seen a few hours after LPS administration (Jilma et al., 1999). Not only aspirin but also flurbiprofen, and NO-donating acetylsalicylic acid (NCX 4016) do not change survival rates in animals administered LPS (Ulu et al., 2015). This may be due to the fact that some antipyretic activity (such as flurbiprofen) is due neither to interference with endogenous pyrogen production, nor to inactivation of circulating endogenous pyrogen (Van Miert & Van Duin, 1977). Instead, some antipyretic effects seem to depend on the virulence of the organism responsible for sepsis. For example, low dose of acetylsalicylic acid administered at the time of bloodstream infection is associated with reduced short-term mortality in patients with *S. aureus* bloodstream infection but not in patients with *E. coli* bloodstream infection (Osthoff et al., 2016). Together, these observations draw attention to the potential importance of the choice of antipyretics depending on the germ responsible for fever.

Reduced food intake

Inflammation-associated anorexia refers to the decrease in appetite and food consumption that occur during both acute and chronic inflammatory conditions in humans and animals. Both bacterial wall components such as LPS (Nava & Carta, 2000; Prendergast, 2008; Ribeiro et

al., 2013; Turner & Berry, 1963) and cytokines such as IL1-β (Deboer, Scarlett, Levasseur, Grant, & Marks, 2010; Lawrence & Rothwell, 2001) and Tumor Necrosis Factor (TNF) (Socher, Friedman, & Martinez, 1988) administrated in the periphery or within the ventricular system in animals induce hypophagy. However, IL-1β suppressed feeding by reducing meal frequency and size while the anorectic effect of LPS was due entirely to a reduction of meal frequency indicating that IL-1β and LPS do not affect feeding through exactly the same mechanism (Langhans, Savoldelli, & Weingarten, 1993). In humans, LPS induces transient anorexia with an initial reduction in food consumption during the first hours after the injection, followed by an increase the next hours (Reichenberg et al., 2002).

Comparison between force-feeding infected mice and infected mice eating *ad libitum* revealed that mortality was increased and survival time shortened in force-fed animals suggesting that anorexia, by reducing energy intake, plays an important role in the early defense of the host against bacterial infection (Murray & Murray, 1979). These initial findings have been confirmed more recently by Wang and colleagues who have shown that anorexia was protective while nutritional supplementation was detrimental in bacterial sepsis (Wang et al., 2016).

According to Hart (1988), sickness-associated anorexia constitutes a behavioral response to preserve energy and maintain blood iron concentrations low. Indeed, lower food motivation can be thought to reduce the organism's search for food and thus save energy that is needed for the increased metabolic costs of fever and reduce heat loss through increased convection and enhanced body surface exposure (Hart, 1988). Anorexia contributes also to reducing other activities such as digestion, which would otherwise consume the energy required to reduce bacterial load, or correct microbiota imbalances and may also limit supply of micronutrients, such as iron, needed by particular bacteria to proliferate (Pacheco-Lopez & Bermudez-Rattoni, 2011). As reviewed by van Niekerk and collaborators (2016) sickness-associated anorexia may also present a mechanism through which autophagy is upregulated systemically, which may play a critical role in clearing pathogens (Van Niekerk, Isaacs, Nell, & Engelbrecht, 2016). Despite being beneficial in the short term, long lasting anorexia delays recovery and is ultimately deleterious for host defense (Exton, 1997; Langhans, 2000).

Increased sleep

Sleep is a period during which activity and alertness decline and that can be distinguished from coma and analgesia by its rapid reversibility (Ibarra-coronado et al., 2015). Sleep can be

divided in two phases depending on the presence of rapid eye movements (REM). REM sleep accounts for about 25% of sleep time and is characterized by episodic bursts of rapid eye movements, irregularities in respiration and heart rate, and paralysis of major muscle groups. Non-REM sleep can be further divided into four stages: light sleep, intermediate sleep and slow-wave sleep (SWS) (Parthasarathy & Tobin, 2004).

Toth and Krueger in 1988 were the first to study the effect of systemic bacterial infection effect on physiological sleep in rabbits inoculated intravenously with *S. aureus* and showed initially increased SWS followed by decreased REM sleep (L. Toth & Krueger, 1989). Intravenous inoculation of rabbits with *E. coli* also produced a large increase in SWS for the first 2-4 h after inoculation. Similar effects occurred when heat-killed *E. coli* were administered, although significantly higher numbers of microorganisms were required to produce equivalent responses (L. A. Toth & Krueger, 1988). CLP surgery also increases the amount of time rats spend in Non-REM sleep and suppresses REM sleep during the first 24 h (Baracchi, Ingiosi, Raymond, & Opp, 2011). Bacterial cell wall components have the same effect on animals as administration of LPS or lipid A enhances the duration of SWS and suppresses REM sleep (Krueger, Kubillus, Shoham, & Davenne, 1986). In humans, responses induced by LPS administration include reduced wakefulness and REM sleep (Pollmächer et al., 1993; Trachsel, Schreiber, Holsboer, & Pollmächer, 1994).

It has been noticed that rabbits that died after being inoculated with *E.coli*, *S.aureus* or *C.albicans*, showed reduced sleep compared to survivors (L. Toth, Tolley, & Krueger, 1993). Imeri & Opp (2009) have proposed that the manner in which sleep is altered during infection facilitates the generation of fever and promotes recovery (Imeri & Opp, 2009). In addition, in animals, sleep is associated with enhanced numbers innate immune and antimicrobial activity of monocytes and neutrophils through increased production of reactive oxygen species (Hahn, Gunter, Bieber, Lange, & Autenrieth, 2017), which may occur independently from the effects of sleep on fever. An important body of literature can therefore be interpreted to suggest that fever, reduced food intake and increased NREM SWS sleep are adaptive organized host responses to limit bacterial proliferation.

Immune-to-brain signaling pathways underlying sickness physiology and behavior

Systemic inflammation is a physiological response to infection initiated by the innate immune cells and inflammatory mediator, but comprises the coordination of many immune, autonomic, and neuroendocrine responses that involve both the peripheral and central nervous

system. Indeed, the fact that fever, reduced food intake and increased non-REM sleep occur in response to systemic inflammation indicate that CNS functioning is modulated by inflammatory signals. However, the BBB prevents hydrophilic pro-inflammatory mediators, such as cytokines, from passively entering the brain parenchyma. This raises the question which immune-to-brain signaling pathways underlie sickness physiology and behavior.

LPS administration is a commonly paradigm used to bring about inflammation-related symptoms and to study associated brain activation. When introduced to the host organism, LPS interact with Toll-Like Receptor 4 (TLR4) expressed on macrophages cell surface to activate the NF-κB pathway (Eva M. Palsson-Mcdremott & O'neill, 2004; Lu, Yeh, & Ohashi, 2008) and enhance transcription of genes responsible for the expression of pro-inflammatory cytokines, chemokines, adhesion molecules, apoptotic factors, and other mediators of the inflammatory response associated with sepsis (Abraham, 2003). Administration of pro-inflammatory cytokines mimics most of the non-specific symptoms of sickness observed during systemic inflammation including fever, altered gastric function, increased metabolism, behavioral changes including anorexia, somnolence, and social withdrawal (Dantzer & Kelley, 2007; Kelley et al., 2003; J. P. Konsman et al., 2008; Rothwell & Hopkins, 1995).

To transmit the peripheral signal into the brain, LPS and pro-inflammatory cytokines (IL1-β, TNF-α and IL-6) may act directly or indirectly via a fast and a slow signaling routes respectively (reviewed by, (Dantzer, 2001, 2009; Goehler et al., 2000; Mccusker & Kelley, 2013). The fast neural route includes the vagus nerve that terminates in the nucleus of the solitary tract. Indeed, vagotomy has been shown to decrease behavioral depression and limbic structures activation induced by LPS or i.p. IL1-β administration in rats (Bluthé RM, Michaud B, Kelley KW, 1996a, 1996b; JP Konsman, Luheshi, Bluthé, & Dantzer, 2000). Although subdiaphragmatic vagus transaction disrupt fever following IL-1β administration (Watkins et al, 1995) this contribution is dose dependent and only low doses of i.p IL-1β induce fever via a vagal route (Hansen, O'Connor, Goehler, Watkins, & Maier, 2001).

Circulating pro-inflammatory cytokines such IL-1β act on the CNS to induce fever, neuroendocrine activation, and behavioral changes, as mentioned above, but cannot passively cross the blood-brain barrier. In the early 1990s, a second isoform of cyclooxygenase catalyzing the production of prostaglandins was discovered and found to be detected in cerebral blood vessels following bacterial LPS (Cao, Matsumura, Yamagata, & Watanabe, 1995) or IL-1 administration (Cao, Matsumura, Yamagata, & Watanabe, 1996). COX-2-like immunoreactive cells were first found at 1.5 h after LPS injection, at which time the fever had not yet developed. After that, the number of COX-

2-like immunoreactive cells and fever followed a similar time course, both being highest at 5 h after the LPS injection and both returning to baseline by 24 h (Matsumura et al., 1998).

Interestingly, in rats receiving i.v LPS in combination with SC-236, a potent selective inhibitor of COX-2, LPS-induced expression of the cellular activation marker c-Fos has been shown to be attenuated in the ventromedial preoptic nucleus and the paraventricular nucleus of the hypothalams (Zhang, Lu, Elmquist, & Saper, 2003). IL-1 receptors are expressed along the cerebrovascular endothelium (Ericsson et al, 1995; Cunningham et al, 1992) and its vascular distribution is consistent with patterns of COX-2 induction after LPS or IL-1β administration (JanPieter Konsman, Vigues, Mackerlova, Bristow, & Blomqvist, 2004). Since endothelial-specific knockdown of the signaling IL-1R1 suppressed IL-1β-induced fever and COX-2 induced expression (Ching et al, 2007), IL-1β seems to act on CNS endothelial cells to induce COX-2 expression and fever.

The BBB is a multicomponent system consisting of cellular and molecular parts (reviewed by (Abbott, 2000; Broadwell & Salcmant, 1981; Hawkins & Davis, 2005)). Indeed, this barrier is composed of endothelial cells in close contact with astrocytic end-feet across a basal lamina and perivascular macrophage and pericytes. Endothelial cells differ from those in the periphery by increased mitochondrial content, a lack of fenestrations, minimal pinocytotic activity, and the presence of tight junction molecules. Endothelial cells are in close contact with pericytes which are attached at irregular intervals to its abluminal membrane. Pericytes and endothelial cells are sheathed by the basal lamina- a membrane 30 to 40-nm thick composed of collagen type IV, heparin sulfate proteoglycans, laminin, fibronectin, and other extracellular matrix proteins- bordered by the plasma membranes of astrocyte end-feet, which sheathes cerebral capillaries.

The BBB is present throughout the CNS except in the choroid plexus and a set of small midline structures bordering the ventricular spaces called circumventricular organs (CVOs). The CVOs are characterized by large perivascular spaces and the absence of tight junctions between endothelial cells and hence a BBB thus allowing the passage of large molecular weight and polar substances. Three of these structures, the subfornical organ (SFO), organum vasculosum of the lamina terminalis (OVLT) and area postrema (AP), are targets for blood-borne molecules and may transmit CNS laying behind the BBB provided that receptors for these molecules are expressed in these CVOs (Johnson & Gross, 1993). CVOs sense multiple signals important in various physiological systems, including fluid balance, metabolic control and reproduction (Ferguson, 2014). LPS and cytokines may also act via slow humoral

pathway which involves production of pro-inflammatory cytokines by phagocytic cells in the circumventricular organs and choroid plexus (J. P. Konsman, Kelley, & Dantzer, 1999). Moreover, the SFO (Takahashi, Smith, Ferguson, & Pittman, 1997) and OVLT (Stitt, 1990) respond to circulating LPS by increasing c-fos.

Part 2: Sepsis associated encephalopathy or neurological impairment

Immune system activation to infection can lead to orchestrated physiological and behavioral changes, such as fever and reduced food intake, thought to reflect adaptive response to fight infection, but also to signs of brain dysfunction and cognitive impairment. Indeed, confusion, seizures, learning, verbal, memory and executive functioning disorders, inattention, disorientation, stupor, *delirium*, loss of consciousness and coma are the main symptoms of altered mental status or awareness that have been described during sepsis-associated encephalopathy (Berisavac et al., 2016; Hosokawa et al., 2014; Stevens & Nyquist, 2007; Young et al., 1990). *Delirium* is a puzzling phenomenon that occurs in up to 80% of ICU patients, mainly in septic patients, and can leading to coma and increased sepsis morbidity and mortality (Girard et al., 2010; Jackson & Hopkins, 2009). The pathophysiology of these neurological dysfunctions is probably multifactorial, but not well understood.

Indeed, with xenon-enhanced computed tomography a significant focal and global cortical hypoperfusion has been shown to occur during *delirium.* After recovery, cerebral blood flow (CBF) returned to normal thus suggesting that a possible cause of *delirium* may be cerebral hypoperfusion (Yokota, Ogawa, Kurokawa, & Yamamoto, 2003). Furthermore, in a small group of patients, a significant association was found between disturbed cerebrovascular autoregulation and sepsis-associated delirium (Pfister et al., 2008). Alternatively, patients with *delirium* and sepsis often show white matter abnormalities in MRI (Morandi et al., 2010; Tarek Sharshar et al., 2007). Moreover, greater *delirium* duration was found to be associated with altered white matter integrity and brain atrophy, which, in turn, was associated with worse cognitive scores including executive functioning and attention at 3 and 12 months after discharge (Girard et al., 2010; Gunther et al., 2012; Jackson & Hopkins, 2009; Marsland et al., 2015; Morandi et al., 2012). In animal models, rats that survived CLP-induced sepsis also show impairment of short- and long-term novel object recognition memory, aversive and spatial memory (Barichello et al., 2005, 2007). Together, these finding suggest that delirium

during sepsis and cognitive impairment occurring after severe sepsis are associated, respectively, with altered CBF and changes in cerebral white matter.

Does overreaction of inflammatory responses lead to dysfunction?

The progressive evolution of sepsis complications is closely linked to hypotension and perfusion changes. As defined by Bone et al, (1992), sepsis is a systemic response to infection, but when this response is associated with organ dysfunction, hypoperfusion, or hypotension; it is termed as severe sepsis. When sepsis-induced hypotension persists despite adequate fluid resuscitation, along with the presence of hypoperfusion abnormalities or organ dysfunction, this is called septic shock (Bone et al., 1992).

LPS has been used at low doses as a nonspecific immune stimulus to study fever, sickness behavior and brain activation in different rodent. Interestingly, low to moderate doses are unable to induce systemic hypotension (Tkacs & Li, 1999; Tkacs, Li, & Strack, 1997), while high doses cause a decrease in mean arterial blood pressure and tachycardia (Lay, Donahue, Tsai, & Castellino, 2007; Perrella et al., 1996; Tkacs et al., 1997) exposing the organism to potentially deleterious organ hypoperfusion.

Low or high dose of LPS may be defined depending on the response of the organism and the route of administration. Intravenously administrated LPS, at low doses (ranging from 0.1 µg/kg to 1 µg/kg) induce monophasic fever (McCarthy, Kluger, & Vander, 1986; Andrej A Romanovsky, Kulchitsky, Simons, Szekely, & Vladimir, 1997), while moderate doses (2 µg/kg to 50 µg/kg) induce a biphasic fever (Al-Saffar et al., 2013; A A Romanovsky, Shido, Sakurada, Sugimoto, & Nagasaka, 1996). The higher the dose, the less pronounced the first and the more pronounced the second phase (Al-Saffar et al., 2013). Also, one needs to bear in mind that biphasic febrile response often consist of more than two phases (Almeida, Steiner, Branco, & Romanovsky, 2006a, 2006b; A A Romanovsky, Simons, & Kulchitsky, 1998). Nevertheless, the common misbelieve that there are two phases depend on several methodological parameters including the dose of LPS, the route of its injection and the ambient temperature (A. Romanovsky, Kulchitsky, Simons, & Sugimoto, 1998). However, a high dose of LPS (200 µg/kg to 5 mg/kg) injected intravenously induces hypothermia or anapyrexia (regulated decrease of body temperature) rather than fever (Almeida et al., 2006a, 2006b; Corrigan, Fonseca, Flatow, Lewis, & Steiner, 2014). Hypothermia may be either monophasic or biphasic. During biphasic hypothermia hypotension or decreased mean arterial pressure may occur simultaneously with the first hypothermic phase at high dose (500 µg/kg)

of i.v. LPS while a tenfold higher dose (5 mg/kg) induce monophasic hypothermia (Almeida et al., 2006b; A A Romanovsky et al., 1996) that may be followed by fever (Almeida et al., 2006a), but is always accompanied by hypotension (Perrella et al., 1996). Fever is a potentially adaptive response as it typically does not present an immediate threat of energy deficit, while hypothermia and cold-seeking behavior are beneficial under conditions of substantial energy deficit (Almeida et al., 2006a). Beyond such conditions, fever or hypothermia becomes detrimental (A A Romanovsky et al., 1996).

In addition to potential detrimental effects of too high or too low body temperatures, complex and multifactorial mechanisms have been described following the peripheral administration of high doses of LPS challenge. High doses of LPS induce endothelial cell dysfunction, eventually leading to perturbations in hemodynamics (Tsai et al., 2015). Both *in vivo* (N. Liu, Li, Zhou, Chen, & Cao, 2015) and *in vitro* (W. Liu et al., 2015; Seok, Kim, Park, Baik, & Lee, 2013; Zhao, Hu, Gao, Liang, & Liu, 2014) experiments showed that high dose of LPS can increase permeability of the BBB and decrease expression of tight-junction proteins. LPS-induced hippocampal alterations are associated with astroglia activation, cells necrosis, NO-initiated regulation of apopototic markers including Bax, Bcl-2 (Semmler, Okulla, Sastre, Dumitrescu-Ozimek, & Heneka, 2005) and caspase-3 (Wei et al., 2015). Interestingly, oxidative stress in the hippocampus during peripheral LPS infusion can also be alleviated by COX-2 inhibition (Ho et al., 2015).

Together, these observations suggest that high doses of LPS can induce neurodegeneration including the loss of interneurons, endothelial cell dysfunction, BBB disruption, microcirculation failure, and cytotoxicity that seem related to increased NF-κB and pro-inflammatory protein expression (COX-2, inducible nitric oxide synthase (iNOS)) and signs of glia cell activation (glial fibrillary acidic protein (GFAP), ED-1).

Models: high and low doses of bacterial LPS vs Cecal Ligation and Puncture

LPS is widely used to study the pathophysiology of sepsis and has the advantage of being easy to administer and to induce a reproducible dose-, yet species-, dependent spectrum of responses. However, its injection is not followed by the complexity of responses and the histopathological changes observed during clinical sepsis. Rather, the intravenous bolus injection of bacterial LPS is considered to reflect intoxication rather than a true septic state since the animal is only responsive to a bacterial fragment that does not colonize and replicate (Cross, Opal, Sadoff, & Gemski, 1993). In addition, human sepsis, except for

meningococcemia, is characterized by low or non-detectable LPS levels which make the presence of live multiplying bacteria in blood and tissue mimics the clinical problem of sepsis more closely than models using LPS. Another limitation is that bolus injection of LPS used in the endotoxic rodents rather than the more progressive bacterial invasion in human sepsis without forgetting that rodents have a much lower sensitivity to LPS than humans (De Cruz, Kenyon, & Sandrock, 2009) which make that large doses of LPS are required in animals to elicit responses similar to those seen in humans with severe sepsis and septic shock, leading to the translational relevance between exogenous administration of bacterial LPS and clinical sepsis questionable (AJ. Lewis, Seymour, & Rosengart, 2016; Buras, Holzmann, Sitkovsky, & Israel, 2005; Cross, Opal, Sadoff, & Gemski, 1993; Fink, 2014; Gonnert et al., 2011; McCarron et al., 2015). Finally, neither the concentration of endotoxin nor that of inflammatory cytokines after LPS injection are comparable to those measured in septic patients (Rittirsch, Hoesel, & Ward, 2007).

To overcome these limitations, other experimental models have been proposed, among which CLP has been widely used. While this model does not fully mimic the whole spectrum of clinical sepsis, it does reproduce the hyperdynamic and hypodynamic phases of clinical sepsis and is therefore often considered as a "gold standard" in sepsis research (Buras et al., 2005; Dejager, Pinheiro, Dejonckheere, & Libert, 2011; Rittirsch, Hoesel, & Ward, 2007; Ruiz et al., 2016; Schabbauer, 2012; Wichterman, Baue, & Chaudry, 1980). The severity of sepsis induced by CLP depends on the number of punctures and needle size and the length of cecal ligation. Thus, this experimental model can be performed with high consistency (Ruiz et al., 2016). CLP results in different kinetic and magnitude of production of cytokines as compared to LPS administration. Indeed, i.p LPS injection induced high plasma and peritoneal concentrations of cytokines (TNF, IL-1, IL-6, and the chemokines KC and MIP-2) with peak levels between 1.5 and 4 h that began to decline at 8 h while cytokine levels in the CLP model continued to increase 8h after surgery (Remick, Newcomb, Bolgos, & Call, 2000). Peripheral hypotension has also been described in the CLP model with a continuous decrease in mean arterial pressure (MAP) that becomes significant after 24 h (Hofer et al., 2008) and which is accompanied by increased cardiac output and heart rate (Barreto, Freitas, de Aquino, de Oliveira-Sales, Campos, & Bergamaschi, 2007; Kafa, Bakirci, Uysal, & Kurt, 2010; Pancoto, Corrêa, Oliveira-Pelegrin, & Rocha, 2008; Su et al., 2015). The early phase of CLP-induced severe sepsis hypotension is caused by iNOS-derived NO as selective iNOS inhibition restored hemodynamics (Kadoi & Goto, 2004).

Following CLP in mice, upregulation of the pro-inflammatory cytokines TNF-α and IL-1β mRNA as well as rapid neurodegenerative changes and BBB injury have been described in the brain (Yokoo et al., 2012). CLP can also induce cerebral edema with ultrastructural changes to cerebral microvessels and adjacent tissue (Brooks, Moss, Davies, Jalan, & Davies, 2014) and selective loss of interneurons, as a result of NADPH oxidase 2 (Nox2) activation (Ji et al., 2015). Interestingly, mice subject to CLP-induced polymicrobial sepsis show long-term expression of pro-inflammatory cytokine and chemokine genes, including TNFα, IFN-c, IL-1b, and IL-6 and CCR2 ligands accompanied by infiltration of monocytes and neutrophils into the CNS until two weeks after sepsis induction (Calsavara, Rodrigues, Miranda, & Teixeira, 2013; Singer et al., 2016).

At thermo-neutral ambient conditions, a single cecal puncture with a 16 gauge needle results in a biphasic thermoregulatory response marked by a significant hypothermia 2 to 2.5 h after CLP followed by significant febrile response at 4.5 h, while two or ten punctures are followed by significant febrile responses without preceding hypothermia (Figueiredo et al., 2012). Fever subsequent to two cecal punctures is mediated by cerebral IL-1β, whereas increases in body temperature during more severe sepsis induced by four cecal punctures depend on IL-6 and COX-2 (Gourine, Rudolph, Tesfaigzi, & Kluger, 1998). Together these findings indicate that similarly to LPS, the mechanism involved in fever depend on the severity of the model.

Although it occurs only in 10 (Arons et al., 1999; Clemmer et al., 1992; Peres Bota, Lopes Ferreira, Mélot, & Vincent, 2004) to 20% (Marik & Zaloga, 2000; Peres Bota et al., 2004) of septic patients, hypothermia is deleterious and associated with higher mortality rate (Arons et al., 1999; Clemmer et al., 1992; Doherty, Fung, Lefkowitz, & Ellrodt, 1985; Peres Bota et al., 2004), lower systemic vascular resistances and higher cardiac indices (Morris, Chambers, Morris, & Sande, 1985), higher incidence of organ dysfunction (Marik & Zaloga, 2000; Peres Bota et al., 2004), failure to recover and higher frequency of CNS dysfunction (Clemmer et al., 1992) in comparison with febrile septic patients or other cause of hypothermia.

Part 3: Contribution of imaging to sepsis-associated encephalopathy

Hemodynamic and metabolic, functional and structural brain imaging approaches have been used to assess cerebral changes during sepsis and sepsis-associated encephalopathy in the clinic and experimental models.

Hemodynamic, metabolic and functional brain imaging

Hemodynamic and metabolic brain imaging

Cerebral blood flow can be defined as the blood volume irrigating 100 g of cerebral parenchyma per minute. It is controlled by many parameters, including CNS-related ones, such as intracranial pressure, cerebral arterial vascular bed resistance, vascular reactivity, neurovascular coupling, cerebral oxygen consumption and systemic ones, such as cardiac output, hypotension, hypocapnia and oxygen delivery. The heterogeneity of all these parameters thus makes CBF sensitive to both central and peripheral disorders.

Alteration of CBF has been proposed as a main contributor to brain dysfunction during sepsis (Taccone, Scolletta, Franchi, Donadello, & Oddo, 2012). A multiplicity of techniques has been used to assess cerebral blood circulation at the macro and microlevel with different temporal and spatial resolutions as well as varying degrees of invasiveness. The first method used to assess CBF was that developed by Kety and Schmidt and consisted of nitrous oxide (N_2O) inhalation and the subsequent determination of its concentration in arterial and cerebral venous blood (Kety & Schmidt, 1948). It allowed the quantification of the cerebral metabolic rate of oxygen ($CMRO_2$), and cerebrovascular resistance in addition to global CBF (Kety and Schmidt 1948). Its reliability and robustness to measure global CBF and cerebral metabolic rates (CMR) have been confirmed over the years and it has more recently been shown that with the use of low tracer concentrations, altered nitrous oxide metabolism is unlikely to affect cerebral hemodynamic function (Taudorf, Berg, Bailey, & Møller, 2009).

Cerebral autoregulation refers to, "a homeostatic mechanism that protects the brain tissue from the potentially damaging effects of hypoperfusion and hyperperfusion" (R. M. Berg et al., 2012). It may be described both in terms of "static" performance, that is, the ability of CBF to respond to longer lasting changes in MAP, and in terms of "dynamic" performance concerning the changes occurring in CBF within the first few seconds after an acute change in MAP" (R. M. Berg et al., 2012). Proposed indices of static autoregulation are based on changes in cerebrovascular resistance, on parameters of the linear regression of flow/velocity versus pressure changes, or on absolute changes in flow induced by drugs, shifts in blood volume or by observing spontaneous changes in CBF in relation to arterial partial pressure of CO_2 ($PaCO_2$) and haematocrit values. Dynamic assessments of autoregulation are based on transient changes in CBF (or velocity) induced by the deflation of thigh cuffs, tilting, Valsalva manoeuvres - moderately forceful attempted exhalation against a closed airway by closing

mouth or nose while pressing out - , or spontaneous oscillations in MAP (Panerai, 1998). Assessment of cerebral autoregulation is an important adjunct to measurement of cerebral blood flow for diagnosis, monitoring or prognosis of cerebrovascular disease. It lost often consists of testing the effects of changes in MAP on cerebral blood flow, known as pressure autoregulation (Panerai, 1998). Patients with severe sepsis or septic shock often represent cases in which CBF is altered and MAP and $PaCO_2$ are not (Bowton, Bertels, Prough, & Stump, 1989; Terborg et al., 2001). However, CBF can also be preserved in other cases in spite of systemic hypotension (Matta & Stow, 1996).

To assess potential impaired autoregulation during sepsis, transcranial Doppler (TCD) has been the most widely-used technique. TCD is a non-invasive transcranial method of determining flow velocities cerebral arteries (Aaslid, Markwalder, & Nornes, 1982; Newell & Winn, 1990). TCD involves use of low-frequency ultrasound waves to insonate cerebral arteries through relatively thin bone windows, namely, the transtemporal, suboccipital (transforaminal), transorbital, and submandibular (retromandibular) (Naqvi, Yap, Ahmad, & Ghosh, 2013). Ultrasound waves emitted from the Doppler probe are transmitted through the skull and reflected by moving red blood cells within the intracerebral vessels. The difference in the frequency between the emitted and reflected waves, referred to as the "Doppler shift frequency," is directly proportional to the speed of the moving red blood cells (blood flow velocity). Because blood flow within the vessel is laminar, the Doppler signal obtained actually represents a mixture of different Doppler frequency shifts that can be transformed to a spectral display of the distribution of the velocities of individual red blood cells (Purkayastha & Sorond, 2012).

Although it does not directly measure CBF, it is a suitable non-invasive tool to assess cerebrovascular reactivity to changes in blood pressure and arterial partial pressure of CO_2 ($PaCO_2$) (Taccone, Scolletta, Franchi, Donadello, & Oddo, 2012). Its main disadvantage is that it is limited to measurements in large cerebral arteries and veins located close to the natural acoustic windows such as the temporal bone and the foramen magnum (Urban et al., 2014). Moreover, the transtemporal window can be absent in up to 5–20% of the patients. Finally, TCD is a 'blind' technique in which the various blood vessels are identified from the window used, the depth of insonation, the direction of blood flow with respect to the probe, and characteristics of the TCD waveform and is therefore a rather operator dependent technique (Sarkar, Ghosh, Ghosh, & Collier, 2007).

Using TCD, Berg et al (R. M. Berg et al., 2012; R. M. G. Berg et al., 2013) have shown that the static and dynamic properties of cerebral autoregulation may disassociate and that dynamic autoregulation was enhanced in humans after i.v LPS administration, but reduced in patients with severe sepsis or septic shock.

In addition to Kety and Schmidt and TCD approaches, Near-infrared spectroscopy (NIRS) is a non-invasive real-time bedside technique that estimates changes in cerebral oxygenation and consequently CBF, but one has to keep in mind that the NIRS signal is susceptible to contamination by changes in blood flow through extracerebral tissues (Toksvang, Plovsing, Petersen, Møller, & Berg, 2014). It measures chromophores, mainly hemoglobin, present in the sampled tissue and the obtained signal is derived mainly from oxy- and deoxyhemoglobin which allows to calculate the overall saturation for tissue hemoglobin or tissue oxygen saturation (StO2). The NIRS signal is dependent on the hemoglobin contained in the entire vascular tree and mainly small vessels (arterioles, capillaries, and venules) present in the sampled area (Mesquida, Gruartmoner, & Espinal, 2013). NIRS values are thought to reflect the blood pool between the arterial and regional venous blood. NIRS findings have been found to correlate well with TCD values (Pfister et al., 2008) and allow to monitor dynamic cerebral autoregulation in healthy adults (Steiner et al., 2009).

With this blood oxygenation sensitive technique, Deutschman and colleagues have shown increased cerebral oxygen extraction in pigs following LPS administration (which corresponds to the difference between oxygen arterial saturation and venous saturation) (Deutschman, Kirsch, Breslow, Miller, & Traystman, 1990). However, others have observed unchanged cerebral oxygen delivery and cerebral oxygen metabolism in human volunteers receiving an intravenous bolus of LPS using the Kety & Scmidt technique (Møller et al., 2002; Pollard et al., 1997). Thus $CMRO_2$ may be a poor marker of alterations in CBF. In addition, $CMRO_2$ was described to increase (EkströmJodal, Häggendal, Larsson, & Westerlind, 1982), decrease (Maekawa et al., 1991) or remain unchanged when CBF decreased (Thees et al., 2007). Furthermore, TCD and NIRS have been found to be in poor agreement to estimate noradrenaline-associated changes in CBF in septic patients. Indeed, measurements of middle cerebral artery flow velocity and jugular bulb oximetry after catecholamine infusion as measured by TCD, show increased cerebral blood flow but unaltered cerebral venous O_2 in stable sepsis patients (Berré et al., 1997). Moreover, TCD has been found to indicate increased middle cerebral artery blood flow velocity (MCAv) associated with increased MAP while NIRS showed no change in cerebral oxygen saturation

(Toksvang, Plovsing, Petersen, Møller, & Berg, 2014). However, the individual recordings in 23 patients with sepsis, severe sepsis, or septic shock revealed that fluctuations in cerebral blood flow velocity as assessed by TCD can be also recorded in the NIRS-derived tissue oxygenation index and that the indices of dynamic autoregulation measured by these two techniques are in agreement (decreased autoregulation in case of vasodilation was associated with increased PaCO2 and decreased MAP) (Steiner et al., 2009). Thus, techniques based on venous oxygen saturation may not seem suitable in all cases of sepsis to assess cerebral blood flow but suggest that alteration of CBF autoregulation during sepsis does not result from changes in cerebral oxygen consumption (Deutschman, Kirsch, Breslow, Miller, & Traystman, 1990). It is important to keep in mind though that the assessment of autoregulation using TCD mainly concerns middle cerebral artery flow velocity and does therefore not necessarily represent whole brain perfusion. Similarly the tissue oxygenation index of dynamic autoregulation quantified by NIRS mainly reflects oxygenation in cerebral blood close to the surface of the skull and can therefore not be expected to provide insight into whole brain perfusion.

The impairment of cerebral autoregulation, when observed, can start early in sepsis and last several hours to over a day after sepsis onset (Pierrakos et al., 2013), can be interpreted to suggest microcirculatory dysfunction (Taccone, Castanares-Zapatero, et al., 2010; Taccone, Su, et al., 2010). Even though microcirculatory dysfunction has been proposed to precede macrocirculatory failure during sepsis (Rosengarten et al., 2007; Tarek Sharshar, Polito, Checinski, & Stevens, 2010), not many studies have addressed the cerebral microcirculation in septic patients. Vasoreactivity to external stimuli is an important parameter to assess microcirculatory function as it informs on vasculature bed health and vascular reserve of the cerebral parenchyma. It refers to changes in cerebral blood flow velocity in response to stimulation by vasodilators (CO_2 inhalation, i.v. injection of acetazolamide or simply by breath holding) and vasoconstrictors (hyperventilation) detected by several techniques. Vasoreactivity is region-dependent and is more important in grey matter than in white matter under physiological conditions. Thus, the vasoreactivity of the cerebral cortex to CO_2 induced by hyperventilation (that reduces arterial $PaCO_2$ and induces vasoconstriction) is greater than that of the cerebellum (Naganawa, Norris, Zysset, & Mildner, 2002; Posse et al., 1997) and basal ganglia (Naganawa, Norris, Zysset, & Mildner, 2002). This may be due to regional differences in metabolic rates and capillary density (Moody, Bell, & Challa, 1990). Patients with sepsis-associated encephalopathy (SAE) showed vascular hyporesponsiveness to a

vasodilatory stimulus (acetazolamide) than control persons, indicating that cerebrovascular reactivity is impaired and cerebral arteriolar function altered in patients with SAE (Szatmári et al., 2010). This altered vasoreactivity seems to be an early pathogenetic phase of SAE, since patients with septic syndrome and multiple-organ failure with hypotension treated with increasing doses of vasopressors are also at risk to develop for encephalopathy (Wijdicks & Stevens, 1992).

Several studies suggest that experimental sepsis affects the mechanical vascular properties of the cerebral vasculature including vascular resistance, vascular tone and reactivity. Vascular resistance refers to the force that opposes the blood flow through its vascular bed and corresponds to the difference between arterial and venous blood pressure divided by cardiac output. The administration of *E. Coli* LPS in dogs induced decreased CBF measured by labeled microspheres in pons, medulla, hypothalamus, thalamus, cortex, cerebellum, pituitry, and decreased regional vascular resistance in pons, medulla, hypothalamus but not in others regions (Bryan & Emerson, 1977).

To overcome the limitations cited above of the Kety & Schmidt, TCD and NIRS techniques based on cerebral oxygenation and external stimuli, estimation of CBF can be performed by magnetic resonance-based approaches. These approaches include magnetic resonance angiography (MRA), non-contrast enhanced time of flight (TOF), contrast-enhanced MRA (CE-MRA), phase contrast (PC) angiography and arterial spin labeling (ASL). TOF is based on the macroscopic motion of water protons, which results in intrinsic contrast between the stationary tissue and incoming blood, CE-MRA on the reduction of T1 relaxation by intravenously-administered contrast agents (Kang et al., 2009), PC on the basis of the shift in the phase of magnetization that occurs when blood moves in the presence of a magnetic field gradient (Huston & Ehman, 1993) and ASL on magnetically "labeling" water molecules as endogenous tracers upstream of the imaged volume (Kim, 1995).

TOF acquisitions can be performed using 2D or 3D sampling, with 2D TOF angiography often being clinically used in the evaluation of carotid arteries and peripheral vasculature, which can easily be chosen to be oriented orthogonal to the imaging plane, while 3D TOF being most commonly used for the more tortuous intracranial vasculature (Hartung, Grist, & François, 2011). Indeed, 3D TOF MRA is a reliable method allowing a rapid noninvasive assessment of the intracranial vasculature and is sensitive and specific enough to render the anatomy of the circle of Willis except for the posterior communicating segment (Ghazali & Shuaib, 2003) due to its small diameter and saturation effects due to slow flow (Talagala et

al., 1995). TOF MRA without contrast agent administration is sensitive to fast flowing blood, as only unsaturated blood entering the imaging volume between subsequent RF pulses produces high signal. Magnetic resonance angiography (MRA) using 3D-TOF technique in 25 patients with infection, clinical sepsis and the posterior reversible encephalopathy syndrome (PRES) indicated that hypertensive patients present vessel irregularities consistent with diffuse constriction of first-, second-, and third-order branch vessels, areas of focal vessel narrowing and string-of-bead (node-like) appearance known as vasospasm, and that normotensive patients even showed vessel disappearance along with reduced second and third order branch visualization (Bartynski, Boardman, Zeigler, Shadduck, & Lister, 2006). In animals, the use of 3D-TOF has allowed to show that i.v. LPS injection reduced outflow from the circle of Willis to the middle and anterior cerebral arteries without affecting filling of the circle of the Willis from the periphery. This indicates that alteration of cerebral blood irrigation may occur independently from peripheral circulation. The main disadvantage of this technique is nevertheless that slowly flowing blood is more difficult to detect. However, detection of slowly incoming blood can be improved by the use of a blood pool contrast agent (Beckmann, Stirnimann, & Bochelen, 1999). The contrast agent provides additional information on the nature of aneurysms and other flow abnormalities (Beckmann, Stirnimann, & Bochelen, 1999; Talagala et al., 1995). Intravenous injection of radioactive microspheres has been used in animal models of sepsis and indicated increased (Felix Wyler, Rutishauser, & Weisser, 1972), decreased (Bryan & Emerson, 1977; Christenson, Kuikka, Owunwanne, & Al-Sarraf, 1986; EkströmJodal, Häggendal, Larsson, & Westerlind, 1982; Tempel, Cook, Wise, Halushka, & Corral, 1986; F Wyler, Forsyth, Nies, Neutze, & Melmon, 1969) or preserved (Booke, Westphal, Hinder, Traber, & Traber, 2003; Hinkelbein et al., 2007; Zhen, 1987) CBF. Species differences or anesthesia may be among the factors explaining these apparent inconsistencies in CBF estimates between sepsis models as decreased CBF and cardiac output has been found in unanesthetized monkeys and increased CBF and cardiac output in anesthetized rabbits (F Wyler et al., 1969; Felix Wyler et al., 1972).

Phase-Contrast MRA allows to identify the direction and velocity of flow in a generated image after the application of a bipolar velocity-encoding gradient during the pulse sequence twice in opposing directions. This results in a phase change in moving blood, thus producing a signal proportional to the velocity of moving blood and to the strength of the bipolar flow encoding gradient, which is prescribed by setting the Velocity Encoding (Venc) value (Hartung, Grist, & François, 2011).

ASL is another MR-based technique to assess CBF. Its non-invasiveness along with the virtual absence of limitations in the depth of measurements makes it very useful in the study of brain perfusion (Ferré, Bannier, & Raoult, 2013). ASL generates an image by magnetically "labeling" water molecules as endogenous tracers upstream of the imaged volume. Briefly, the application of radiofrequency to the neck region inverting the magnetization of local arterial blood water is followed after a short delay by imaging of brain regions of interest more downstream. Subtraction of the unlabeled and labeled images provides perfusion-weighted maps that can then be used to quantify CBF (Grade et al., 2015; Kim, 1995). Bos et al, 2012, evaluated the quantitative accuracy of ASL-Flow-sensitive Alternating Inversion Recovery (ASL-FAIR) for brain imaging in rats by a direct comparison with radioactive microspheres, which is an accepted gold standard for perfusion quantification, and concluded that ASL-FAIR is suitable to quantify brain perfusion in the rat at low, normal, and moderately increased flows (Boś et al., 2012). To our knowledge, no study so far has employed PC-MRA or ASL to quantify CBF during clinical or experimental sepsis.

Systemic alterations that may alter CBF during sepsis

Altered CBF may be caused by systemic changes in cardiovascular parameters often occurring in septic patients, such as decreased cardiac output and reduced arterial carbon dioxide partial pressure (Thees et al., 2007). Indeed, several studies have shown that decreased CBF is associated with decreased cardiac output (Tempel, Cook, Wise, Halushka, & Corral, 1986; F Wyler, Forsyth, Nies, Neutze, & Melmon, 1969) and, conversely, that increased CBF is associated with increased cardiac output in septic conditions (Hariri, Ghajar, Bahramian, Sharif, & Barie, 1993; Lingnau et al., 1996; Smith, Padayachee, Modaresi, Smithies, & Bihari, 1998; Felix Wyler, Rutishauser, & Weisser, 1972). However, as we have already seen above, increased cardiac output despite increased (Berré et al., 1997; Hariri et al., 1993; Lingnau et al., 1996; Smith et al., 1998; Felix Wyler et al., 1972), decreased (Maekawa et al., 1991) or unchanged CBF (Booke, Westphal, Hinder, Traber, & Traber, 2003; Taccone, Castanares-Zapatero, et al., 2010) have also been described. Although these apparent inconsistencies cannot yet be explained, it is important to bear in mind that the brain can regulate its own blood supply in large part independently from cardiac output under healthy conditions and that the heart and brain vasculature may respond differently to the presence of circulating bacterial fragments (Møller et al., 2002). Nevertheless, Martinell et al (Martinell, Högström, & Haglund, 1987) have shown that in "early" septic shock following i.p injection

of live *E.coli* bacteria in rat, cardiac output and blood flow distribution to vital organs were maintained at the normal range. But even during "late" shock, when cardiac output had decreased markedly, myocardial and cerebral blood flow remained nevertheless in the control range. Similarly, after the administration of LPS to pigs and despite the deterioration of microcirculatory perfusion observed in the myocardium, a macro-hemodynamical high flow state was maintained so that the cerebral blood flow remained with the control range (Zhen, 1987). However, it is important to point out that when brain hypoperfusion during sepsis occurs, it may alter cerebral function and lead to severe complications including *delirium* (Pierrakos et al., 2014; Yokota, Ogawa, Kurokawa, & Yamamoto, 2003) and PRES (Bartynski, 2008) as well as CNS structural changes (see below).

Functional imaging: fMRI, PET, SEP and EEG

The main functional neuroimaging techniques used to determine the effects of brain injury on cognition and behavior related systems are electroencephalography (EEG), functional magnetic resonance imaging (fMRI) and positron emission tomography (PET). Functional imaging allows measuring of neuronal activity by measuring changes in electrical activity as clusters of neurons become active (EEG) or by detecting regional metabolic changes as a proxy for neuronal activity (fMRI and PET). The latter approach is based on tagging molecules of interest with a positron emitting isotope (^{18}F or ^{15}O) and has frequently been used to measure changes in brain blood flow and metabolism with intravenously-injected water and deoxyglucose, respectively, containing a positron emitting isotope. fMRI allows measurement of hemodynamic responses related to neuronal activity through it sensitivity to changes in blood oxygenation (Crosson et al., 2013).

Electroencephalography (EEG) is the primary means to study neocortical dynamics on the millisecond time scale at which information is processed by neurons. However, the information content of conventional EEG is limited by its poor spatial resolution (Nunez, 1993). This brain mapping method is a non-invasive procedure which allows as many control tests as needed to survey the course of a disease or to monitor drug effects. EEG and evoked potential (EP) data recorded from multiple scalp electrodes are graphically displayed on a computer-driven video screen. The main advantage of EEG mapping is that different frequencies appearing simultaneously, can be visualized and their topographic peculiarities can be shown by consecutive maps. In addition, subtle slow-wave asymmetries are detected and can be summarized concisely in spectral plots. However, a simple look at such maps does

not provide enough information to discriminate between real EEG activity and possible artifacts. It is, therefore, necessary to monitor the subject's EEG during data acquisition (Maurer & Dierks, 1987).

SEP and EEG

In patients with sepsis and in animals under septic conditions somatosensoriel evoked potentials (SEP) have been used to evaluate global cerebral electrophysiological function. SEP has been used to detect SAE in critically ill patients and has been described as a prolongation of SEP peak latencies beyond the upper limit of the reference range of subcortical and cortical SEP pathways, as well as asymmetry of peak latencies. Both subcortical and cortical SEP pathways have been found to be impaired and subclinical cerebral focal signs to be present in the subcortical SEP pathways and to a lesser extent in the cortical SEP pathways 48 hrs after the development of severe sepsis or septic shock (Zauner et al., 2002). Metabolic encephalopathy refers to a series of neurological disorders not caused by primary structural abnormalities but by lack of glucose, oxygen or metabolic cofactors and those linked to peripheral organ dysfunction (Roger, 1999). In order to determine metabolic encephalopathy in critically ill patients with multiple organ failure as a result of septic or surgery, measurement of median nerve-stimulated short-latency and long-latency sensory evoked potentials have been performed. Peak latencies in septic patients with multiple organ dysfunction were significantly prolonged compared with peak latencies of healthy controls but did not differ from surgery patients, indicating that the peak latency was correlated with the severity of illness but not with the presence or absence of sepsis (Zauner et al., 2000).

Electroencephalography (EEG), revealed mainly non-specific but generalized cerebral dysfunction associated with sepsis (Jackson & Hopkins, 2009; Morandi et al., 2010; Pereira et al., 2015; Thees et al., 2007) that were significantly more frequent in patients who died (Polito et al., 2013). These diffuse brain dysfunctions were also more evident in the cerebral cortex in patients with PRES (Pereira et al., 2015).

In animals, the evoked flow velocity responses in the somatosensorial cortex are calculated from the averaged relative flow velocity signals during electrical stimulation of, for example, the forepaw with rectangular pulses at a repetition frequency. Amplitudes and latencies of somatosensory evoked potentials 60 min after injection of 0.1 mg/kg *E. coli* LPS intravenously in pigs were shown to be unchanged, even though, MAP, cerebral perfusion pressure, and systemic vascular resistance fell by 50% and cerebral oxygen extraction

increased (Deutschman, Kirsch, Breslow, Miller, & Traystman, 1990). Moreover, it has been shown in rats that the intravenous administration of 1 mg/kg LPS increased local CBF, measured with TCD, and evoked potentials occurred concomitantly, whereas subsequent to 5mg/kg LPS the increase in blood flow was lower 60 min later and evoked potentials decreased 180 min later (Rosengarten et al., 2007). Interestingly, both doses of intravenously administered LPS induced comparable systemic hypotension starting 30 min after injection (Rosengarten et al., 2007). Taken together, these experimental studies indicate that decreased SEP in response to circulating bacterial fragments are neither the necessary consequence of systemic hypotension nor of deficits in local cerebral hyperemia. Impaired EEG has also been described in rats after CLP surgery with elongated latencies and increased amplitudes in somatosensory recordings, while electrocorticograms revealed slight decrease in median and spectral edge frequencies amplitudes and significantly increased delta activities in 50% of CLP rats (Kafa, Bakirci, Uysal, & Kurt, 2010).

Structural imaging

Different MR imaging modalities can be employed to characterize with high sensitivity various acute CNS pathological features like ischemic and hemorrhagic stroke, edema formation and white matter disorganization and disruption associated with inflammation.

CT, T2, susceptibility-weighted MRI: Ischemia and hemorrhage

Computed tomography (CT) is a computer-controlled transverse axial scanning system using a frame with an x-ray tube and two detectors opposite to the tube. During scanning, a narrow x-ray beam passes through the patient's head and emergent photons are received by detectors. A third detector is used in a reference mode to measure the intensity of the primary x-ray beam. Permanent recording then allows for quantitative assessment of the x-ray absorption values in different brain structures (Hassani, Khomeini, & Bard, 1976). CT is similar to magnetic resonance angiography and conventional angiography in its sensitivity to detect the anterior, middle, or posterior cerebral arteries or the anterior communicating artery of the circle of Willis (Katz, Marks, Napel, Bracci, & Roberts, 1995) and provides complementary information to other techniques of CBF assessment, such as TCD (Tsivgoulis, Sharma, Lao, Malkoff, & Alexandrov, 2007).

Initial studies with CT scans suggested that ischemia and hemorrhage were not common during sepsis since the majority of in septic patients showed no abnormalities (Coppens, Sztern, Korman, & Lustman, 1995; Egyed et al., 2008; Fabbian et al., 2010; Finelli & Uphoff,

2004; Nagase et al., 1995; Pereira et al., 2015; Taccone, Castanares-Zapatero, et al., 2010; Wijdicks & Stevens, 1992). However other studies have shown signs of ischemic stroke in one third of septic patients (Pereira et al., 2015; Polito et al., 2013) with different aspects and sizes seen in CT and T2-weighted MR images. When present, ischemia is especially affecting the subcortical white matter of frontal lobes and temporal regions and is associated with the presence of disseminated intravascular coagulation as well as increased mid-term neurological disability and mortality (Fabbian et al., 2010; Jackson & Hopkins, 2009). It is important to point out that no association was found between duration or severity of hypotension and cerebral ischemia (Polito et al., 2013).

Dynamic susceptibility contrast-enhanced MRI is based on the detection of the first passage of a bolus of non-diffusible contrast media that alters signal decay in T2*-weighted and often used to perform perfusion-weighted MRI (Macdonald & Frayne, 2015; Viallon et al., 2015). However, when the blood–brain barrier is compromised, extravasation of the contrast agent through the leaky capillaries can be detected on T1-weighted sequences (Heye, Culling, Valdés Hernández, Thrippleton, & Wardlaw, 2014). Hence, susceptibility-weighted MRI is particularly sensitive to detect hemorrhages, brain abscesses, and sinus thrombosis in septic patients (Mizuhara et al., 2011; Nagase et al., 1995; Polito et al., 2013; Weon, Marsot-Dupuch, Ducreux, & Lasjaunias, 2005).

Diffusion-weighted MRI: white matter disorganization and disruption

Diffusion weighted imaging (DWI) is a method of signal contrast generation based on the random Brownian motion of water molecules driven by thermal energy. This technique allows assessing the micro-architecture of both human and animal tissues. Diffusion can be quantified by parameters, such as the apparent diffusion coefficient (ADC) and fractional anisotropy (FA). The ability to detect and quantify of diffusion in many different directions allows for so-called diffusion tensor imaging (DTI), which is an interesting tool for the assessment of organs with a highly organized fiber structure. Water diffusion is anisotropic in brain white matter, because myelinated axons limit molecular movement perpendicular to these fibers. DTI exploits this property to produce micro-architectural detail of white matter tracts and thus provides information about white matter integrity (Baliyan, Das, Sharma, & Gupta, 2016).

White matter abnormalities are frequently seen in septic patients (Morandi et al., 2010, 2012; Tarek Sharshar et al., 2007). Indeed, leukoencephalopathy with reduced diffusion has been

found in 21% of in septic patients (Egyed et al., 2008; Polito et al., 2013; Tarek Sharshar et al., 2007). However, often times, classic MRI modalities may not show any lesions or abnormalities during sepsis. In 71 septic shock patients with acute brain dysfunction including coma, *delirium*, focal neurological deficits or seizures, approximatively the half of patients (52%) showed normal: T1- and T2-weighted MRI, as well as FLuid Attenuated Inversion Recovery (FLAIR) MRI and DWI (Polito et al., 2013). In addition, in some cases MRI may be normal at sepsis onset and show multiple abnormalities later on even with advanced modalities. As shown by Morandi et al (2012) and using DTI, septic patients may show white matter abnormalities associated with cognitive impairment 3 months after discharge that were absent at sepsis onset. On the contrary, some initial abnormalities found during sepsis are reversible and patients may show normal brain imaging and functioning subsequently (Fabbian et al., 2010) and recover or have better overall cognitive functioning than initially (Jackson & Hopkins, 2009; Mizuhara et al., 2011). For example, Takanashi et al (Takanashi, Hirasawa, & Tada, 2006) showed reversible lesions with transiently increased diffusion in the entire corpus callosum based on T1- and T2-MRI as well as on ADC and DTI maps.

Numerous mechanisms may alter diffusion parameters and contribute to MRI abnormalities and especially edema formation. Cytotoxic edema is characterized by swelling of cellular elements of brain parenchyma while vasogenic type is characterized by an increased vascular permeability leading to accumulation of edema fluid in the extracellular spaces (Klatzo, 1987). While T2/FLAIR hypersignals may be indicative of the presence of vasogenic edema with evidence of BBB disruption (Tarek Sharshar et al., 2007), DWI-derived ADC can indicate the occurrence of cytotoxic edema when ADC is low (Höllinger, Zürcher, Schroth, & Mattle, 2000). These two forms of increased water content in the brain may coexist during sepsis (Höllinger et al., 2000).

Rosengarten et al (2008) did not find any difference in brain water content in rats 3.5 h after LPS injection (5 mg/kg) (Rosengarten et al., 2008). But after CLP in mice, T2-WI indicating vasogenic edematic fluid accumulation has been observed at the base of the brain after cecal ligation, while ADC maps suggest cytotoxic edema formation both in the cortex and thalamus (Bozza et al., 2010).

Brain imaging with different approaches both in septic patients and experimental animal models of sepsis, show that the forebrain, and in particular, subcortical white matter of frontal and temporal lobes, corpus callosum and the basal ganglia, seems to be the location of the major structural and functional abnormalities occurring during sepsis with the cerebellum and

brainstem being less affected (Finelli & Uphoff, 2004; F Wyler, Forsyth, Nies, Neutze, & Melmon, 1969).

Post mortem analysis

Post mortem analysis in septic patients has revealed the presence of diffuse cerebral edema with white matter swelling, dilation of perivascular spaces containing haemosiderin-laden macrophages, separation of myelinated fibers without myelin destruction and the presence of intra myelin vacuoles interpreted as cytotoxic edema (Sharshar et al. 2007). In addition, acute hemorrhages, hypercoagulability syndrome, micro-abscesses, multifocal necrotizing leukoencephalopathy, ischemic lesions and neuronal apoptosis have been found with different frequencies and intensities in autonomic brain regions (Sharshar et al. 2004). Multiple foci of infarction has been observed in the cortex, basal ganglia and the splenium of the corpus callosum that were characterized by necrotic lesions and marked acute inflammatory reaction with some abscess formation in cortex and basal ganglia and associated with occlusion of small arteries (Finelli & Uphoff, 2004). Histological modifications suggestive of edema have been described surrounding microvessels (<10 μm diameter), but not larger vessels, in the frontal cerebral of rats that had been subject to CLP (Brooks, Moss, Davies, Jalan, & Davies, 2014).

Part 4: Contribution of histology to the understanding of sepsis-associated encephalopathy

Endothelial cells (BBB)

It has been reported that both LPS and CLP result in changes of the BBB that are due to effects of inflammatory mediators rather than to the presence of live bacteria (Hofer et al., 2008). Both disruptive and non-disruptive changes may occur during sepsis (as reviewed by (Varatharaj & Galea, 2017)). During sepsis the BBB can be altered by several mechanisms including hemodynamic, structural and molecular changes depending on the components of the BBB that are affected Following *E. coli* administration to mice, the transient increase in BBB permeability was maximal 3 h later (Tsao, Hsu, Wu, Liu, & Lei, 2001). However, up to 3 h after i.p. injection of high doses of bacterial LPS, no evidence of non-specific disruption of the BBB has been observed indicating that circulating LPS does not acutely disrupt the BBB (Bickel, Grave, Kang, & Voigt, 1998). Nevertheless, 6-24 h after LPS injection in mice

interrupted basal lamina, detached pericytes and increased cerebrovascular permeability have been observed (Nishioku et al., 2009). Interestingly, after CLP increased BBB permeability in cortex and hippocampus is related to the increase of matrix metalloproteinases MMP-9 and MMP-2 expression in microvessels and could be reversed by administration of inhibitors of either MMP. However, only the inhibition of both MMP-9 and MMP-2 was able to improve acute cognitive alterations associated with sepsis (Dal-Pizzol et al., 2013).

Astroglia

The term 'astrocyte' was coined by Michael von Lenhossék in 1893 to describe the star-shaped neuroglial cells in the CNS. Astrocytes constitute the most abundant cell type in the CNS and outnumber neurons (Bass, Hess, Pope, & Thalheimer, 1971) and microglia (Savchenko, Nikonenko, Skibo, & McKanna, 1997). Astrocytes participate in the formation of the BBB and maintenance of its integrity by regulating cerebral endothelium properties, release neurotrophic factors, modulate neurotransmission through the release of synaptically active molecules, maintain fluid, ion, pH, and transmitter homeostasis of the synaptic interstitial fluid and furnish energy metabolites to different neural elements in gray and white matter (Sofroniew & Vinters, 2010). They also play an important role in the coupling of increased blood flow to neuronal activity by releasing vasoactive molecules (Jakovcevic & Harder, 2007). Indeed, astrocytes have been proposed to control cerebrovascular activity and induce both constriction and dilation of adjacent arterioles via the release of prostaglandins (PGE), nitric oxide and potassium (Gordon, Choi, Ellis-Davies, & MacVicar, 2008).

Astrocytes express water channels, such as aquaporin 4 (AQP4), the presence of which is particularly abundant in astrocytic endfeet close to brain endothelial cells and pia mater (Jung et al., 1994). Water flux via AQP4 follows osmotic gradients (Verkman, 2005; Verkman, Binder, Bloch, Auguste, & Papadopoulos, 2006) and AQP4 regulates water movement across the BBB, neutralizes changes of extra-cellular space volume and contributes to water reflux from presynaptic astrocytes (Haj-Yasein et al., 2011) and more generally to resorption of extra-cellular fluid (Papadopoulos, 2004).

In response to local injury, the shape of astrocytes changes and their number may increase, a process called astrogliosis, which can seal off the injured area. Astrogliosis includes astrocytic hypertrophy with different morphologies depending on lesion severity and localization (Sofroniew & Vinters, 2010) and increased expression of GFAP (Eng, Yu, & Lee, 1992). GFAP an intermediate filament protein present in the main branches, but absent from the fine

terminal branches of astrocytes (Sofroniew & Vinters, 2010). During the initial response to insult, a reactive astrocyte adjacent to the core of a lesion may have a beneficial role in preventing degeneration of surrounding tissue, whereas one at a more distant location may have a deleterious effect (Sun & Jakobs, 2012). Interestingly, AQP4 facilitates astrocytic inflation during cytotoxic edema, (Manley et al., 2000), whereas AQP4 facilitates the clearance of vasogenenic edema (Papadopoulos, 2004) during which it is expressed in the whole astrocytic membrane (Tourdias et al., 2011).

Microglia

Microglia survey their microenvironment with their extremely motile processes and protrusions, which allow, through the expression of specific receptors, for the detection of accumulated metabolic products and deteriorated tissue components (Nimmerjahn, Kirchhoff, & Helmchen, 2005). Indeed, microglia express a variety of surface receptors recognizing purine, fractalkine, complement, immunoglobulins, adhesion molecules, and inflammatory molecules (Nimmerjahn et al., 2005). Microglia are the first cells to respond to CNS insults, and can rapidly migrate to the lesion site and release cytotoxic or trophic factors there (Dheen, Kaur, & Ling, 2007). Microglia cells exhibit two forms of motility, constant movement of filopodia probing surrounding brain tissue, and outgrowth of larger processes in response to nearby damage (Hines, Hines, Mulligan, & Macvicar, 2009). Activation of microglia occurs predictably after acute CNS insults and is characterized by changes in cell morphology, size and number as well as in the pattern of surface molecules, cytokines and growth factors expressed (Streit, Walter, & Pennell, 1999).

In patients who died from sepsis, morphological signs of microglia activation have been observed in the grey matter (Lemstra et al., 2007). In animals impaired memory during experimental septic conditions after LPS or pro-inflammatory cytokine administration has been associated with microglial activation in the hippocampus (Terrando et al., 2010). The induction of glial cytokine expression after systemic LPS injection in mice peaked 2 to 4 h after injection in microglia and around 12 h post-injection in astrocytes, and preceded increased Ionized calcium binding adaptor molecule-1 (Iba-1) or GFAP immunoreactivity (24 and 48 h, respectively) (Norden, Trojanowski, Villanueva, Navarro, & Godbout, 2016). Iba-1 is a microglia/macrophage-specific calcium-binding protein acting as an adapter molecule binding calcium signals that has actin-bundling activity and participates in membrane ruffling and phagocytosis in activated microglia (Imai, Ibata, Ito, Ohsawa, & Kohsaka, 1996; Ohsawa,

Imai, Sasaki, & Kohsaka, 2004). As suggested by Michels et al (Michels, Danielski, Dal-Pizzol, & Petronilho, 2014), microglial activation represents one of the cerebral responses during SAE and may contribute to altered behavior and mental state through the production of free radicals and neuroactive and vasoactive mediators. In addition, microglia may control CNS infection through inflammatory responses, phagocyte cell debris and repair tissue through the release of growth factors. Interestingly, i.c.v administration of minocycline, a potential anti-inflammatory drugs that inhibits microglial activity and microgliosis, has been shown to decrease hippocampal pro-inflammatory cytokine concentrations, oxidative damage and BBB disruption as well as long-term cognitive impairment in a CLP rat model (Michels et al., 2015).

Oligodendroglia

Oligodendrocytes, the myelin-forming cells of the central nervous system, are found in short rows, appearing like beads on a string, running parallel to axons in brain white matter (Edgar & Griffiths, 2014). Myelination is a complex process by which an axon becomes insulated by sheets of the proteolipid oligodendroglial membrane known as myelin. Oligodendrocytes express several myelin associated enzymes. 2',3'-cyclic nucleotide 3'-phosphodiesterase (CNPase) is a myelin-specific protein detected in developing oligodendrocytes that continues to be expressed in adult animals (Trapp, Bernier, Andrews, & Colman, 1988). It represents the major enzyme in myelin and constitutes about 4% of total CNS myelin protein (Pfeiffer, Warrington, & Bansal, 1993). The loss of myelin sheath around an axon slows the conduction of action potential in affected nerves, thus causing impaired sensation, movement, or cognition depending on which nerves are affected (Jing, He, Zhang, & Andy Li, 2013). After brain insults, oligodendrocytes are similar to neurons in their susceptibility to damage (reviewed by (Bradl & Lassmann, 2010; Ludwin, 1997)), but display a higher regenerative potential even in the adult (reviewed by (Baumann & Pham-Dinh, 2001)). During SAE edema formation, oligodendrocytes show vacuoles (Tarek Sharshar et al., 2007). CNPase has been shown to be downregulated in the neonatal cerebral white matter after intracerebral LPS injection in rodents (Xie et al., 2015). However the effect of systemic inflammation on myelin and it associated enzymes has not been studied following LPS administration or CLP.

The presence of cytokines in low concentrations in the brain during the acute phase of sepsis is essential for the expression sickness behavior as an adaptive response. The transition from physiology to pathology may be either progressive or sudden, marked by an event such as

BBB breakdown (Varatharaj and Galea, 2017). Neuroinflammation has become a commonly used term in the context of sepsis, Alzheimer's disease, Parkinson's disease, multiple sclerosis and brain tumors to describe endogenous CNS tissue responses to injury and the implication of inflammatory processes in the pathogenesis of these diseases. It comprises "reactive gliosis" and increased pro-inflammatory cytokine production as well as immune cell infiltration and possibly neurodegenerative processes (Streit, Mrak, & Griffin, 2004).

Conclusion

Immune system activation to infection can lead to orchestrated physiological and behavioral changes, such as fever, reduced food intake and increased sleep thought to reflect adaptive response to fight infection. After systemic challenge, the signal rich the brain via LPS and pro-inflammatory cytokines that act directly or indirectly via a fast vagal route and a slow signaling route involving CVO to induce these adaptive response but may also result in brain dysfunction and cognitive impairment.

Hemodynamic, metabolic, functional and structural brain imaging approaches have been used to assess cerebral changes during sepsis and sepsis-associated encephalopathy in the clinic and experimental models. However, SAE pathophysiology still questionable because of the multiplicity of peripheral and central factors involved in the genesis of neuroinflammation and brain as well as other organs damage. Despite its privileged status and difference in peripheral and cerebral vasculature response to the presence of circulating bacterial fragments, brain vasculature is sensitive to hypotension and peripheral changes that are responsible for increased morbidity and severity of sepsis. SAE symptoms have been proposed to be related to a decrease in CBF, cerebral autoregulation failure, microcirculatory dysfunction and white matter damage making the well understanding of these mechanisms crucial for the its treatment or prevention of many neurological deficits, mental deficiency and motor response alteration.

Neurological deficits such as delirium, memory and learning are strongly associated with altered brain during SAE induced by activated glial cells both in grey and white matter.

Outstanding questions and objectives

One of the prerequisites to improve our understanding of sepsis-associated encephalopathy or brain dysfunction is to extend already existing knowledge on this condition and to clarify some of its still unrecognized aspects by combining different approaches to obtain a better description of how hemodynamic, neurochemical and structural changes are related in time and space. As the early phase of SAE often only concerns some neurological or cognitive symptoms, which in some cases even lead to suspect sepsis, it is virtually impossible to obtain hemodynamic, metabolic and structural information during this early phase in patients. Addressing the question of how hemodynamic, neurochemical and structural changes are related during SAE needs therefore to be addressed experimentally in well-described animal models. Our work proposes to do just that and employs *in vivo* MRI approaches to assess hemodynamical changes and indications of structural modification in the CNS followed by *post mortem* histological approaches to describe neurochemical and cellular modifications in brains of animals that either underwent intraperitoneal injection of bacterial LPS or CLP. In particular, we set out to study *in vivo* cerebral blood perfusion with Arterial Spin Labeling and brain structure with Diffusion-Weighted Imaging as well as to detect the production of inflammatory mediators, modifications of blood-brain barrier permeability and glial cell morphology on brain sections of the same septic animals.

Thesis structure

The present thesis is structured as follows; after introducing the outstanding questions based on an analysis of the available literature and the ensuing aims, the first chapter contains a literature review introducing the essential concepts and approaches used in this study. The second chapter relates findings obtained in an experimental sepsis model consisting of the intraperitoneal injection of LPS in which animals were subject to perfusion and diffusion imaging before being sacrificed 2.5 h later to detect blood-brain barrier breakdown, pro-inflammatory cytokine production, vasoactive prostaglandin synthesis and glial cell morphology. The third chapter concerns the assessment of the same parameters in the more pathophysiologically-relevant CLP model. The fourth chapter addresses the possible influence of MRI under anesthesia on histological measures of vasoactive prostaglandin production, BBB integrity and glia cell responses during CLP-induced sepsis in a comparison to

histological findings from animals that have not undergone anesthesia and imaging. Finally, the last part presents conclusions and perspectives of the thesis work.

References

Aaslid, R., Markwalder, T.-M., & Nornes, H. (1982). Noninvasive transcranial Doppler ultrasound recording of flow velocity in basal cerebral arteries. *Journal of Neurosurgery*, *57*(6), 769–774. https://doi.org/10.3171/jns.1982.57.6.0769

Abbott, N. J. (2000). Inflammatory Mediators and Modulation of Blood – Brain Barrier Permeability. *Cellular and Molecular Neurobiology*, *20*(2), 131–147.

Abraham, E. (2003). Nuclear Factor – k B and Its Role in Sepsis- Associated Organ Failure, *80262*(Suppl 2).

AJ. Lewis, Seymour, C., & Rosengart, M. (2016). Current Murine Models of Sepsis. *Surgical Infection*, *17*(4), 385–393.

Al-Saffar, H., Lewis, K., Liu, E., Schober, A., Corrigan, J. J., Shibata, K., & Steiner, A. A. (2013). Lipopolysaccharide-induced hypothermia and hypotension are associated with inflammatory signaling that is triggered outside the brain. *Brain, Behavior, and Immunity*, *28*(November), 188–195. https://doi.org/10.1016/j.bbi.2012.11.015

Almeida, M. C., Steiner, A. A., Branco, L. G. S., & Romanovsky, A. A. (2006a). Cold-seeking behavior as a thermoregulatory strategy in systemic inflammation. *European Journal of Neuroscience*, *23*(12), 3359–3367. https://doi.org/10.1111/j.1460-9568.2006.04854.x

Almeida, M. C., Steiner, A. A., Branco, L. G. S., & Romanovsky, A. A. (2006b). Neural substrate of cold-seeking behavior in endotoxin shock. *PLoS ONE*, *1*(1). https://doi.org/10.1371/journal.pone.0000001

Arons, M., Wheeler, A., Bernard, G., Christman, B., Russell, J., Schein, R., … Swindell, B. (1999). Effects of ibuprofen on the physiology and survival of hypothermic sepsis. Ibuprofen in Sepsis Study Group. *Crit Care Med.*, *27*(4), 699–707.

Baliyan, V., Das, C. J., Sharma, R., & Gupta, A. K. (2016). Diffusion weighted imaging: Technique and applications. *World Journal of Radiology*, *8*(9), 785. https://doi.org/10.4329/wjr.v8.i9.785

Baracchi, F., Ingiosi, A., Raymond, R. J., & Opp, M. (2011). Sepsis-induced alterations in sleep of rats. *Am J Physiol Regul Integr Comp Physiol*, *301*(5), 1467–1478.

Barichello, T., Martins, M. R., Reinke, A., Constantino, L. S., Machado, R. A., Valvassori, S. S., … Dal-Pizzol, F. (2007). Behavioral deficits in sepsis-surviving rats induced by cecal ligation and perforation. *Brazilian Journal of Medical and Biological Research*, *40*(6), 831–837. https://doi.org/S0100-879X2007000600013 [pii]

Barichello, T., Martins, M., Reinke, A., Feier, G., Ritter, C., Quevedo, J., & Dal-Pizzol, F. (2005). Cognitive impairment in sepsis survivors from cecal ligation and perforation. *Crit Care Med.*, *33*(1), 221–223.

Barreto, C. R., Freitas, de Aquino, R. R., de Oliveira-Sales, E. B., Campos, R. R. de, & Bergamaschi, C. T. (2007). Sympathic activation in sepsis induced by cecal ligation and puncture. *FASEB J.*, *21*((Meeting Abstract Supplement) A591), 618–626.

Bartynski, W. S. (2008). Posterior reversible encephalopathy syndrome, Part 2: Controversies surrounding pathophysiology of vasogenic edema. *American Journal of Neuroradiology*, *29*(6), 1043–1049. https://doi.org/10.3174/ajnr.A0929

Bartynski, W. S., Boardman, J. F., Zeigler, Z. R., Shadduck, R. K., & Lister, J. (2006). Posterior reversible encephalopathy syndrome in infection, sepsis, and shock. *American Journal of Neuroradiology*, *27*(10), 2179–2190. https://doi.org/10.1016/S0098-1672(08)70231-5

Bass, N. H., Hess, H. H., Pope, A., & Thalheimer, C. (1971). Quantitative cytoarchitectonic

distribution of neurons, glia, and DNA in rat cerebral cortex. *Journal of Comparative Neurology*, *143*(4), 481–490. https://doi.org/10.1002/cne.901430405

Baumann, N., & Pham-Dinh, D. (2001). Biology of oligodendrocyte and myelin in the mammalian central nervous system. *Physiological Reviews*, *81*(2), 871–927. https://doi.org/10.1111/j.1365-2427.2009.02340.x

Beckmann, N., Stirnimann, R., & Bochelen, D. (1999). High-resolution magnetic resonance angiography of the mouse brain: application to murine focal cerebral ischemia models. *Journal of Magnetic Resonance (San Diego, Calif. : 1997)*, *140*(2), 442–450. https://doi.org/10.1006/jmre.1999.1864

Berg, R. M. G., Plovsing, R. R., Evans, K. A., Christiansen, C. B., Bailey, D. M., Holstein-Rathlou, N.-H., & Møller, K. (2013). Lipopolysaccharide infusion enhances dynamic cerebral autoregulation without affecting cerebral oxygen vasoreactivity in healthy volunteers. *Critical Care (London, England)*, *17*(5), R238. https://doi.org/10.1186/cc13062

Berg, R. M., Plovsing, R. R., Ronit, A., Bailey, D. M., Holstein-Rathlou, N. H., & Moller, K. (2012). Disassociation of static and dynamic cerebral autoregulatory performance in healthy volunteers after lipopolysaccharide infusion and in patients with sepsis. *Am J Physiol Regul Integr Comp Physiol*, *303*(11), R1127-35. https://doi.org/10.1152/ajpregu.00242.2012

Berisavac, I. I., Padjen, V. V., Ercegovac, M. D., Beslać-Bumbaširević, L. G., Stanarčević, P. D., Stefanović-Budimkić, M. S., … Jovanović, D. R. (2016). Focal epileptic seizures, electroencephalography and outcome of sepsis associated encephalopathy—A pilot study. *Clinical Neurology and Neurosurgery*, *148*, 60–66. https://doi.org/10.1016/j.clineuro.2016.06.013

Bernheim, H., & Kluger, M. (1976). Fever: effect of drug-induced antipyresis on survival. *Science*, *193*(4249), 237–239.

Berré, J., De Backer, D., Moraine, J., Mélot, C., Kahn, R., & Vincent, J. (1997). Dobutamine increases cerebral blood flow velocity and jugular bulb hemoglobin saturation in septic patients. *Crit Care Med.*, *25*(3), 392–398.

Bickel, U., Grave, B., Kang, Y., & Voigt, K. (1998). No increase in blood – brain barrier permeability after intraperitoneal injection of endotoxin in the rat. *J.Neuroimmunol.*, *85*(2), 131–136.

Blatteis, C. M. (2003). Fever : pathological or physiological , injurious or beneficial ? *Journal of Thermal Biology*, *28*, 1–13.

Bluthé RM, Michaud B, Kelley KW, D. R. (1996a). Vagotomy attenuates behavioural effects of interleukin-1 injected peripherally but not centrally.

Bluthé RM, Michaud B, Kelley KW, D. R. (1996b). Vagotomy blocks behavioural effects of interleukin-1 injected via the intraperitoneal route but not via other systemic routes.

Bone, R. C., Balk, R. A., Cerra, F. B., Dellinger, R. P., Fein, A. M., Knaus, W. A., … Sibbald, W. J. (1992). Definitions for sepsis and organ failure and guidelines for the use of innovative therapies in sepsis. *Chest*, *101*(6), 1644–1655. https://doi.org/10.1378/chest.101.6.1644

Booke, M., Westphal, M., Hinder, F., Traber, L. D., & Traber, D. L. (2003). Cerebral blood flow is not altered in sheep with Pseudomonas aeruginosa sepsis treated with norepinephrine or nitric oxide synthase inhibition. *Anesthesia and Analgesia*, *96*(4), 1122–8, table of contents. https://doi.org/10.1213/01.ANE.0000052516.86497.B6

Boś, A., Bergmann, R., Strobel, K., Hofheinz, F., Steinbach, J., & den Hoff, J. Van. (2012). Cerebral blood flow quantification in the rat: a direct comparison of arterial spin labeling MRI with radioactive microsphere PET. *EJNMMI Research*, *2*(1), 47.

https://doi.org/10.1186/2191-219X-2-47
Bowton, D., Bertels, N., Prough, D., & Stump, D. (1989). Cerebral blood flow is reduced in patients with sepsis syndrome. *Crit Care Med.*, *17*(5), 399–403.
Bozza, F. A., Garteiser, P., Oliveira, M. F., Doblas, S., Cranford, R., Saunders, D., … Castro-Faria-Neto, H. C. (2010). Sepsis-associated encephalopathy: a magnetic resonance imaging and spectroscopy study. *Journal of Cerebral Blood Flow and Metabolism : Official Journal of the International Society of Cerebral Blood Flow and Metabolism*, *30*(2), 440–8. https://doi.org/10.1038/jcbfm.2009.215
Bradl, M., & Lassmann, H. (2010). Oligodendrocytes: Biology and pathology. *Acta Neuropathologica*, *119*(1), 37–53. https://doi.org/10.1007/s00401-009-0601-5
Broadwell, R. D., & Salcmant, M. (1981). Expanding the definition of the blood-brain barrier to protein. *Proc. Natl. Acad. Sci. USA*, *78*(12), 7820–7824.
Brooks, H. F., Moss, R. F., Davies, N. A., Jalan, R., & Davies, D. C. (2014). Caecal ligation and puncture induced sepsis in the rat results in increased brain water content and perimicrovessel oedema. *Metabolic Brain Disease*, *29*(3), 837–843. https://doi.org/10.1007/s11011-014-9555-y
Bryan, W. J., & Emerson, T. E. (1977). Blood flow in seven regions of the brain during endotoxin shock in the dog. *Proceedings of the Society for Experimental Biology and Medicine*, *156*(2), 205–8. https://doi.org/10.3181/00379727-156-39907
Bryant, R. E., Hood, A. F., Hood, C. E., & Al, E. (1971). Factors Affecting Mortality of Gram-Negative Rod Bacteremia. *Arch Intern Med*, *127*(1), 120–128.
Buras, J. A., Holzmann, B., Sitkovsky, M., & Israel, B. (2005). ANIMAL MODELS OF SEPSIS : SETTING THE STAGE. *NATURE REVIEWS, DRUG DISCOVERY*, *4*, 854–866. https://doi.org/10.1038/nrd1854
Calsavara, A. C., Rodrigues, D. H., Miranda, A. S., & Teixeira, L. (2013). Late Anxiety-Like Behavior and Neuroinflammation in Mice Subjected to Sublethal Polymicrobial Sepsis. *Neurotox Res*, *24*, 103–108. https://doi.org/10.1007/s12640-012-9364-1
Cao, C., Matsumura, K., Yamagata, K., & Watanabe, Y. (1995). Induction by lipopolysaccharide of cyclooxygenase-2 mRNA in rat brain; its possible role in the febrile response. *Brain Research*, *697*(1–2), 187–196. https://doi.org/10.1016/0006-8993(95)00839-I
Cao, C., Matsumura, K., Yamagata, K., & Watanabe, Y. (1996). Endothelial cells of the rat brain vasculature express cyclooxygenase-2 mRNA in response to systemic interleukin-1beta: A possible site of prostaglandin synthesis responsible for fever. *Brain Research*, *733*(2), 263–272. https://doi.org/10.1016/0006-8993(96)00575-6
Christenson, J., Kuikka, J., Owunwanne, A., & Al-Sarraf, A. (1986). Cerebral circulation during endotoxic shock with special emphasis on the regional cerebral blood flow in vivo. *Nucl Med Commun.*, *7*(7), 531–540.
Clemmer, T. P., Fisher, C. J., Bone, R. C., Slotman, G. J., Metz, C. A., & Thomas, F. O. (1992). Hypothermia in the sepsis syndrome and clinical outcome. *Critical Care Medicine*. Retrieved from http://www.ncbi.nlm.nih.gov/pubmed/1395659
Coppens, L., Sztern, B., Korman, D., & Lustman, F. (1995). Yersinia enterolitica bacteremia with intracranial extension. *Scand J Infect Dis*, *27*(4), 409–410. https://doi.org/10.3109/00365549509032742
Corrigan, J. J., Fonseca, M. T., Flatow, E. A., Lewis, K., & Steiner, A. A. (2014). Hypometabolism and hypothermia in the rat model of endotoxic shock: independence of circulatory hypoxia. *The Journal of Physiology*, *592*(17), 3901–3916. https://doi.org/10.1113/jphysiol.2014.277277
Cross, A. S., Opal, S. M., Sadoff, J. C., & Gemski, P. (1993). Choice of bacteria in animal

models of sepsis. *Infection and Immunity*, *61*(7), 2741–2747.
Crosson, B., Ford, A., McGregor, K. M., Meinzer, M., Cheshkov, S., Li, X., … Briggs, R. W. (2013). Functional Imaging and Related Techniques: An Introduction for Rehabilitation Researchers. *J Rehabil Res Dev.*, *47*(2), 7–34. https://doi.org/10.1111/j.1747-0285.2012.01428.x.Identification
Dal-Pizzol, F., Rojas, H., dos Santos, E., Vuolo, F., Constantino, L., Feier, G., … Ritter, C. (2013). Matrix metalloproteinase-2 and metalloproteinase-9 activities are associated with blood-brain barrier dysfunction in an animal model of severe sepsis. *Mol Neurobiol.*, *48*(1), 62–70.
Dantzer, R. (2001). Cytokine-Induced Sickness Behavior: Where Do We Stand? *Brain, Behavior, and Immunity*, *15*(1), 7–24. https://doi.org/10.1006/brbi.2000.0613
Dantzer, R. (2009). Cytokine, Sickness Behavior, and Depression. *Immunol Allergy Clin North Am*, *29*(2), 247–264. https://doi.org/10.1016/j.iac.2009.02.002.Cytokine
Dantzer, R., & Kelley, K. W. (2007). Twenty years of research on cytokine-induced sickness behavior. *Brain, Behavior, and Immunity*, *21*(2), 153–160. https://doi.org/10.1016/j.bbi.2006.09.006
De Cruz, S. J., Kenyon, N. J., & Sandrock, C. E. (2009). Bench-to-bedside review: the role of nitric oxide in sepsis. *Expert Review of Respiratory Medicine*, *3*(5), 511–521. https://doi.org/10.1586/ers.09.39
Deboer, M. D., Scarlett, J. M., Levasseur, P. R., Grant, W. F., & Marks, D. L. (2010). Administration of IL-1β to the 4th ventricle causes anorexia that is blocked by agouti-related peptide and that coincides with activation of tyrosine-hydroxylase neurons in the nucleus of the solitary tract. *Peptides*, *30*(2), 210–218. https://doi.org/10.1016/j.peptides.2008.10.019.Administration
Dejager, L., Pinheiro, I., Dejonckheere, E., & Libert, C. (2011). Cecal ligation and puncture: The gold standard model for polymicrobial sepsis? *Trends in Microbiology*, *19*(4), 198–208. https://doi.org/10.1016/j.tim.2011.01.001
Deutschman, C., Kirsch, J., Breslow, M., Miller, C., & Traystman, R. (1990). Failure of endotoxic shock to elicit superoxide anion production in pig brain. *Circ Shock.*, *31*(2), 149–158.
Dhar, R., & Diringer, M. N. (2008). The burden of the systemic inflammatory response predicts vasospasm and outcome after subarachnoid hemorrhage. *Neurocritical Care*, *8*(3), 404–412. https://doi.org/10.1007/s12028-008-9054-2.The
Dheen, S. T., Kaur, C., & Ling, E.-A. (2007). Microglial activation and its implications in the brain diseases. *Current Medicinal Chemistry*, *14*(11), 1189–97.
Doherty, N. E., Fung, P., Lefkowitz, M., & Ellrodt, A. G. (1985). Hypothermia and Sepsis. *Ann Intern Med.*, *103*(2), 308.
Edgar, J. M., & Griffiths, I. R. (2014). White Matter Structure: A Microscopist's View. In *Diffusion MRI From Quantitative Measurement to In vivo Neuroanatomy* (Second, pp. 127–154). Heidi Johansen-Berg & Timothy E.J. Behrens.
Egyed, M., Rajnics, P., Kollar, B., Sinko, J., Zsoldos, E., & Repa, I. (2008). Severe hemolytic anemia and acute psychosis caused by Clostridium perfringens sepsis. *Medical Science Monitor : International Medical Journal of Experimental and Clinical Research*, *14*(3), CS13-6. https://doi.org/836568 [pii]
Eisen, D. P., Moore, E. M., Leder, K., Lockery, J., McBryde, E. S., McNeil, J. J., … Woods, R. L. (2017). AspiriN To Inhibit SEPSIS (ANTISEPSIS) randomised controlled trial protocol. *BMJ Open*, *7*(1), e013636. https://doi.org/10.1136/bmjopen-2016-013636
EkströmJodal, B., Häggendal, J., Larsson, L. E., & Westerlind, A. (1982). Cerebral Hemodynamics, Oxygen Uptake and Cerebral Arteriovenous Differences of

Catecholamines Following E. coli Endotoxin in Dogs. *Acta Anaesthesiologica Scandinavica*, *26*(5), 446–452. https://doi.org/10.1111/j.1399-6576.1982.tb01797.x

Eng, L. F., Yu, A. C. H., & Lee, Y. L. (1992). Astrocytic response to injury. *Progress in Brain Research*. https://doi.org/10.1016/S0079-6123(08)61764-1

Eva M. Palsson-Mcdremott, & O'neill, L. A. J. (2004). Signal transduction by the lipopolysaccharide receptor, Toll-like receptor-4 ˚. *Immunology*, *113*, 153–162. https://doi.org/10.1111/j.1365-2567.2004.01976.x

Exton, M. S. (1997). Infection-Induced Anorexia : Active Host Defence Strategy. *Appetite*, *29*, 369–383.

Fabbian, F., Pala, M., Fallica, E., Capone, J., Monetti, V. C., Fratti, D., & Fainardi, E. (2010). Posterior reversible encephalopathy syndrome in an 87-year-old woman with Escherichia coli bloodstream infection. *Clinical and Experimental Nephrology*, *14*(2), 176–179. https://doi.org/10.1007/s10157-009-0234-y

Ferguson, A. V. (2014). *Circumventricular Organs - Neurobiology of Fluid Homeostasis: Transduction and integration*.

Ferré, J., Bannier, E., & Raoult, H. (2013). Arterial spin labeling (ASL) perfusion :

Figueiredo, M. J., De Melo Soares, D., Martins, J. M., De Resende Machado, R., Sorgi, C. A., Faccioli, L. H., … Souza, G. E. P. (2012). Febrile response induced by cecal ligation and puncture (CLP) in rats: Involvement of prostaglandin E 2 and cytokines. *Medical Microbiology and Immunology*, *201*(2), 219–229. https://doi.org/10.1007/s00430-011-0225-y

Finelli, P. F., & Uphoff, D. F. (2004). Magnetic resonance imaging abnormalities with septic encephalopathy. *Journal of Neurology, Neurosurgery, and Psychiatry*, *75*(8), 1189–1191. https://doi.org/10.1136/jnnp.2003.030833

Fink, M. P. (2014). Animal models of sepsis. *Virulence*, *5*(1), 143–153.

Ghazali, R. M., & Shuaib, I. L. (2003). Comparison between 3D TOF magnetic resonance angiography and intraarterial digital subtraction angiography in imaging the circle of Willis. *Malaysian Journal of Medical Sciences*, *10*(1), 37–42.

Girard, T., Jackson, J. C., Pandharipande, P. P., Pun, B. T., Thompson, J. L., Shintani, A. K., … Ely, E. W. (2010). Delirium as a Predictor of Long-Term Cognitive Impairment in Survivors of Critical Illness. *Crit Care Med*, *38*(7), 1513–1520. https://doi.org/10.1097/CCM.0b013e3181e47be1.Delirium

Goehler, L. E., Gaykema, R. P. A., Hansen, M. K., Anderson, K., Maier, S. F., & Watkins, L. R. (2000). Vagal immune-to-brain communication: A visceral chemosensory pathway. *Autonomic Neuroscience: Basic and Clinical*, *85*(1–3), 49–59. https://doi.org/10.1016/S1566-0702(00)00219-8

Gonnert, F. A., Recknagel, P., Seidel, M., Jbeily, N., Dahlke, K., Bockmeyer, C. L., … Bauer, M. (2011). Characteristics of clinical sepsis reflected in a reliable and reproducible rodent sepsis model. *Journal of Surgical Research*, *170*(1), 123–134. https://doi.org/10.1016/j.jss.2011.05.019

Gordon, G. R. J., Choi, H. B., Ellis-Davies, G. C. R., & MacVicar, B. A. (2008). Brain metabolic state dictates the polarity of astrocyte control over the cerebrovasculature. *Nature*, *456*(7223), 745–749. https://doi.org/10.1002/ana.22528.Toll-like

Gourine, A. V, Rudolph, K., Tesfaigzi, J., & Kluger, M. J. (1998). Role of hypothalamic interleukin-1beta in fever induced by cecal ligation and puncture in rats. *The American Journal of Physiology*, *275*, R754–R761.

Grade, M., Hernandez Tamames, J. A., Pizzini, F. B., Achten, E., Golay, X., & Smits, M. (2015). A neuroradiologist's guide to arterial spin labeling MRI in clinical practice. *Neuroradiology*, *57*(12), 1181–1202. https://doi.org/10.1007/s00234-015-1571-z

Gunther, M. L., Morandi, A., Krauskopf, E., Pandharipande, P., Girard, T. D., Jackson, J. C., … Ely, E. W. (2012). Association between Brain Volumes, Delirium Duration and Cognitive Outcomes in Intensive Care Unit Survivors: A Prospective Exploratory Cohort Magnetic. *Critical Care …*, *40*(7), 2022–2032. https://doi.org/10.1097/CCM.0b013e318250acc0.The

Hahn, J., Gunter, M., Bieber, K., Lange, T., & Autenrieth, S. E. (2017). No Title. In *Sleep enhance numbers and function of monocytes and improves bacterial infection outcome in mice*.

Haj-Yasein, N. N., Vindedal, G. F., Eilert-Olsen, M., Gundersen, G. A., Skare, O., Laake, P., … Nagelhus, E. A. (2011). Glial-conditional deletion of aquaporin-4 (Aqp4) reduces blood-brain water uptake and confers barrier function on perivascular astrocyte endfeet. *Proceedings of the National Academy of Sciences*, *108*(43), 17815–17820. https://doi.org/10.1073/pnas.1110655108

Hansen, M. K., O'Connor, K. a, Goehler, L. E., Watkins, L. R., & Maier, S. F. (2001). The contribution of the vagus nerve in interleukin-1beta-induced fever is dependent on dose. *Am J Physiol Regul Integr Comp Physiol*, *280*(4), R929–R934. Retrieved from http://www.ncbi.nlm.nih.gov/pubmed/11247812

Harbi, S. A. Al, Tamim, H. M., Al-dorzi, H. M., Sadat, M., & Arabi, Y. M. (2016). Association between aspirin therapy and the outcome in critically ill patients : a nested cohort study. *BMC Pharmacology and Toxicology*, *17*(5), 1–7. https://doi.org/10.1186/s40360-016-0047-z

Harden, L. M., Kent, S., Pittman, Q. J., & Roth, J. (2015). Fever and sickness behavior : Friend or foe ? *Brain Behavior and Immunity*, *50*, 322–333. https://doi.org/10.1016/j.bbi.2015.07.012

Hariri, R., Ghajar, J., Bahramian, K., Sharif, S., & Barie, P. (1993). Alterations in intracranial pressure and cerebral blood volume in endotoxemia. *Surg Gynecol Obstet.*, *176*(2), 155–166.

Hart, B. L. (1988). Biological Basis of the Behavior of Sick Animals. *Neuroscience & Biobehavioral Reviews*, *12*, 123–137.

Hartung, M. P., Grist, T. M., & François, C. J. (2011). Magnetic resonance angiography: {Current} status and future directions. *Journal of Cardiovascular Magnetic Resonance*, *13*, 19. https://doi.org/10.1186/1532-429X-13-19

Hassani, N., Khomeini, R., & Bard, R. (1976). Principles of Computerized Axial Tomography. *Journal of the National Medical Association*, *68*(2), 110–112. https://doi.org/10.1148/119.2.336

Hawkins, B. T., & Davis, T. P. (2005). The Blood-Brain Barrier / Neurovascular Unit in Health and Disease. *Pharmacological Reviews*, *57*(2), 173–185. https://doi.org/10.1124/pr.57.2.4.173

Heye, A. K., Culling, R. D., Valdés Hernández, M. D. C., Thrippleton, M. J., & Wardlaw, J. M. (2014). Assessment of blood-brain barrier disruption using dynamic contrast-enhanced MRI. A systematic review. *NeuroImage: Clinical*, *6*, 262–274. https://doi.org/10.1016/j.nicl.2014.09.002

Hines, D. J., Hines, R. M., Mulligan, S. J., & Macvicar, B. A. (2009). Microglia processes block the spread of damage in the brain and require functional chloride channels. *Glia*, *57*(15), 1610–1618. https://doi.org/10.1002/glia.20874

Hinkelbein, J., Schroeck, H., Peterka, A., Schubert, C., Kuschinsky, W., & Kalenka, A. (2007). Local cerebral blood flow is preserved in sepsis. *Current Neurovascular Research*, *4*(1), 39–47. https://doi.org/10.2174/156720207779940671

Ho, Y., Lin, Y., Wu, C. J., Chao, Y., Chang, A. Y. W., & Chan, J. Y. H. (2015). Peripheral

inflammation increases seizure susceptibility via the induction of neuroinflammation and oxidative stress in the hippocampus. *Journal of Biomedical Science*, *22*(46), 1–14. https://doi.org/10.1186/s12929-015-0157-8

Hofer, S., Bopp, C., Hoerner, C., Plaschke, K., Faden, R. M., Martin, E., … Weigand, M. A. (2008). Injury of the Blood Brain Barrier and Up-Regulation of ICAM-1 in Polymicrobial Sepsis. *Journal of Surgical Research*, *146*(2), 276–281. https://doi.org/10.1016/j.jss.2007.07.021

Höllinger, P., Zürcher, R., Schroth, G., & Mattle, H. P. (2000). Diffusion magnetic resonance imaging findings in cerebritis and brain abscesses in a patient with septic encephalopathy. *Journal of Neurology*, *247*(3), 232–234. https://doi.org/10.1007/s004150050573

Hosokawa, K., Gaspard, N., Su, F., Oddo, M., Vincent, J.-L., & Taccone, F. S. (2014). Clinical neurophysiological assessment of sepsis-associated brain dysfunction: a systematic review. *Critical Care*, *18*(6), 674. https://doi.org/10.1186/s13054-014-0674-y

Huston, J. 3rd, & Ehman, R. L. (1993). Comparison of time-of-flight and phase-contrast MR neuroangiographic techniques. *Radiographics : A Review Publication of the Radiological Society of North America, Inc*, *13*(1), 5–19. https://doi.org/10.1148/radiographics.13.1.8426937

Ibarra-coronado, E. G., Pantaleón-martínez, A. M., Velazquéz-moctezuma, J., Prospéro-garcía, O., Méndez-díaz, M., Pérez-tapia, M., … Morales-montor, J. (2015). The Bidirectional Relationship between Sleep and Immunity against Infections. *Journal of Immunology Research*, *2015*.

Imai, Y., Ibata, I., Ito, D., Ohsawa, K., & Kohsaka, S. (1996). A novel gene iba1 in the major histocompatibility complex class III region encoding an EF hand protein expressed in a monocytic lineage. *Biochem Biophys Res Commun*, *224*(3), 855–862. Retrieved from papers://af3eb3cd-aba3-4891-9345-6bc903d7765e/Paper/p4909

Imeri, L., & Opp, M. R. (2009). How (and why) the immune system makes us sleep. *Nat Rev Neurosci.*, *10*(3), 199–210. https://doi.org/10.1038/nrn2576.How

Jackson, J., & Hopkins, R. (2009). Acute respiratory distress syndrome, sepsis, and cognitive decline: a review and case study. *Southern Medical …*, *102*(11), 1150–1157. https://doi.org/10.1097/SMJ.0b013e3181b6a592.Acute

Jakovcevic, D., & Harder, D. R. (2007). Role of Astrocytes in Matching Blood Flow to Neuronal Activity. *Current Topics in Developmental Biology*, *79*(6), 75–97. https://doi.org/10.1016/S0070-2153(06)79004-4

Ji, M.-H., Qiu, L.-L., Tang, H., Ju, L.-S., Sun, X.-R., Zhang, H., … Yang, J.-J. (2015). Sepsis-induced selective parvalbumin interneuron phenotype loss and cognitive impairments may be mediated by NADPH oxidase 2 activation in mice. *Journal of Neuroinflammation*, *12*(1), 182. https://doi.org/10.1186/s12974-015-0401-x

Jilma, B., Blann, A., Pernerstorfer, T., Stohlawetz, P., Eichler, H., Vondrovec, B., … Wagner, O. F. (1999). Regulation of Adhesion Molecules during Human Endotoxemia No Acute Effects of Aspirin. *AM J RESPIR CRIT CARE MED*, *159*, 857–863.

Jing, L., He, Q., Zhang, J. Z., & Andy Li, P. (2013). Temporal profile of astrocytes and changes of oligodendrocyte-based myelin following middle cerebral artery occlusion in diabetic and non-diabetic rats. *International Journal of Biological Sciences*, *9*(2), 190–199. https://doi.org/10.7150/ijbs.5844

Johnson, A. K., & Gross, P. M. (1993). Sensory circumventricular organs and brain homeostatic pathways. *The FASEB Journal*, *7*(8), 678–686.

Jung, J. S., Bhat, R. V, Preston, G. M., Guggino, W. B., Baraban, J. M., & Agre, P. (1994). Molecular characterization of an aquaporin cDNA from brain: candidate osmoreceptor

and regulator of water balance. *Proceedings of the National Academy of Sciences*, *91*(26), 13052–13056. https://doi.org/10.1073/pnas.91.26.13052

Kadoi, Y., & Goto, F. (2004). Selective inducible nitric oxide inhibition can restore hemodynamics, but does not improve neurological dysfunction in experimentally-induced septic shock in rats. *Anesthesia and Analgesia*, *99*(1), 212–20. https://doi.org/10.1213/01.ANE.0000118111.94913.22

Kafa, I. M., Bakirci, S., Uysal, M., & Kurt, M. A. (2010). Alterations in the brain electrical activity in a rat model of sepsis-associated encephalopathy. *Brain Research*, *1354*, 217–226. https://doi.org/10.1016/j.brainres.2010.07.049

Kang, B., Jang, D., Gu, S., Kim, Y., Lim, C., Lee, J., & Woo, E. (2009). Three-Dimensional Time-of-Flight Magnetic Resonance Angiography of Intracranial Vessels in a Canine Model of Ischemic Stroke with Permanent Occlusion of the Middle Cerebral Artery, *59*(1), 72–77.

Katz, D., Marks, M., Napel, S., Bracci, P., & Roberts, S. (1995). Circle of Willis: evaluation with spiral CT angiography, MR angiography, and conventional angiography. *Radialogy.*, *195*(2), 445–449.

Kelley, K. W., Bluthe, R.-M., Dantzer, R., Zhou, J.-H., Shen, W.-H., Johnson, R. W., & Broussard, S. R. (2003). Cytokine-induced sickness behavior. *Brain Behavior and Immunity*, *17*, 112–118. https://doi.org/10.1016/S0889-1591(02)00077-6

Kety, S. S., & Schmidt, C. F. (1948). the Nitrous Oxide Method for the Quantitative Determination of Cerebral Blood Flow in Man: Theory, Procedure and Normal Values. *The Journal of Clinical Investigation*, *27*(4), 476–483. https://doi.org/10.1172/JCI101994

Kim, S. G. (1995). Quantification of Relative Cerebral Blood-Flow Change by Flow-Sensitive Alternating Inversion-Recovery (FAIR) Technique - Application to Functional Mapping. *Magnetic Resonance in Medicine*, *34*(3), 293–301. https://doi.org/DOI 10.1002/mrm.1910340303

Klatzo, I. (1987). Pathophysiological aspects of brain edema. *Acta Neuropathol.*, *72*(3), 236–239.

Kluger, J., & Vaughn, L. K. (1978). Fever and Survival In Rabbits Infected With Pasteurella Multocida. *J. Physiol.*, *282*, 243–251.

Kluger, M., Ringler, D., & Anver, M. (1975). Fever and survival. *Science.*, *188*(4184), 166–168.

Konsman, J., Luheshi, G., Bluthé, R., & Dantzer, R. (2000). The vagus nerve mediates behavioural depression, but not fever, in response to peripheral immune signals; a functional anatomical analysis. *Eur J Neurosci.*, *12*(12), 4434–4446.

Konsman, J. P., Kelley, K., & Dantzer, R. (1999). Temporal a n d spatial relationships between lipopolysaccharide-induced expression of fos, interleukin-i[3 a n d inducible nitric oxide synthase in rat brain. *Neuroscience*, *89*(2), 535–548.

Konsman, J. P., Veeneman, J., Combe, C., Poole, S., Luheshi, G. N., Dantzer, R., & Se, V. (2008). Central nervous action of interleukin-1 mediates activation of limbic structures and behavioural depression in response to peripheral administration of bacterial lipopolysaccharide. *European Journal of Neuroscience, Vol.*, *28*, 2499–2510. https://doi.org/10.1111/j.1460-9568.2008.06549.x

Konsman, J., Vigues, S., Mackerlova, L., Bristow, A., & Blomqvist, A. (2004). Rat Brain Vascular Distribution of Immunoreactivity : Relationship to Patterns of Inducible Cyclooxygenase Expression by Peripheral Inflammatory Stimuli. *The Journal of Comparative Neurology*, *472*, 113–129. https://doi.org/10.1002/cne.20052

Krueger, J., Kubillus, S., Shoham, S., & Davenne, D. (1986). Enhancement of slow-wave

sleep by endotoxin and lipid A. *Am J Physiol.*, *251*(3 Pt 2), 591–597.
Langhans, W. (2000). Anorexia of infection_ current prospects. *Nutrition*, *16*(10), 996–1005.
Langhans, W., Savoldelli, D., & Weingarten, S. (1993). Comparison of the feeding responses to bacterial lipopolysaccharide and interleukin-1 beta. *Physiol Behav*, *53*(4), 643–649.
Lawrence, C., & Rothwell, N. (2001). Anorexic but not pyrogenic actions of interleukin-1 are modulated by central melanocortin-3/4 receptors in the rat. *J Neuroendocrinol*, *13*(6), 490–495.
Lay, A. J., Donahue, D., Tsai, M. J., & Castellino, F. J. (2007). Acute inflammation is exacerbated in mice genetically predisposed to a severe protein C deficiency. *Blood*, *109*(5), 1984–1991. https://doi.org/10.1182/blood-2006-07-037945
Lemstra, A. W., Groen in't Woud, J. C. M., Hoozemans, J. J. M., van Haastert, E. S., Rozemuller, A. J. M., Eikelenboom, P., & van Gool, W. A. (2007). Microglia activation in sepsis: a case-control study. *Journal of Neuroinflammation*, *4*(II), 4. https://doi.org/10.1186/1742-2094-4-4
Lingnau, W., McGuire, R., Dehring, D., Traber, L., Linares, H., Nelson, S., … Traber, D. (1996). Changes in regional hemodynamics after nitric oxide inhibition during ovine bacteremia. *Am J Physiol.*, *270*(1 Pt 2), R207-216.
Liu, N., Li, A.-L., Zhou, X.-P., Chen, Q., & Cao, W. (2015). P120 catenin attenuates lipopolysaccharide-induced blood-brain barrier dysfunction and inflammatory responses in human brain microvascular endothelial cells. *International Journal of Clinical and Experimental Pathology*, *8*(4), 4204–4212.
Liu, W., Wang, Z., Wang, Y., Tong, L., Li, Y., Wei, X., … Li, L. (2015). Increasing the Permeability of the Blood – brain Barrier in Three Different Models in vivo. *CNS Neuroscience & Therapeutics*, *21*, 568–574. https://doi.org/10.1111/cns.12405
Lu, Y., Yeh, W., & Ohashi, P. S. (2008). LPS / TLR4 signal transduction pathway, *42*, 145–151. https://doi.org/10.1016/j.cyto.2008.01.006
Ludwin, S. K. (1997). The pathobiology of the oligodendrocyte. *Journal of Neuropathology and Experimental Neurology*, *56*(2), 111–124.
Macdonald, M. E., & Frayne, R. (2015). Cerebrovascular MRI: A review of state-of-the-art approaches, methods and techniques. *NMR in Biomedicine*, *28*(7), 767–791. https://doi.org/10.1002/nbm.3322
Mackowiak, P. A. (1981). Direct Effects of Hyperthermia on Pathogenic Microorganisms: Teleologic Implications with Regard to Fever. *REVIEWS OF INFECTIOUS DISEASES*, *3*(3), 33–41.
Mackowiak, P., Browne, R., Southern, P. J., & Smith, J. (1980). Polymicrobial sepsis_ an analysis of 184 cases using log linear models, *280*(2), 73–80.
Maekawa, T., Fujii, Y., Sadamitsu, D., Yokota, K., Soejima, Y., Ishikawa, T., … Takeshita, H. (1991). Cerebral circulation and metabolism in patients with septic encephalopathy. *American Journal of Emergency Medicine*, *9*(2), 139–143. Retrieved from http://www.ncbi.nlm.nih.gov/pubmed/1994941
Manley, G., Fujimura, M., Ma, T., Noshita, N., Filiz, F., Bollen, A., … Verkman, A. (2000). Aquaporin-4 deletion in mice reduces brain edema after acute water intoxication and ischemic stroke. *Nat Med.*, *6*(2), 159–163.
Marik, P., & Zaloga, G. (2000). Hypothermia and cytokines in septic shock. Norasept II Study Investigators. North American study of the safety and efficacy of murine monoclonal antibody to tumor necrosis factor for the treatment of septic shock. *Intensive Care Medicine*, *26*(6), 716–721.
Marsland, A. L., Gianaros, P. J., Kuan, D. C. H., Sheu, L. K., Krajina, K., & Manuck, S. B. (2015). Brain morphology links systemic inflammation to cognitive function in midlife

adults. *Brain, Behavior, and Immunity*, *48*, 195–204. https://doi.org/10.1016/j.bbi.2015.03.015

Martinell, S., Högström, H., & Haglund, U. (1987). Cardiac output and its distribution in peritonitis - (Septic) Shock in the Rat. *Research in Experimental Medicine*, *187*(2), 87–94. https://doi.org/10.1007/BF01851970

Matsumura, K., Cao, C., Ozaki, M., Morii, H., Nakadate, K., & Watanabe, Y. (1998). Brain Endothelial Cells Express Cyclooxygenase-2 during Lipopolysaccharide-Induced Fever : Light and Electron Microscopic Immunocytochemical Studies, *18*(16), 6279–6289.

Matta, B. F., & Stow, P. J. (1996). Sepsis-induced vasoparalysis does not involve the cerebral vasculature: indirect evidence from autoregulation and carbon dioxide reactivity studies. *British Journal of Anaesthesia*, *76*(6), 790–794. https://doi.org/10.1093/bja/76.6.790

Maurer, K., & Dierks, T. (1987). Functional imaging of the brain in psychiatry - mapping of EEG and evoked potentials. *Neurosurg. Rev.*, *10*(4), 275–282.

McCarron, E. P., Williams, D. P., Antoine, D. J., Kipar, A., Lemm, J., Stehr, S., & Welters, I. D. (2015). Exploring the translational disconnect between the murine and human inflammatory response: Analysis of LPS dose???response relationship in murine versus human cell lines and implications for translation into murine models of sepsis. *Journal of Inflammation Research*, *8*, 201–209. https://doi.org/10.2147/JIR.S89097

McCarthy, D. O., Kluger, M. J., & Vander, A. J. (1986). Effect of centrally administered interleukin-1 and endotoxin on food intake of fasted rats. *Physiology and Behavior*, *36*(4), 745–749. https://doi.org/10.1016/0031-9384(86)90363-X

Mccusker, R. H., & Kelley, K. W. (2013). Immune – neural connections : how the immune system ’ s response to infectious agents influences behavior, 84–98. https://doi.org/10.1242/jeb.073411

Mesquida, J., Gruartmoner, G., & Espinal, C. (2013). Skeletal Muscle Oxygen Saturation (StO 2) Measured by Near-Infrared Spectroscopy in the Critically Ill Patients. *Biomed Research International*, *2013*, 8 pages. https://doi.org/10.1155/2013/502194

Michels, M., Danielski, L., Dal-Pizzol, F., & Petronilho, F. (2014). Neuroinflammation: Microglial Activation During Sepsis. *Current Neurovascular Research*, *11*(3), 262–270. https://doi.org/10.2174/1567202611666140520122744

Michels, M., Vieira, A. S., Vuolo, F., Zapelini, H. G., Mendonça, B., Mina, F., … Dal-Pizzol, F. (2015). The role of microglia activation in the development of sepsis-induced long-term cognitive impairment. *Brain, Behavior, and Immunity*, *43*, 54–59. https://doi.org/10.1016/j.bbi.2014.07.002

Mizuhara, Y., Choi, H., Kohigashi, M., Hata, Y., Nishizawa, S., Fujimori, A., … Fukui, K. (2011). A Case of Anorexia Nervosa Complicated by Brain Abscess due to Sepsis After Pneumonia. *Psychosomatics*, *52*(5), 478–481. https://doi.org/10.1016/j.psym.2011.01.018

Møller, K., Strauss, G. I., Qvist, J., Fonsmark, L., Knudsen, G. M., Larsen, F. S., … Pedersen, B. K. (2002). Cerebral blood flow and oxidative metabolism during human endotoxemia. *Journal of Cerebral Blood Flow and Metabolism*, *22*(10), 1262–1270. https://doi.org/10.1097/00004647-200210000-00014

Moody, D. M., Bell, M. A., & Challa, V. R. (1990). Features of the Cerebral Vascular Pattern That Predict Vulnerability to Perfusion or Oxygenation Deficiency : An Anatomic Study. *American Society of Neuroradiology*, *11*, 431–439.

Morandi, A., Gunther, M. L., Vasilevskis, E. E., Girard, T. D., Hopkins, R. O., Jackson, J. C., … Ely, E. W. (2010). Neuroimaging in delirious intensive care unit patients: a preliminary case series report. *Psychiatry (Edgmont (Pa. : Township))*, *7*(9), 28–33. Retrieved from

http://www.ncbi.nlm.nih.gov/pmc/articles/PMC2952644/%5Cnpapers2://publication/uuid/E9A0998E-684A-4A58-9D23-64610B23EB04

Morandi, A., Rogers, B. P., Gunther, M. L., Merkle, K., Pandharipande, P., Girard, T. D., … Hopkins, R. O. (2012). The Relationship between Delirium Duration, White Matter Integrity, and Cognitive Impairment in Intensive Care Unit Survivors as Determined by Diffusion Tensor Imaging. *Critical Care Medicine*, *40*(7), 2182–2189. https://doi.org/10.1097/CCM.0b013e318250acdc.

Morris, D., Chambers, H., Morris, M., & Sande, M. (1985). Hemodynamic characteristics of patients with hypothermia due to occult infection and other causes. *Ann Intern Med.*, *102*(2), 153–157.

Murray, M. J., & Murray, A. B. (1979). Anorexia of infection as a mechanism of host defense. *American Journal of Clinical Nutrition*, *32*(3), 593–596.

Naganawa, S., Norris, D. G., Zysset, S., & Mildner, T. (2002). Regional differences of fMR signal changes induced by hyperventilation: Comparison between SE-EPI and GE-EPI at 3-T. *Journal of Magnetic Resonance Imaging*, *15*(1), 23–30. https://doi.org/10.1002/jmri.10028

Nagase, T., Wada, S., Nakamura, R., Morisako, T., Kamakura, K., Kugai, N., … Nagata, N. (1995). Magnetic resonance imaging of multiple brain abscesses of the bilateral basal ganglia. *Internal Medicine (Tokyo, Japan)*, *34*(6), 554–558.

Naqvi, J., Yap, K. H., Ahmad, G., & Ghosh, J. (2013). Transcranial Doppler Ultrasound: A Review of the Physical Principles and Major Applications in Critical Care. *Int J Vasc Med*, *2013*(March), 629378. https://doi.org/10.1155/2013/629378

Nava, F., & Carta, G. (2000). Repeated lipopolysaccharide administration produces tolerance to anorexia and fever but not to inhibition of thirst in rat. *International Journal of Immunopharmacology*, *22*, 943–953.

Newell, D., & Winn, H. (1990). Transcranial Doppler in cerebral vasospasm. *Neurosurg Clin N Am.*, *1*(2), 319–328.

Nimmerjahn, A., Kirchhoff, F., & Helmchen, F. (2005). Resting microglial cells are highly dynamic surveillants of brain parenchyma in vivo. *Neuroforum*, *11*(3), 95–96. https://doi.org/10.1126/science.1110647

Nishioku, T., Dohgu, S., Takata, F., Eto, T., Ishikawa, N., Kodama, K., … Kataoka, Y. (2009). Detachment of brain pericytes from the basal lamina is involved in disruption of the blood-brain barrier caused by lipopolysaccharide-induced sepsis in mice. *Cell Mol Neurobiol.*, *29*(3), 309–316.

Norden, D. M., Trojanowski, P. J., Villanueva, E., Navarro, E., & Godbout, J. P. (2016). Sequential activation of microglia and astrocyte cytokine expression precedes increased iba-1 or GFAP immunoreactivity following systemic immune challenge. *Glia*, *64*(2), 300–316. https://doi.org/10.1002/glia.22930

Nunez, P. L. (1993). High resolution EEG : applications in medicine and cognitive science. *Spie*, *1887*, 22–39.

Ohsawa, K., Imai, Y., Sasaki, Y., & Kohsaka, S. (2004). Microglia/macrophage-specific protein Iba1 binds to fimbrin and enhances its actin-bundling activity. *Journal of Neurochemistry*, *88*(4), 844–856. https://doi.org/10.1046/j.1471-4159.2003.02213.x

Osthoff, M., Sidler, J., Lakatos, B., Frei, R., Dangel, M., Weisser, M., … Widmer, A. (2016). Low-Dose Acetylsalicylic Acid Treatment and Impact on Short-Term Mortality in Staphylococcus aureus Bloodstream Infection: A Propensity Score-Matched Cohort Study. *Crit Care Med.*, *44*(4), 773–781.

Pacheco-Lopez, G., & Bermudez-Rattoni, and F. (2011). Brain – immune interactions and the neural basis of disease-avoidant ingestive behaviour. *Phil. Trans. R. Soc.*, *366*, 3389–

3405. https://doi.org/10.1098/rstb.2011.0061
Pancoto, J. A. T., Corrêa, P. B. F., Oliveira-Pelegrin, G. R., & Rocha, M. J. A. (2008). Autonomic dysfunction in experimental sepsis induced by cecal ligation and puncture. *Autonomic Neuroscience: Basic and Clinical*, *138*(1–2), 57–63. https://doi.org/10.1016/j.autneu.2007.10.006
Panerai, R. (1998). Assessment of cerebral pressure autoregulation in humans-a review of measurement methods. *Physiol Meas.*, *19*(3), 305–338.
Papadopoulos, M. C. (2004). Aquaporin-4 facilitates reabsorption of excess fluid in vasogenic brain edema. *The FASEB Journal*, *18*, 1–18. https://doi.org/10.1096/fj.04-1723fje
Parthasarathy, S., & Tobin, M. J. (2004). Sleep in the intensive care unit. *Intensive Care Medicine*, *30*(2), 197–206.
Pereira, P. R., Pinho, J., Rodrigues, M., Rocha, J., Sousa, F., Amorim, J., … Ferreira, C. (2015). Clinical, imagiological and etiological spectrum of posterior reversible encephalopathy syndrome. *Arquivos de Neuro-Psiquiatria*, *73*(1), 36–40. https://doi.org/10.1590/0004-282X20140176
Peres Bota, D., Lopes Ferreira, F., Mélot, C., & Vincent, J. L. (2004). Body temperature alterations in the critically ill. *Intensive Care Medicine*, *30*(5), 811–816. https://doi.org/10.1007/s00134-004-2166-z
Perrella, M. A., Hsieh, C. M., Lee, W. S., Shieh, S., Tsai, J. C., Patterson, C., … Lee, M. E. (1996). Arrest of endotoxin-induced hypotension by transforming growth factor beta1. *Proc Natl Acad Sci U S A*, *93*(5), 2054–2059. https://doi.org/10.1073/pnas.93.5.2054
Pfeiffer, Warrington, & Bansal. (1993). The oligodendrocyte and its many cellular processes. *Trends in Cell Biology*, *3*(6), 191–197. https://doi.org/10.1016/0962-8924(93)90213-K
Pfister, D., Siegemund, M., Dell-Kuster, S., Smielewski, P., Rüegg, S., Strebel, S. P., … Steiner, L. A. (2008). Cerebral perfusion in sepsis-associated delirium. *Critical Care*, *12*(3), R63. https://doi.org/10.1186/cc6891
Pierrakos, C., Antoine, A., Velissaris, D., Michaux, I., Bulpa, P., Evrard, P., … Dive, A. (2013). Transcranial doppler assessment of cerebral perfusion in critically ill septic patients: a pilot study. *Annals of Intensive Care*, *3*(1), 28. https://doi.org/10.1186/2110-5820-3-28
Pierrakos, C., Attou, R., Decorte, L., Kolyviras, A., Malinverni, S., Gottignies, P., … De Bels, D. (2014). Transcranial Doppler to assess sepsis-associated encephalopathy in critically ill patients. *BMC Anesthesiology*, *14*(1), 45. https://doi.org/10.1186/1471-2253-14-45
Polito, A., Eischwald, F., Maho, A.-L. Le, Polito, A., Azabou, E., Annane, D., … Sharshar, T. (2013). Pattern of Brain Injury in the Acute Setting of Human Septic Shock. *Critical Care (London, England)*, *17*(5), R204. https://doi.org/10.1186/cc12899
Pollard, V., Prough, D., Deyo, D., Conroy, B., Uchida, T., Daye, A., … Traber, D. (1997). Cerebral blood flow during experimental endotoxemia in volunteers. *Crit Care Med.*, *25*(10), 1700–1706.
Pollmächer, T., Schreiber, W., Gudewill, S., Vedder, H., Fassbender, K., Wiedemann, K., … Holsboer, F. (1993). Influence of endotoxin on nocturnal sleep in humans. *Am J Physiol.*, *264*(6 Pt 2), 1077–1083.
Posse, S., Olthoff, U., Weckesser, M., Jäncke, L., Müller-Gärtner, H. W., & Dager, S. R. (1997). Regional dynamic signal changes during controlled hyperventilation assessed with blood oxygen level-dependent functional MR imaging. *American Journal of Neuroradiology*, *18*(9), 1763–1770.
Prendergast, B. J. (2008). Behavioral Tolerance to Endotoxin is Enhanced by Adaptation to Winter Photoperiods. *Psychoneuroendocrinology*, *33*(4), 540–545. https://doi.org/10.1016/j.psyneuen.2007.12.008.Behavioral

Purkayastha, S., & Sorond, F. (2012). Transcranial Doppler Ultrasound: Technique and Application. *Semin Neurol*, *32*(4), 411–420. https://doi.org/10.1055/s-0032-1331812.Transcranial

Reichenberg, A., Kraus, T., Haack, M., Schuld, A., Pollmacher, T., & Yirmiya, R. (2002). Endotoxin-induced changes in food consumption in healthy volunteers are associated with TNF-?? and IL-6 ... *Psychoneuroendocrinology*, *27*, 945–956. https://doi.org/10.1016/S0306-4530(01)00101-9

Remick, D., Newcomb, D., Bolgos, G., & Call, D. (2000). Comparison of the mortality and inflammatory response of two models of sepsis: lipopolysaccharide vs. cecal ligation and puncture. *Shock.*, *13*(2), 110–116.

Ribeiro, D. E., Maiolini, V. M., Soncini, R., Antunes-rodrigues, J., Elias, L. L. K., Vilela, F. C., & Giusti-paiva, A. (2013). Pharmacology , Biochemistry and Behavior Inhibition of nitric oxide synthase accentuates endotoxin-induced sickness behavior in mice. *Pharmacology, Biochemistry and Behavior*, *103*, 535–540. https://doi.org/10.1016/j.pbb.2012.09.022

Rittirsch, D., Hoesel, L. M., & Ward, P. A. (2007). The disconnect between animal models of sepsis and human sepsis Abstract : Frequently used experimental models of sepsis include cecal ligation and puncture , as-. *Journal of Leukocyte Biology*, *81*(1), 137–143. https://doi.org/10.1189/jlb.0806542

Roger, F. B. (1999). Metabolic Encephalopathies. In *Basic Neurochemistry: Molecular, Cellular and Medical Aspects. 6th edition.* (p. Chapter 38).

Romanovsky, A. A., Kulchitsky, A., Simons, T., Szekely, M., & Vladimir, A. K. (1997). The vagus nerve in the thermoregulatory response to systemic inflammation The vagus nerve in the thermoregulatory to systemic inflammation. *The American Physiological Society*, *1*(August 1997), R407-413. Retrieved from https://www.researchgate.net/profile/Vladimir_Kulchitsky/publication/13969702_The_vagus_nerve_in_the_thermoregulatory_response_to_systemic_inflammation/links/53eb6d190cf23b8116a9bf2f.pdf

Romanovsky, A. A., Shido, O., Sakurada, S., Sugimoto, N., & Nagasaka, T. (1996). Endotoxin shock: thermoregulatory mechanisms. *The American Journal of Physiology*. Retrieved from http://www.ncbi.nlm.nih.gov/pubmed/8967396

Romanovsky, A. A., Simons, C. T., & Kulchitsky, V. A. (1998). "Biphasic" fevers often consist of more than two phases. *The American Journal of Physiology*, *275*(1 Pt 2), R323-31. Retrieved from http://www.ncbi.nlm.nih.gov/pubmed/9688995

Romanovsky, A., Kulchitsky, V., Simons, C., & Sugimoto, N. (1998). Methodology of fever research: why are polyphasic fevers often thought to be biphasic? *Am J Physiol.*, *275*(1 Pt 2), R332-338.

Rosengarten, B., Hecht, M., Auch, D., Ghofrani, H. A., Schermuly, R. T., Grimminger, F., & Kaps, M. (2007). Microcirculatory dysfunction in the brain precedes changes in evoked potentials in endotoxin-induced sepsis syndrome in rats. *Cerebrovascular Diseases*, *23*(2–3), 140–147. https://doi.org/10.1159/000097051

Rosengarten, B., Walberer, M., Allendoerfer, J., Mueller, C., Schwarz, N., Bachmann, G., & Gerriets, T. (2008). LPS-induced endotoxic shock does not cause early brain edema formation - An MRI study in rats. *Inflammation Research*, *57*(10), 479–483. https://doi.org/10.1007/s00011-008-8042-5

Rothwell, N. J., & Hopkins, S. J. (1995). Cytokines and the nervous system II: actions and mechanisms of action. *Trends Neurosci.*, *18*, 130–136.

Ruiz, S., Vardon-Bounes, F., Merlet-Dupuy, V., Conil, J.-M., Buléon, M., Fourcade, O., … Minville, V. (2016). Sepsis modeling in mice: ligation length is a major severity factor in

cecal ligation and puncture. *Intensive Care Medicine Experimental*, *4*(1), 22. https://doi.org/10.1186/s40635-016-0096-z

Sarkar, S., Ghosh, S., Ghosh, S. K., & Collier, A. (2007). Role of transcranial Doppler ultrasonography in stroke. *Postgraduate Medical Journal*, *83*(985), 683–689. https://doi.org/10.1136/pgmj.2007.058602

Savchenko, V. L., Nikonenko, I. R., Skibo, G. G., & McKanna, J. A. (1997). Distribution of microglia and astrocytes in different regions of the normal adult rat brain. *Neurophysiology*, *29*(6), 343–351. https://doi.org/10.1007/BF02463354

Schabbauer, G. (2012). Polymicrobial sepsis models: CLP versus CASP. *Drug Discovery Today: Disease Models*, *9*(1), e17–e21. https://doi.org/10.1016/j.ddmod.2011.10.002

Semmler, A., Okulla, T., Sastre, M., Dumitrescu-Ozimek, L., & Heneka, M. T. (2005). Systemic inflammation induces apoptosis with variable vulnerability of different brain regions. *Journal of Chemical Neuroanatomy*, *30*(2–3), 144–157. https://doi.org/10.1016/j.jchemneu.2005.07.003

Seok, S., Kim, J., Park, T., Baik, E., & Lee, S. (2013). Fructose-1,6-bisphosphate ameliorates lipopolysaccharide-induced dysfunction of blood-brain barrier. *Arch Pharm Res.*, *36*(9), 1149–1159.

Sharshar, T., Annane, D., de la Grandmaison, G., Brouland, J., Hopkinson, N., & Françoise, G. (2004). The neuropathology of septic shock. *Brain Pathol.*, *14*(1), 21–33.

Sharshar, T., Carlier, R., Bernard, F., Guidoux, C., Brouland, J. P., Nardi, O., … Annane, D. (2007). Brain lesions in septic shock: A magnetic resonance imaging study. *Intensive Care Medicine*, *33*(5), 798–806. https://doi.org/10.1007/s00134-007-0598-y

Sharshar, T., Polito, A., Checinski, A., & Stevens, R. D. (2010). Septic-associated encephalopathy--everything starts at a microlevel. *Critical Care (London, England)*, *14*(5), 199. https://doi.org/10.1186/cc9254

Singer, B. H., Newstead, M. W., Zeng, X., Cooke, C. L., Thompson, R. C., Singer, K., … Parent, J. M. (2016). Cecal Ligation and Puncture Results in Long- Term Central Nervous System Myeloid Inflammation, 1–22. https://doi.org/10.1371/journal.pone.0149136

Smith, S. M., Padayachee, S., Modaresi, K. B., Smithies, M. N., & Bihari, D. J. (1998). Cerebral blood flow is proportional to cardiac index in patients with septic shock. *Journal of Critical Care*, *13*(3), 104–9. https://doi.org/http://dx.doi.org/10.1016/S0883-9441%2898%2990013-2

Socher, S. H., Friedman, A., & Martinez, D. (1988). RECOMBINANT HUMAN TUMOR NECROSIS FACTOR INDUCES ACUTE REDUCTIONS IN FOOD INTAKE AND BODY WEIGHT IN MICE. *J. Exp. MED*, *167*(June), 1957–1962.

Sofroniew, M. V., & Vinters, H. V. (2010). Astrocytes: Biology and pathology. *Acta Neuropathologica*, *119*(1), 7–35. https://doi.org/10.1007/s00401-009-0619-8

Steiner, L. A., Pfister, D., Strebel, S. P., Radolovich, D., Smielewski, P., & Czosnyka, M. (2009). Near-infrared spectroscopy can monitor dynamic cerebral autoregulation in adults. *Neurocritical Care*, *10*(1), 122–128. https://doi.org/10.1007/s12028-008-9140-5

Stevens, R. D., & Nyquist, P. A. (2007). Coma, Delirium, and Cognitive Dysfunction in Critical Illness. *Critical Care Clinics*, *22*(4), 787–804. https://doi.org/10.1016/j.ccc.2006.11.006

Stitt, J. T. (1990). Passage of immunomodulators across the blood-brain barrier. *Yale Journal of Biology and Medicine*, *63*(2), 121–131.

Straver, J., Keunen, R., Stam, C., Tavy, D., De Ruiter, G., Smith, S., & Thijs, L. (1996). Transcranial Doppler and systemic hemodynamic studies in septic shock. *Neurol Res.*, *18*(4), 313–318.

Streit, W. J., Mrak, R. E., & Griffin, W. S. T. (2004). Microglia and neuroinflammation: a pathological perspective. *Journal of Neuroinflammation*, *1*(doi:10.1186/1742-2094-1-14), 4 pages. https://doi.org/10.1186/1742-2094-1-14

Streit, W. J., Walter, S. A., & Pennell, N. A. (1999). Reactive microgliosis. *Progress in Neurobiology*, *57*(6), 563–581. https://doi.org/10.1016/S0301-0082(98)00069-0

Su, Y., Qu, Y., Zhao, F., Li, H., Mu, D., & Li, X. (2015). Regulation of autophagy by the nuclear factor κB signaling pathway in the hippocampus of rats with sepsis. *Journal of Neuroinflammation*, *12*(1), 116. https://doi.org/10.1186/s12974-015-0336-2

Sun, D., & Jakobs, T. C. (2012). Structural Remodeling of Astrocytes in the Injured CNS. *Neuroscientist.*, *18*(6), 567–588. https://doi.org/10.1086/498510.Parasitic

Szatmári, S., Végh, T., Csomós, A., Hallay, J., Takács, I., Molnár, C., & Fülesdi, B. (2010). Impaired cerebrovascular reactivity in sepsis-associated encephalopathy studied by acetazolamide test. *Critical Care (London, England)*, *14*(2), R50. https://doi.org/10.1186/cc8939

Taccone, F. S., Castanares-Zapatero, D., Peres-Bota, D., Vincent, J.-L., Berre', J., & Melot, C. (2010). Cerebral autoregulation is influenced by carbon dioxide levels in patients with septic shock. *Neurocritical Care*, *12*(1), 35–42. https://doi.org/10.1007/s12028-009-9289-6

Taccone, F. S., Scolletta, S., Franchi, F., Donadello, K., & Oddo, M. (2012). Brain perfusion in sepsis. *Current Vascular Pharmacology*, *11*(2), 170–86. https://doi.org/10.2174/157016111311020007

Taccone, F. S., Su, F., Pierrakos, C., He, X., James, S., Dewitte, O., … De Backer, D. (2010). Cerebral microcirculation is impaired during sepsis: an experimental study. *Critical Care (London, England)*, *14*(4), R140. https://doi.org/10.1186/cc9205

Takahashi, Y., Smith, P., Ferguson, A., & Pittman, Q. J. (1997). Circumventricular organs and fever. *Am J Physiol Regul Integr Comp Physiol*, *273*(6), 1690–1695. Retrieved from http://ajpregu.physiology.org/content/273/5/R1690.full#ref-list-1%5Cn

Takanashi, J. ichi, Hirasawa, K. ichi, & Tada, H. (2006). Reversible restricted diffusion of entire corpus callosum. *Journal of the Neurological Sciences*, *247*(1), 101–104. https://doi.org/10.1016/j.jns.2006.03.015

Talagala, S. L., Jungreis, C. A., Kanal, E., Meyers, S. P., Foo, T. K. F., Rubin, R. A., & Applegate, G. R. (1995). Fast three-dimensional time-of-flight MR angiography of the intracranial vasculature. *Journal of Magnetic Resonance Imaging*, *5*(3), 317–323. https://doi.org/10.1002/jmri.1880050316

Taudorf, S., Berg, R. M. G., Bailey, D. M., & Møller, K. (2009). Cerebral blood flow and oxygen metabolism measured with the Kety-Schmidt method using nitrous oxide. *Acta Anaesthesiologica Scandinavica*, *53*(2), 159–167. https://doi.org/10.1111/j.1399-6576.2008.01788.x

Tempel, G., Cook, J., Wise, W., Halushka, P., & Corral, D. (1986). Improvement in organ blood flow by inhibition of thromboxane synthetase during experimental endotoxic shock in the rat. *J Cardiovasc Pharmacol.*, *8*(3), 514–519.

Terborg, C., Schummer, W., Albrecht, M., Reinhart, K., Weiller, C., & Röther, J. (2001). Dysfunction of vasomotor reactivity in severe sepsis and septic shock. *Intensive Care Medicine, Supplement*, *27*(1), 1231–1234. https://doi.org/10.1007/s001340101005

Terrando, N., Rei Fidalgo, A., Vizcaychipi, M., Cibelli, M., Ma, D., Monaco, C., … Maze, M. (2010). The impact of IL-1 modulation on the development of lipopolysaccharide-induced cognitive dysfunction. *Critical Care*, *14*(3), R88. https://doi.org/10.1186/cc9019

Thees, C., Kaiser, M., Scholz, M., Semmler, A., Heneka, M. T., Baumgarten, G., … Putensen, C. (2007). Cerebral haemodynamics and carbon dioxide reactivity during sepsis

syndrome. *Critical Care (London, England)*, *11*(6), R123. https://doi.org/10.1186/cc6185

Tkacs, N. C., & Li, J. (1999). Immune stimulation induces Fos expression in brainstem amygdala afferents. *Brain Research Bulletin*, *48*(2), 223–231. https://doi.org/10.1016/S0361-9230(98)00167-1

Tkacs, N. C., Li, J., & Strack, A. M. (1997). Central amygdala Fos expression during hypotensive or febrile, nonhypotensive endotoxemia in conscious rats. *Journal of Comparative Neurology*, *379*(4), 592–602. https://doi.org/10.1002/(SICI)1096-9861(19970324)379:4<592::AID-CNE9>3.0.CO;2-Y

Toksvang, L. N., Plovsing, R. R., Petersen, M. W., Møller, K., & Berg, R. M. G. (2014). Poor agreement between transcranial Doppler and near-infrared spectroscopy-based estimates of cerebral blood flow changes in sepsis. *Clinical Physiology and Functional Imaging*, *34*(5), 405–409. https://doi.org/10.1111/cpf.12120

Toner, P., Mcauley, D. F., & Shyamsundar, M. (2015). Aspirin as a potential treatment in sepsis or acute respiratory distress syndrome. *Critical Care*, *19*(374), 1–9. https://doi.org/10.1186/s13054-015-1091-6

Toth, L. A., & Krueger, J. M. (1988). Alteration of Sleep in Rabbits by Staphylococcus aureus Infection. *Infection and Immunity*, *56*(7), 1785–1791.

Toth, L., & Krueger, J. (1989). Effects of microbial challenge on sleep in rabbits. *FASEB J.*, *3*(9), 2062–2066.

Toth, L., Tolley, E., & Krueger, J. (1993). Sleep as a prognostic indicator during infectious disease in rabbits. *Proc Soc Exp Biol Med.*, *203*(2), 179–92.

Tourdias, T., Mori, N., Dragonu, I., Cassagno, N., Boiziau, C., Aussudre, J., … Dousset, V. (2011). Differential aquaporin 4 expression during edema build-up and resolution phases of brain inflammation. *Journal of Neuroinflammation*, *8*(1), 143. https://doi.org/10.1186/1742-2094-8-143

Trachsel, L., Schreiber, W., Holsboer, F., & Pollmächer, T. (1994). Endotoxin enhances EEG alpha and beta power in human sleep. *Sleep*, *17*(2), 132–139.

Trapp, B., Bernier, L., Andrews, S., & Colman, D. (1988). Cellular and subcellular distribution of 2',3'-cyclic nucleotide 3'-phosphodiesterase and its mRNA in the rat central nervous system. *J Neurochem*, *51*(3), 859–868.

Tsai, T., Lou, S., Wong, K., Wang, M., Su, T., Liu, Z., … Leung, Y. (2015). Suppression of Ca 2+ influx in endotoxin-treated mouse cerebral cortex endothelial bEND . 3 cells. *European Journal of Pharmacology*, *755*, 80–87. https://doi.org/10.1016/j.ejphar.2015.03.001

Tsao, N., Hsu, H. P., Wu, C. M. Ã., Liu, C. C., & Lei, H. Y. (2001). Tumour necrosis factor-á causes an increase in blood-brain barrier permeability during sepsis. *J. Med. Microbiol*, *50*, 812–821.

Tsivgoulis, G., Sharma, V. K., Lao, A. Y., Malkoff, M. D., & Alexandrov, A. V. (2007). Validation of transcranial Doppler with computed tomography angiography in acute cerebral ischemia. *Stroke*, *38*(4), 1245–1249. https://doi.org/10.1161/01.STR.0000259712.64772.85

Turek, J., Templeton, C., Bottoms, G., & JF., F. (1985). Flunixin meglumine attenuation of endotoxin-induced damage to the cardiopulmonary vascular endothelium of the pony. *Am J Vet Res.*, *46*(3), 591–596.

Turner, M. M., & Berry, L. J. (1963). Inhibition of gastric emptying in mice by bacterial endotoxins. *AJP Legacy*, *205*, 1113–1116.

Ulu, N., Iskit, A., Sökmensüer, C., & Güç, M. (2015). The effects of aspirin, flurbiprofen, and NO-donating acetylsalicylic acid (NCX 4016) on mice models of endotoxic and septic

shock. *Turk J Med Sci.*, *45*(4), 812–819.
Urban, A., Mace, E., Brunner, C., Heidmann, M., Rossier, J., & Montaldo, G. (2014). Chronic assessment of cerebral hemodynamics during rat forepaw electrical stimulation using functional ultrasound imaging. *NeuroImage*, *101*, 138–149. https://doi.org/10.1016/j.neuroimage.2014.06.063
Vallery-Radot, R. (1923). *The life of pasteur*.
Van Miert, A., & Van Duin, C. (1977). The antipyretic effect of flurbiprofen. *Eur J Pharmacol.*, *44*(3), 197–204.
Van Niekerk, G., Isaacs, A. W., Nell, T., & Engelbrecht, A. (2016). Sickness-Associated Anorexia : Mother Nature ' s Idea of Immunonutrition ? *Mediators of Inflammation*, *2016*. https://doi.org/10.1155/2016/8071539
Varatharaj, A., & Galea, I. (2017). Brain , Behavior , and Immunity The blood-brain barrier in systemic inflammation. *Brain Behavior and Immunity*, *60*, 1–12. https://doi.org/10.1016/j.bbi.2016.03.010
Verkman, A. S. (2005). More than just water channels: unexpected cellular roles of aquaporins. *Journal of Cell Science*, *118*(15), 3225–3232. https://doi.org/10.1242/jcs.02519
Verkman, A. S., Binder, D. K., Bloch, O., Auguste, K., & Papadopoulos, M. C. (2006). Three distinct roles of aquaporin-4 in brain function revealed by knockout mice. *Biochemical et Biophysical Acta.-Biomembranes*, *1758*(8), 1085–1093.
Viallon, M., Cuvinciuc, V., Delattre, B., Merlini, L., Barnaure-Nachbar, I., Toso-Patel, S., … Haller, S. (2015). State-of-the-art MRI techniques in neuroradiology: principles, pitfalls, and clinical applications. *Neuroradiology*, *57*(5), 441–467. https://doi.org/10.1007/s00234-015-1500-1
Wagner-Jauregg, J. (1965). The Treatment of Dementia Paralytica by Malaria Inoculation. *Nobel Lecture*.
Wang, A., Huen, S., Luan, H., Yu, S., Zhang, C., Gallezot, J., … Medzhitov, R. (2016). Opposing Effects of Fasting Metabolism on Tissue Tolerance in Bacterial and Viral Inflammation. *Cell*, *166*(6), 1512–1525.
Wei, P., Liu, Q., Li, D., Zheng, Q., Zhou, J., & Li, J. (2015). Acute nicotine treatment attenuates lipopolysaccharide-induced cognitive dysfunction by increasing BDNF expression and inhibiting neuroinflammation in the rat hippocampus. *Neuroscience Letters*, *604*, 161–166. https://doi.org/10.1016/j.neulet.2015.08.008
Weinstein, M., Iannini, P., Stratton, C., & Eickhoff, T. (1978). Spontaneous bacterial peritonitis. A review of 28 cases with emphasis on improved survival and factors influencing prognosis. *Am J Med.*, *64*(4), 592–598.
Weon, Y. C., Marsot-Dupuch, K., Ducreux, D., & Lasjaunias, P. (2005). Septic thrombosis of the transverse and sigmoid sinuses: Imaging findings. *Neuroradiology*, *47*(3), 197–203. https://doi.org/10.1007/s00234-004-1313-0
Wichterman, K., Baue, A. E., & Chaudry, I. H. (1980). Sepsis and Septic Shock -A Review of Laboratory and a Proposal Models. *Journal of Surgical Research*, *29*, 189–201.
Wijdicks, E. F. M., & Stevens, M. (1992). The Role of Hypotension in Septic Encephalopathy Following Surgical Procedures. *Archives of Neurology*, *49*(6), 653–656. https://doi.org/10.1001/archneur.1992.00530300093015
Wyler, F., Forsyth, R. P., Nies, a S., Neutze, J. M., & Melmon, K. L. (1969). Endotoxin-induced regional circulatory changes in the unanesthetized monkey. *Circulation Research*, *24*(6), 777–786. Retrieved from http://www.ncbi.nlm.nih.gov/pubmed/1557064
Wyler, F., Rutishauser, M., & Weisser, K. (1972). Endotoxin induced regional circulatory

reactions in the rabbit with and without halothane anesthesia. *Journal of Surgical Research*, *13*, 13–19.

Xie, D., Shen, F., He, S., Chen, M., Han, Q., Fang, M., … Deng, Y. (2015). IL-1β induces hypomyelination in the periventricular white matter through inhibition of oligodendrocyte progenitor cell maturation via FYN/MEK/ERK signaling pathway in septic neonatal rats. *Glia*. https://doi.org/10.1002/glia.22950

Yokoo, H., Chiba, S., Tomita, K., Takashina, M., Sagara, H., Yagisita, S., … Hattori, Y. (2012). Neurodegenerative Evidence in Mice Brains with Cecal Ligation and Puncture-Induced Sepsis: Preventive Effect of the Free Radical Scavenger Edaravone. *PLoS ONE*, *7*(12), 1–11. https://doi.org/10.1371/journal.pone.0051539

Yokota, H., Ogawa, S., Kurokawa, A., & Yamamoto, Y. (2003). Regional cerebral blood flow in delirium patients. *Psychiatry and Clinical Neurosciences*, *57*(3), 337–339. https://doi.org/10.1046/j.1440-1819.2003.01126.x

Yoshimoto, Y., Tanaka, Y., & Hoya, K. (2001). Acute Systemic Inflammatory Response Syndrome in Subarachnoid Hemorrhage. *Stroke*, *32*(9), 1989–1993. https://doi.org/10.1161/hs0901.095646

Young, G., Bolton, C., Austin, T., Archibald, Y., Gonder, J., & Wells, G. (1990). The encephalopathy associated with septic illness. *Clin Invest Med.*, *13*(6), 297–304.

Zauner, C., Gendo, A., Kramer, L., Funk, G., Bauer, E., Schenk, P., … Madl, C. (2002). Impaired subcortical and cortical sensory evoked potential pathways in septic patients. *Crit Care Med.*, *30*(5), 1136–1139.

Zauner, C., Gendo, A., Kramer, L., Kranz, A., Grimm, G., & Madl, C. (2000). Metabolic encephalopathy in critically ill patients suffering from septic or nonseptic multiple organ failure. *Crit Care Med.*, *28*(5), 1310–1315.

Zhang, Y.-H., Lu, J., Elmquist, J. K., & Saper, C. B. (2003). Specific Roles of Cyclooxygenase-1 and Cyclooxygenase-2 in Lipopolysaccharide- Induced Fever and Fos Expression in Rat Brain. *The Journal of Comparative Neurology*, *12*(April), 3–12. https://doi.org/10.1002/cne.10743

Zhao, Z., Hu, J., Gao, X., Liang, H., & Liu, Z. (2014). Activation of AMPK attenuates lipopolysaccharide-impaired integrity and function of blood-brain barrier in human brain microvascular endothelial cells. *Experimental and Molecular Pathology*, *97*(3), 386–392. https://doi.org/10.1016/j.yexmp.2014.09.006

Zhen, Y. (1987). Regional Changes in Cerebral Blood Flow during Acute Endotoxemia. *Journal of Tongji Medical University*, *7*(3), 131–135.

Chapter 2

Bacterial lipopolysaccharide-induced systemic inflammation alters perfusion of white matter-rich regions without altering flow in brain-irrigating arteries: relationship to blood-brain barrier breakdown?

Ibtihel Dhaya[a,b,c], Marion Griton[a,b,d], Gérard Raffard[a,b], Mohamed Amri[c], Bassem Hiba[a,b#] and Jan Pieter Konsman[a,b#*]

[a] CNRS, Résonance Magnétique des Systèmes Biologiques, UMR 5536, Bordeaux, France

[b] Univ. Bordeaux, RMSB, UMR 5536, Bordeaux, France

[c] Laboratoire de Neurophysiologie Fonctionnelle et Pathologies, UR/11ES09, Faculté des Sciences Mathématiques, Physiques et Naturelles, Université de Tunis El Manar, Tunis, Tunisie

[d] Service de Réanimation Anesthésie Neurochirurgicale, Centre Hospitalier Universitaire (CHU) de Bordeaux, Bordeaux, France

Running title: LPS increases brain white matter perfusion

co-senior authors

Abbreviations used:

ACA: anterior cerebral artery;
ADC : apparent diffusion coefficient;
ASL: aterial spin labeling;
Az: pericallosal azygos artery;
BBB: blood-brain barrier;
cc: corpus callosum;
COX-2: cyclooxygenase-2;
CP: caudate putamen;
dMCA: dorsal branch of middle cerebral artery;
dMRI: diffusion-weighted magnetic resonance imaging;
ec: external capsule;
FA: fractional anisotropy;
fi: fimbria;
GFAP: glial fibrillary acidic protein;
IgG: immunoglobulin G;
Iba-1: ionized calcium-binding adaptor molecule;
IL-1beta: interleukin-1β;
LPS: lipopolysaccharides;
MCA: middle cerebral artery;
MO: motor cortex;
MRA: magnetic resonance angiography;
MRI : magnetic resonance imaging;
NS: non-significant;
PhC: Phase contrast;
ROI: Regions Of Interest;
Sal: saline;
SS: somatosensory cortex;
st: stria terminalis;
T1: T1-weighted imaging;
TOF: time-of-flight;
vhc: ventral hippocampal commissure.

Abstract

To better understand brain dysfunction during sepsis, cerebral arterial blood flow was assessed with Phase Contrast Magnetic Resonance Imaging, perfusion with Arterial Spin Labeling and structure with diffusion-weighted Magnetic Resonance Imaging in rats after intraperitoneal administration of bacterial lipopolysaccharides. Although cerebral arterial flow was not altered, perfusion of the corpus callosum region and diffusion parallel to its fibers were higher after lipopolysaccharide administration as compared to saline injection. In parallel, lipopolysaccharide induced perivascular immunoglobulin-immunoreactivity in white matter. These findings indicate that systemic inflammation can result in increased perfusion, blood-brain barrier breakdown and altered water diffusion in white matter.

Keywords

Arterial spin labeling, blood-brain barrier, cerebral artery, cerebral blood flow, diffusion magnetic resonance imaging, lipopolysaccharide, sepsis

Introduction

Nervous system dysfunction often occurs during sepsis or sepsis-associated encephalopathy (Baron et al., 2006; Levy et al., 2003) with altered mental status, ranging from lethargy to coma, being observed in 25-70% of patients (Ebersoldt et al., 2007; Sprung et al., 1990; Wilson and Young, 2003). Septic patients with encephalopathy display reduced global cerebral blood flow compared to healthy controls (Bowton et al., 1989; Maekawa et al., 1991). Moreover, clinical studies using time-of-flight (TOF) Magnetic Resonance Angiography (MRA) have provided evidence of vasospasms in branches of the anterior and middle cerebral arteries (ACA and MCA) during sepsis-associated encephalopathy (Bartynski et al., 2006; Polito et al., 2013). Furthermore, white matter perivascular hyperintensities on FLuid-Attenuated Inversion Recovery (FLAIR) magnetic resonance (MR) images and altered water diffusion in diffusion-Magnetic Resonance Imaging (dMRI) occur during sepsis-associated encephalopathy indicating edema due to blood-brain barrier (BBB) breakdown (Bartynski et al., 2006; Sharshar et al., 2007). Indeed, autopsies of fatal cases of encephalopathy associated with sepsis have shown white matter perivascular edema and hemorrhages (Jackson et al., 1985; Sharshar et al., 2007).

Reduced global cerebral blood flow and lower flow speed in the territory of the MCA are also observed after intravenous (iv) administration of bacterial lipopolysaccharides (LPS) in human volunteers (Brassard et al., 2012; Moller et al., 2002). Time-resolved 3D TOF MRA allowed us to expand some of these clinical observations in rodents and show that blood flow in the first segments of the mouse ACA and MCA is lower after iv LPS injection as compared to administration of its vehicle (Villega et al., 2017). However, it is unknown how these changes relate to vasodilation of downstream subpial arterioles and venules observed with intravital microscopy and increased resting blood flow in the sensory cortex found with laser Doppler after iv LPS administration in rodents (Rosengarten et al., 2007; Rosengarten et al., 2008a; Ruiz-Valdepenas et al., 2011). Interestingly, in other neuropathologies involving inflammation increased perfusion has been to be closely associated with breakdown of the BBB in subcortical white matter (Ge et al., 2005; Ingrisch et al., 2012). Although changes of CBF and BBB-breakdown have both been shown to occur in clinical sepsis and after systemic LPS administration, their spatial and temporal relationships remain to be determined.

In the present work, we therefore set out to study blood flow in the dorsal branches of the ACA and MCA with Phase Contrast MRI (PhC-MRI) and perfusion of white and grey matter

brain structures with Arterial Spin Labeling (ASL) over time after intraperitoneal (ip) LPS administration. In addition, we analyzed white matter microstructure with dMRI. Then, we performed histological stains on the brains of the same animals to detect the vasoactive prostaglandin-synthesizing enzyme cyclooxygenase-2 (COX-2), the expression of which can be upregulated in response to LPS (Konsman et al., 2004), to assess the presence of perivascular immunoglobulins (Ig) indicating BBB leakage and to study glia cell morphology.

Experimental procedures

Animals

Experiments were conducted according to European recommendations (European Council Directive of 24 November 1986 (86/609/EEC) and European Parliament and Council Directive of 22 September 2010 (2010/63/UE)). Eighteen male Wistar rats (Charles Rivers, L'arbresle, France), weighing a mean 310 g, were housed two per cage in a temperature-controlled room (22°± 1 °C; humidity 55-60 %) on a 12 h dark-light cycle with free access to water and food during one week before the start of experiments. During this acclimation period, animals were manipulated daily and only by persons who took part in the experiment.

Anesthesia and animal preparation

Rats were anesthetized with isoflurane (induction 3-5%; maintenance 1.5% in air) and equipped with an intraperitoneal catheter that contained either *E. Coli.* LPS or its saline vehicle. Animals were next gently positioned in a body restrainer with a tooth-bar and ear-bar-equipped head holder and provided with ECG electrodes and an anal temperature probe while being positioned on a pressure-sensitive pad. Heart and respiration rate as well as colonic temperature were monitored continuously throughout the experiment with thoracic electrodes and an anally-inserted thermocouple, respectively. A thermostatically regulated water flow system maintained colonic temperature between 35.5 and 39 °C thus allowing for some potential fever and hypothermic responses to occur after LPS administration.

Magnetic Resonance Imaging

MRI experiments were performed on a 7T horizontal-bore scanner (Advance III console, Bruker, Ettlingen, Germany) equipped with a magnetic field gradient system providing a maximum gradient strength of 650 mT/m), a quadrature coil for radio-frequency emission and a 4-element phased-array surface coil for MR signal reception. Intracolonic temperature was

constantly monitored and the animal was heated when colonic temperature dropped below 35.5°C by warm water circulating in the bed used to position the rat inside MRI scanner. Respiration was assessed with a ventral pressure sensor and heart rate recorded using an MRI compatible electrode. After careful second-order shimming, the following images were acquired.

Anatomical T1-weighted MRI

T1-weighted images were obtained through a FLASH (Fast Low Angle Shot) pulse sequence with the following parameters: Repetition Time [TR]/Echo Time [TE]: 15/2.68 ms; flip angle: 30°; voxel size: 117×117×234 μm^3; Field Of View (FOV): 30×30×30 mm^3; acquisition time: 8 min 12 sec.

Flow velocity mapping with Phase Contrast magnetic resonance imaging

A blood velocity map of a three consecutive 0.5 mm thick axial virtual slices of the rat forebrain centered at the level of the anterior commissure were obtained using PhC-MRI (Dumoulin, 1995; Dumoulin et al., 1991; Underwood et al., 1987). The axial level was chosen because flow in the arteries of interest (ventral anterior and middle cerebral arteries, dorsal branches of the latter and pericallosal artery) was perpendicular to the imaging slice. Mean diastolic velocity map was acquired with ECG triggering and the velocity range (velocity encoding) parameter set to 10 cm/sec based on previous studies using Doppler ultrasonography (Kreis et al., 2011). The following acquisition parameters were used for velocity maps: TR/TE: 15/5.5 ms; flip angle: 30°; voxel size: 130×154 μm^2; FOV: 30×25 mm^2; number of averages: 8; mean acquisition duration: around 1 min.

Cerebral perfusion mapping with Arterial Spin Labeling

ASL data were acquired from a single 1.5 mm-thick axial slice, with a FOV of 3.5×3.5 cm^2 centered on phase contrast imaging slices, using a Flow-sensitive Alternating Inversion Recovery – Echo Planar Imaging (FAIR-EPI) pulse sequence (Kim and Tsekos, 1997). This placement allowed for measurement of blood perfusion of those areas that were supplied through smaller arteries and arterioles with the flow measured by phase contrast in the dorsal branches of the MCAs and the pericallosal artery and contained important regions of both white (corpus callosum, external capsule) and grey (cortex) matter. The acquisition was performed twice first with selective inversion of the slice and then with a global inversion recovery technique (Kober et al., 2004). For each of these acquisitions, and based on previous

publications (Carr et al., 2007), the following parameters were used: TE/TR 30.5/16000 ms; flip angle: 90°; voxel size: 273×547 μm^2; number of averages: 6; inversion times: 0.2, 0.6, 0.8, 0.9, 1.0, 1.1, 1.2, 1.5, 2.0, and 2.5 sec; acquisition duration: 3 min 12 sec.

Diffusion-weighted imaging

A Stejskal-Tanner Echo Planar Imaging (EPI) pulse sequence was used to collect diffusion-weighted images (Stejskal and Tanner, 1965). A pulse sequence based on 3D sampling of Fourier space was used to increase the sensitivity of diffusion-weighted MRI (dMRI) (Nicolas et al., 2013). One image was acquired without diffusion weighting (b-value= 0 s/mm^2) and six with diffusion-weighting with a b-value of 1500 s/mm^2 and six different diffusion encoding directions in space. Diffusion-weighted images were recorded with the following parameters: TE/TR=58.97/1300 ms; voxel size: 203×195×750 μm^3; FOV: 30×25×24 mm^3; acquisition duration 4 min 51 sec.

Image processing

All pre-treatments, parametric map computing, definition of Regions Of Interest (ROIs) and measurements of ROIs were performed using ParaVision software (Bruker, Ettlingen, Germany). The phase contrast images calibrated for flow velocity (cm/sec) were displayed and mean velocities during the diastole of the heart cycle measured in the center of the ACAs, the pericallosal azygos artery as well as of the MCAs and its dorsal branches (Figure 1). Two (selective and global) T1 maps were computed using selective and global FAIR data sets. Relative cerebral blood flow (rCBF) map was then computed pixel by pixel according to (Kober et al., 2004). Blood T1 was set to 2070 ms as measured previously on rat and bovine blood (Dobre et al., 2007; Esparza-Coss et al., 2010).

To analyze perfusion-weighted ASL images, ROIs corresponding to the global brain or hemisphere, to the grey matter of the superficial and deep layers of the primary motor and sensory cortices and striatum as well as to the white matter of the corpus callosum and the external capsule were traced manually on each individual's selective inversion 1100 ms FAIR image using a rat brain atlas (Swanson, 1998) for guidance. The ROIs were then copied and pasted on perfusion-weighted images (Figure 1). For the ROIs covering the global brain or hemispheres cerebrospinal fluid-containing voxels were excluded. The ROI covering the combined white matter of the corpus callosum, cingulum and external capsule was used for the sake of comparison with previously published ASL studies in rats (Danker and Duong, 2007; Shen et al., 2015). For the ROI centered on the corpus callosum alone, the lateral limits

were the medial borders of the lateral ventricle to avoid inclusion of the cingulum. To limit operator bias, the ROI tracing step was repeated by two different operators with no knowledge of the condition of each animal. No difference was observed between these two independent operators (correspondence in coefficient of variation of 92% for the striatum, which was considered to have the least clear anatomical borders on images).

The following diffusion tensor parametric maps were computed from dMRI data: 1) Fractional Anisotropy (FA) map indicating the degree of anisotropy, 2) Tensor Trace map depicting the Apparent Diffusion Coefficients (ADC) and 3) Eigenvalue maps (λ1, λ2 and λ3) corresponding to the three diffusivities along the principal axes of the diffusion tensor, where: λ1 represents the ADC of water along the length of white matter fibers and λ2, λ3 represent the ADC of water perpendicular to the fibers. On images at a level comparable to that used for phase contrast and ASL imaging, A ROI was positioned manually on the corpus callosum carefully avoiding its interfaces with the cortex, septum and cerebrospinal fluid. Other ROIs were placed on the cortex (including both its superficial and deep layers) and striatum (Figure 1). Mean values of FA, ADC, λ1, λ2 and λ3 were then determined in these ROIs.

Experimental protocol

Six blocks of imaging sequences alternating phase-contrast imaging and ASL-imaging were repeated over time with the first "baseline" block occurring before intraperitoneal injection. Upon completion of baseline imaging, ten rats received an intraperitoneal injection of, on average (depending on body weight), 1 ml of 4.0 mg/ml *E. Coli* lipopolysaccharides (LPS; serotype 0127:B8, Sigma-Aldrich, St-Fallavier, France), thus corresponding to 12.5 mg/kg, and eight an injection of its vehicle, 1 ml of saline. The dose of LPS injected ip was based on our previous work showing that 1.25 mg/kg of LPS given iv reduced blood flow in the anterior cerebral arteries (Villega et al., 2017) and on the fact that ip administration of LPS results in ten times lower circulating concentrations as compared to iv administration (Yasui et al., 1995). After ip injection, blocks of imaging sequences were repeated every 30 minutes up to 150 minutes later. In addition, dMRI was performed right before and 150 min after injection. Animals were sacrificed after the last imaging sequence.

Immunohistochemistry

At the end of the experiment, rats were deeply anaesthetized by intraperitoneal injection of 60mg/kg of Sodium Pentobarbital. Bodies were rinsed from blood by intracardiac perfusion with 0.1 M phosphate-buffered saline (PBS; pH 7.4 at room temperature) and subsequently

fixed by 300 ml of 4% paraformaldehyde in 0.1 M PBS. Brains were removed from the skull, post-fixed for 24 h in the same fixative, and then cryoprotected in 30% sucrose in 0.1 M phosphate buffer. Forty-micrometer thick sections were cut on a vibratome (Leica VM 1000, Leica Microsystems, Nussloch, Germany) from the rostral limit of the optic chiasm to the caudal end of the central amygdala (Swanson, 1998) and collected in cold cryoprotectant solution (0.05 M PBS, 20 % glycerol, 30% ethylene glycol) and stored at -20°C until processing. For immunohistochemistry four animals (two injected ip with saline and two injected ip with LPS) that had neither undergone isoflurane anesthesia nor MRI were perfusion-fixed and their brains processed in the same way.

Immunohistochemistry was performed as previously described (Konsman and Blomqvist, 2005; Konsman et al., 2008; Konsman et al., 2004). Briefly, free-floating sections were washed four times in 0.1 M PBS (pH 7.4). Non-specific binding sites were blocked by a 45-minute incubation of sections in PBS containing 0.3% Triton X-100 and 1.0% BSA. The first antibody was then diluted (indicated below for every antiserum used) in the same buffer and added to the sections overnight at room temperature. Commercially available antisera raised against the cellular activation marker c-Fos (rabbit anti-c-Fos; sc-52, Santa Cruz Biotechnology, Heidelberg, Germany) diluted 1:2000, COX-2 (goat anti-COX-2; sc-1747, Santa Cruz Biotechnology, Heidelberg, Germany) diluted 1:750, the astrocyte specific glial fibrillary acidic protein (GFAP; mouse anti-GFAP; clone GA5, MAB360, Merck Millipore, Fontenay sous Bois, France) diluted 1:1000, the microglia-macrophage specific ionized calcium-binding adaptor molecule (Iba-1; rabbit anti-Iba-1; 019-19741, Wako Chemicals GmbH, Neuss, Germany) diluted 1:1000 and rat immunoglobulin G (IgG; biotinylated goat anti IgG, BA-9401, Vector Laboratories, Burlingame, CA, USA) diluted 1:750 were used. To detect rat IL-1beta, a sheep antiserum generated to recombinant rat IL-1beta (Dr. S. Poole, NIBSC, Potters Bar, UK) was used diluted 1:500.

The c-Fos, COX-2, GFAP and Iba-1 antisera used in the present work are part of the Journal of Comparative Neurology antibody database that contains collected information on the antibodies used for immunohistochemistry based on that journal's policy requiring rigorous characterization for antibodies. The c-Fos antiserum 1) has been characterized by the vendor to recognize a 62 kDa protein, corresponding to the molecular weight of c-Fos, on Western blots, and 2) has previously been used by us (Konsman and Blomqvist, 2005; Konsman et al., 2008) and others (Engler et al., 2011; Farzi et al., 2015) at comparable dilutions in streptavidin–biotin–immunoperoxidase immunohistochemistry protocols on formaldehyde-

fixed rat brain tissue. The COX-2 antiserum has been characterized by the vendor to recognize a 70-72 kDa protein corresponding to the molecular weight of COX-2, on Western blots of the LPS-stimulated macrophage cell line RAW 264.7 and 2) has been widely used by us and others in *in vivo* conditions comparable to the ones in the present study (Konsman et al., 2000; Konsman et al., 2004; Laflamme et al., 1999; Schiltz and Sawchenko, 2002; Yamagata et al., 2001). The Iba-1 antiserum has been shown by the vendor to recognize rat Iba-1 in macrophages and microglia and has been widely used by others. The IgG antiserum has been characterized by the vendor to show <1% cross-reactivity with rat IgM. The rat IL-1beta antiserum has previously been shown to specifically recognize the pro- and mature form of IL-1beta in rat microglia (Chauvet et al., 2001). Since brain sections were obtained from animals that had undergone imaging under isoflurane anesthesia and isoflurane has been shown to attenuate LPS-induced cytokine expression in peripheral tissues (de Rossi et al., 2004; Flondor et al., 2008) and potentially c-Fos expression (Villega et al., 2017), IL-1beta and c-Fos induction in the brain were used as positive controls for the effects of systemic LPS administration on the CNS.

After four rinses in PBS, sections were treated for 30 minutes with 0.3% (v/v) hydrogen peroxide to block endogenous peroxidases followed by rinses in PBS. With the exception of those sections exposed to biotinylated rat IgG, sections were then incubated for 2 h with biotinylated antisera raised against IgGs of the species of the first antibody (Vector Laboratories, Burlingame, CA, USA) diluted 1:500 in PBS, 0.3% Triton X-100, 1% BSA. After four washes in PBS, sections were incubated for 2 h with a complex of avidin and biotinylated peroxidase (Vector Laboratories, Burlingame, CA, USA) diluted 1:500 in PBS. Finally, sections were transferred to a sodium acetate buffer and stained using diaminobenzidine as a chromogen in the presence of Ni-ions, thus providing yielding a dark grey to black precipitate.

Stained sections were examined with a light-microscope (Leica DM5500B, Leica Microsystems, Nanterre, France) and images were captured by a high-resolution digital camera system Leica DFC425C, Leica Microsystems, Nanterre, France) and stored onto a personal computer. In every brain section between bregma +4.85 and -2.85 mm the occurrence and extent (scored as restricted (1), intermediate (2) or extensive (3)) of perivascular IgG diffusion in a given structure was noted. As each region or structure considered covered at least two, but a varying number (depending on the length of the structure) of, brain sections (with two consecutive sections being separated by 240 µm), the

number of occurrences of perivascular IgG diffusion for a structure were then divided by the number of brain sections in which the structure was present. Similarly, the cumulative score of the extent of IgG diffusion for a given brain region or structure was also divided by the number of sections that contained the region or structure in question.

The number of c-Fos positive cells in a section of a brain structure of interest was determined by applying a particle size criterion on fixed-thresholded 8-bit images with Image J (http://imagej.nih.gov/ij/). Iba-1- and GFAP-immunopositive glia cells in the corpus callosum, were characterized both in terms of cellular density and morphology using the Image J plugin Fraclac (http://rsb.info.nih.gov/ij/plugins/fraclac/fraclac.html). Briefly, on binary images of brain sections between bregma -0.11 and -1.33 mm glia cells were enclosed by a Hull convex and bounding circle after which the surface, perimeter, diameter and circularity (defined as $4*\pi*\text{Area} / \text{Perimeter}^2$) were determined in addition to the width and height of the cells. In addition, as both white matter microglia and astrocytes retract their most distant processes when they become activated, Iba-1- and GFAP-immunoreactive fragments were also quantified. Image editing software (Adobe Photoshop, Adobe Systems, San Jose, CA, USA) was used only to adjust contrast and brightness for photomicrographs composing illustrating figures.

Data representation and analysis

Data were expressed as means ± standard error of the mean (SEM). Maximum, minimum and final body temperature and heart and respiration rate were analyzed by analyses of variance (ANOVA) with ip treatment as a between factor. Phase contrast and ASL data after injection were analyzed by a repeated measures ANOVA with ip treatment as a between factor and post-injection time as a within factor. In addition, and to assess blood redistribution between brain structures, ASL perfusion of cerebral structures was also expressed relative to perfusion of brain hemispheres or to that of the global brain parenchyma in the case of the ROI centered on the corpus callosum that is situated between the two hemispheres and analyzed with similar repeated measures ANOVA. Significant effects of time and interactions were further analyzed by the Newman-Keuls *post-hoc* test. dMRI data were expressed as changes relative to baseline and analyzed by a one-way ANOVA with ip treatment as a between factor. Image analysis data obtained on immunohistochemically-stained brain sections were analyzed by a one-way ANOVA with ip treatment as a between factor. When data were not normally

distributed, the non-parametric Mann-Whitney U test was used. In all cases, a level of $p<0.05$ was considered as statistically significant.

Results

Ip LPS increased minimum body temperature

Central components of the acute phase response like fever indicate that inflammation-related messages have reached and acted upon the central nervous system to alter body temperature (Konsman et al., 2002). Although no statistically significant differences in heart and respiration rate were observed between anesthetized animals given LPS (12.5 mg/kg ip) and those administered saline, a significant difference in minimum body temperature was found. Indeed, the minimum body temperature observed was significantly higher in LPS-treated rats (36.45 ± 0.20 °C) as compared to their saline-injected conspecifics (35.86 ± 0.17 °C; $F_{1,22}$: 4.38, $p<0.05$).

Ip LPS did not alter flow in the major forebrain-irrigating arteries

PhC-MRI data indicated that the direction of blood flow in the ACAs and MCAs (white to light grey in Figure 1B) on the ventral side of the brain was opposite to that of their dorsal branches (dark grey to black in Figure 1B). Ventral to the ACAs and MCAs, blood velocities in the center of the internal carotids clearly were superior to the velocity encoding parameter that was set to 10 cm/sec in the present work (black on white signal in Figure 1B). However, in the ACAs and MCAs this occurred much less frequently, and only exceptionally in all of the three slices considered (in the one case that this happened for the ACA, the animal was excluded from analysis). In the dorsal arteries, the maximum velocity of 10 cm/s was never reached.

ANOVAs on blood flow velocities in the center of the left and right MCAs (Figure 2A, C) and left (Figure 2B) and right ACAs with treatment as a between factor and time after injection as a within subject factor did neither show a significant treatment effect nor a significant interaction between treatment and time. Similar analysis on blood flow velocities in the center of the dorsal left and right branches of the MCAs (Figure 2D, F) and pericallosal azygos artery (Figure 2E) with treatment as a between factor and time after injection as a within subject factor did not show any global treatment effect, but did reveal a significant interaction between treatment and time in the dorsal right MCA branch ($F_{4,56}=2.65$, $p<0.05$).

Post-hoc analysis showed that this interaction was due to a tendency for higher blood flow velocity at 120 min as compared to 30 min after ip LPS injection (p=0.075; Figure 2C). In addition, these ANOVAs indicated a significant increase in blood flow velocities over time in the right ACA (F4,56=2.69, p<0.05) and in the dorsal left branch of the MCA ($F_{4,56}$=2.74, p<0.05).

Ip LPS shunted perfusion towards the corpus callosum

ANOVAs on perfusion values measured in the global brain brain or hemispheres with treatment as a between factor and time after injection as a within subject factor did neither show a global treatment effect nor an interaction between treatment and time. Application of these analyses on perfusion in the ROI covering the combined white matter of the corpus callosum, cingulum and the external capsule also did not indicate a treatment effect or interaction (Figure 3A). An ANOVA on perfusion in the ROI centered on the corpus callosum revealed a significant interaction between treatment and time in the corpus callosum ($F_{4,52}$=3.18, p<0.05). *Post-hoc* analysis showed that this interaction was due to significantly higher perfusion of the corpus callosum 90, 120 and 150 min after ip LPS injection as compared to the 30 min post-injection time point (p<0.05; Figure 3C). An ANOVA on perfusion values in the ROI that covered the external capsule with treatment as a between factor and time after injection as a within subject factor did neither show a global effect of treatment nor an interaction between treatment and time (Figure 3E). Similar analyses of perfusion in the ROIs covering grey matter did not reveal any global treatment effects or interactions in the superficial and deep cortical layers (Figure 3B and D) and striatum (Figure 3F). In addition, ANOVAs indicated a significant increase in blood perfusion over time in the global brain ($F_{4,28}$=4.41, p<0.01, brain hemispheres ($F_{4,28}$=4.44, p<0.01 and $F_{4,28}$=3.56, p<0.05), the superficial and deep cortical layers ($F_{4,48}$=3.77, p<0.01 and $F_{4,56}$=3.29, p<0.05, respectively Figure 3B and D) and striatum ($F_{4,52}$=13.4, p<0.001; Figure 3F).

Perfusion values measured in brain areas were next expressed relative to that of the hemisphere (or to that of the global brain parenchyma in the case of the ROI centered on the corpus callosum that is situated between the two hemispheres) to assess the distribution of blood between different brain structures. ANOVAs on these data with treatment as a between factor and time after injection as a within subject factor indicated a significant redistribution of perfusion towards the corpus callosum after LPS injection ($F_{1,13}$=9.88, p<0.01; Figure 4C) and a significant interaction between LPS treatment and time in the ROI covering the

combined white matter of the corpus callosum, cingulum and the external capsule ($F_{4,56}$: 2.95, $p<0.05$) and in the ROI centered on the external capsule alone ($F_{4,52}$: 3.81, $p<0.01$). *Post-hoc* analysis showed that these interactions were due to significant lower perfusion between the 60 and 150 min time points in the former ROI (combined white matter of the corpus callosum, cingulum and the external capsule; $p<0.05$; Figure 4A) and a trend for decreased perfusion between the 30 and 150 min time points in the latter ROI (external capsule alone; $p=0.074$; Figure 4E) of ip LPS-treated animals. In the grey matter, ANOVAs on relative perfusion of brain areas with treatment as a between factor and time after injection as a within subject factor revealed a trend for increased perfusion in the deep cortical layers after ip LPS injection compared to ip saline administration ($F_{1,13}=4.22$, $p=0.061$; Figure 4D). In addition, these analyses indicated a significant increase over time in the striatum ($F_{4,52}=4.73$, $p<0.001$; Figure 4F), but no main effect or interaction with LPS treatment.

Ip LPS increased horizontal water diffusion in the corpus callosum

One-way ANOVAs on diffusion parameters 150 min after ip injection did neither reveal any differences in ADC in the cortex (Figure 5A), striatum and corpus callosum nor any changes in corpus callosum diffusion directions (Figure 5B) between treatments. In addition, a one-way ANOVAs on the change of mean water diffusion in each subject's cortex between the start and end of the experiment did not indicate an effect of treatment (Figure 5C). However, a one-way ANOVAs on the change of water diffusion parameters in the corpus callosum of each animal between the start and end of the experiment showed a significantly increase in water diffusion in the horizontal plane, that is parallel to corpus callosum fibers, in rats that were administered LPS ip as compared to saline ($F_{1,15}$: 6.32, $p<0.05$; Figure 5D) without any effect on other diffusion directions.

Ip LPS induced cerebral Interleukin-1ß, but not c-Fos, expression

Since, Interleukin-1ß is known to be expressed in brain circumventricular organs and choroid plexus as early as 2 h after ip LPS injection in awake rats (Konsman et al., 1999), this response was studied as a positive control for the effects of LPS on the brain in the present work. In accordance with our previous work, Interleukin-1ß-immunoreactivity was observed in the circumventricular subfornical organ and the choroid plexus (Figure 6B) of ip LPS-treated animals that had undergone isoflurane anesthesia and MRI, whereas no stained cellular processes were found in saline-injected rats (Figure 6A).

Induction of the c-Fos transcription factor in the hypothalamus is another potential positive control for the effects of LPS on the brain (Konsman et al., 1999). However, a one-way ANOVA on the number of c-Fos-immunoreactive cells in the preoptic area did not reveal significant differences between ip saline- and LPS-treated rats that had undergone MRI under anesthesia (Figure 7A-C). A similar analysis of c-Fos expression in the supraoptic and paraventricular nucleus of the hypothalamus also did not indicate significant differences between ip saline and LPS administration under isoflurane anesthesia (Figure 7D-F).

Ip LPS moderately induced cerebrovascular COX-2 expression

As COX-2 is constitutively expressed by cortical neurons and robustly induced perivascularly throughout the neuraxis already 2 h after ip LPS injection in awake rats (Konsman et al., 2004), these were studied as positive controls for COX-2 immunohistochemistry in the present work. Indeed, in those two animals that were injected ip with LPS without having undergone isoflurane anesthesia and MRI, robust perivascular COX-2 induction was observed 2.5 h later in the meninges and preoptic area (Supplementary figure 1B, D) as compared to their two saline-administered counterparts (Supplementary figure 1A, C), and in addition to constitutive expression in the cortex (Supplementary figure 1A, C).

Two and a half hours after ip administration of saline or LPS under isoflurance anesthesia, constitutive COX-2-positive neuron-like cells were found in cortex (Figure 8A). After ip LPS administration, moderate COX-2 immunolabeling was however seen in the meninges between the two cortical hemispheres (Figure 8C) and around some blood vessels in the striatum and medial preoptic area (Figure 8D). However, unlike our previous observations in awake animals, except for the optic chiasm, no induction of COX-2 immunoreactive blood vessels or perivascular cells was found in the white matter of ip LPS-injected rats that had undergone anesthesia and MRI.

Ip LPS induced BBB breakdown in white matter

In all animals, IgG was found in brain circumventricular organs, choroid plexus and meninges, where there is no functional BBB at the endothelial cell level. In the white matter of anesthetized animals injected with saline, weak, and occasionally moderate, IgG-immunoreactivity could be observed in some vessel walls in the white matter of the transition zone between the corpus callosum and the external capsule, the internal capsule, the fimbria, the stria terminalis and the ventral hippocampal commissure (Figure 9A). In the grey matter of these animals weak to moderate IgG-immunoreactivity was seen around blood vessel walls

of the grey matter parenchyma of the deep layers of the somatosensory (Figure 9B), motor, insular and piriform cortices, caudate putamen (Figure 9C), nucleus accumbens, amygdala, lateral septum median preoptic area and lateral hypothalamus.

Compared to saline injection, ip LPS administration under anesthesia resulted in increased occurrence of perivascular plume-like diffusion clouds of IgG staining in sections containing white matter when all forebrain fiber bundles were considered ($F_{1,14}$: 12.1, $p<0.01$; Table 1). This effect was in large part due to trends for increased occurrence of perivascular IgG staining in sections of the ventral hippocampal commissure (($F_{1,14}$: 4.46, $p=0.053$; Table 1; Figure 9D), the fimbria ($F_{1,14}$: 3.65, $p=0.077$; Table 1) and the stria terminalis ($F_{1,14}$: 3.18, $p=0.096$; Table 1). However, similar one-way ANOVAs did not reveal any significant differences in perivascular IgG-immunoreactivity in the corpus callosum and external capsule between animals that were given saline and those rats administered LPS (Table 1). In the grey matter of LPS-treated animals, the deep layers of the cerebral cortex occasionally showed important perivascular plumes of IgG staining (Figure 9E), a phenomenon that was also regularly encountered in striatal structures (Figure 9F). ANOVAs indicated that compared to saline injection, ip LPS administration did not significantly increase the occurrence of perivascular IgG staining in sections containing cortical structures, whereas it did in striatal structures ($F_{1,14}$: 5.45, $p<0.05$; Table 1). The latter effect was in large part due to significantly increased occurrence of perivascular IgG staining in sections of the caudate putamen (($F_{1,14}$: 4.78, $p<0.05$; Table 1).

Ip LPS did not alter corpus callosum glia cell morphology

Although signs of morphological activation of Iba-1-positive cells were observed in the vicinity of circumventricular organs of LPS-treated animals, a one-way ANOVA on the relative surface occupied by Iba-1-immunoreactive cell bodies and processes in the corpus callosum did not show a difference between saline and LPS injection. Similar analyses of the height, width (Figure 10A-D), perimeter, area and circularity of Iba-1-positive cells and fragments also did not indicate any differences between treatments when all levels between bregma -0.11 and -1.33 mm were considered. However, one-way ANOVA on these latter parameters established a trend for decreased height of Iba-1-immunoreactive cells in LPS-treated animals as compared to saline-injected rats at bregma -0.83 mm ($F_{1,11}$: 3.99, $p=0.083$). Finally, one-way ANOVAs on the relative surface occupied by GFAP-positive cell bodies and processes and on the height, width, perimeter, area and circularity of GFAP-1-

immunoreactive cells and fragments in the corpus callosum did not show any difference between saline and LPS injection (Figure 10E-H).

Discussion

The main finding of the present work was that, compared to ip injection of saline, administration of bacterial LPS in rats increased blood perfusion in the ROI centered on the white matter of the corpus callosum without affecting blood flow in the dorsal forebrain-irrigating arteries. In addition, a trend for a distribution of blood perfusion in favor of the deep cortical regions was found in LPS-injected animals. Over the duration of the experiment ip LPS injection also resulted in higher water diffusion parallel to the fibers of the corpus callosum as compared to saline. These changes in perfusion and diffusion were not related to global perivascular COX-2 induction or glia cell activation, but may be linked, at least in part, to BBB breakdown.

Compared to our previous TOF MRA findings indicating reduced blood flow in the ACA and MCA after iv LPS administration in mice, no changes in flow velocities were found in the ACAs and MCAs and their dorsal branches using phase contrast imaging after ip LPS injection in rats. Several reasons may explain this apparent inconsistency. On the other hand, other studies have indicated increased resting blood flow velocities in the sensory cortex with laser Doppler flowmetry after iv LPS administration in rats (Rosengarten et al., 2007; Rosengarten et al., 2008a). Several factors need to be taken into account when considering these apparent inconsistencies. First, phase contrast MRA yields quantitative flow data, whereas TOF MRA and laser Doppler data are typically provided as arbitrary units (Rosengarten et al., 2007; Rosengarten et al., 2008a; Kiruluta and Gonzalez, 2016; MacDonald and Frayne, 2015). Secondly, TOF MRA is well-suited for the extensive high blood flow systems downstream of and in the circle of Willis while laser Doppler flowmetry adequately assesses local flow velocities in much more circumscribed parts of the cortex. Phase contrast imaging perfect probes flow velocities at the level of the whole brain downstream of the circle of Willis and upstream of the penetrating arterioles in the cortex. And because distinct mechanisms regulate flow in these diverse parts of the cerebrovascular tree, different phenomena may be observed after systemic LPS administration. Lastly, ip LPS results in a more progressive and pathophysiologically-relevant appearance of bacterial fragments in the blood stream as compared to an iv bolus injection of LPS (Yasui et al.,

1995). Therefore, and even though signs of vasospasms have been observed with TOF MRA in septic patients with encephalopathy (Bartynski et al., 2006; Polito et al., 2013), progressively increasing circulating concentrations of bacterial LPS after its ip injection did not alter flow in the dorsal forebrain-irrigating arteries of rodents.

The increase in blood perfusion of the cortex and striatum with time, but independently from treatment, as found in the present work, is in accordance with previous studies employing ASL in intact rats under isoflurane anesthesia (Sicard et al., 2003, Duong, 2007). This isoflurane-induced hyperemia is due to increased cerebral NO production (Kehl et al., 2002, Sjakste et al., 2005) and even more important for other inhaled anesthetics (Holmstrom and Akeson, 2005). The lack of differences in flow in the ventral and dorsal branches of the MCAs and the pericallosal artery may explain why overall blood perfusion of forebrain hemispheres and cortices did not differ between ip saline and LPS treatments. However, intravital microscopy has shown rapid vasodilation of subpial arterioles and venules in the cortex after iv LPS administration in rodents (Ruiz-Valdepenas et al., 2011). With respect to this latter finding it is important to keep in mind that arterioles and venules, which can be assessed with intravital microscopy on the cortical surface, irrigate and drain the whole depth of the cortex, respectively, and that we did observed a tendency for increased perfusion of the deep cortical layers.

Interestingly, we found increased perfusion in the ROI centered on the corpus callosum as well increased perfusion distribution to this area relative to that of the brain after ip LPS administration as compared to saline injection. The ASL perfusion values found for the corpus callosum ROI were in agreement with those obtained by Sicard and colleagues (2003). This being said, ASL-based perfusion data are known to vary even between studies of the same group (Danker and Duong, 2007; Shen et al., 2015; Sicard et al., 2003) and the aim of the present work was not to obtain absolute quantitative data. Instead, our main aim was to compare cerebral arterial flow and grey and white matter perfusion after ip administration of LPS and saline in animals under the same conditions. As any MRI technique, ASL values obtained in a ROI are exposed to a risk of partial volume. However, the corpus callosum at the level where the ROI was placed is bordered ventrally by the white matter of the dorsal fornix and in its rostral part also by that of ventral hippocampal commissure and dorsally only in part by the cortex (Barazany et al., 2009). The partial volume included in our corpus callosum ROI thus concerned in large part other white matter. Our findings that despite unaltered blood flow in the pericallosal azygos artery that supplies the white matter of the

corpus callosum and the dorsal fornix as well as to a lesser extent the ventral hippocampal commissure, and the grey matter of the overlying induseum griseum and cingulate cortex (Coyle, 1975), ip LPS did increase perfusion in the ROI centered on the corpus callosum, but that likely also contained the dorsal fornix and ventral hippocampal commissure, indicate that inflammation shunted cerebral perfusion towards dorsal white matter.

Systemic administration of bacterial LPS in awake rats induces expression of the prostaglandin-synthesizing enzyme COX-2 in grey and white matter venules (Konsman et al., 2004). In the cortex, COX-2 is essential for neurovascular coupling (Niwa et al., 2000; Stefanovic et al., 2006), that is the increase in local arteriole, capillary and venous blood supply after neuronal activation (Drew et al., 2011). Although it is not known if increased blood supply to the white matter involves COX-2, we did not observe LPS-induced COX-2 expresson in vessels of the corpus callosum, external capsule and deep cortical layers where blood was shunted towards after ip LPS injection in anesthetized rats. Therefore, increased perfusion distribution to the white matter, as observed in the present study, does not seem to involve COX-2-mediated inflammatory signaling.

In mutiple sclerosis patients, increased perfusion has been shown to be associated with breakdown of the BBB in subcortical white matter (Ge et al., 2005; Ingrisch et al., 2012). Rupture of the BBB is a dose- and time-dependent gradual process with low, but not high, molecular weight molecules entering the brain 2-4 h after injection, even in response to moderate doses of LPS (Bickel et al., 1998; Singh and Jiang, 2004). One day after high doses of LPS (2-3 mg/kg) injected ip, high molecular weight dextran, albumin and immunnoglobulins can be detected in the brain (Singh and Jiang, 2004; Xaio et al., 2001). Since we used a slightly higher dose of ip LPS (12.5 mg/kg) to mimic severe sepsis conditions, it was relevant to study if BBB permeability to high-molecular weight markers occurred during the first hours after injection. Several vessel walls showed staining for IgG of which some were associated with perivascular diffusion clouds of staining indicating BBB leakage in both saline- and LPS-injected animals. This phenomenon may be explained by the fact that all animals underwent isoflurane anesthesia for MRI. Indeed, isoflurane can render the BBB in the cortex and subcortical structures permeable to Evans blue and IgG (Acharya et al., 2015; Tetrault et al., 2008). Given the need for stable long-term anesthesia and that fact that sevoflurane results in more important BBB breakdown than isoflurane (Acharya et al., 2015), an informed choice in favor of the latter was made in the present study.

Quantification of the occurrence of perivascular IgG clouds in brain sections containing white matter showed that BBB-breakdown occurred more frequently after ip LPS administration as compared to saline. While a trend for increased occurrence of perivascular IgG staining was found in sections of the ventral hippocampal commissure in LPS-treated rats as compared to saline-injected rodents, no differences were observed in the corpus callosum. Thus, increased perfusion in the ROI centered on the corpus callosum, but likely also containing the dorsal fornix and ventral hippocampal commissure, may, in part, be related to local BBB breakdown in the ventral hippocampal commissure.

Contrary to a previous study showing decreased ADC in the cortex of mice 24 h after cecal ligature and puncture (Bozza et al., 2010), no changes in diffusion parameters were observed in the cortex 2.5 h after ip LPS administration in the present work. This may due to the fact that no edema formation occurs during the first hours after systemic LPS injection (Rosengarten et al., 2008b). Interestingly, we did observe that between the start and end of the experiment the change of water diffusion in the horizontal plane of the corpus callosum, that is parallel to callosal fibers, was higher in rats that were administered LPS than in those given saline. This finding may seem at variance with the reported lower FA in the genu and splenium of the corpus callosum of intensive care patients at discharge after an episode of delirium, many of which related to sepsis (Morandi et al., 2012). However, one should keep in mind that in the present work the corpus callosum proper, and not its genu and splenium parts, was assessed while, and not after, the organism was exposed to bacterial fragments. Furthermore, increased ADC has been reported in white matter during septic encephalopathy (Sharshar et al., 2007). Taken together, the previous and present findings suggest that during inflammation axial diffusion in the corpus callosum first increases to subsequently decrease when white matter integrity is altered.

Increased perfusion combined with BBB breakdown in the corpus callosum after systemic LPS administration, as observed in the present work, may have augmented water diffusion parallel to callosal fibers. Alternatively, retraction of the processes of microglia or astrocytes that occupy the space between white matter fibers may explain increased horizontal water diffusion in the corpus callosum after ip LPS injection. Although we did not find any change in glia cell morphology when considering all levels of the corpus callosum proper, we observed a trend for a decrease in the height of microglia in the corpus callosum at the level where this structure overlies the subfornical organ. This may reflect a progressive activation

of microglia spreading from circumventricular organs after peripheral LPS administration similar to what we observed previously (Konsman et al., 1999).

Contrary to the effects of LPS at the blood-brain interface, which, albeit seeming somewhat less intense than in awake animals, did occur in anesthesized rats, the induction of the activation marker c-Fos in the parenchyma of the preoptic area and paraventricular hypothalamus was found to be variable and not to significantly differ between saline and LPS treatment. This is at variance with previous reports, including our own, showing increased c-Fos expression in these rodent brain structures after systemic LPS administration in awake animals (Konsman et al., 1999). Although anesthesia-maintaining concentrations of isoflurane (0.6-1.5 %) are not sufficient to induce c-Fos expression in the paraventricular hypothalamus (Sawamura et al., 2004), higher anesthesia-inducing concentrations may be. Moreover, isoflurane most likely interfered with the activation of nervous pathways leading to c-Fos expression in the preoptic area and paraventricular hypothalamus after LPS administration. Hence, LPS administration under gaseous anesthesia to perform MRI in animals may be adequate to address systemic inflammation-related events at the blood-brain interface, even though the effects may be less important, but not to study neuronal activation.

In conclusion, our present findings indicate that LPS-induced systemic inflammation can result, without altering flow in dorsal forebrain-irrigating arteries, in increased perfusion, blood-brain barrier breakdown and altered water diffusion in the cerebral white matter. Since the association between plasma LPS and bacteremia is consistent for different types of Gram-negative bacteria (Hurley, 2009), these findings bear relevance for brain dysfunction observed during those infections.

Acknowledgements

We thank Richard Rouland for skillful assistance. Ibtihel Dhaya was a laureate of a stipend from the Ministère de l'Enseignement Supérieur et de Recherche Scientifique in Tunisia. Administrative help from Adera (Pessac, France) is gratefully acknowledged.

References

Acharya, N.K., Goldwaser, E.L., Forsberg, M.M., Godsey, G.A., Johnson, C.A., Sarkar, A., DeMarshall, C., Kosciuk, M.C., Dash, J.M., Hale, C.P., Leonard, D.M., Appelt, D.M., Nagele, R.G., 2015. Sevoflurane and Isoflurane induce structural changes in brain vascular endothelial cells and increase blood-brain barrier permeability: Possible link to postoperative delirium and cognitive decline. Brain Res 1620, 29-41.

Barazany, D., Basser, P.J., Assaf, Y., 2009. In vivo measurement of axon diameter distribution in the corpus callosum of rat brain. Brain 132, 1210-1220.

Baron, R.M., Baron, M.J., Perrella, M.A., 2006. Pathobiology of sepsis: are we still asking the same questions? Am J Respir Cell Mol Biol 34, 129-134.

Bartynski, W.S., Boardman, J.F., Zeigler, Z.R., Shadduck, R.K., Lister, J., 2006. Posterior reversible encephalopathy syndrome in infection, sepsis, and shock. AJNR Am J Neuroradiol 27, 2179-2190.

Bickel, U., Grave, B., Kang, Y.S., del Rey, A., Voigt, K., 1998. No increase in blood-brain barrier permeability after intraperitoneal injection of endotoxin in the rat. J Neuroimmunol 85, 131-136.

Bowton, D.L., Bertels, N.H., Prough, D.S., Stump, D.A., 1989. Cerebral blood flow is reduced in patients with sepsis syndrome. Crit Care Med 17, 399-403.

Bozza, F.A., Garteiser, P., Oliveira, M.F., Doblas, S., Cranford, R., Saunders, D., Jones, I., Towner, R.A., Castro-Faria-Neto, H.C., 2010. Sepsis-associated encephalopathy: a magnetic resonance imaging and spectroscopy study. J Cereb Blood Flow Metab 30, 440-448.

Brassard, P., Kim, Y.S., van Lieshout, J., Secher, N.H., Rosenmeier, J.B., 2012. Endotoxemia reduces cerebral perfusion but enhances dynamic cerebrovascular autoregulation at reduced arterial carbon dioxide tension. Crit Care Med 40, 1873-1878.

Carr, J.P., Buckley, D.L., Tessier, J., Parker, G.J.M., 2007. What levels of precision are achievable for quantification of perfusion and capillary permeability surface area product using ASL? Magnetic Resonance In Medicine 58, 281-289.

Chauvet, N., Palin, K., Verrier, D., Poole, S., Dantzer, R., Lestage, J., 2001. Rat microglial cells secrete predominantly the precursor of interleukin-1beta in response to lipopolysaccharide. Eur J Neurosci 14, 609-617.

Coyle, P., 1975. Arterial patterns of the rat rhinencephalon and related structures. Exp Neurol 49, 671-690.

Danker, J.F., Duong, T.Q., 2007. Quantitative regional cerebral blood flow MRI of animal model of attention-deficit/hyperactivity disorder. Brain Res 1150, 217-224.

de Rossi, L.W., Brueckmann, M., Rex, S., Barderschneider, M., Buhre, W., Rossaint, R., 2004. Xenon and isoflurane differentially modulate lipopolysaccharide-induced activation of the nuclear transcription factor KB and production of tumor necrosis factor-alpha and interleukin-6 in monocytes. Anesth Analg 98, 1007-1012, table of contents.

Dobre, M.C., Ugurbil, K., Marjanska, M., 2007. Determination of blood longitudinal relaxation time (T1) at high magnetic field strengths. Magn Reson Imaging 25, 733-735.

Drew, P.J., Shih, A.Y., Kleinfeld, D., 2011. Fluctuating and sensory-induced vasodynamics in rodent cortex extend arteriole capacity. Proc Natl Acad Sci U S A 108, 8473-8478.

Dumoulin, C.L., 1995. Phase contrast MR angiography techniques. Magn Reson Imaging Clin N Am 3, 399-411.

Dumoulin, C.L., Souza, S.P., Darrow, R.D., Pelc, N.J., Adams, W.J., Ash, S.A., 1991. Simultaneous acquisition of phase-contrast angiograms and stationary-tissue images with Hadamard encoding of flow-induced phase shifts. J Magn Reson Imaging 1, 399-404.

Duong, T. Q., 2007. Cerebral blood flow and BOLD fMRI responses to hypoxia in awake and anesthetized rats. Brain Res 1135, 186-194.

Ebersoldt, M., Sharshar, T., Annane, D., 2007. Sepsis-associated delirium. Intensive Care Med 33, 941-950.

Engler, H., Doenlen, R., Engler, A., Riether, C., Prager, G., Niemi, M.B., Pacheco-Lopez, G., Krugel, U., Schedlowski, M., 2011. Acute amygdaloid response to systemic inflammation. Brain Behav Immun 25, 1384-1392.

Esparza-Coss, E., Wosik, J., Narayana, P.A., 2010. Perfusion in rat brain at 7 T with arterial spin labeling using FAIR-TrueFISP and QUIPSS. Magn Reson Imaging 28, 607-612.

Farzi, A., Reichmann, F., Meinitzer, A., Mayerhofer, R., Jain, P., Hassan, A.M., Frohlich, E.E., Wagner, K., Painsipp, E., Rinner, B., Holzer, P., 2015. Synergistic effects of NOD1 or NOD2 and TLR4 activation on mouse sickness behavior in relation to immune and brain activity markers. Brain Behav Immun 44, 106-120.

Flondor, M., Hofstetter, C., Boost, K.A., Betz, C., Homann, M., Zwissler, B., 2008. Isoflurane inhalation after induction of endotoxemia in rats attenuates the systemic cytokine response. Eur Surg Res 40, 1-6.

Ge, Y., Law, M., Johnson, G., Herbert, J., Babb, J.S., Mannon, L.J., Grossman, R.I., 2005. Dynamic susceptibility contrast perfusion MR imaging of multiple sclerosis lesions: characterizing hemodynamic impairment and inflammatory activity. AJNR Am J Neuroradiol 26, 1539-1547.

Holmstrom, A. and Akeson, J., 2005. Desflurane induces more cerebral vasodilation than isoflurane at the same A-line autoregressive index level. Acta Anaesthesiol Scand 49, 754-758.

Hurley, J.C., 2009. Diagnosis of endotoxemia with gram-negative bacteremia is bacterial species dependent: a meta-analysis of clinical studies. J Clin Microbiol 47, 3826-3831.

Ingrisch, M., Sourbron, S., Morhard, D., Ertl-Wagner, B., Kumpfel, T., Hohlfeld, R., Reiser, M., Glaser, C., 2012. Quantification of perfusion and permeability in multiple sclerosis: dynamic contrast-enhanced MRI in 3D at 3T. Invest Radiol 47, 252-258.

Jackson, A.C., Gilbert, J.J., Young, G.B., Bolton, C.F., 1985. The encephalopathy of sepsis. Can J Neurol Sci 12, 303-307.

Kehl, F., Shen, H., Moreno, C., Farber, N. E., Roman, R. J., Kampine, J. P. and Hudetz, A. G., 2002. Isoflurane-induced cerebral hyperemia is partially mediated by nitric oxide and epoxyeicosatrienoic acids in mice in vivo. Anesthesiology 97, 1528-1533.

Kim, S.G., Tsekos, N.V., 1997. Perfusion imaging by a flow-sensitive alternating inversion recovery (FAIR) technique: application to functional brain imaging. Magn Reson Med 37, 425-435.

Kiruluta, A.J., Gonzalez, R.G., 2016. Magnetic resonance angiography: physical principles and applications. Handb Clin Neurol 135, 137-149.

Kober, F., Iltis, I., Izquierdo, M., Desrois, M., Ibarrola, D., Cozzone, P.J., Bernard, M., 2004. High-resolution myocardial perfusion mapping in small animals in vivo by spin-labeling gradient-echo imaging. Magn Reson Med 51, 62-67.

Konsman, J.P., Blomqvist, A., 2005. Forebrain patterns of c-Fos and FosB induction during cancer-associated anorexia-cachexia in rat. Eur J Neurosci 21, 2752-2766.

Konsman, J.P., Kelley, K., Dantzer, R., 1999. Temporal and spatial relationships between lipopolysaccharide-induced expression of Fos, interleukin-1beta and inducible nitric oxide synthase in rat brain. Neuroscience 89, 535-548.

Konsman, J.P., Luheshi, G.N., Bluthe, R.M., Dantzer, R., 2000. The vagus nerve mediates behavioural depression, but not fever, in response to peripheral immune signals; a functional anatomical analysis. Eur J Neurosci 12, 4434-4446.

Konsman, J.P., Parnet, P., Dantzer, R., 2002. Cytokine-induced sickness behaviour: mechanisms and implications. Trends in Neurosciences 25, 154-159.

Konsman, J.P., Veeneman, J., Combe, C., Poole, S., Luheshi, G.N., Dantzer, R., 2008. Central nervous action of interleukin-1 mediates activation of limbic structures and behavioural depression in response to peripheral administration of bacterial lipopolysaccharide. Eur J Neurosci 28, 2499-2510.

Konsman, J.P., Vigues, S., Mackerlova, L., Bristow, A., Blomqvist, A., 2004. Rat brain vascular distribution of interleukin-1 type-1 receptor immunoreactivity: relationship to patterns of inducible cyclooxygenase expression by peripheral inflammatory stimuli. Journal of Comparative Neurology 472, 113-129.

Kreis, D., Schulz, D., Stein, M., Preuss, M., Nestler, U., 2011. Assessment of parameters influencing the blood flow velocities in cerebral arteries of the rat using ultrasonographic examination. Neurological Research 33, 389-395.

Laflamme, N., Lacroix, S., Rivest, S., 1999. An essential role of interleukin-1beta in mediating NF-kappaB activity and COX-2 transcription in cells of the blood-brain barrier in response to a systemic and localized inflammation but not during endotoxemia. J Neurosci 19, 10923-10930.

Levy, M.M., Fink, M.P., Marshall, J.C., Abraham, E., Angus, D., Cook, D., Cohen, J., Opal, S.M., Vincent, J.L., Ramsay, G., 2003. 2001 SCCM/ESICM/ACCP/ATS/SIS International Sepsis Definitions Conference. Intensive Care Med 29, 530-538.

MacDonald, M.E., Frayne, R., 2015. Cerebrovascular MRI: a review of state-of-the-art approaches, methods and techniques. NMR Biomed 28, 767-791.

Maekawa, T., Fujii, Y., Sadamitsu, D., Yokota, K., Soejima, Y., Ishikawa, T., Miyauchi, Y., Takeshita, H., 1991. Cerebral circulation and metabolism in patients with septic encephalopathy. Am J Emerg Med 9, 139-143.

Moller, K., Strauss, G.I., Qvist, J., Fonsmark, L., Knudsen, G.M., Larsen, F.S., Krabbe, K.S., Skinhoj, P., Pedersen, B.K., 2002. Cerebral blood flow and oxidative metabolism during human endotoxemia. J Cereb Blood Flow Metab 22, 1262-1270.

Morandi, A., Rogers, B.P., Gunther, M.L., Merkle, K., Pandharipande, P., Girard, T.D., Jackson, J.C., Thompson, J., Shintani, A.K., Geevarghese, S., Miller, R.R., 3rd, Canonico, A., Cannistraci, C.J., Gore, J.C., Ely, E.W., Hopkins, R.O., 2012. The relationship between delirium duration, white matter integrity, and cognitive impairment in intensive care unit survivors as determined by diffusion tensor imaging: the VISIONS prospective cohort magnetic resonance imaging study*. Crit Care Med 40, 2182-2189.

Niwa, K., Araki, E., Morham, S.G., Ross, M.E., Iadecola, C., 2000. Cyclooxygenase-2 contributes to functional hyperemia in whisker-barrel cortex. J Neurosci 20, 763-770.

Polito, A., Eischwald, F., Maho, A.L., Polito, A., Azabou, E., Annane, D., Chretien, F., Stevens, R.D., Carlier, R., Sharshar, T., 2013. Pattern of brain injury in the acute setting of human septic shock. Crit Care 17, R204.

Renaud, N., Sachez, S., Raffard, G., I., S., Franconi, J.M., Konsman, J.P., Hiba, B., 2013. In vivo 3D-q-space imaging of the adult rat brain during energy failure European Society Magnetic Resonance in Medicine and Biology, Springer, Toulouse.

Rosengarten, B., Hecht, M., Auch, D., Ghofrani, H.A., Schermuly, R.T., Grimminger, F., Kaps, M., 2007. Microcirculatory dysfunction in the brain precedes changes in evoked potentials in endotoxin-induced sepsis syndrome in rats. Cerebrovasc Dis 23, 140-147.

Rosengarten, B., Hecht, M., Wolff, S., Kaps, M., 2008a. Autoregulative function in the brain in an endotoxic rat shock model. Inflamm Res 57, 542-546.

Rosengarten, B., Walberer, M., Allendoerfer, J., Mueller, C., Schwarz, N., Bachmann, G., Gerriets, T., 2008b. LPS-induced endotoxic shock does not cause early brain edema formation - an MRI study in rats. Inflamm Res 57, 479-483.

Ruiz-Valdepenas, L., Martinez-Orgado, J.A., Benito, C., Millan, A., Tolon, R.M., Romero, J., 2011. Cannabidiol reduces lipopolysaccharide-induced vascular changes and inflammation in the mouse brain: an intravital microscopy study. J Neuroinflammation 8, 5.

Sawamura, S., Obara-Nawata, M., Takeda, K. and Hanaoka, K., 2004. General anesthetics inhibit the nitrous-oxide-induced activation of corticotropin releasing factor containing neurons in rats. Eur J Pharmacol 503, 49-53.

Schiltz, J.C., Sawchenko, P.E., 2002. Distinct brain vascular cell types manifest inducible cyclooxygenase expression as a function of the strength and nature of immune insults. Journal of Neuroscience 22, 5606-5618.

Sharshar, T., Carlier, R., Bernard, F., Guidoux, C., Brouland, J.P., Nardi, O., de la Grandmaison, G.L., Aboab, J., Gray, F., Menon, D., Annane, D., 2007. Brain lesions in septic shock: a magnetic resonance imaging study. Intensive Care Med 33, 798-806.

Shen, Q., Huang, S., Duong, T.Q., 2015. Ultra-high spatial resolution basal and evoked cerebral blood flow MRI of the rat brain. Brain Res 1599, 126-136.

Sicard, K., Shen, Q., Brevard, M.E., Sullivan, R., Ferris, C.F., King, J.A., Duong, T.Q., 2003. Regional cerebral blood flow and BOLD responses in conscious and anesthetized rats under basal and hypercapnic conditions: implications for functional MRI studies. J Cereb Blood Flow Metab 23, 472-481.

Singh, A.K., Jiang, Y., 2004. How does peripheral lipopolysaccharide induce gene expression in the brain of rats? Toxicology 201, 197-207.

Sprung, C.L., Peduzzi, P.N., Shatney, C.H., Schein, R.M., Wilson, M.F., Sheagren, J.N., Hinshaw, L.B., 1990. Impact of encephalopathy on mortality in the sepsis syndrome. The Veterans Administration Systemic Sepsis Cooperative Study Group. Crit Care Med 18, 801-806.

Stefanovic, B., Bosetti, F., Silva, A.C., 2006. Modulatory role of cyclooxygenase-2 in cerebrovascular coupling. Neuroimage 32, 23-32.

Stejskal, E.O., Tanner, J.E., 1965. Spin diffusion measurements: spin echoes in the presence of a time-dependent field gradient. J Chem Phys 42, 282-292.

Swanson, L.W., 1998. Brain Maps: Structure of the Rat Brain. Elsevier, Amsterdam.

Tetrault, S., Chever, O., Sik, A., Amzica, F., 2008. Opening of the blood-brain barrier during isoflurane anaesthesia. Eur J Neurosci 28, 1330-1341.

Underwood, S.R., Firmin, D.N., Klipstein, R.H., Rees, R.S., Longmore, D.B., 1987. Magnetic resonance velocity mapping: clinical application of a new technique. Br Heart J 57, 404-412.

Villega, F., Delpech, J.C., Griton, M., Andre, C., Franconi, J.M., Miraux, S., Konsman, J.P., 2017. Circulating bacterial lipopolysaccharide-induced inflammation reduces flow in brain-irrigating arteries independently from cerebrovascular prostaglandin production. Neuroscience 346, 160-172.

Wilson, J.X., Young, G.B., 2003. Progress in clinical neurosciences: sepsis-associated encephalopathy: evolving concepts. Can J Neurol Sci 30, 98-105.

Xaio, H., Banks, W.A., Niehoff, M.L., Morley, J.E., 2001. Effect of LPS on the permeability of the blood-brain barrier to insulin. Brain Res 896, 36-42.

Yamagata, K., Matsumura, K., Inoue, W., Shiraki, T., Suzuki, K., Yasuda, S., Sugiura, H., Cao, C., Watanabe, Y., Kobayashi, S., 2001. Coexpression of microsomal-type prostaglandin E synthase with cyclooxygenase-2 in brain endothelial cells of rats during endotoxin-induced fever. J Neurosci 21, 2669-2677.

Yasui, M., Nakao, A., Yuuki, T., Harada, A., Nonami, T., Takagi, H., 1995. Immunohistochemical detection of endotoxin in endotoxemic rats. Hepato-Gastroenterology 42, 683-690.

Table and figures

Region	Occurrence / section	ANOVA	Occurrence x extent /section	ANOVA
Cortex	Sal: 0.640 ± 0.284	NS	Sal: 0.750 ± 0.333	NS
	LPS: 1.102 ± 0.221		LPS: 1.244 ± 0.299	
deep MO-SS	Sal: 0.016 ± 0.010	NS	Sal: 0.016 ± 0.010	NS
	LPS: 0.062 ± 0.027		LPS: 0.073 ± 0.030	
Striatum	Sal: 0.105 ± 0.039	LPS > Sal p<0.05	Sal: 0.105 ± 0.039	LPS > Sal p<0.05
	LPS: 0.559 ± 0.167		LPS: 0.636 ± 0.167	
CP	Sal: 0.105 ± 0.039	LPS > Sal p<0.05	Sal: 0.105 ± 0.0039	LPS > Sal p<0.05
	LPS: 0.389 ± 0.109		LPS: 0.430 ± 0.121	
White matter	Sal: 0.301 ± 0.054	LPS > Sal	Sal: 0.400 ± 0.082	LPS > Sal
	LPS: 1.066 ± 0.188	p<0.01	LPS: 1.232 ± 0.222	p<0.01
cc-ec	Sal: 0.141 ± 0.053	NS	Sal: 0.157 ± 0.059	NS
	LPS: 0.198 ± 0.082		LPS: 0.294 ± 0.128	
vhc	Sal: 0.046 ± 0.031	LPS > Sal p=0.053	Sal: 0.064 ± 0.042	LPS > Sal p=0.068
	LPS: 0.201 ± 0.059		LPS: 0.217 ± 0.060	

Table 1: Occurrence and extent of perivascular immunoglobulin G diffusion in forebrain sections of animals injected ip with saline or LPS. cc: corpus callosum; CP: caudate putamen; ec: external capsule; fi: fimbria; IgG: immunoglobulin G; MO: motor cortex; NS: non-significant; SS: somatosensory cortex; st: stria terminalis; vhc: ventral hippocampal commissure. Group sizes Sal: n=9; LPS: n=12.

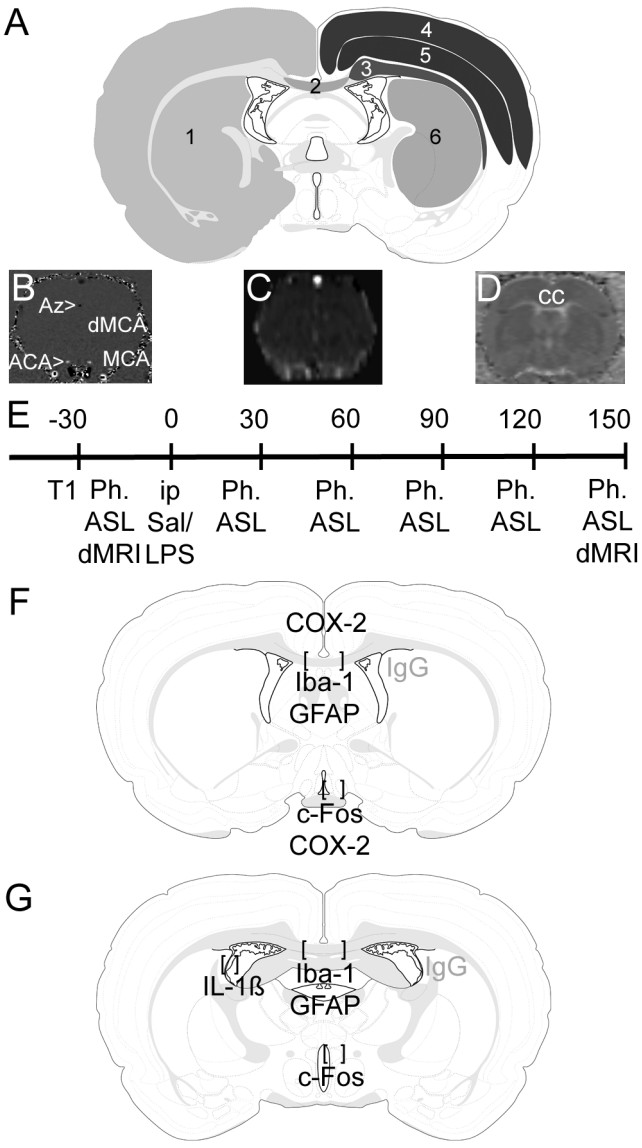

Figure 1 :

Placement of different Region Of Interest (ROIs; A) to analyze phase contrast (example in B), perfusion-weighted (example in C) and diffusion-weighted images (example in D), timeline (E in min) representing when different imaging sequences were performed and text labels indicating which parts of the brain were studied with immunohistochemistry (F and G). 1: hemisphere; 2: corpus callosum; 3 external capsule; 4 and 5: superficial and deep layers of the primary motor and sensory cortices (considered separately for perfusion-weighted images and together for diffusion-weighted images); and 6: striatum. ACA: anterior cerebral artery; ASL: aterial spin labeling; Az: pericallosal azygos artery; cc: corpus callosum; COX-2: cyclooxygenase-2; dMCA: dorsal branch of middle cerebral artery; dMRI: diffusion-weighted imaging; GFAP: glial fibrillary acidic protein; Iba-1: ionized calcium-binding adaptor molecule-1; IgG: immunoglobulin G; IL-1β: interleukin-1β; LPS: lipopolysaccharides; MCA: middle cerebral artery; Ph.: Phase contrast imaging; Sal: saline; T1; T1-weighted imaging..

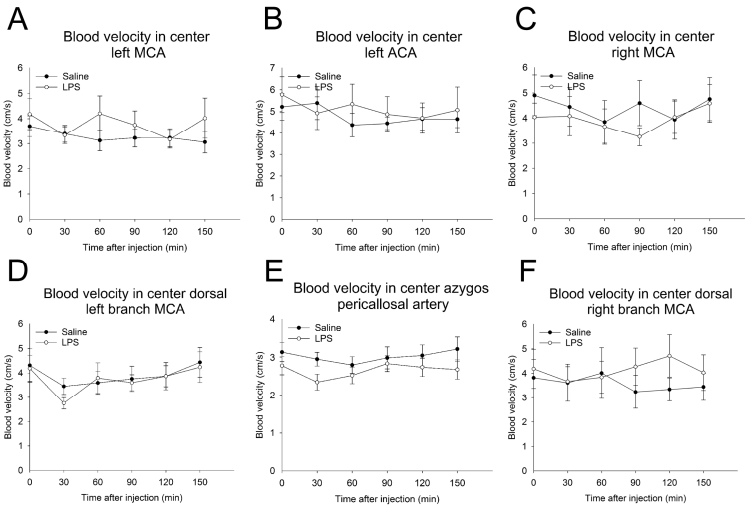

Figure 2 :

Blood flow velocities in the center of the ventral left and right middle cerebral arteries (A, C), ventral left anterior cerebral artery (Figure 2B), dorsal left and right branches of middle cerebral arteries (D, F), and pericallosal azygos artery (E) obtained with phase contrast imaging. Graphs represent flow velocity over post-injection time points after ip saline or LPS administration in isoflurane-anesthetized rats. Group sizes Sal: n=8; LPS: n=9-10.

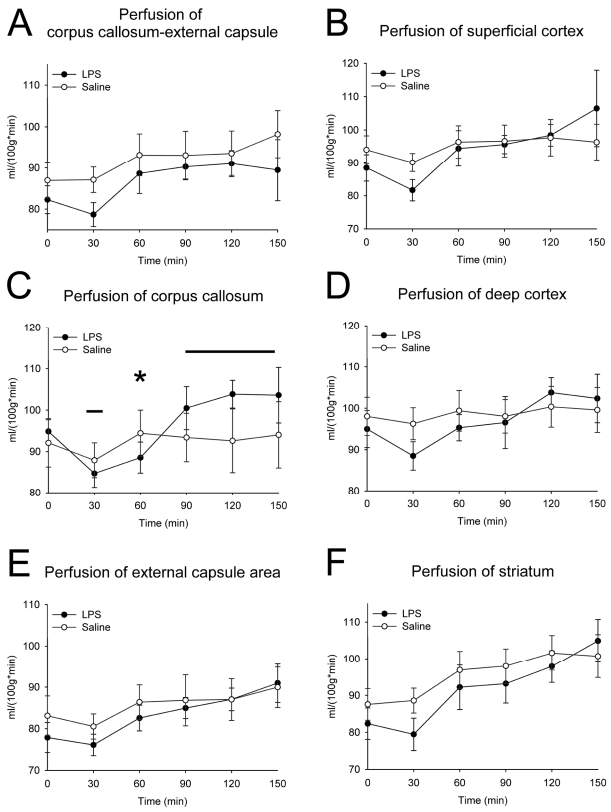

Figure 3 :

Perfusion of the white matter of the corpus callosum, cingulum and external capsule combined (A), and of the corpus callosum (C) and external capsule (E) alone as well as of the grey matter of the superficial (B) and deep cortical layers (D) and striatum (F). Graphs represent perfusion over post-injection time points after ip saline or LPS administration in isoflurane-anesthetized rats. *: $p < 0.05$. Group sizes Sal: n=8; LPS: n=8

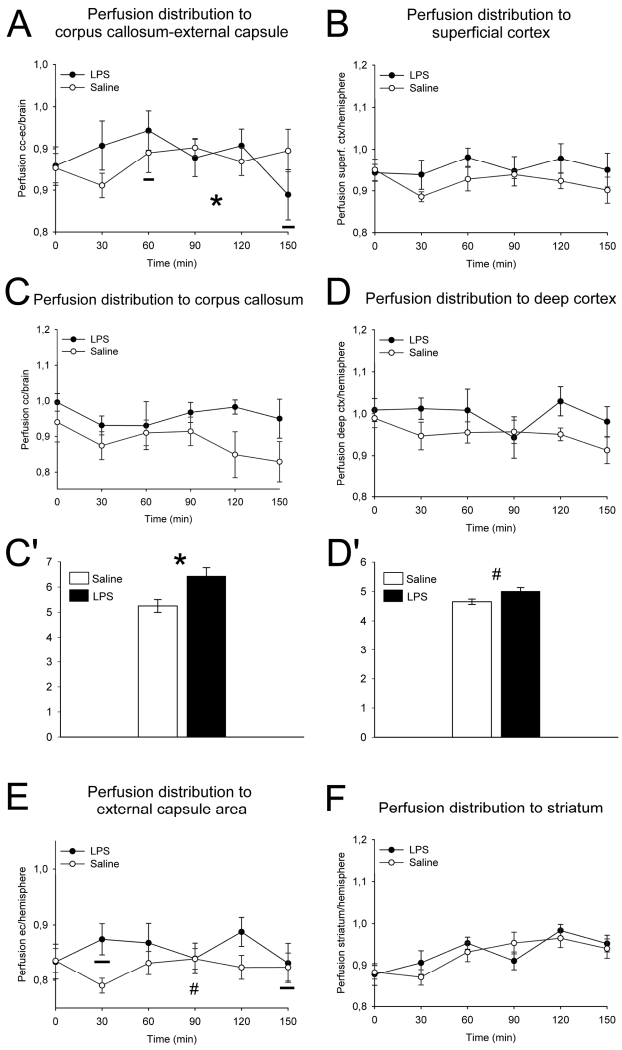

Figure 4

Perfusion distribution to the white matter of the corpus callosum, cingulum and external capsule combined (A), and to the corpus callosum (C and C') and external capsule (E) alone, as well as to the grey matter of the superficial (B) and deep cortical layers (D and D') and striatum (F). Graphs represent perfusion relative to the global brain (corpus callosum) or ipsilateral hemisphere (cortex) over post-injection time points after ip saline or LPS administration in isoflurane-anesthetized rats. C' and D' represent cumulated perfusion relative to global brain (corpus callosum) or ipsilateral hemisphere (cortex) after ip saline or LPS administration. *: $p < 0.05$ or $p < 0.01$ (between saline and LPS treatment in C' and between underscored _ time points in LPS-treated animals in A); #: $p < 0.10$ (between saline and LPS treatment in D' and between underscored _ time points in LPS-treated animals in E). Group sizes Sal: n=8; LPS: n=8.

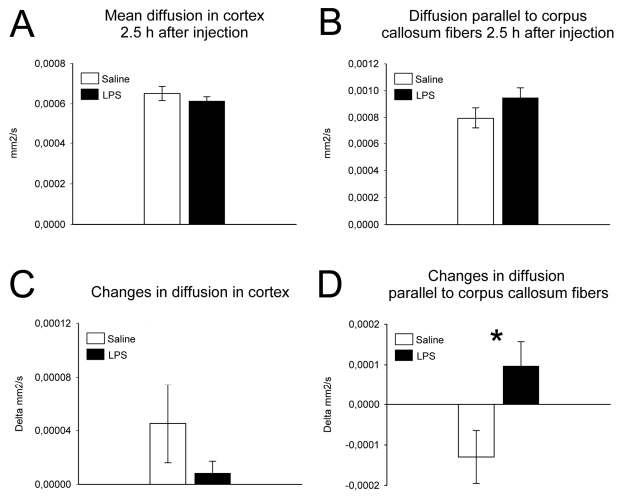

Figure 5:

Mean diffusion in the cortex (A) and diffusion parallel to fibers of the corpus callosum (B) 2.5 h after intraperitoneal injection of saline or bacterial LPS in isoflurane-anesthetized rats. Changes in water diffusion in the cortex (C) and horizontal water diffusion in the corpus callosum (D) after ip saline or LPS administration in isoflurane-anesthetized rats. *: $p < 0.05$. Group sizes Sal: n=7; LPS: n=9

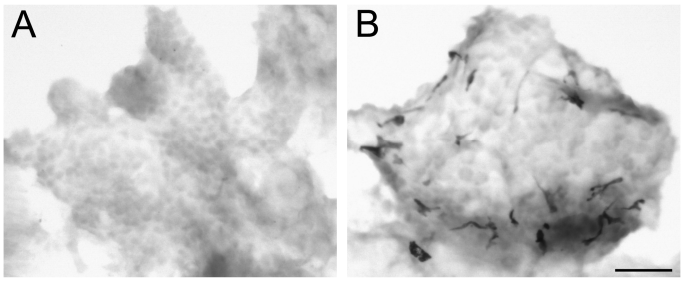

Figure 6 :

Photomicrographs illustrating Interleukin-1beta-ir in choroid plexus 2.5 h after intraperitoneal injection of saline (A) or bacterial LPS (B) in isoflurane-anesthetized rats. Scale bar = 50 µm.

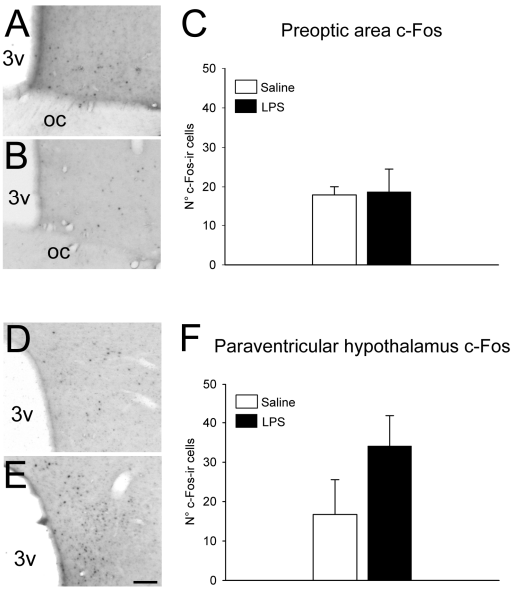

Figure 7 :

Quantitative analysis of the number of c-Fos-positive cells in the preoptic area (A-C) and paraventricular nucleus (D-F) of the hypothalamus and 2.5 h after intraperitoneal injection of saline or bacterial LPS in isoflurane-anesthetized rats. Sal: n=5-7; LPS: n=5-8. Scale bar = 100 µm.

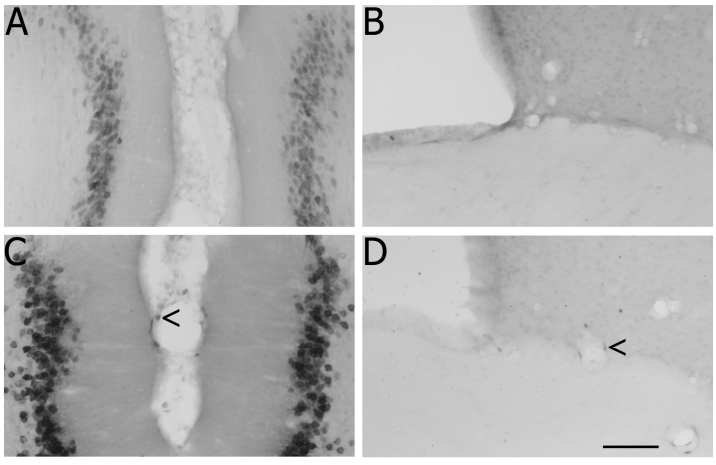

Figure 8 :

Photomicrographs illustrating the distribution of COX-2-ir in and between the cortical hemispheres (A and C) and in the ventromedial preoptic area (B and D) 2.5 h after intraperitoneal injection of saline (A, B) or bacterial LPS (C, D) in isoflurane-anesthetized rats. 3v: third ventricle; oc: optic chiasm. Arrow heads > and < indicate labeling. Scale bar = 100 µm.

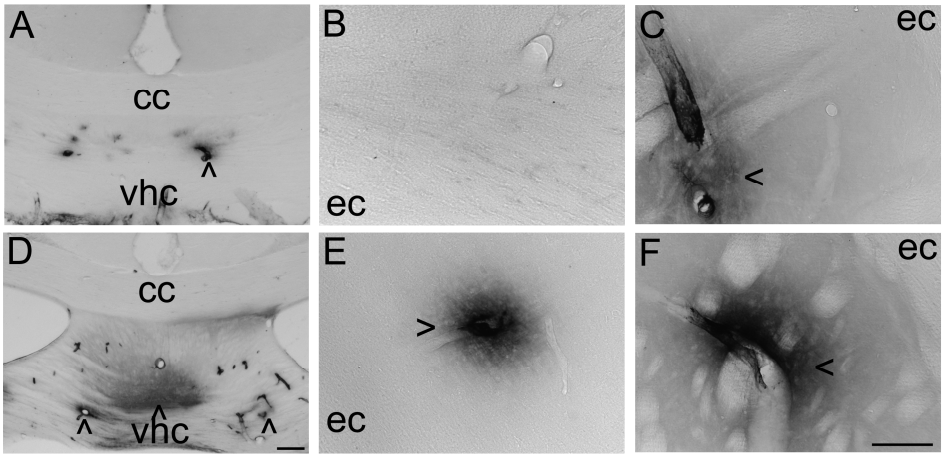

Figure 9:

Photomicrographs illustrating the distribution of rat IgG-ir in the corpus callosum and ventral hippocampal commissure (A and D), deep layers of the somatosensory cortex (B and E) and dorsoslateral caudate putamen (C and F) 2.5 h after intraperitoneal injection of saline (A to C) or bacterial LPS (D to F) in isoflurane-anesthetized rats. cc: corpus callosum; ec: external capsule; vhc: ventral hippocampal commissure. Arrow heads >, < and ^ indicate perivascular diffuse cloud-like labeling. Scale bar = 100 µm.

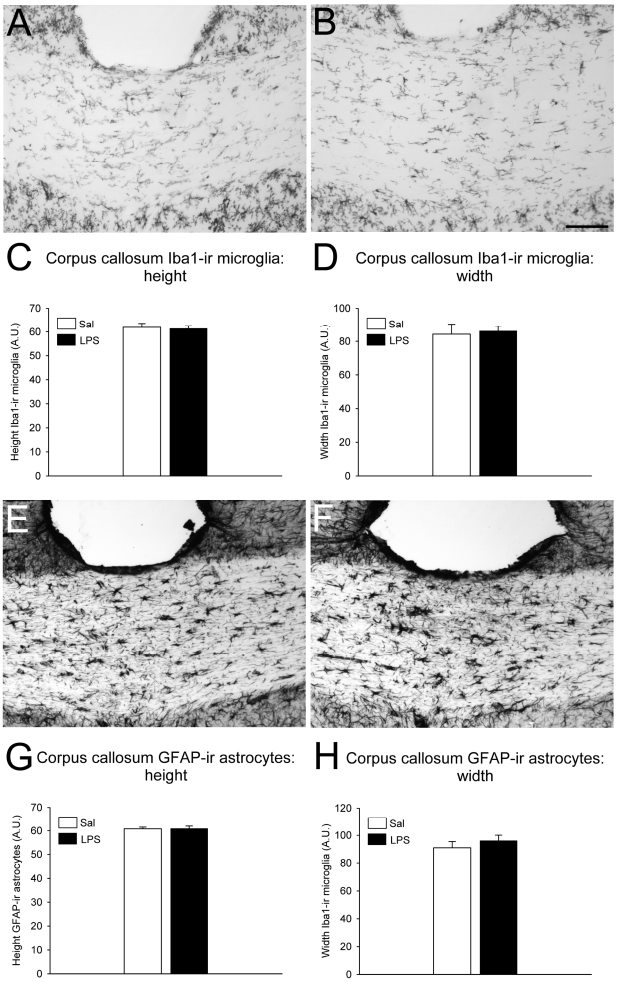

Figure 10 :

Photomicrographs illustrating Iba1-ir microglia (A-D) and GFAP-ir astrocytes (E-H) in the corpus callosum 2.5 h after intraperitoneal injection of saline (A, E) or bacterial LPS (B, F) in isoflurane-anesthetized rats. Quantitative Fraclac-based analysis of microglial height (C, G) and width (D, H) in the corpus callosum on brain sections situated between bregma -0.11 and -1.33 mm. Group sized Sal: n=7; LPS: n=9. Scale bar = 100 µm.

Chapter 3

Cecal ligature and puncture-induced systemic inflammation increases water diffusion in white matter-rich regions in the absence of blood-brain barrier breakdown: relationships to changes in glial cell morphology

Marion Griton[a,b,c$] ,Ibtihel Dhaya[a,b,d$], Gérard Raffard[e,f], Mohamed Amri[d], Olivier Periot[a,b,g], Bassem Hiba[a,b#] and Jan Pieter Konsman[a,b#*]

a INCIA, Institut de Neurosciences Cognitive et Intégrative d'Aquitaine, UMR 5287, Bordeaux, France

b Univ. Bordeaux, INCIA, UMR 5287, Bordeaux, France

c Service de Réanimation Anesthésie Neurochirurgicale, Centre Hospitalier Universitaire (CHU) de Bordeaux, Bordeaux, France

d Laboratoire de Neurophysiologie Fonctionnelle et Pathologies, UR/11ES09, Faculté des Sciences Mathématiques, Physiques et Naturelles, Université de Tunis El Manar, Tunis, Tunisie

e CNRS, Résonance Magnétique des Systèmes Biologiques, UMR 5536, Bordeaux, France

f Univ. Bordeaux, RMSB, UMR 5536, Bordeaux, France

g Service de Médecine Nucléaire, Centre Hospitalier Universitaire (CHU) de Bordeaux, Bordeaux, France

Running title: CLP increases white matter axial diffusion

$ contributed equally to the present work

co-senior authors

Abbreviations used:

AD: axial diffusivity ;
ADC : apparent diffusion coefficient;
AFNI: Analysis of Functional NeuroImages;
AQP4: aquaporin 4;
ASL: aterial spin labeling;
BBB: blood-brain barrier;
CBF: cerebral blood flow;
cc: corpus callosum;
CLP: cecal ligation and puncture;
CNPase: 2',3'-cyclic nucleotide 3'-phosphodiesterase;
COX-2: cyclooxygenase-2;
DTI: diffusion-tensor imaging;
DWI: diffusion-weighted imaging;
ec: external capsule;
EPI : Echo Planar Imaging;
FA: fractional anisotropy;
FAIR: Flow-sensitive Alternating Inversion Recovery;
fi: fimbria;
fMRI: functional magnetic resonance imaging;
FSL: FMRIB's Software Library
GFAP: glial fibrillary acidic protein;
Iba-1: ionized calcium-binding adaptor molecule;
IgG: immunoglobulin G;
LPS: lipopolysaccharide;
MCA: middle cerebral area;
MD: mean diffusivity;
MRI : magnetic resonance imaging;
NS: non-significant;
och: optic chiasm.
RD: radial diffusivity;
ROI: Regions Of Interest;
SAE: sepsis-associated encephalopathy;
SFO: subfornical organ;
T1: T1-weighted imaging;
T2: T2-weighted imaging;
TBSS: tract-based spatial statistics;
TFCE: threshold-free cluster enhancement;
vhc: ventral hippocampal commissure;
VOI: Volume Of Interest.

Abstract

Sepsis-associated encephalopathy (SAE) has been proposed to be due to reduced cerebral blood flow (CBF), blood-brain barrier breakdown (BBB), edema, white matter damage and glia cell activation, but their exact relationships remain to be determined. In the present work, we therefore set out to study CBF using Arterial Spin Labeling (ASL) and gray and white structure with T2- and Diffusion-Weighted imaging (DWI) in rats with cecal ligature and puncture (CLP)-induced signs of central nervous system dysfunction. The vasoactive prostaglandin-synthesizing enzyme cyclooxygenase-2 (COX-2), perivascular immunoglobulins G (IgG), aquaporin-4 (AQP4) and glia cells were subsequently detected in the brains of the same animals using immunohistochemical approaches. CLP induced deficits in the righting reflex and resulted in higher T2-weighted contrast intensities in the cortex, striatum and base of the brain, decreased blood perfusion distribution to the cortex and increased the anisotropy of water diffusion in the corpus callosum and ventral striatum compared to sham surgery. In these same animals, CLP reduced the number of fragments staining for microglia- and astrocytic-specific proteins, decreased neuronal COX-2 and AQP4 expression in the cortex while inducing perivascular COX-2 expression while , but not widespread perivascular IgG diffusion. In conclusion, our findings indicate that experimental SAE can occur in the absence of BBB breakdown and is accompanied by increased of water diffusion anisotropy and altered glia cell morphology in brain white matter.

Keywords

Arterial spin labeling, blood-brain barrier, cecal ligation and puncture, cerebral blood flow, diffusion magnetic resonance imaging, glia, sepsis

Introduction

Sepsis-associated encephalopathy (SAE), including *delirium*, has been proposed to be related to reduced cerebral blood flow (CBF) and oxygen extraction as well as blood-brain barrier breakdown and edema (Papadopoulos, Davies, Moss, Tighe, & Bennett, 2000), but the exact relationships between these phenomena remain to be determined. Indeed, during SAE global or incoming baseline CBF has been shown to be reduced (Bowton, Bertels, Prough, & Stump, 1989; Maekawa et al., 1991; Pfister et al., 2008; Pierrakos et al., 2013, 2014; S M Smith, Padayachee, Modaresi, Smithies, & Bihari, 1998; Yokota, Ogawa, Kurokawa, & Yamamoto, 2003). Moreover, systematic assessment of middle cerebral artery (MCA) blood velocity to variations in arterial blood pressure indicates that impaired cerebral autoregulation is associated with sepsis-associated *delirium* (Pfister et al., 2008; Schramm et al., 2012).

Concomitantly with vasospasms in the MCA of patients with sepsis and brain dysfunction, T2- and diffusion-weighted Magnetic Resonance Imaging (MRI) have indicated white matter edema (Bartynski, 2008; Sharshar et al., 2007). Interestingly, *delirium* has been found to be associated with white matter disruption at hospital discharge and 3 months later, which, in turn, was associated with long-term cognitive impairment (Morandi et al., 2012). Hence, SAE has been shown to be associated with reduced CBF and signs of edema formation.

Intravenous administration of bacterial lipopolysaccharide (LPS) fragments in human volunteers is sufficient to reduce global or incoming CBF (Møller et al., 2002; Pollard et al., 1997), but enhances cerebral autoregulation (R. M. Berg et al., 2012; R. M. G. Berg et al., 2013; R. M. G. Berg, Plovsing, Bailey, Holstein-Rathlou, & Møller, 2016) After systemic administration of LPS in animals, some studies have also observed rapidly decreased global or incoming CBF (Bryan & Emerson, 1977; Christenson, Kuikka, Owunwanne, & Al-Sarraf, 1986; EkströmJodal, Häggendal, Larsson, & Westerlind, 1982; Tempel, Cook, Wise, Halushka, & Corral, 1986; Villéga et al., 2017; F Wyler, Forsyth, Nies, Neutze, & Melmon, 1969; Felix Wyler, Rutishauser, & Weisser, 1972; Zhen, 1987)

However, other studies have shown increased CBF in cortical MCA territories, but dose-dependent impaired autoregulation of CBF, after intravenous LPS administration (Rosengarten et al., 2007; Rosengarten, Hecht, Wolff, & Kaps, 2008), yet in the absence of edema (Rosengarten, Walberer, et al., 2008). So, even though systemic LPS administration mimics some of the cerebral alterations observed in clinical SAE, it far more reproduces all and may, therefore, not be the best model to improve our understanding SAE.

Cecal ligature and puncture (CLP) is a more clinically-relevant sepsis model than systemic LPS administration in that it involves live bacteria and mimics the different hemodynamic phases observed in clinical sepsis. Interestingly, during the first 24 h after CLP, CBF has been shown to be preserved (Hinkelbein et al., 2007) while increased T2-weighted contrast at the base of the brain suggested vasogenic edema and restricted apparent diffusion coefficient (ADC) indicated cytotoxic edema in the cortex and hippocampus (Bozza et al., 2010). Yet, neither of these studies addressed SAE in animals that underwent CLP.

In the present work, we therefore set out to study CBF and brain gray and white microstructure using Arterial Spin Labeling (ASL) and Diffusion Weighted imaging (DWI), respectively, in animals with CLP-induced signs of SAE. In addition, we also detected the vasoactive prostaglandin-synthesizing enzyme cyclooxygenase-2 (COX-2), which is upregulated under inflammatory response, the presence of perivascular immunoglobulins G (IgG) as a measure of BBB integrity, and modifications of glia cell morphology in the brains of the same animals.

Materials and methods

Animals

Twenty-one male 3.5 month old Wistar rats (Charles River, l'Abresle, France) weighing 340.3 ± 3.6 g were used. Animals were treated according to European recommendations on animal research (European Council Directive of 24 November 1986 (86/609/EEC) and European Parliament and Council Directive of 22 September 2010 (2010/63/UE)), housed 2 per cage in a temperature-controlled room (22.0 ± 1.0°C) with lights on from 8 AM to 8 PM with free access to water and food. After arrival rats were left undisturbed for at least a week except for daily handling starting three days before surgery.

Surgery

On the day of surgery, animals were anesthetized with isoflurane (induction 3-5%; maintenance 1.5% in air). Once anesthetized, seventeen rats underwent polymicrobial intra-abdominal infection induced by CLP as previously described (Rittirsch, Huber-lang, Flierl, & Ward, 2009; Wichterman, Baue, & Chaudry, 1980). Briefly, after a 2-3-cm midline abdominal incision, the cecum was exposed in sterile saline on laboratory film (Parafilm, Neenah, WI, USA) and ligated with a 3-0 silk suture (Ethicon, Issy les Moulineaux, France) just below the ileocecal valve and subsequently punctured twice with a 22 G sterile needle.

Next, a small drop of cecal contents was gently pushed out, before the cecum was gently placed back into the peritoneal cavity and the abdomen was sutured in two layers. At the end of the operation, animals received 5 ml of saline and analgesia (butrophanol, Torbugesic®; 2 mg/kg subcutaneously) and were placed in a clean individual cage. For the ten rats that were sham-operated rats, the same manipulations were performed except cecal ligation and puncture and saline injection. Thirty minutes after the end of surgery animals were awake and moving around.

Behavioral evaluation

Daily food and water intake and body weight were measured prior and posterior to surgery. Sham and CLP -operated rats were tested at different time points before and after surgery for two simple non-postural (pinna and corneal reflexes) and one complex postural somatomotor reflex (Righting reflex).

The pinna reflex was assessed by lightly touching the auditory meatus with a cotton stick tip and recording the occurrence and rapidity of ear retraction or head shake. The corneal reflex was tested by gently touching the cornea with a cotton stick tip and scoring the occurrence and rapidity of eye blinks. The righting reflex consisted of picking up the animal behind the forepaws and holding its trunk horizontally back upwards before putting the animal's back down and evaluating the time required to turn over to an upright position.

Magnetic Resonance Imaging

Twenty-four hours after surgery, animals were anesthetized again with isoflurane (induction 3-5%, maintenance 1.5%) and introduced into a 7 T horizontal-bore scanner (Advance III console, Bruker, Ettlingen, Germany) equipped with a magnetic field gradient system providing a maximum magnetic field gradient amplitude of 650 mT/m. A quadrature coil was used for radio-frequency emission and a 4-element phased-array surface coil for signal reception. Intracolonic temperature was constantly monitored and the animal was heated when colonic temperature dropped below 35.5°C by warm water circulating in the bed used to position the rat inside MRI scanner. Respiration was assessed with a ventral pressure sensor and heart rate recorded using an MRI compatible electrode. After careful second-order shimming, the following images were acquired.

Anatomical T1-weighted MRI

T1-weighted images were obtained with a FLASH (Fast Low Angle Shot) pulse sequence with the following parameters: repetition time [TR]/echo time [TE]: 15/2.5 ms; flip angle: 30°; voxel size: 117×117×234 μm^3; Field of View (FOV): 30×30×30 mm^3; acquisition time: 6 min.

Morphological T2-weighted MRI

T2-weighted images were acquired using a Rapid Acquisition with Relaxation Enhancement (RARE) sequence with the following parameters: repetition time: 3.64 s, echo time: 70 ms, flip angle: 90°, RARE factor: 16, number adjacent (non-contiguous) axial slices: 20, slice thickness: 0.7 mm, image matrix size: 196×196 pixels, FOV: 25×25 mm^2 and in plan spatial resolution of 128 µm, 8 averages were acquired giving a total acquisition time of 4 min 51 s.

Arterial Spin Labeling (ASL)

The accuracy of ASL-FAIR to quantify brain perfusion in the rat at low, normal, and moderately increased flows has been validated by a direct comparison with the cerebral distribution of intravenously-injected radioactive microspheres (Boś et al., 2012). Arterial Spin Labeling data were acquired from a single 1.5 mm-thick axial slice, with a FOV of 35×35 mm^2 using a Flow-sensitive Alternating Inversion Recovery–Echo Planar Imaging) pulse sequence (FAIR-EPI) (Kim & Tsekos, 1997). The acquisition was performed twice, first with selective inversion of the slice and then with a global inversion recovery technique (Kober et al., 2004). For each of these acquisitions, and based on previous publications (Carr, Buckley, Tessier, & Parker, 2007), the following parameters were used: TR/TE 16000/15 ms; flip angle: 90°; number of averages: 6; inversion times: 0.2, 0.6, 0.8, 0.9, 1.0, 1.1, 1.2, 1.5, 2.0, and 2.5 sec; acquisition duration: 14 min 25 s.

Diffusion-weighted imaging (DWI)

A Stejskal-Tanner Echo Planar Imaging (EPI) pulses sequence was used to collect diffusion-weighted images (Stejskal & Tanner, 1965). A multi-shot 3D EPI sampling of Fourier space was used to increase the sensitivity of diffusion- weighted MRI (Nicolas et al., 2013). Twenty-one DW-images were acquired with b-value =1000 s/mm^2 applied along 21 non-collinear diffusion encoding directions (B1000 images). One other DW image was acquired with b-value = 0 s/mm2 (B0 image). DW-images were recorded with the following

parameters: TR/TE=1200/36.86 ms; voxel size: 153×148×333 μm^3; FOV: 30×22×16 mm^3; flip angle: 90°; acquisition duration: 22 min 4 s.

Image processing

All pre-treatments, parametric map computing, definition of Regions Of Interest (ROIs) and measurements of ROIs were performed using ParaVision software (Bruker, Ettlingen, Germany) unless otherwise indicated.

T2 data processing

Analysis of T2-weighted images was performed using mipav (https://mipav.cit.nih.gov). In this study, an approximation of the T2 quantification, based on one T2-weighted image, was used to determine the presence rather than quantifying the edematic fluid. Volumes Of Interest (VOIs) were defined in the brain and in the skull muscles. Max intensity, sum intensities and average intensities obtained in brain VOIs were divided by those obtained in the skull muscle VOIs following Abdel-Aty et al., 2005 (Abdel-Aty et al., 2005), then compared between the two groups.

The first VOI at the base of the brain was made up of 3 parts (right, left and center) to avoid blood vessels. The corresponding areas were summed together to cover the base of the rat brain (in bregma ~ -0,46 mm). The other VOIs were cortex, striatum (right and left) and corpus callosum.

ASL data processing

Two (selective and global) T1 maps were computed using selective and global FAIR data sets. Relative cerebral blood flow (rCBF) map was then computed pixel by pixel according to Kober et al. (2004). Blood T1 measured on rat blood at 7 T was set at 2070 ms (Dobre, Uğurbil, & Marjanska, 2007; Esparza-Coss, Wosik, & Narayana, 2010). To analyze perfusion data, ROIs corresponding to the global brain or hemisphere, to the grey matter of the primary motor and sensory cortices and striatum as well as to the white matter of the corpus callosum and the external capsule were traced manually on each individual's selective inversion 1100 ms FAIR image using a rat brain atlas (Swanson, 1998) for guidance. These ROIs were then copied onto perfusion-weighted images (Figure 1). For the ROIs covering the global brain or hemispheres cerebrospinal fluid-containing voxels were excluded. For the ROI centered on the corpus callosum, the lateral limits were the medial borders of the lateral ventricle to avoid inclusion of the cingulum.

Diffusion MRI data processing

The *3dSkullStrip* command included in Analysis of Functional NeuroImages software (AFNI) (https://afni.nimh.nih.gov) was used with the rat parameter: 1) to extract the brain from the surrounding within the DWI data, 2) to create a mask for the following reconstruction steps, carefully checked and manually adjusted when it was necessary. Using *dtifit* which is part of the FMRIB's Software Library (FSL) (http://www.fmrib.ox.ac.uk/fsl), the twenty-one diffusion-weighted images and the B0 image were corrected for eddy currents, The following diffusion-tensor maps were computed: 1) Eigenvalues ($\lambda1$, $\lambda2$ and $\lambda3$) corresponding to the three diffusivities along the principal axes of the diffusion tensor, 2) Axial Diffusivity (AD=$\lambda1$) representing water diffusivity along the length of the white mater fibers, 3) Radial Diffusivity (RD=($\lambda1$+$\lambda2$)/2) representing water diffusivity perpendicular to the white mater fibers, 4) Mean Diffusivity (MD) corresponding to the Apparent Diffusion Coefficient (ADC) of water and 5) Fractional Anisotropy (FA) indicating the degree of anisotropy of water diffusivity.

ROI-based analyses

ROIs were positioned manually on the corpus callosum at two different rostrocaudal levels (1) the level where the third ventricle is traversed by the junction of the white matter and 2) the level where the third ventricle is divided in its ventral and dorsal part by the grey matter of the paraventricular thalamus) because the cytoarchitecture of this structure is known to vary along the rostrocaudal axis (Barazany, Basser, & Assaf, 2009). Other ROIs were placed on the cortex and striatum at the level where the third ventricle is traversed by the junction of the white matter (Figure1).

Tract-based spatial statistical analyses

To explore diffusion data in a non-hypothesis driven manner, a whole brain voxelwise statistical method adapted to the rat brain was performed using Tract-Based Spatial Statistics (TBSS) which is part of FSL (Stephen M. Smith et al., 2006). FA maps from each rat were co-registered to the *DTI Rat Atlas at Postnatal Day 72* (DTI-RAPnD72) template (https://www.nitrc.org/projects/dti_rat_atlas/) using *fnirt* a nonlinear registration command adapted to take into account rat brain. After image registration, FA maps were averaged to produce a group mean FA image. A skeletonization algorithm was applied to the group mean FA image to define a group template of the lines of maximum FA, thought to correspond to

centers of white matter tracts. FA values for each individual subject were then projected onto the group template skeleton by searching along perpendiculars from the skeleton to find local maxima. Non-FA maps (AD, RD, and MD) were skeletonized according to non-linear warps of the FA registrations described above. Voxelwise analyses across subjects on the skeleton space were carried out for DTI metrics to obtain regions of difference between the control and the CLP animals.

Tissue processing and immunohistochemistry

At the end of MRI, rats were deeply anaesthetized by intraperitoneal injection of 60mg/kg of sodium pentobarbital. Bodies were rinsed from blood by intracardiac perfusion with 0.1 M phosphate-buffered saline (PBS; pH 7.4) and subsequently fixed by 300 ml of 4% paraformaldehyde in 0.1 M PBS. Brains were removed from the skull, post-fixed for 4 h in the same fixative, and then cryoprotected in 30% sucrose in 0.1 M phosphate buffer. Thirty-micrometer thick sections were cut on a cryostat (CM3050 S, Leica Microsystems, Nussloch, Germany) from the rostral limit of the optic chiasm to the caudal end of the central amygdala (Swanson, 1998) and collected in cold cryoprotectant solution (0.05 M PBS, 20 % glycerol, 30% ethylene glycol) and stored at -20°C until processing.

Immunohistochemistry was performed as previously described (J. Konsman, Vigues, Mackerlova, Bristow, & Blomqvist, 2004; Jan Pieter Konsman & Blomqvist, 2005; J P Konsman et al., 2008). Briefly, free-floating sections were washed four times in 0.1 M PBS (pH 7.4). Non-specific binding sites were blocked by a 45-minute incubation of sections in PBS containing 0.3% Triton X-100 and 2.0% normal serum or 1.0% BSA. The first antibody was then diluted (indicated below for every antiserum used) in the same buffer and added to the sections overnight at room temperature.

Commercially available antisera raised against COX-2 (goat anti-COX-2; M-19 sc-1747, lot# F2512,Santa Cruz Biotechnology, Heidelberg, Germany) diluted 1:750, the microglia-macrophage specific ionized calcium-binding adaptor molecule (Iba-1; rabbit anti-Iba-1; 019-19741, Wako Chemicals GmbH, Neuss, Germany) diluted 1:1000 and rat immunoglobulin G (IgG; biotinylated goat anti IgG, BA-9401, Vector Laboratories, Burlingame, CA, USA) diluted 1:2000, the astrocytic aquaporin-4 water channel (rabbit anti-AQP4, cat # AB2218, lot # 2506432, Millipore) diluted 1:2000, the intermediate filament Glial fibrillary acidic protein GFAP (mouse anti-GFAP mAb, clone GA5, MAB360, Merck Millipore, Fontenay sous Bois, France) diluted 1:500, the myelin-associated enzyme 2',3'-Cyclic-nucleotide 3'-

phosphodiesterase also known as CNPase (mouse anti-CNPase, Abcam, Paris, France) diluted 1:8000 were used.

After four rinses in PBS, sections were treated for 30 minutes with 0.3% (v/v) hydrogen peroxide to block endogenous peroxidases followed by four rinses in PBS. With the exception of those sections exposed to biotinylated rat IgG, sections were then incubated for 2h with biotinylated antisera raised against IgGs of the species of the first antibody (Vector Laboratories, Burlingame, CA, USA) diluted 1:500 in PBS, 0.3% Triton X-100, 1% BSA or normal serum. After four washes in PBS, sections were incubated for 2 h with avidin and biotinylated peroxidase complex (Vector Laboratories, Burlingame, CA, USA) diluted in PBS to 1:750 in IgG immunostaining and 1:500 in others. Finally, sections were transferred to a sodium acetate buffer (0.1 M; pH 6.0) and stained using diaminobenzidine as a chromogen in the presence of Ni-ions, thus yielding a dark grey to black precipitate.

Microscopy and image analysis

Staining reactions were stopped by rinses in sodium acetate and PBS, after which sections were mounted on slides in 0.5% gelatin in distilled water containing chromo-potassium sulphate, dehydrated in alcohol, defatted in xylene and coverslipped with Eukitt (O.Kindler GmbH & CO, Freiburg, Brisgau, Germany). Stained sections were examined with a light-microscope (Leica DM5500B, Leica Microsystems, Nanterre, France) and images were captured by a high-resolution digital camera system (Leica DFC425C, Leica Microsystems, Nanterre, France) and stored onto a personal computer. In every brain section between bregma +4,85 and -2,85 mm the occurrence and extent (scored as restricted (1), intermediate (2) or extensive (3)) of perivascular IgG diffusion in a given structure was noted. As each region or structure considered covered at least two, but a varying number (depending on the length of the structure) of, brain sections (with two consecutive sections being separated by 180 µm), the number of occurrences of perivascular IgG diffusion for a structure were then divided by the number of brain sections in which the structure was present. Similarly, the cumulative score of the extent of IgG diffusion for a given brain region or structure was also divided by the number of sections that contained the region or structure in question.

The counts and relative surfaces of AQP4, CNPase, COX-2, GFAP and Iba-1-immunoreactive elements were quantified after application of fixed particle size and intensity criteria on 8-bit images with Image J (http://imagej.nih.gov/ij/). In addition, Iba-1- and GFAP-immunostaining was characterized using the Image J plugin Fraclac

(http://rsb.info.nih.gov/ij/plugins/fraclac/fraclac.html). Briefly, on binary images of brain sections between bregma -0.11 and -1.33 mm, Iba-1-positive cells (size between 300-6000 pixels) and GFAP-immunoreactive cells (size between 300-8000 pixels) were enclosed by a Hull convex (a boundary enclosing the foreground pixels of an image using straight line segments to each outermost point) and bounding circle after which the surface, perimeter and circularity (defined as $4*\pi*Area / Perimeter^2$) were determined in addition to the width and height of the cells. Iba-1 cell size and activation was also evaluated as described by Hovens et al (2014) with Image J. Briefly, a minimum size filter was applied on cell body size (>150 pixels) before cell and cell body size were distinguished based on an intensity criterion. Finally, three different categories of sizes of GFAP-positive elements (GFAP: <300 pixels considered as astrocytic fragments; 300<pixels<8000 considered as astrocytes; pixels>8000 considered as astrocytes in contact) were quantified in terms of number and relative surface after application of either an automatic or manually-fixed intensity threshold.

Image editing software (Adobe Photoshop, Adobe Systems, San Jose, CA, USA) was used only to adjust contrast and brightness for photomicrographs composing illustrating figures.

Data representation and analysis

Food intake and water intake were expressed relative to 100 g of body weight and 100 g of food intake respectively. Maximum intensity obtained from T2-weighted images analysis was expressed relative to skull muscle. To assess blood redistribution between brain structures, ASL values in cerebral structures were also expressed relative to perfusion of brain hemispheres or to that of the global brain parenchyma in the case of the corpus callosum that is situated between the two hemispheres. All data, except TBSS data, were expressed as means ± standard error of the mean (SEM) and analyzed by a one-way ANOVA/student-t test with surgery as a between factor. When data were not normally distributed, a log10 or square root transformation was performed, and if still not normally distributed then the non-parametric Mann-Whitney U test was used. In all cases, a level of $p<0.05$ was considered as statistically significant.

For statistical analysis of TBSS data, a nonparametric voxel-wise statistical procedure was carried out using *randomise,* a permutation testing algorithm, with 500 and 5000 permutations. Threshold-free cluster enhancement (TFCE) method (Stephen M. Smith & Nichols, 2009) was used to define clusters with significant differences at $p < 0.05$ fully corrected for multiple comparisons across space. Contrasts were performed for sham-operated

vs. CLP animals. TBSS results were displayed on top of the group mean_FA map, the DTI-RAPnD72_template and the DTI-RAPnD72_labels.

Results

CLP reduced food intake and induced encephalopathy

Within the 23 h following the end of surgery, no mortality was observed in the sham-operated group (One animal did die however at the induction of anesthesia for imaging) while CLP resulted in 12.5% mortality. Student-t-tests on food consumption relative to body weight during the 24 h before surgery did not reveal any differences between animals to be allocated to treatment groups. However, a Mann-Whitney U-tests on food consumption relative to body weight during the 24 h after the start of surgery showed a significant lower food intake in animals that underwent CLP as compared to sham-operated rats (U: 26.0, $p<0.05$) (Figure 2A).

Mann-Whitney tests on corneal, pinna and righting reflexes showed that CLP significantly reduced the righting reflex 8 (U:=10.0, $p<0.001$) and 24 h (U: 4.50, $p<0.001$) later as compared to sham surgery (Figure 2D) without affecting the pinna and corneal reflexes (Figure 2B, C).

CLP increased T2-weighted intensities in cortex and striatum

One way ANOVAs on T2-weighted intensities relative to that of skull muscle showed a significantly greater maximum intensity in the cortex (Sham: 3.08 ± 0.17; CLP: 3.78 ± 0.22; $F_{1,18}$: 5,41, $p<0.05$), striatum (Sham: 1.91 ± 0.17; CLP: 2.92 ± 0.07; $F_{1,18}$: 5.39, $p < 0.05$) and at the base of the brain (Sham: 4.91 ± 0.36; CLP: 6.18 ± 0.25; $F_{1,17}$: 8.98, $p < 0,01$) and a tendency for increased maximum intensity in the corpus callosum (Sham 1,96 ± 0.13; CLP 2.36 ± 0.14; $F_{1,18}$: 4.08, $p = 0,059$) of CLP animals as compared to sham-operated rats (Figure 3).

CLP decreased perfusion towards the cerebral cortex

One-way ANOVAs on perfusion values measured in brain hemispheres or in the global brain 24 h after surgery did not show any differences between CLP and sham surgery. Application of similar analyses on perfusion in the ROIs covering the white matter of the corpus callosum or that of the external capsule also did not indicate any difference between CLP and sham surgery (data not shown). Finally, one-way ANOVAs or Mann-Whitney tests of perfusion in

the ROIs covering the cortex or the striatum also did not reveal between the CLP- and sham surgery group.

To assess the distribution of blood between brain structures perfusion values measured in brain areas were also analyzed relative to that of the hemisphere (or to that of the global brain parenchyma in the case of the ROI centered on the corpus callosum that is situated between the two hemispheres). One-way ANOVAs on these data indicated a significant redistribution of blood at the detriment of the cortex ($F_{1,18}$: 4.69, $p<0.05$; Figure 4A) without affecting perfusion distribution towards the corpus callosum (Figure 4B), external capsule region (Figure 4C) or striatum (Figure 4D).

CLP increased axial water diffusion in the corpus callosum

One-way ANOVAs or Mann-Whitney tests on water diffusion parameters in the cortex and striatum revealed neither differences in ADC nor in the means of diffusion directions (data not shown). Similar analyses on water diffusion parameters in the corpus callosum at the anatomical level where the third ventricle is traversed by the junction of the white matter anterior commissure indicated significantly higher $\lambda 1$ (mean axial water diffusion: $F_{1,17}$: 7.13, $p<0.05$; Figure 5A) in rats that underwent CLP surgery as compared to sham-operated rats without any effect on $\lambda 2$, $\lambda 3$ (Figure 5B), FA (Figure 5C) or ADC (Figure 5D). One-way ANOVAs or Mann-Whitney tests on water diffusion parameters in the corpus callosum where the third ventricle is divided in its ventral and dorsal part by the grey matter of the paraventricular thalamus indicated a significant increase in FA (U: 15.0, $p<0.05$; Figure 6C) and a significant decrease in $\lambda 2$ (U: 15.0, $p<0.05$) and radial diffusion ($(\lambda 2 + \lambda 3)/2$) (U: 10.0, $p<0.05$; Figure 6B) in rats that underwent CLP surgery as compared to sham-operated rats without any effect on $\lambda 1$ (Figure 6A) or ADC (Figure 6D).

Tract-based spatial statistics

With 5000 random permutations, a significant higher FA was found in the ventral caudate putamen and globus pallidus of CLP rats than in sham-operated animals between the coronal level where the third ventricle is traversed by the junction of the white matter anterior commissure and that where the interventricular foramen appears (Figure 7).

CLP did not induce BBB breakdown

In all animals, IgG was found in brain regions lacking a functional BBB including the choroid plexus, meninges and circumventricular organs from which it spread to surrounding regions

(Figure 8A, B). A one-way ANOVA or Mann-Whitney tests on the occurrence of perivascular plume-like diffusion clouds of IgG staining in the white matter revealed a significantly increased frequency in the fimbria (U: 30.0, $p<0.05$), but not in the corpus callosum (Figure 8C, D) or elsewhere in the white matter, of rats that underwent sham surgery as compared to CLP animals. Similar analyses on grey matter did not indicate any differences with light to moderate perivascular IgG diffusion occasionally being observed in the cortex, striatum and hippocampus of both sham-operated and CLP animals (Figure 8E-J).

CLP decreased cortical COX-2-immunoreactivity

No or very weak COX-2 immunoreactivity was found associated with blood vessels in the preoptic area (Figure 9A), caudate putamen (Figure 9C), external capsule (Figure 9E), cortex (Figure 9G) or hippocampus (Figure 9I) of animals subjected to sham-surgery. However, distinct perivascular disc-like COX-2-immunoreactive cells were frequently observed in these structures, with the exception of the hippocampus, in rats that underwent CLP (Figure 9B, D, F, H and J).

Constitutive COX-2 expression was detected in neurons of the hippocampus and to a lesser extent, in neurons of the cortex. Interestingly, and in spite of perivascular induction of COX-2 in the cortex after CLP (Figure 9H), but not after sham-surgery (Figure 9G), one-way ANOVAs on cortical COX-2-immunoreactivity showed a significant decrease in the number of cells ($F_{1,11}$: 22.2, $p<0,001$), the total ($F_{1,11}$: 8.37, $p<0.05$) and relative ($F_{1,11}$: 8.90, $p<0.05$) surface labeled after CLP in comparison to sham-surgery.

CLP altered corpus callosum microglia cell morphology

CLP as compared to Sham surgery resulted in Iba-1-immunoreactive cells with larger cell bodies and more intensely stained cellular processes in brain parenchyma at some few hundred micrometers from circumventricular organs, such as the median eminence (see Figure 10A, B upper right corners).

One-way ANOVAs on Iba-1 staining in the cortex between bregma -0.11 and -1.33 mm revealed a significant increase in the number ($F_{1,15}$: 8.68, $p<0.05$) and relative surface ($F_{1,15}$: 7.46, $p<0.05$) of positive elements in CLP rats as compared to sham-operated animals. Similar analyses on Iba-1-immunoreactivity in the whole striatum between bregma -0.11 and -1.33 indicated a significant increase in number ($F_{1,16}$: 6.15, $p<0.05$) and relative surface labeled (($F_{1,16}$: 6.29, $p<0.05$) in animals that underwent CLP rats as compared to those subject to sham surgery. Similar analyses on values measured at individual bregma levels revealed

tendencies for higher numbers ($F_{1,13}$: 3.39, p=0.089) and relative surface ($F_{1,13}$: 4.44, p=0.055) of Iba-1-positive elements at bregma -0.51 mm, but not at any other level, in animals that underwent CLP surgery compared to sham-surgery. One-way ANOVAs on Iba-1 staining in the ventral part of the striatum at bregma levels -0.51 to -0.83 mm, that was indicated by tract-based spatial statistics of water diffusion data, indicated a significant increase in relative surface ($F_{1,16}$: 5.48, $p<0.05$) of positive elements in CLP rats as compared to sham-operated animals.

One-way ANOVA on Iba-1 staining in the corpus callosum between bregma -0.11 and -1.33 mm revealed a tendency for an increase in relative surface ($F_{1,18}$: 3.38, p=0.082) of positive elements in CLP rats as compared to sham-operated animals. Similar analyses on values measured at individual bregma levels did not reveal any differences between treatment groups.

One-way ANOVAs or Mann-Whitney tests on fractal parameters obtained on Iba-1-positive cells in the corpus callosum indicated a significant decrease in the number of labeled divided by the total number of pixels in the convex hull ($F_{1,17}$: 9.40, $p<0.01$), and a significant increase in area (U: 21.0, $p<0.05$), perimeter (U=21.0, $p<0.05$), height ($F_{1,18}$: 14.9, $p<0.01$; Figure 11C) and width ($F_{1,18}$: 6.93, $p<0.05$; Figure 11D) and tendency for decreased circularity ($F_{1,18}$: 3.24, p=0.089) in CLP rats compared to sham-operated animals when all rostrocaudal levels between bregma -0.11 and -1.33 mm were considered. Similar analyses on fractal parameters of Iba-1-positive elements at bregma levels -0.51 and -1.33 mm revealed that microglia were significantly higher in CLP animals than in rats that underwent sham-surgery ($F_{1,13}$: 14.4: $p<0.01$ and $F_{1,7}$: 7.17, $p< 0.05$, respectively) without any other differences.

One-way ANOVAs or Mann-Whitney tests on parameters generated by the method of Hovens et al. indicated a significant decrease in Iba-1-positive cell size (U:18.0, $p<0.05$) and cell processes (U: 18.0, $p<0.05$) and a significantly increased cell body size (U: 0.0, $p<0.001$) as well as a significantly increased microglial activation measure (cell body size/cell size; $F_{1,17}$: 6.94, $p<0.05$) in CLP animals as compared to sham-operated rats when all rostrocaudal levels between bregma -0.11 and -1.33 mm were considered. Similar analyses on these parameters at individual bregma levels revealed a significantly increased cell body size ($F_{1,8}$: 23.6, $p<0.01$) and activation state ($F_{1,8}$: 7.77, $p<0.05$) at -1.33 mm and not at any other level.

As the minimum labeling size to be taken into account differed between fractal analysis (all elements>300 pixels) and the Hoven's method (all elements>0 pixels and cell body size>150

pixels), an additional analysis using Hoven's method was done considering cellular elements of the size criteria of the fractal analysis (300<pixels< 6000) to be able to compare between these two approach. One-way ANOVAs or Mann-Whitney tests on these values parameters indicated significantly higher cell size (U=14.0, $p<0.05$) and cell body size ($F_{1,17}$: 7.68, $p<0.05$) with no change in the microglial activation measure in CLP animals as compared to sham-operated rats when all rostrocaudal levels between bregma -0.11 and -1.33 mm were considered. Similar analyses on values measured at individual bregma levels revealed a significantly increased cell body size ($F_{1,7}$: 9.95, $p<0.05$), cell size ($F_{1,7}$: 8.37, $p<0.05$) and microglial activation measure ($F_{1,7}$: 7.36, $p<0.05$) at bregma -1.33, but not at any other level.
One-way ANOVAs on counts of Iba-1-positive fragments using an automatic threshold on all levels of the corpus callosum considered revealed a significantly lower number ($F_{1,17}$: 6.06, $p<0.05$) in CLP animals than in sham-operated rats. Similar analyses on values measured at individual bregma levels revealed a significantly lower relative surface ($F_{1,8}$: 6.32, $p<0.05$) and a tendency for a lower count ($F_{1,8}$: 4.95, $p=0.057$) of Iba-1-positive fragments at bregma -1.33, but not at any other level in animals that underwent CLP surgery compared to sham-surgery. One-way ANOVAs on counts of Iba-1-positive fragment sizes using a fixed threshold at all levels of the corpus callosum considered did not reveal any differences. Similar analyses on values measured at individual bregma levels indicated tendencies for a lower relative surface at bregma -0.26 ($F_{1,8}$: 4.19, $p=0.075$) and bregma -1.33 ($F_{1,8}$: 4.41, $p=0.072$) in CLP animals than in sham-operated rats.

CLP alter corpus callosum astroglia morphology but not density

One-way ANOVAs on GFAP staining in the cortex between bregma -0.11 and -1.33 mm revealed a significant increase in the number ($F_{1,19}$: 4.91, $p<0.05$) and relative surface ($F_{1,19}$: 4.55, $p<0.05$) of positive elements in CLP rats as compared to sham-operated animals. Similar analyses on GFAP-immunoreactivity in the whole striatum between bregma -0.11 and -1.33 indicated a significant increase in number ($F_{1,19}$: 6.14, $p<0.05$) and relative surface labeled ($F_{1,19}$: 5.82, $p<0.05$) in animals that underwent CLP rats as compared to those subject to sham surgery. Similar analyses on values measured at individual bregma levels revealed significantly higher numbers ($F_{1,12}$: 7.40, $p<0.05$) and relative surface ($F_{1,12}$ 7.1, $p<0.05$) of GFAP-positive elements at bregma -0.83, and tendencies for higher counts ($F_{1,14}$: 4.49, $p=0.053$) and relative surface ($F_{1,14}$: 4.33, $p=0.056$) of GFAP-positive cells at bregma -1.08, in animals that underwent CLP surgery compared to sham-surgery. In the striatum**,** GFAP was

also quantified in the ventral region at bregma levels -0.51 and -0.83 mm, indicated by tract-based spatial statistics to show changes in water diffusion. One-way ANOVA on GFAP staining in this part of the striatum showed tendencies for an increase in number ($F_{1,13}$: 4.57, p=0.052) and relative surface ($F_{1,13}$: 3.58, p=0.081).

One-way ANOVAs or Mann-Whitney tests on GFAP staining in the corpus callosum between bregma -0.11 and -1.33 mm did not reveal any differences in number or relative surface of positive elements between CLP rats and sham-operated animals. Similar analyses on values measured at individual bregma levels did not reveal any differences between treatment groups.

One-way ANOVAs on fractal parameters obtained on GFAP-1-positive cells in the corpus callosum did not indicate significant differences in the parameters considered (number of labeled pixels divided by the total number of pixels in the convex hull, height (Figure 12C), width (Figure 12D), perimeter, surface and circularity when all rostrocaudal levels between bregma -0.11 and -1.33 mm were considered. One-way ANOVAs or Mann-Whitney tests on fractal parameters of GFAP-1-positive elements measured at individual bregma levels revealed also no differences in CLP animals compared to rats that underwent sham-surgery.

One-way ANOVAs on GFAP-positive element of different sizes using an automatic threshold on all levels of the corpus callosum considered only revealed a tendency for a decreased relative surface of labeled fragments (pixels<300; ($F_{1,18}$: 4.00, p=0.061)) in CLP animals as compared to sham-operated rats. Similar analyses of GFAP-positive fragments (pixels<300) measured at individual bregma levels revealed a significantly lower count ($F_{1,10}$: 9.44, p<0.05) and a tendency for lower relative surface ($F_{1,10}$: 4.90, p=0.051) at bregma -0.26 as well as a significantly lower relative surface ($F_{1,17}$: 8.48, p<0.05) at bregma -0.51 in animals that underwent CLP surgery compared to sham-surgery. One-way ANOVAs on GFAP-positive fragment sizes using a fixed threshold on all levels of the corpus callosum indicated a significantly lower number of counts ($F_{1,17}$: 8.45, p<0.05) and relative surface ($F_{1,17}$: 18.49, p<0.001) of fragments in the CLP group as compared to sham surgery. Similar analyses on values measured at individual bregma levels revealed significantly lower numbers ($F_{1,9}$: 9.88, p<0.05) and relative surface ($F_{1,9}$: 21.0, p<0.01) of GFAP-positive fragments at bregma -0.26 as well as at bregma -0.51 (number: $F_{1,15}$: 4.74, p<0.05 and relative surface ($F_{1,15}$: 19.1, p<0.001) in CLP animals than in sham-operated rats. More rostrally, one-way ANOVA's showed a significantly lower relative surface occupied by GFAP-immunoreactive fragments at bregma -0.83 and -1.08 ($F_{1,12}$: 5.97, p<0.05 and $F_{1,10}$: 5.70, p<0.05, respectively) and a

tendency for a lower number at bregma -1.08 ($F_{1,10}$: 4.65, p=0.056) in animals that underwent CLP surgery compared to sham-surgery.

CLP decreased cortical AQP4 expression

One way ANOVA showed that cortical AQP4-immunoreactivity between bregma -0.46 and -1.08 mm, which corresponded to the T2-weighted analyzed image, was significantly lower 24 h after CLP-induced sepsis than consecutive after sham surgery (count: $F_{1,14}$:9.74, $p<0.01$; Figure 13C; % surface: $F_{1,14}$:8.66, $p<0.05$; Figure 13D). Similar analyses on AQP-4-positive staining in the corpus callosum and striatum did not indicate differences between groups.

CLP did not alter the myelin-associated enzyme: CNPase

One-way ANOVAs on the density of CNPase immunoreactivity showed no differences between CLP and sham-operated rats in the corpus callosum.

CLP surgery did not affect the corpus callosum dimensions

One-way ANOVAs on the dimensions of the corpus callosum at the center and on both sides revealed no differences between Sham and CLP groups.

Discussion

The main findings of the present work were that CLP induced sepsis-associated CNS dysfunction resulted in higher T2-weighted contrast intensities in the cortex, striatum and base of the brain, decreased blood perfusion distribution to the cortex and increased water diffusion in the corpus callosum and ventral striatum compared to sham surgery. In these same animals CLP induced perivascular COX-2 expression and changes in glial cell morphology.

Decreased food intake is a classic non-specific symptom of systemic inflammation in response to bacterial infection (Hart, 1988) and was observed following CLP. In addition, the loss of the righting reflex in animals that underwent CLP is in agreement with previous studies (Kadoi & Goto, 2004; Kafa, Bakirci, Uysal, & Kurt, 2010; Kafa, Uysal, Bakirci, & Ayberk Kurt, 2010)and indicates deteriorated neurological status and SAE**.**

Using the perivascular diffusion of IgG as endogenous of BBB breakdown, no indication of increased BBB permeability was found in the parenchyma of the grey and white matter after CLP in the present work except for the fimbria. This was neither due to technical failure nor lack of sensitivity as perivascular IgG was readily observed in brain circumventricular organs and meninges, where the endothelial BBB is absent, and ip LPS was previously shown to

increase perivascular IgG diffusion in the white matter using the same protocol (Dhaya et al., J. Neuroimmunol., accepted). It is important to keep in mind however that the severity of CLP-induced sepsis depends on the size of the needle used to puncture as well as the number of punctures (Rittirsch et al., 2009) and that the needle size used here was smaller than previous work reporting BBB breakdown after CLP in rodents (Avtan et al., 2011; Comim et al., 2011; Imamura et al., 2011; Jeppsson et al., 1981; Vachharajani et al., 2012; Yokoo et al., 2012) Hence, our experimental model is interesting in that it induces signs of neurological impairment in the absence of BBB breakdown for molecules of high molecular weight.

Neurological impairment was associated with signs of fluid accumulation at the base of the brain as indicated by increased T2-weigthed contrast, which is in accordance with results of T2-weighted imaging in a murine CLP model (Bozza et al., 2010). In addition, increased T2-weighted contrast intensities were also found in the cortex and striatum in the present work. As diffusion imaging did not indicate altered ADC in the cortex and striatum the increase in T2 intensities were considered as indicating vasogenic rather than cytotoxic edema. Interestingly, lower perivascular expression of the water channel AQP4 was observed in the cortex of CLP animals as compared to those subject to sham surgery. Reduced water clearance may therefore, in part, explain the increased T2-weighted contrast intensity found in the cortex after CLP.

Since in addition to edema, SAE has been proposed to be related to reduced CBF and oxygen extraction (Papadopoulos et al., 2000), the perfusion of the brain and that of some of its major structures were assessed with ASL. Global perfusion of the brain in sham-operated animals was in accordance with that observed in some previous studies (Detre, Leigh, Williams, & Koretsky, 1992; Zhang, Williams, Detre, & Koretsky, 1992), but higher than that described by others (Danker & Duong, 2007; Shen, Huang, & Duong, 2015), yet lower than that measured in still other published work (Carr et al., 2007; Moffat, Chenevert, Hall, Rehemtulla, & Ross, 2005; Williams, Detre, Leigh, & Koretsky, 1992). These discrepancies may be due to differences in anesthesia, ASL sequences used and the way the global brain was defined (in our case both cerebral hemispheres without the ventricular system and the large vessels at the base of the brain). This being said, ASL-based perfusion data are known to vary even between studies of the same group (Duong, 2007; Shen et al., 2015; Sicard et al., 2003)and the aim of the present work was not to obtain absolute quantitative, but to compare between CLP and sham-surgery. Nevertheless, all CBF values observed in the present work were in agreement

with those observed in our previous study addressing the effects of intraperitoneal LPS injection on cerebral perfusion.

Like in our previous work with LPS (Dhaya et al., accepted), perfusion of the global brain, striatum and cortex was not found to be altered by CLP-induced sepsis. In addition, to absolute perfusion values, the distribution of blood between brain structures is an important value as this distribution can vary as a function of local cerebral metabolism. In this respect it is interesting to note that the distribution of blood to the cortex relative to that of the ipsilateral hemisphere was lower 24 h after CLP as compared to sham-surgery. This relative hypoperfusion of the cortex may be related to a local loss of cerebral autoregulation or uncoupling between CBF and cerebral metabolism (Feng et al., 2010; Rosengarten et al., 2007). The reported local decrease of glucose utilization in cortical areas (Soejima, Fujii, Ishikawa, Takeshita, & Maekawa, 1990) and altered cortical electric activity (Kafa, Bakirci, et al., 2010) during sepsis support the possibility of altered cortical metabolism. Cortical COX-2 plays an important role in neurovascular coupling between neuronal activity and CBF (Niwa, Araki, Morham, Ross, & Iadecola, 2000; Stefanovic, Bosetti, & Silva, 2006). Interestingly, and although increased perivascular de novo induction of perivascular COX-2 was observed after CLP, overall cortical COX-2-immunoreactivity was decreased as compared to sham-surgery. Thus, decreased neuronal COX-2 may explain the observed decrease in blood distribution towards the cerebral cortex during sepsis.

Contrary to our findings obtained after systemic LPS administration (Dhaya et al., accepted), no changes in perfusion in the ROI centered on the white matter of the corpus callosum body were detected after CLP. This difference may be related to the fact that IgG perivascular leakage indicating BBB breakdown was observed in the ventral hippocampal commissure, which was part of the ASL ROI centered on the corpus callosum, after LPS injection, but not after CLP. Since increased perfusion has been shown to be associated with BBB breakdown in the subcortical white matter of multiple sclerosis patients (Ge et al., Am. J. Neuroradiol., 2005; Ingrisch et al., Invest. Radiol., 2012), the absence of massive BBB breakdown in the white matter after CLP may explain the lack of increased ASL values in the corpus callosum ROI in the present work.

However, in accordance with our previous work on LPS, increased axial water diffusion was observed in the corpus callosum body after CLP. Interestingly, three months after hospital discharge, septic patients that had suffered from SAE showed inverse correlation between delirium duration and FA in the body of the corpus callosum (Morandi et al., 2012). The body

of the corpus callosum is characterized by large axonal diameter distribution and a higher diffusivity suggesting that the space between axons may be larger at the body than that at the genu and splenium (Barazany et al., 2009). Taken together, the previous and present findings suggest that during inflammation axial diffusion in the corpus callosum first increases to subsequently decrease when white matter integrity is altered.

Recently, disruption of the tubulin network inside white matter axons has been shown in rats rendered septic by intraperitoneal injection of fecal slurry (Ehler et al., 2017). If the same phenomenon occurred after CLP, this would be expected to alter axial diffusion in the corpus callosum. Alternatively, retraction of the processes of microglia or astrocytes that occupy the space between white mater fibers may explain increased horizontal water diffusion in the corpus callosum after CLP. Indeed, in the corpus callosum, microglia have several long cytoplasmic processes that run mostly parallel, but also perpendicularly to the longitudinal axis of myelinated axons (Lawson, Perry, Dri, & Gordon, 1990; Mori & Leblond, 1969). In the present work, a decrease in the surface of total Iba-1 labeling per cell and an increased cell body to cell size ratio, microglial activation measure according to the method developed by Hovens and colleagues, were observed in the corpus callosum of CLP animals as compared to that of rats that underwent sham-surgery. This occurred in spite of the increase in maximum height and width of Iba-1-positive cells with their primary processes, as indicated by fractal analysis, and was most likely due to a decrease in Iba-1-immunoreactive fragments considered to represent most distal microglial processes. The decrease in the most distal microglial processes then results in less hindrance for axial water diffusion in the corpus callosum. When white matter astrocytes are activated, they retract their higher order processes, increase their soma and lose their transverse orientation (Sun, Lye-Barthel, Masland, & Jakobs, 2011). Less GFAP-irmmunorreactive fragments were found in the corpus callosum after CLP than after sham-surgery. Although GFAP does not mark astrocytic endfeet (Sun & Jakobs, 2012), this finding can be interpreted to suggest astroglial activation and retraction of their processes, which , like for microglia, allows for increased diffusion of water molecules parallel to corpus callosum fibers.

A non-hypothesis- driven tract-based analysis indicated that white matter in the ventral striatum is affected by CLP-induced sepsis and showed increase FA values compared to sham surgery. This was accompanied by tendencies for higher relative surface of Iba-1- and GFAP-staining in this area of CLP rat than in the ventral striatum of sham-operated animals. However, the presence of numerous small white matter fiber bundles intermingled with grey

matter in the striatum complicates the comparison between DTI and histology in this structure.

In conclusion, our findings confirm the existence of brain dysfunction and increased T2-weighted contrast at the base of the brain 24 h after CLP in rodents. In addition, they expand previous findings in showing increased T2-weighted contrast in the striatum and cortex, decreased perfusion distribution to the cortex and augmented FA as well as increased axial water diffusion in the corpus callosum. Importantly, these imaging findings were accompanied by lower numbers of Iba-1- and GFAP-immunoreactive fragments in the corpus callosum, decreased neuronal COX-2 and AQP4 expression in the cortex, but not by widespread perivascular IgG diffusion indicating breakdown of the BBB

Acknowledgements

We thank Renauld Nicolas for skillful assistance. Ibtihel Dhaya was a laureate of a stipend from the Ministère de l'Enseignement Supérieur et de Recherche Scientifique in Tunisia. Administrative help from Adera (Pessac, France) is gratefully acknowledged.

References

Abdel-Aty, H., Boyé, P., Zagrosek, A., Wassmuth, R., Kumar, A., Messroghli, D., … Schulz-Menger, J. (2005). Diagnostic performance of cardiovascular magnetic resonance in patients with suspected acute myocarditis: Comparison of different approaches. *Journal of the American College of Cardiology*, *45*(11), 1815–1822. https://doi.org/10.1016/j.jacc.2004.11.069

Avtan, S. M., Kaya, M., Orhan, N., Arslan, A., Arican, N., Toklu, A. S., … Ahishali, B. (2011). The effects of hyperbaric oxygen therapy on blood-brain barrier permeability in septic rats. *Brain Research*, *1412*, 63–72. https://doi.org/10.1016/j.brainres.2011.07.020

Barazany, D., Basser, P. J., & Assaf, Y. (2009). In vivo measurement of axon diameter distribution in the corpus callosum of rat brain. *Brain*, *132*(5), 1210–1220. https://doi.org/10.1093/brain/awp042

Bartynski, W. S. (2008). Posterior reversible encephalopathy syndrome, Part 2: Controversies surrounding pathophysiology of vasogenic edema. *American Journal of Neuroradiology*, *29*(6), 1043–1049. https://doi.org/10.3174/ajnr.A0929

Berg, R. M. G., Plovsing, R. R., Bailey, D. M., Holstein-Rathlou, N.-H., & Møller, K. (2016). Dynamic cerebral autoregulation to induced blood pressure changes in human experimental and clinical sepsis. *Clinical Physiology and Functional Imaging*, *36*(6), 490–6. https://doi.org/10.1111/cpf.12256

Berg, R. M. G., Plovsing, R. R., Evans, K. A., Christiansen, C. B., Bailey, D. M., Holstein-Rathlou, N.-H., & Møller, K. (2013). Lipopolysaccharide infusion enhances dynamic cerebral autoregulation without affecting cerebral oxygen vasoreactivity in healthy volunteers. *Critical Care (London, England)*, *17*(5), R238. https://doi.org/10.1186/cc13062

Berg, R. M., Plovsing, R. R., Ronit, A., Bailey, D. M., Holstein-Rathlou, N. H., & Moller, K. (2012). Disassociation of static and dynamic cerebral autoregulatory performance in healthy volunteers after lipopolysaccharide infusion and in patients with sepsis. *Am J Physiol Regul Integr Comp Physiol*, *303*(11), R1127-35. https://doi.org/10.1152/ajpregu.00242.2012

Boś, A., Bergmann, R., Strobel, K., Hofheinz, F., Steinbach, J., & den Hoff, J. Van. (2012). Cerebral blood flow quantification in the rat: a direct comparison of arterial spin labeling MRI with radioactive microsphere PET. *EJNMMI Research*, *2*(1), 47. https://doi.org/10.1186/2191-219X-2-47

Bowton, D., Bertels, N., Prough, D., & Stump, D. (1989). Cerebral blood flow is reduced in patients with sepsis syndrome. *Crit Care Med.*, *17*(5), 399–403.

Bozza, F. A., Garteiser, P., Oliveira, M. F., Doblas, S., Cranford, R., Saunders, D., … Castro-Faria-Neto, H. C. (2010). Sepsis-associated encephalopathy: a magnetic resonance imaging and spectroscopy study. *Journal of Cerebral Blood Flow and Metabolism : Official Journal of the International Society of Cerebral Blood Flow and Metabolism*, *30*(2), 440–8. https://doi.org/10.1038/jcbfm.2009.215

Bryan, W. J., & Emerson, T. E. (1977). Blood flow in seven regions of the brain during endotoxin shock in the dog. *Proceedings of the Society for Experimental Biology and Medicine*, *156*(2), 205–8. https://doi.org/10.3181/00379727-156-39907

Carr, J. P., Buckley, D. L., Tessier, J., & Parker, G. J. M. (2007). What levels of precision are achievable for quantification of perfusion and capillary permeability surface area product using ASL? *Magnetic Resonance in Medicine*, *58*(2), 281–289. https://doi.org/10.1002/mrm.21317

Christenson, J., Kuikka, J., Owunwanne, A., & Al-Sarraf, A. (1986). Cerebral circulation during endotoxic shock with special emphasis on the regional cerebral blood flow in vivo. *Nucl Med Commun.*, *7*(7), 531–540.

Comim, C., Vilela, M., Constantino, L., Petronilho, F., Vuolo, F., Lacerda-Queiroz, N., … Dal-Pizzol, F. (2011). Traffic of leukocytes and cytokine up-regulation in the central nervous system in sepsis. *Intensive Care Medicine*, *37*, 711–718. https://doi.org/10.1007/s11046-013-9679-3

Danker, J. F., & Duong, T. Q. (2007). Quantitative Regional Cerebral Blood Flow MRI of Animal Model of Attention-Deficit/Hyperactivity Disorder. *Brain Res*, *1150*, 217–224.

Detre, J. A., Leigh, J. S., Williams, D. S., & Koretsky, A. P. (1992). Perfusion imaging. *Magnetic Resonance in Medicine*, *23*(1), 37–45. https://doi.org/10.1002/mrm.1910230106

Dobre, M. C., Uğurbil, K., & Marjanska, M. (2007). Determination of blood longitudinal relaxation time (T1) at high magnetic field strengths. *Magnetic Resonance Imaging*, *25*(5), 733–735. https://doi.org/10.1016/j.mri.2006.10.020

Duong, T. (2007). Cerebral blood flow and BOLD fMRI responses to hypoxia in awake and anesthetized rats. *Brain Research*, *1135*(1), 186–194. https://doi.org/10.1016/j.brainres.2006.11.097.Cerebral

Ehler, J., Barrett, L. K., Taylor, V., Groves, M., Scaravilli, F., Wittstock, M., … Petzold, A. (2017). Translational evidence for two distinct patterns of neuroaxonal injury in sepsis: a longitudinal, prospective translational study. *Critical Care*, *21*(1), 262. https://doi.org/10.1186/s13054-017-1850-7

EkströmJodal, B., Häggendal, J., Larsson, L. E., & Westerlind, A. (1982). Cerebral Hemodynamics, Oxygen Uptake and Cerebral Arteriovenous Differences of Catecholamines Following E. coli Endotoxin in Dogs. *Acta Anaesthesiologica Scandinavica*, *26*(5), 446–452. https://doi.org/10.1111/j.1399-6576.1982.tb01797.x

Esparza-Coss, E., Wosik, J., & Narayana, P. A. (2010). Perfusion in Rat Brain at 7 T with Arterial Spin Labeling Using FAIR-TrueFISP and QUIPSS. *Magnetic Resonance Imaging*, *28*(4), 607–312. https://doi.org/10.1007/s11103-011-9767-z.Plastid

Feng, S. Y. S., Samarasinghe, T., Phillips, D. J., Alexiou, T., Hollis, J. H., Yu, V. Y. H., & Walker, A. M. (2010). Acute and chronic effects of endotoxin on cerebral circulation in lambs. *American Journal of Physiology. Regulatory, Integrative and Comparative Physiology*, *298*(3), R760–R766. https://doi.org/10.1152/ajpregu.00398.2009

Hart, B. L. (1988). Biological Basis of the Behavior of Sick Animals. *Neuroscience & Biobehavioral Reviews*, *12*, 123–137.

Hinkelbein, J., Schroeck, H., Peterka, A., Schubert, C., Kuschinsky, W., & Kalenka, A. (2007). Local cerebral blood flow is preserved in sepsis. *Current Neurovascular Research*, *4*(1), 39–47. https://doi.org/10.2174/156720207779940671

Imamura, Y., Wang, H., Matsumoto, N., Muroya, T., Shimazaki, J., Ogura, H., & Shimazu, T. (2011). Interleukin-1β causes long-term potentiation deficiency in a mouse model of septic encephalopathy. *Neuroscience*, *187*, 63–69. https://doi.org/10.1016/j.neuroscience.2011.04.063

Jeppsson, B., Freund, H. R., Gimmon, Z., James, J. H., von Meyenfeldt, M. F., & Fischer, J. E. (1981). Blood-brain barrier derangement in sepsis: Cause of septic encephalopathy? *The American Journal of Surgery*, *141*(1), 136–142. https://doi.org/10.1016/0002-9610(81)90026-X

Kadoi, Y., & Goto, F. (2004). Selective inducible nitric oxide inhibition can restore hemodynamics, but does not improve neurological dysfunction in experimentally-induced septic shock in rats. *Anesthesia and Analgesia*, *99*(1), 212–20.

https://doi.org/10.1213/01.ANE.0000118111.94913.22
Kafa, I. M., Bakirci, S., Uysal, M., & Kurt, M. A. (2010). Alterations in the brain electrical activity in a rat model of sepsis-associated encephalopathy. *Brain Research*, *1354*, 217–226. https://doi.org/10.1016/j.brainres.2010.07.049
Kafa, I. M., Uysal, M., Bakirci, S., & Ayberk Kurt, M. (2010). Sepsis induces apoptotic cell death in different regions of the brain in a rat model of sepsis. *Acta Neurobiologiae Experimentalis*, *70*, 246–260.
Kim, S., & Tsekos, N. V. (1997). Perfusion imaging by a flow-sensitive alternating inversion recovery (FAIR) technique: application to functional brain imaging. *Magnetic Resonance in Medicine : Official Journal of the Society of Magnetic Resonance in Medicine / Society of Magnetic Resonance in Medicine*, *37*(3), 425–435.
Kober, F., Iltis, I., Izquierdo, M., Desrois, M., Ibarrola, D., Cozzone, P. J., & Bernard, M. (2004). High-Resolution Myocardial Perfusion Mapping in Small Animals in Vivo by Spin-Labeling Gradient-Echo Imaging. *Magnetic Resonance in Medicine*, *51*(1), 62–67. https://doi.org/10.1002/mrm.10676
Konsman, J. P., & Blomqvist, A. (2005). Forebrain patterns of c-Fos and FosB induction during cancer-associated anorexia-cachexia in rat. *European Journal of Neuroscience*, *21*(10), 2752–2766. https://doi.org/10.1111/j.1460-9568.2005.04102.x
Konsman, J. P., Veeneman, J., Combe, C., Poole, S., Luheshi, G. N., Dantzer, R., & Se, V. (2008). Central nervous action of interleukin-1 mediates activation of limbic structures and behavioural depression in response to peripheral administration of bacterial lipopolysaccharide. *European Journal of Neuroscience, Vol.*, *28*, 2499–2510. https://doi.org/10.1111/j.1460-9568.2008.06549.x
Konsman, J., Vigues, S., Mackerlova, L., Bristow, A., & Blomqvist, A. (2004). Rat Brain Vascular Distribution of Immunoreactivity : Relationship to Patterns of Inducible Cyclooxygenase Expression by Peripheral Inflammatory Stimuli. *The Journal of Comparative Neurology*, *472*, 113–129. https://doi.org/10.1002/cne.20052
Lawson, L. J., Perry, V. H., Dri, P., & Gordon, S. (1990). Heterogeneity in the distribution and morphology of microglia in the normal adult mouse brain. *Neuroscience*, *39*(1), 151–170. https://doi.org/10.1016/0306-4522(90)90229-W
Maekawa, T., Fujii, Y., Sadamitsu, D., Yokota, K., Soejima, Y., Ishikawa, T., … Takeshita, H. (1991). Cerebral circulation and metabolism in patients with septic encephalopathy. *American Journal of Emergency Medicine*, *9*(2), 139–143. Retrieved from http://www.ncbi.nlm.nih.gov/pubmed/1994941
Moffat, B. A., Chenevert, T. L., Hall, D. E., Rehemtulla, A., & Ross, B. D. (2005). Continuous arterial spin labeling using a train of adiabatic inversion pulses. *Journal of Magnetic Resonance Imaging*, *21*(3), 290–296. https://doi.org/10.1002/jmri.20268
Møller, K., Strauss, G. I., Qvist, J., Fonsmark, L., Knudsen, G. M., Larsen, F. S., … Pedersen, B. K. (2002). Cerebral blood flow and oxidative metabolism during human endotoxemia. *Journal of Cerebral Blood Flow and Metabolism*, *22*(10), 1262–1270. https://doi.org/10.1097/00004647-200210000-00014
Morandi, A., Rogers, B. P., Gunther, M. L., Merkle, K., Pandharipande, P., Girard, T. D., … Hopkins, R. O. (2012). The Relationship between Delirium Duration, White Matter Integrity, and Cognitive Impairment in Intensive Care Unit Survivors as Determined by Diffusion Tensor Imaging. *Critical Care Medicine*, *40*(7), 2182–2189. https://doi.org/10.1097/CCM.0b013e318250acdc.
Mori, S., & Leblond, C. P. (1969). Identification of microglia in light and electron microscopy. *Journal of Comparative Neurology*, *135*(1), 57–79. https://doi.org/10.1002/cne.901350104

Nicolas, R., Sanchez, S., Raffard, G., Sibon, I., Franconi, J., Konsman, J.-P., & Hiba, B. (2013). In vivo 3D q-space imaging of the adult rat brain during energy failure . In *European Society Magnetic Resonance in Medicine and Biology, Springer, Toulouse*. https://doi.org/10.13140/2.1.1534.8808

Niwa, K., Araki, E., Morham, S. G., Ross, M. E., & Iadecola, C. (2000). Cyclooxygenase-2 contributes to functional hyperemia in whisker-barrel cortex. *The Journal of Neuroscience*, *20*(2), 763–770.

Papadopoulos, M. C., Davies, D. C., Moss, R. F., Tighe, D., & Bennett, E. D. (2000). Pathophysiology of septic encephalopathy: a review. *Critical Care Medicine*, *28*(8), 3019–3024. https://doi.org/10.1097/00003246-200008000-00057

Pfister, D., Siegemund, M., Dell-Kuster, S., Smielewski, P., Rüegg, S., Strebel, S. P., … Steiner, L. A. (2008). Cerebral perfusion in sepsis-associated delirium. *Critical Care*, *12*(3), R63. https://doi.org/10.1186/cc6891

Pierrakos, C., Antoine, A., Velissaris, D., Michaux, I., Bulpa, P., Evrard, P., … Dive, A. (2013). Transcranial doppler assessment of cerebral perfusion in critically ill septic patients: a pilot study. *Annals of Intensive Care*, *3*(1), 28. https://doi.org/10.1186/2110-5820-3-28

Pierrakos, C., Attou, R., Decorte, L., Kolyviras, A., Malinverni, S., Gottignies, P., … De Bels, D. (2014). Transcranial Doppler to assess sepsis-associated encephalopathy in critically ill patients. *BMC Anesthesiology*, *14*(1), 45. https://doi.org/10.1186/1471-2253-14-45

Pollard, V., Prough, D., Deyo, D., Conroy, B., Uchida, T., Daye, A., … Traber, D. (1997). Cerebral blood flow during experimental endotoxemia in volunteers. *Crit Care Med.*, *25*(10), 1700–1706.

Rittirsch, D., Huber-lang, M. S., Flierl, M. a, & Ward, P. a. (2009). Immunodesign of experimental sepsis by cecal lingation and puncture. *Nat Protoc*, *4*(1), 31–36. https://doi.org/10.1038/nprot.2008.214.Immunodesign

Rosengarten, B., Hecht, M., Auch, D., Ghofrani, H. A., Schermuly, R. T., Grimminger, F., & Kaps, M. (2007). Microcirculatory dysfunction in the brain precedes changes in evoked potentials in endotoxin-induced sepsis syndrome in rats. *Cerebrovascular Diseases*, *23*(2–3), 140–147. https://doi.org/10.1159/000097051

Rosengarten, B., Hecht, M., Wolff, S., & Kaps, M. (2008). Autoregulative function in the brain in an endotoxic rat shock model. *Inflammation Research*, *57*(11), 542–546. https://doi.org/10.1007/s00011-008-7199-2

Rosengarten, B., Walberer, M., Allendoerfer, J., Mueller, C., Schwarz, N., Bachmann, G., & Gerriets, T. (2008). LPS-induced endotoxic shock does not cause early brain edema formation - An MRI study in rats. *Inflammation Research*, *57*(10), 479–483. https://doi.org/10.1007/s00011-008-8042-5

Schramm, P., Klein, K., Falkenberg, L., Berres, M., Closhen, D., Werhahn, K. J., … Engelhard, K. (2012). Impaired cerebrovascular autoregulation in patients with severe sepsis and sepsis-associated delirium. *Critical Care*, *16*(5), R181. https://doi.org/10.1186/cc11665

Sharshar, T., Carlier, R., Bernard, F., Guidoux, C., Brouland, J. P., Nardi, O., … Annane, D. (2007). Brain lesions in septic shock: A magnetic resonance imaging study. *Intensive Care Medicine*, *33*(5), 798–806. https://doi.org/10.1007/s00134-007-0598-y

Shen, Q., Huang, S., & Duong, T. Q. (2015). Ultra-high spatial resolution basal and evoked cerebral blood flow MRI of the rat brain. *Brain Research*, *1599*, 126–136. https://doi.org/10.1016/j.brainres.2014.12.049

Sicard, K., Shen, Q., Brevard, M. E., Sullivan, R., Ferris, C. F., King, J. A., & Duong, T. Q. (2003). Regional Cerebral Blood Flow and BOLD Responses in Conscious and

Anesthetized Rats Under Basal and Hypercapnic Conditions: Implications for Functional MRI Studies. *J Cereb Blood Flow Metab.*, *23*(4), 472–481. https://doi.org/10.1111/j.1747-0285.2012.01428.x.Identification

Smith, S. M., Jenkinson, M., Johansen-Berg, H., Rueckert, D., Nichols, T. E., Mackay, C. E., … Behrens, T. E. J. (2006). Tract-based spatial statistics: Voxelwise analysis of multi-subject diffusion data. *NeuroImage*, *31*(4), 1487–1505. https://doi.org/10.1016/j.neuroimage.2006.02.024

Smith, S. M., & Nichols, T. E. (2009). Threshold-free cluster enhancement: Addressing problems of smoothing, threshold dependence and localisation in cluster inference. *NeuroImage*, *44*(1), 83–98. https://doi.org/10.1016/j.neuroimage.2008.03.061

Smith, S. M., Padayachee, S., Modaresi, K. B., Smithies, M. N., & Bihari, D. J. (1998). Cerebral blood flow is proportional to cardiac index in patients with septic shock. *Journal of Critical Care*, *13*(3), 104–9. https://doi.org/http://dx.doi.org/10.1016/S0883-9441%2898%2990013-2

Soejima, Y., Fujii, Y., Ishikawa, T., Takeshita, H., & Maekawa, T. (1990). Local cerebral glucose utilization in septic rats. *Crit Care Med.*, *18*(4), 423–427.

Stefanovic, B., Bosetti, F., & Silva, A. C. (2006). Modulatory role of cyclooxygenase-2 in cerebrovascular coupling. *NeuroImage*, *32*(1), 23–32. https://doi.org/10.1016/j.neuroimage.2006.03.014

Stejskal, E. O., & Tanner, J. E. (1965). Spin Diffusion Measurements: Spin Echoes in the Presence of a Time-Dependent Field Gradient. *The Journal of Chemical Physics*, *42*(1), 288–292. https://doi.org/10.1063/1.1695690

Sun, D., & Jakobs, T. C. (2012). Structural Remodeling of Astrocytes in the Injured CNS. *Neuroscientist.*, *18*(6), 567–588. https://doi.org/10.1086/498510.Parasitic

Sun, D., Lye-Barthel, M., Masland, R. H., & Jakobs, T. C. (2011). Structural Remodeling of Fibrous Astrocytes after Axonal Injury. *J Neurosci.*, *30*(42), 14008–14019. https://doi.org/10.1086/498510.Parasitic

Swanson, L. W. (1998). *Swanson, L.W. (1998) Brain maps: structure of the rat brain. Elsevier Amsterdam.*

Tempel, G., Cook, J., Wise, W., Halushka, P., & Corral, D. (1986). Improvement in organ blood flow by inhibition of thromboxane synthetase during experimental endotoxic shock in the rat. *J Cardiovasc Pharmacol.*, *8*(3), 514–519.

Vachharajani, V., Cunningham, C., Yoza, B., Jr, J. C., Vachharajani, T. J., & McCall, C. (2012). Adiponectin-Deficiency Exaggerates Sepsis-Induced Microvascular Dysfunction in the Mouse Brain. *Obesity (Silver Spring)*, *20*(3), 498–504. https://doi.org/10.1038/oby.2011.316.Adiponectin-Deficiency

Villéga, F., Delpech, J. C., Griton, M., André, C., Franconi, J. M., Miraux, S., & Konsman, J. P. (2017). Circulating bacterial lipopolysaccharide-induced inflammation reduces flow in brain-irrigating arteries independently from cerebrovascular prostaglandin production. *Neuroscience*, *346*(January), 160–172. https://doi.org/10.1016/j.neuroscience.2017.01.018

Wichterman, K. A., Baue, A. E., & Chaudry, I. H. (1980). Sepsis and septic shock—A review of laboratory models and a proposal. *Journal of Surgical Research*, *29*(2), 189–201. https://doi.org/10.1016/0022-4804(80)90037-2

Williams, D. S., Detre, J. A., Leigh, J. S., & Koretsky, A. P. (1992). Magnetic resonance imaging of perfusion using spin inversion of arterial water. *Proceedings of the National Academy of Sciences of the United States of America*, *89*(1), 212–6. https://doi.org/10.1073/pnas.89.9.4220e

Wyler, F., Forsyth, R. P., Nies, a S., Neutze, J. M., & Melmon, K. L. (1969). Endotoxin-

induced regional circulatory changes in the unanesthetized monkey. *Circulation Research*, *24*(6), 777–786. Retrieved from http://www.ncbi.nlm.nih.gov/pubmed/1557064

Wyler, F., Rutishauser, M., & Weisser, K. (1972). Endotoxin induced regional circulatory reactions in the rabbit with and without halothane anesthesia. *Journal of Surgical Research*, *13*, 13–19.

Yokoo, H., Chiba, S., Tomita, K., Takashina, M., Sagara, H., Yagisita, S., … Hattori, Y. (2012). Neurodegenerative Evidence in Mice Brains with Cecal Ligation and Puncture-Induced Sepsis: Preventive Effect of the Free Radical Scavenger Edaravone. *PLoS ONE*, *7*(12), 1–11. https://doi.org/10.1371/journal.pone.0051539

Yokota, H., Ogawa, S., Kurokawa, A., & Yamamoto, Y. (2003). Regional cerebral blood flow in delirium patients. *Psychiatry and Clinical Neurosciences*, *57*(3), 337–339. https://doi.org/10.1046/j.1440-1819.2003.01126.x

Zhang, W., Williams, D. S., Detre, J. A., & Koretsky, A. P. (1992). Measurement of brain perfusion by volume-localized NMR spectroscopy using inversion of arterial water spins: Accounting for transit time and cross???relaxation. *Magnetic Resonance in Medicine*, *25*(2), 362–371. https://doi.org/10.1002/mrm.1910250216

Zhen, Y. (1987). Regional Changes in Cerebral Blood Flow during Acute Endotoxemia. *Journal of Tongji Medical University*, *7*(3), 131–135.

Figures

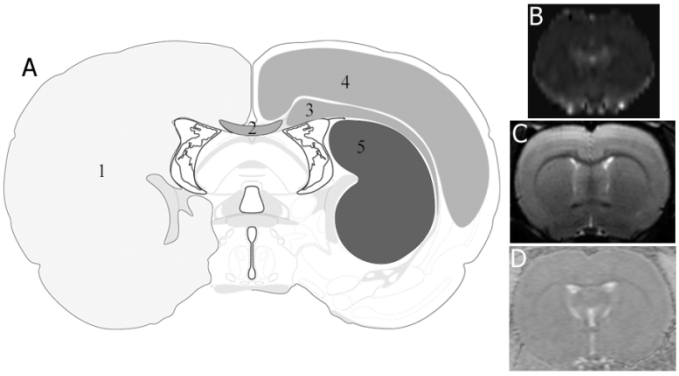

Figure 1 :

Placement of different Region Of Interest (ROIs; A) to analyze perfusion-weighted (example in B), T2-weighted (example in C) and diffusion-weighted images (example in D). 1: hemisphere; 2: corpus callosum; 3 external capsule; 4 primary motor and sensory cortices and 5: striatum.

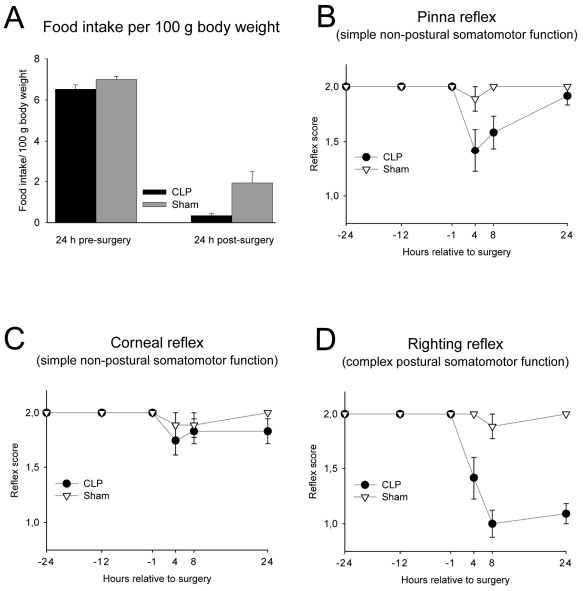

Figure 2:

Food intake relative to body weight (A) during 24h after CLP or sham surgery. Group size Sham: n=9; CLP: n=11-12. Reflex scores: Pinna (B), corneal (C) and righting (D) reflexes at 24h, 12h, and 1h prior to surgery then 4h, 8h and 24h later. Group size Sham: n=8-9; CLP: n=8-12

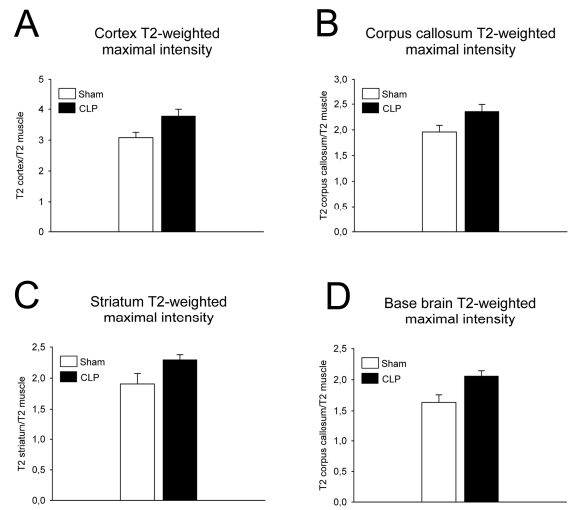

Figure 3: Changes in T2-weighted intensity in the cortex (A), corpus callosum (B) the striatum (C) and the base of the brain (D). Graphs represent max, average and sum intensities in the VOI relative to the muscle 24h after cecal ligation and puncture or laparotomy. *: $p < 0.05$. Group sizes Sham: n=8; CLP: n=11.

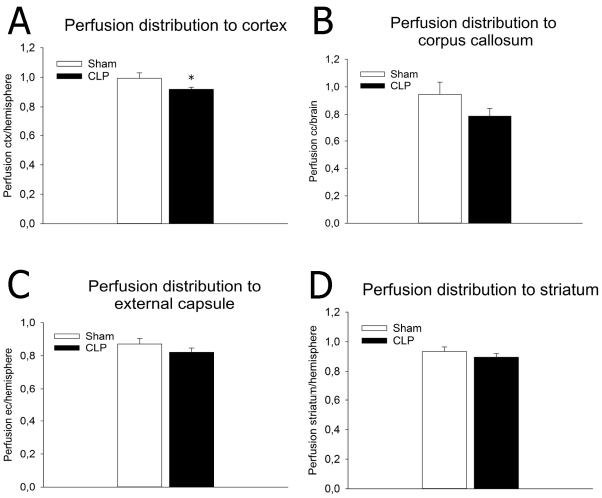

Figure 4:

Perfusion distribution to rat cortical layers (A) and corpus callosum (B), external capsule (C) and striatum (D).Graphs represent perfusion relative to both hemispheres for all structures except for the corpus callosum that was expressed relative to global brain 24h after surgery. *: $p < 0.05$; Group sizes Sham: n=8; CLP: n=12.

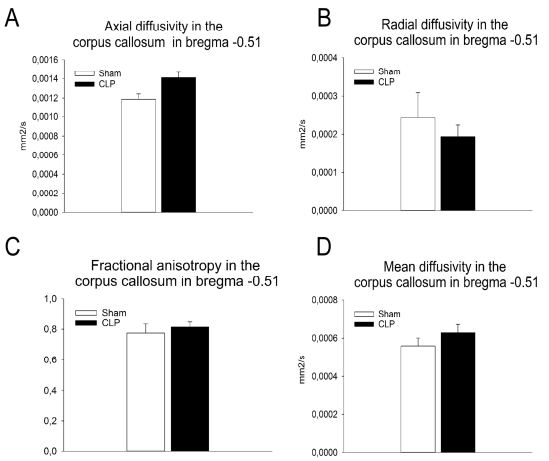

Figure 5:

Changes in axial diffusivity (A), radial diffusivity (B), fractional anisotropy (C) and mean diffusivity (D) in the corpus callosum in bregma -0.51mm, 24h after cecal ligation and puncture or laparotomy. *: $p < 0.05$. Group sizes Sham: n=7; CLP: n=12.

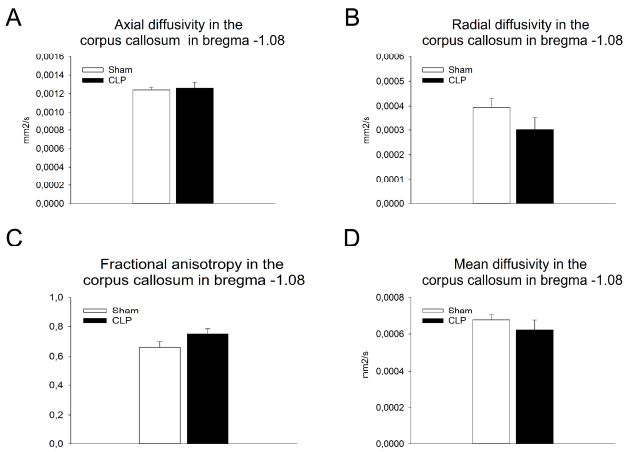

Figure 6:

Changes in axial diffusivity (A), radial diffusivity (B), fractional anisotropy (C) and mean diffusivity (D) in the corpus callosum in bregma -1.08mm, 24h after cecal ligation and puncture or laparotomy. *: $p < 0.05$. Group sizes Sham: n=7; CLP: n=12.

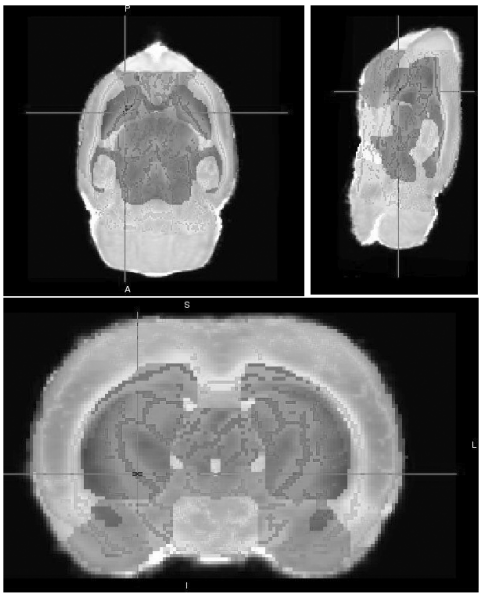

Figure 7:

Placement of differences observed in the striatum using Voxel-based analysis using tract-based spatial statistics (TBSS) with 5000 permutations demonstrating an increase of FA in the base of striatum (Caudate putamen+ Globus Pallidus) in the bregma between -0.51 and -0.83 mm.

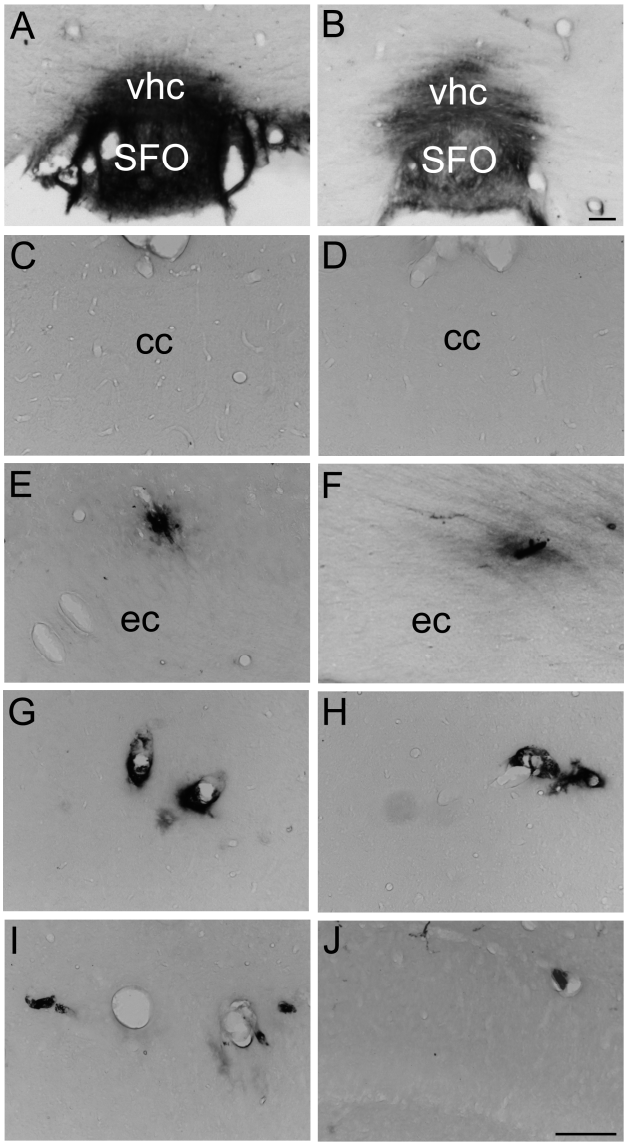

Figure 8:

Photomicrographs illustrating the distribution of rat IgG-ir in ventral hippocampal comissure (A,B), the corpus callosum (C,D), deep layers of the somatosensory cortex (E,F), dorsoslateral striatum (G,H) and hippocampus (I,J), 24 h after laparotomy or cecal ligation and puncture in rats. cc: corpus callosum; ec: external capsule; vhc: ventral hippocampal comissure; SFO: subfornical organ. Scale bar = 100 µm.

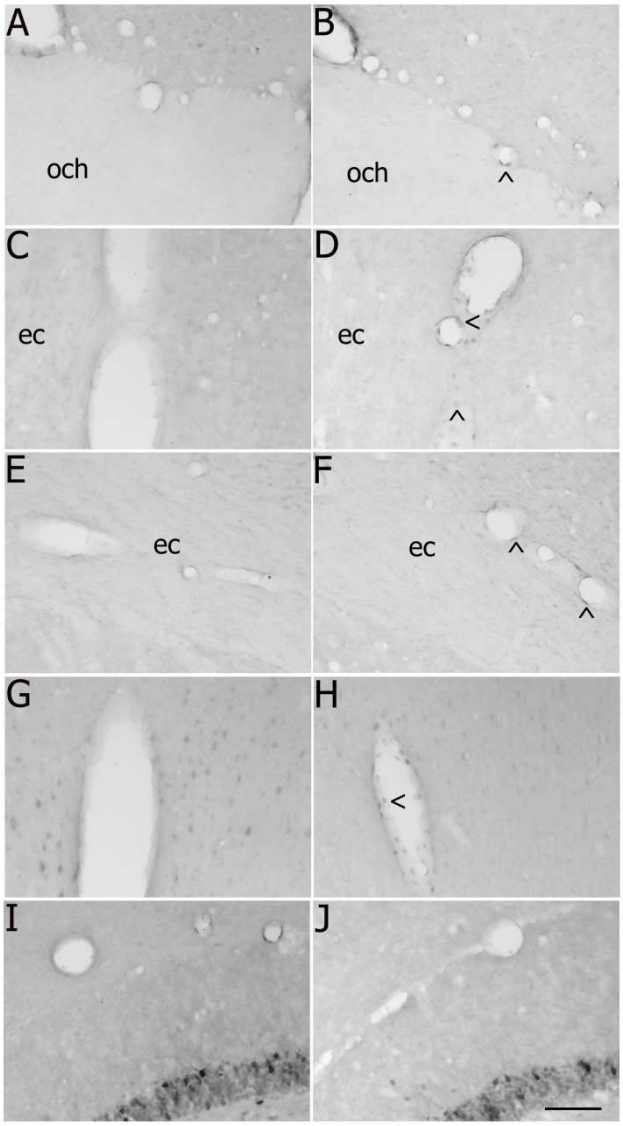

Figure 9:

Photomicrographs illustrating the distribution of COX-2-ir in para-suprachiasmatic nucleus (A,B), caudate putamen (C,D), external capsule (E,F), the cortical hemispheres (G,H) and hippocampus (I,J) 24h after laparotomy or cecal ligation and puncture in rats.

och: optic chiasm; ec: external capsule. Arrow heads > and < indicate labeling. Scale bar = 100 μm.

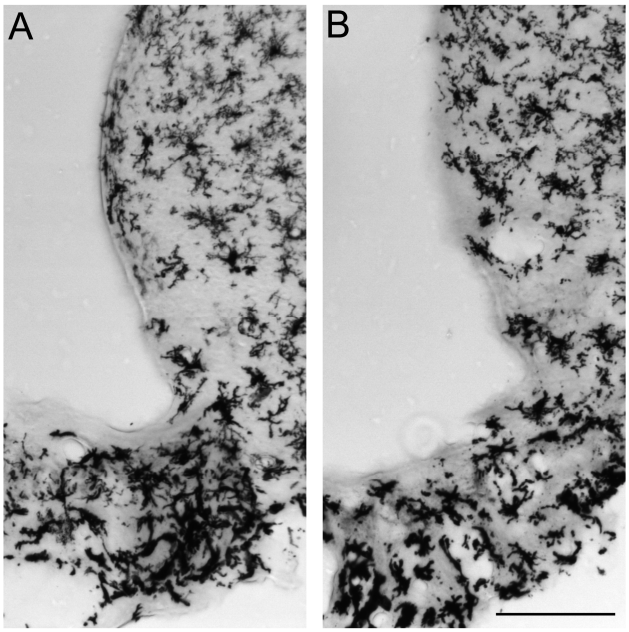

Figure 10 :

Photomicrographs illustrating the microglia activation around median eminence 24h after laparotomy (A) or cecal ligation and puncture (B) in rats. Scale bar = 100 µm.

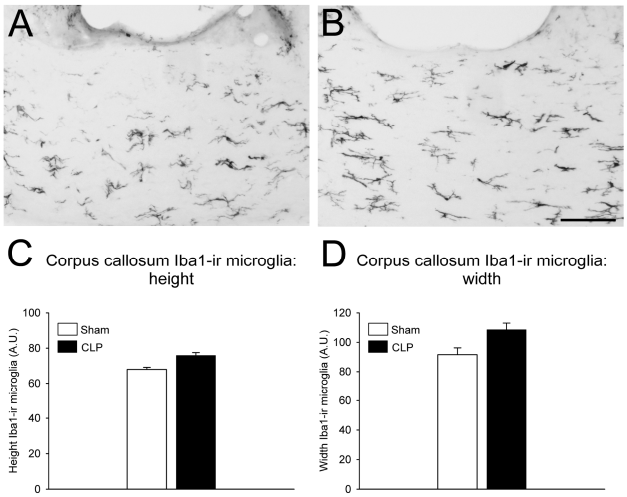

Figure 11:

Photomicrographs illustrating Iba1-ir microglia in the corpus callosum after laparotomy (A) or cecal ligation and puncture (B) in rats. Quantitative Fraclac-based analysis of microglial height (C), width (D) in the corpus callosum on brain sections situated between bregma -0.11 and -1.33 mm. Sham: n=9; CLP: n=11. Scale bar = 100 µm.

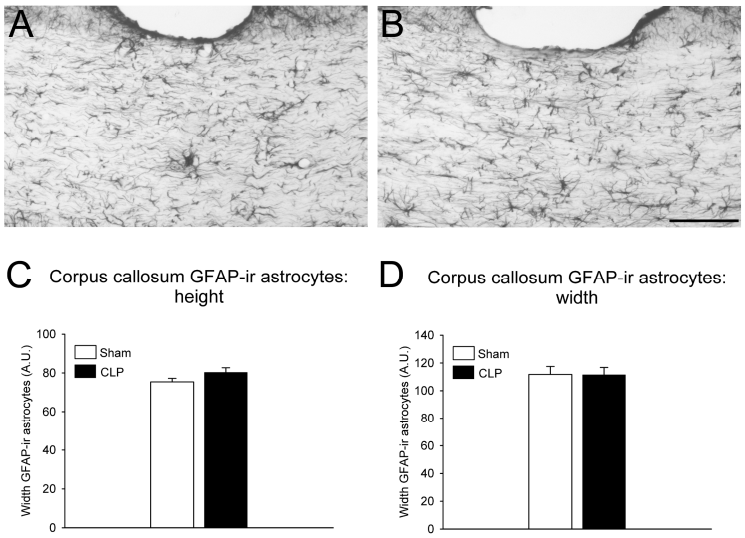

Figure 12:

Photomicrographs illustrating GFAP-ir astrocytes in the corpus callosum after laparotomy (A) or cecal ligation and puncture (B) in rats. Quantitative Fraclac-based analysis of microglial height (C), width (D) in the corpus callosum on brain sections situated between bregma -0.11 and -1.33 mm. Sham: n=9; CLP: n=11. Scale bar = 100 µm.

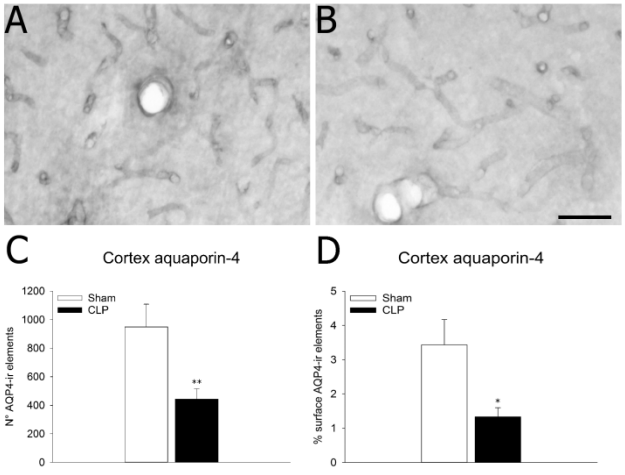

Figure 13:

Photomicrographs illustrating AQP4-ir astrocytes end-feet in the cortex after laparotomy (A) or cecal ligation and puncture (B) in rats and the surface occupied by AQP-4. Quantification of the number (C) and % of the surface occupied by AQP-4-ir elements (D) in the cortex on sections between bregma -0.46 and -1.08 nmm. Sham: n=7; CLP: n=9. Scale bar = 50 µm.

Chapter 4

Magnetic resonance imaging under isoflurane anesthesia alters blood-brain barrier permeability and glial cell morphology during sepsis-associated encephalopathy in rats

Ibtihel Dhaya[a,b,c] Marion Griton[a,b,d], Mohamed Amri[c] and Jan Pieter Konsman[a,b]*

a INCIA, Institut de Neurosciences Cognitive et Intégrative d'Aquitaine, UMR 5287, Bordeaux, France

b Univ. Bordeaux, INCIA, UMR 5287, Bordeaux, France

c Laboratoire de Neurophysiologie Fonctionnelle et Pathologies, UR/11ES09, Faculté des Sciences Mathématiques, Physiques et Naturelles, Université de Tunis El Manar, Tunis, Tunisie

d Service de Réanimation Anesthésie Neurochirurgicale, Centre Hospitalier Universitaire (CHU) de Bordeaux, Bordeaux, France

Running title: MRI under anesthesia alters blood-brain interface and glia

Abbreviations used:

AI: agranular insular area;

BBB: blood-brain barrier;

cc: corpus callosum;

ccg: genus of the corpus callosum;

CLP: cecal ligation and puncture;

CLP+: CLP/MRI+

CLP-: CLP/MRI-

CNS: central nervous system;

COX-2: cyclooxygenase-2;

CP: caudate putamen;

ec: external capsule;

fi: fimbria;

GFAP: glial fibrillary acidic protein;

GPe: external segment of globus pallidus;

Gu: gustatory area;

Iba-1: ionized calcium-binding adaptor molecule;

IgG: immunoglobulin G;

IL-1beta: interleukin-1β;

LPS: lipopolysaccharide;

MRI : magnetic resonance imaging;

NS: non-significant;

PET: Positron Emission Tomography;

ROI: Regions Of Interest;

SAE: sepsis-associated encephalopathy;

Sh.+: sham/MRI+

Sh.-: sham/MRI-

SSs: supplemental somatosensory area

vhc: ventral hippocampal commissure;

VISC: visceral area.

Abstract

Magnetic Resonance Imaging (MRI) of rodents under anesthesia followed by histology is a very promising approach to determine what mechanisms may be underlying functional and structural changes in the brain during sepsis-associated encephalopathy (SAE). As isoflurane anesthesia is a method of choice for MRI, but has the potential to modify the blood-brain interface and glia cells, this study addressed the effect of MRI under isoflurane anesthesia on BBB integrity, COX-2 expression and glial cells activation during CLP-induced SAE in rats. CLP reduced food intake and induced deficits in the righting reflex indicating SAE. MRI under isoflurane anesthesia after laparotomy under isoflurane anesthesia reduced BBB breakdown, decreased circularity of white matter astrocytes and increased neuronal COX-2 immunoreactivity in the cortex of rodents. In addition, it annihilated CLP-induced sepsis-associated increased circularity of white matter glial cells, but without altering perivascular COX-2 induction. These findings indicate that, depending on the measure of interest, MRI under isoflurane anesthesia can modify neurovascular and glial responses and should, therefore, be interpreted with caution.

Keywords

Anesthesia, blood-brain barrier, cecal ligation and puncture, glia, isoflurane, magnetic resonance imaging, sepsis

Introduction

The invention of anesthesia has been instrumental for medicine and the life sciences, because it allowed for surgery and intervention studies while limiting suffering. More recently, anesthesia of animals has made it possible to implement low-invasive medical imaging techniques, such as Positron Emission Tomography (PET) and Magnetic Resonance Imaging (MRI) modalities, in laboratory animals. Indeed, as these techniques, which are now the methods of choice in exploring human brain structure and function, require that the subject does not move, anesthesia enabled to apply these to animals and minimize movement artefacts and stress.

But both clinical and experimental evidence has accumulated indicating that anesthesia has acute and long-term effects on the central nervous system (CNS) beyond that of simply reducing neuronal activity (see for review (Colon et al., 2017)). For example, it has been known for some time now that the widely used gaseous anesthetic isoflurane increases cerebral blood flow over time and alters cerebral autoregulation in rodents (Hendrich et al., 2001; Kehl et al., 2002; Aksenov, Eassa, Lakhoo, Wyrwicz, & Linsenmeier, 2012; Sicard et al., 2003). However, some other anesthetic molecules have even more profound effects on cerebral blood flow (Holmström & Åkeson, 2005). So, notwithstanding its cerebrovascular effects, isoflurane has been recommended as the anesthesia of choice for longitudinal experiments involving the study of neurovascular coupling because it provides robust activity-induced vascular response, easy control and good recovery (Masamoto & Kanno, 2012).

When studying brain function or dysfunction in response to stimuli that affect the body, like stimulation of the sense organs or exposure to microbial fragment, under anesthesia, one also needs to consider the effects that anesthesia may have on bodily processes. In the case of the systemic inflammatory response to infection or sepsis, isoflurane, but not other anesthetics, has been found to neither affect survival of Cecal Ligature and Puncture (CLP; (Herrmann et al., 2013)) nor systemic hemodynamic changes following intravenous administration of bacterial lipopolysaccharide (LPS) fragments (Schaefer et al., 1987). Nevertheless, beyond these broad measures, isoflurane has been shown to reduce LPS-induced pro-inflammatory cytokine production (Plachinta, Hayes, Cerilli, & Rich, 2003; Boost et al., 2007; Hofstetter et al., 2005; Fuentes et al., 2006; Hofstetter et al., 2007; Adams, Radhakrishnan, Helmer, & Mercer, 2008; Flondor et al., 2008).

In the case of sepsis-associated encephalopathy (SAE), breakdown of the blood-brain barrier, altered glial cell function and neuronal cell death have all been proposed to play in the brain

dysfunction that characterizes this syndrome (Papadopoulos, Davies, Moss, Tighe, & Bennett, 2000). Interestingly, isoflurane results in BBB breakdown (Tétrault, Chever, Sik, & Amzica, 2008; Acharya et al., 2015) and attenuates LPS-induced microglial activation and pro-inflammatory cytokine synthesis both *in vitro* and *in vivo* (Kim, Liaoliao, & Zhiyi, 2009; Tanaka et al., 2013; Shuangmei Yang et al., 2016). Isoflurane thus has the potential to be an important confounding factor in the study of SAE in animals.

In our recent work, we have used MRI combined with histology in a first attempt to determine what mechanism may be underlying functional and structural changes in the brain during SAE. In doing so, we have noticed that LPS-induced perivascular COX-2 expression seemed lower in animals isoflurane-anesthetized animals that had undergone MRI (Dhaya et al., J. Neuroimmunol., accepted) in comparison to that previously observed in awake animals (J. Konsman, Vigues, Mackerlova, Bristow, & Blomqvist, 2004). This study will address the effect of MRI under isoflurane anesthesia on BBB integrity, COX-2 expression and glial cells activation during CLP-induced SAE.

Materials and methods

Animals

Experiments were conducted according to European recommendations on animal research (European Council Directive of 24 November 1986 (86/609/EEC) and European Parliament and Council Directive of 22 September 2010 (2010/63/UE)). Forty-two male Wistar rats (Charles Rivers, L'arbresle, France), weighing a mean 343.4 ± 2.4 g were housed two per cage in a temperature-controlled room (22°± 1 °C) in a 12 h dark-light cycle with free access on water and food during one week before starting experiments. During this acclimation period, animals were left undisturbed except for daily handling starting three days before surgery.

Surgery

On the day of surgery, animals were anesthetized with isoflurane (induction 3-5%; maintenance 1.5% in air). Once anesthetized, twenty-four rats underwent polymicrobial intra-abdominal infection induced by CLP as previously described (Wichterman, Baue, & Chaudry, 1980). Briefly, after a 2-3-cm midline abdominal incision, the cecum was exposed in sterile saline on laboratory film (Parafilm, Neenah, WI, USA) and ligated with a 3-0 silk suture (Ethicon, Issy les Moulineaux, France) just below the ileocecal valve and subsequently

punctured twice with a 22 G sterile needle. Next, a small drop of cecal contents was gently pushed out, before the cecum was gently placed back into the peritoneal cavity and the abdomen was sutured in two layers. At the end of the operation, animals received 5 ml of saline and analgesia (butrophanol, Torbugesic®; 2 mg/kg subcutaneously) and were placed in a clean individual cage. For the seventeen rats that were sham-operated, the same manipulations were performed except cecal ligation and puncture and saline injection. Thirty minutes after the end of surgery animals were awake and moving around.

Behavioral evaluation

Daily food and water intake and body weight were measured prior and posterior to surgery. Sham and CLP-operated rats were tested at different time points before and after surgery for two simple non-postural (pinna and corneal reflexes) and one complex postural somatomotor reflex (Righting reflex).

The pinna reflex was assessed by lightly touching the auditory meatus with a cotton stick tip and recording the occurrence and rapidity of ear retraction or head shake. The corneal reflex was tested by gently touching the cornea with a cotton stick tip and scoring the occurrence and rapidity of eye blinks. The righting reflex consisted of picking up the animal behind the forepaws and holding its trunk horizontally back upwards before putting the animal's back down and evaluating the time required to turn over to an upright position.

Magnetic resonance imaging

MRI experiments were performed on a 7T horizontal-bore scanner (Advance III console, Bruker, Ettlingen, Germany) equipped with a magnetic field gradient system providing a maximum gradient strength of 650 mT/m), a quadrature coil for radio-frequency emission and a 4-element phased-array surface coil for signal reception. Intracolonic temperature was constantly monitored and the animal was heated when colonic temperature dropped below 35.5°C by warm water circulating in the bed used to position the rat inside MRI scanner.

Respiration was assessed with a ventral pressure sensor and heart rate recorded using an MRI compatible electrode. After careful second-order shimming, images were acquired and processed as previously described in chapter 3.

Immunohistochemistry

At the end of MRI or 26 h after CLP without MRI, rats were deeply anaesthetized by intraperitoneal injection of 60mg/kg of Sodium Pentobarbital. Bodies were rinsed from blood

by intracardiac perfusion with 0.1 M phosphate-buffered saline (PBS; pH 7.4 at room temperature) and subsequently fixed by 300 ml of 4% paraformaldehyde in 0.1 M PBS. Brains were removed from the skull, post-fixed for 4 h in the same fixative, and then cryoprotected in 30% sucrose in 0.1 M phosphate buffer. Forty-micrometer thick sections were cut on a cryostat (CM3050 S, Leica Microsystems, Nussloch, Germany) from the rostral limit of the optic chiasm to the caudal end of the central amygdala (Swanson, 1998) and collected in cold cryoprotectant solution (0.05 M PBS, 20 % glycerol, 30% ethylene glycol) and stored at -20°C until processing.

Immunohistochemistry was performed as previously described (J. Konsman et al., 2004; Jan Pieter Konsman & Blomqvist, 2005; J P Konsman et al., 2008). Briefly, free-floating sections were washed four times in 0.1 M PBS (pH 7.4). Non-specific binding sites were blocked by a 45-minute incubation of sections in PBS containing 0.3% Triton X-100 and 2.0% normal serum or 1.0% BSA. The first antibody was then diluted (indicated below for every antiserum used) in the same buffer and added to the sections overnight at room temperature. Antisera raised against the different markers to which we were interested are resumed in the table below.

Commercially available antisera raised against COX-2 (goat anti-COX-2; M-19 sc-1747, lot# F2512,Santa Cruz Biotechnology, Heidelberg, Germany) diluted 1:750, the microglia-macrophage specific ionized calcium-binding adaptor molecule (Iba-1; rabbit anti-Iba-1; 019-19741, Wako Chemicals GmbH, Neuss, Germany) diluted 1:1000 and rat immunoglobulin G (IgG; biotinylated goat anti IgG, BA-9401, Vector Laboratories, Burlingame, CA, USA) diluted 1:2000 and the intermediate filament Glial fibrillary acidic protein GFAP (mouse anti-GFAP mAb, clone GA5, MAB360, Merck Millipore, Fontenay sous Bois, France) diluted 1:500 were used.

After four rinses in PBS, sections were treated for 30 minutes with 0.3% (v/v) hydrogen peroxide to block endogenous peroxidases followed by rinses in PBS. With the exception of those sections exposed to biotinylated rat IgG, sections were then incubated for 2 h with biotinylated antisera raised against IgGs of the species of the first antibody (Vector Laboratories, Burlingame, CA, USA) diluted 1:500 in PBS, 0.3% Triton X-100, 1% BSA or normal serum. After four washes in PBS, sections were incubated for 2 h with avidin and biotinylated peroxidase complex (Vector Laboratories, Burlingame, CA, USA) diluted in PBS to 1:750 in IgG immunostaining and 1:500 in others. Finally, sections were transferred to a

sodium acetate buffer and stained using diaminobenzidine as a chromogen in the presence of Ni-ions, thus providing yielding a dark grey to black precipitate.

Microscopy and image analysis

Staining reactions were stopped by rinses in sodium acetate and PBS, after which sections were mounted on slides in 0.5% gelatin in distilled water containing chromo-potassium sulphate, dehydrated in alcohol, defatted in xylene and coverslipped with Eukitt (O.Kindler GmbH & CO, Freiburg, Brisgau, Allemagne). Stained sections were examined with a light-microscope (Leica DM5500B, Leica Microsystems, Nanterre, France) and images were captured by a high-resolution digital camera system (Leica DFC425C, Leica Microsystems, Nanterre, France) and stored onto a personal computer. In every brain section between bregma +4,85 and -2,85 mm the occurrence and extent (scored as restricted (1), intermediate (2) or extensive (3)) of perivascular IgG diffusion in a given structure was noted. As each region or structure considered covered at least two, but a varying number (depending on the length of the structure) of brain sections (with two consecutive sections being separated by 240 µm), the number of occurrences of perivascular IgG diffusion for a structure were then divided by the number of brain sections in which the structure was present. Similarly, the cumulative score of the extent of IgG diffusion for a given brain region or structure was also divided by the number of sections that contained the region or structure in question.

The counts and relative surfaces of COX-2, GFAP and Iba-1-immunoreactive elements were quantified after application of fixed particle size and intensity criteria on 8-bit images with Image J (http://imagej.nih.gov/ij/). In addition, Iba-1- and GFAP- immunostaining was characterized using the Image J plugin Fraclac (http://rsb.info.nih.gov/ij/plugins/fraclac/fraclac.html). Briefly, on binary images of brain sections between bregma -0.11 and -1.33 mm, Iba-1-positive cells (size between 300-6000 pixels) and GFAP-immunoreactive cells (size between 300-8000 pixels) were enclosed by a Hull convex (a boundary enclosing the foreground pixels of an image using straight line segments to each outermost point) and bounding circle after which the surface, perimeterand circularity (defined as $4*\pi*\text{Area} / \text{Perimeter}^2$) were determined in addition to the width and height of the cells. Iba-1 cell size and activation was also evaluated as described by Hovens et al (2014) with Image J. Briefly, a minimum size filter was applied on cell body size (>150 pixels) before cell and cell body size were distinguished based on an intensity criterion. Finally, three different categories of sizes of GFAP-positive elements (GFAP: <300 pixels

considered as astrocytic fragments; 300<pixels<8000 considered as astrocytes; pixels>8000 considered as astrocytes in contact) were quantified in terms of number and relative surface after application of either an automatic or manually-fixed intensity threshold.
Image editing software (Adobe Photoshop, Adobe Systems, San Jose, CA, USA) was used only to adjust contrast and brightness for photomicrographs composing illustrating figures.

Data representation and analysis

Food intake and water intake were expressed relative to 100 g of body weight and 100 g of food intake respectively. All data were expressed as means ± standard error of the mean (SEM) and analyzed by either a one-way ANOVA/student-t test with surgery as a between factor (food and water intake) or a two-way ANOVA with surgery and imaging between factors (immunohistochemistry data). When data were not normally distributed, a log10 or square root transformation was performed, and if still not normally distributed then the non-parametric Kruskall-Wallis test was used. In all cases, a level of $p<0.05$ was considered as statistically significant.

Results

CLP reduced food intake and induced encephalopathy

One animal died at the induction of anesthesia for surgery while another died at the end of sham-surgery. Within the 23 h following the end of surgery, no mortality was observed in the sham-operated group (One animal did die however at the induction of anesthesia for imaging.) while 3 out of 24 CLP animals died (12.5% mortality).
A Mann-Whitney U-tests on food consumption relative to body weight during the 24h after the start of surgery showed a significant lower food intake in animals that underwent CLP as compared to sham-operated rats (U: 67.0, $p<0.05$) (Figure 1A). Mann-Whitney tests on reflexes showed that CLP significantly reduced the righting reflex 4 h (U: 102, $p<0.05$), 8 h (U: 24.5, $p<0.001$) and 24 h (U: 19.5, $p<0.001$) (Figure 1D) and had a tendency to decrease the pinna reflex 4 h (U: 137.0, $p=0.054$) (Figure 1B) later as compared to sham surgery without affecting the corneal reflex (Figure 1C).

Imaging under anesthesia attenuates BBB breakdown following abdominal surgery

In all animals, IgG was found in brain regions lacking a functional BBB including the choroid plexus, meninges and circumventricular organs from which it spread to surrounding regions (Figure 2A-D).

A two-way ANOVA on the occurrence of perivascular plume-like diffusion clouds of IgG staining in the whole cortex between bregma +4,85 and -2,85 mm revealed a significant effect of imaging under anesthesia ($F_{1,26}$: 7.75, $p<0.01$; Table 1) and a tendency for an interaction between surgery and imaging under anesthesia ($F_{1,26}$: 3.09, $p=0.091$; Table 1). *Post-hoc* tests revealed that perivascular IgG diffusion was more frequent in animals that did not undergo imaging as compared to in rats that underwent imaging under anesthesia ($p<0.05$). In the hippocampus, a Kruskal-Wallis test on the occurrence of BBB breakdown revealed by perivascular IgG diffusion did not show any significant main effect or interaction.

When considering all striatal structures together, a two-way ANOVA on the occurrence of perivascular IgG showed a tendency for interaction between surgery and imaging under anesthesia ($F_{1,26}$: 3.64, $p=0.068$; Table 1). However, *post-hoc* tests revealed no significant differences between the four groups. When considering all white matter bundles between bregma +4,85 and -2,85 mm, a two-way ANOVA revealed a significantly lower occurrence of perivascular plume-like diffusion clouds of IgG staining in animals that underwent imaging under anesthesia as compared to rats that did not undergo a second anesthesia after surgery ($F_{1,26}$: 5.49, $p<0.05$; Table 1).

Imaging under anesthesia does not alter CLP induced perivascular COX-2 expression, but affects constitutive cortical COX-2

No or very weak COX-2 immunoreactivity was found associated with blood vessels in the preoptic area (Figure 3A, C), caudate putamen (Figure 3E, G), external capsule (Figure 3I, K), cortex (Figure 3M, O) or hippocampus (Figure 3Q, S) of animals subjected to sham-surgery. However, distinct perivascular disc-like COX-2-immunoreactive cells were frequently observed in these structures in rats that underwent CLP (Figure 9B, D, F, H, J, L, N, P, R and T). Except for hippocampal vessels where perivascular COX-2-staining was stronger after CLP without subsequent imaging, no major differences in perivascular COX-2-immunoreactivity were observed between animals that underwent imaging under anesthesia and that those that did not.

Constitutive COX-2 expression was detected in neurons of the hippocampus (Figure 3Q-T) and to a lesser extent, in neurons of the cortex (Figure 3M-P). A two-way ANOVA on the number of COX-2-positive elements in the cortex revealed significant effects of surgery ($F_{1,18}$=13.7, p<0.01) and imaging under anesthesia ($F_{1,18}$=16.6, p<0.001) as well as a significant interaction between these factors ($F_{1,18}$=13.2, p<0.01). *Post-hoc* analysis indicated more COX-2-immunoreactive cells in the cortex of animals that underwent sham surgery followed by imaging under anesthesia than in that of sham-operated animals not undergoing imaging (p<0.001) and significant less COX-2 positive cells in CLP as compared to sham-surgery in animals that underwent imaging (p<0.001).

A two-way ANOVA on the relative surface occupied by COX-2-immunoreactivity in the cortex indicated a significant effect of surgery ($F_{1,18}$=4.86, p<0.05) and tendencies for an effect of imaging under anesthesia ($F_{1,18}$=3.69, p=0.071) as well as for an interaction between factors ($F_{1,18}$=3.85, p=0.066). *Post-hoc* analysis showed a significantly lower relative surface of COX-2-immunoreactivity in the cortex of animals that underwent CLP as compared to sham-surgery (p<0.05).

CLP increases microglial circularity in the corpus callosum in rats that were not imaged

Two-way ANOVAs on the number of and relative surface occupied by Iba-1-positive elements in the corpus callosum between bregma -0.11 and -1.33 mm with surgery and imaging under anesthesia as between factors did not indicate any significant differences. Similar analyses on the activation state of Iba-1-stained microglia according to Hovens and collegues (Hovens et al, 2014) revealed a tendency for an effect of imaging under anesthesia of cell size ($F_{1,23}$=3.00, p=0.096) and a tendency for an interaction between surgery and imaging under anesthesia for cell body size ($F_{1,23}$=3.34, p=0.081) and activation state ($F_{1,23}$=3.18, p=0.09). *Post-hoc* tests only showed a tendency for decreased cell size in CLP as compared to sham surgery in those animals that underwent imaging under anesthesia (p=0.092).

Two-way ANOVAs on values measured at individual bregma levels revealed a tendency for an effect of imaging under anesthesia on Iba-1 stained cell size ($F_{1,18}$=5.83, p<0.05) at bregma level -0.51 mm.

Two-way ANOVAs on fractal parameters of Iba-1-positive cells in the corpus callosum between bregma -0.11 and -1.33 mm revealed a significant interaction between surgery and imaging under anesthesia for circularity ($F_{1,24}$=7.00, p<0.05) and cell width ($F_{1,24}$=7.32,

$p<0.05$) and a tendency for an interaction between treatments for cell height ($F_{1,24}=3.08$, $p=0.091$). *Post-hoc* analyses indicated a significantly increased circularity in CLP compared to sham surgery in animals that did not undergo imaging anesthesia ($p<0.05$) and tendencies for increased circularity in sham-operated animals that underwent imaging under anesthesia as compared to sham-operated rats that did not ($p=0.062$) and for decreased circularity in CLP rats that were imaged as compared to CLP animals that were not ($p=0.088$) In addition, post-hoc analyses showed a significantly lower width in CLP rats that did not undergo subsequent imaging in comparison to CLP animals that subsequently were imaged under anesthesia ($p<0.05$) as well as significantly higher width after CLP than after sham surgery in those animals that underwent imaging ($p<0.05$). Two-way ANOVAs on values measured at individual bregma levels revealed that imaging under anesthesia had a tendency to increase the area ($F_{1,19}=4.18$, $p=0.055$) and width ($F_{1,19}=3.32$, $p=0.084$) and a tendency for an interaction for height ($F_{1,19}=3.55$, $p=0.075$) of Iba-1 positive cells at bregma level -0.51 mm. However, *post-hoc* tests did not indicate any significant differences between groups.

Imaging under anesthesia alters astrocyte morphology

Two-way ANOVAs on the number of and relative surface occupied by GFAP-positive elements in the corpus callosum between bregma -0.11 and -1.33 mm with surgery and imaging under anesthesia as between factors revealed no significant differences.

Similar analyses on fractal parameters of GFAP-positive cells in the corpus callosum between bregma -0.11 and -1.33 mm indicated that imaging under anesthesia significantly increased cell width ($F_{1,24}=4.56$, $p<0.05$) and decreased circularity ($F_{1,24}=4.52$, $p<0.05$), but also had a tendency to increase cell perimeter ($F_{1,24}=3.95$, $p=0.058$) while CLP had a tendency to increase cell height ($F_{1,23}=3.04$, $p=0.094$). No significant or tendencies for interactions between surgery and imaging under anesthesia were found for fractal parameters.

Two way ANOVAs on fractal parameters of GFAP-positive elements measured at individual bregma levels showed a tendency for an effect of surgery on cell circularity ($F_{1,23}=3.51$, $p=0.074$) and a tendency for an interaction between surgery and imaging under anesthesia on circularity ($F_{1,23}=3.53$, $p=0.073$) at bregma -0.51 mm. *Post-hoc* analysis indicated a significantly higher circularity in CLP animals that were not subject to imaging under anesthesia than in CLP rats that were imaged ($p<0.05$) and a tendency for increased circularity in CLP rats compared to sham-operated animals that did not undergo subsequent imaging ($p=0.06$).

Discussion

The main finding of the present study was that imaging under isoflurane anesthesia one day after abdominal surgery reduced the frequency of perivascular diffusion of IgG into brain parenchyma, altered white matter astrocyte morphology and increased cortical COX-2 immunoreactivity. In addition, it annihilated CLP-induced increased circularity of white matter glial cells, but did not affect CLP-induced perivascular COX-2 expression.

The concept of tissue pre-conditioning was introduced in the context of research on ischemia to describe the idea that tissue exposure to brief subcritical ischemia can activate protective mechanisms that increase the tolerance to subsequent more critical ischemia (Steiger & Hänggi, 2007). Interestingly, pre-exposure to isoflurane also protects brain tissue against ischemic damage (Bedirli et al., 2012; Kitano, Kirsch, Hurn, & Murphy, 2007; Nasu et al., 2006). Moreover, a second exposure to isoflurane 24 h later has been shown to inhibit some of the effects of a single exposure to isoflurane on neuronal cell death (J. Peng et al., 2014). Hence, in the present work it was of interest to study if a second exposure to isoflurane anesthesia during imaging altered the BBB, COX-2 expression and glia cell morphology in rats that had undergone an abdominal sham-surgery or CLP under isoflurane anesthesia 24 h earlier.

Three hours of isoflurane anesthesia of 3-5 month old rats has been found to not significantly alter the frequency of perivascular diffusion of IgG in the cortex compared to unanesthetized controls (Acharya et al., 2015). In the present study, perivascular diffusion of IgG was occasionally found in the cerebral cortex as well as in the hippocampus, striatum and white matter of rats that underwent sham-surgery under approximately 1 h of isoflurane anesthesia the day before. Thus, our finding indicates that the BBB breakdown after laparotomy under isoflurane anesthesia, previously shown to be important 6 h later (Siming Yang et al., 2017), may still be somewhat present 24 h later. Interestingly, perivascular diffusion of IgG was less frequently encountered in the cortex and white matter of rats that underwent 2 h of MRI under isoflurane anesthesia one day after surgery as compared to those that underwent abdominal surgery without subsequent imaging under anesthesia. Since exposure to radiowaves has not been shown to tighten the BBB (Stam, 2010), this effect is likely to be related to the second isoflurane anesthesia. The finding that BBB breakdown was less frequently observed in animals on which abdominal surgery was performed being imaged under anesthesia than in those that just underwent surgery can be interpreted to suggest that isoflurane exerts a protective effect on the BBB one day after laparotomy.

Breakdown of the blood-brain barrier has been proposed to play a role in brain dysfunction and *delirium* during sepsis (Papadopoulos et al., 2000). Here, the loss of the righting reflex in animals that underwent CLP indicated brain dysfunction in agreement with previous studies (Kadoi & Goto, 2004; Kafa, Bakirci, Uysal, & Kurt, 2010; Kafa, Uysal, Bakirci, & Ayberk Kurt, 2010). However, in a previous study using the CLP model for combined brain imaging and histology, no indication of increased BBB permeability, based on the perivascular diffusion of IgG, was found in the parenchyma of the grey and white matter except for the fimbria (Griton et al., in preparation). This negative finding was at variance with numerous previous studies indicating BBB breakdown after CLP, but that did not use imaging (Avtan et al., 2011; Comim et al., 2011; Imamura et al., 2011; Jeppsson et al., 1981; Vachharajani et al., 2012; Yokoo et al., 2012). Importantly, the lack of CLP-associated BBB breakdown in our experimental paradigm was neither due to technical failure nor lack of sensitivity as perivascular IgG was readily observed in brain circumventricular organs and meninges, where the endothelial BBB is absent.

Since isoflurane anesthesia is known to induce delirium in patients (Lee, Kwan, Tsai, Chen, & Cheng, 1993; Locatelli et al., 2013; Meyer et al., 2013) and to alter behavior (M. Peng et al., 2016) and affect the BBB in rodents (Tétrault, Chever, Sik, & Amzica, 2008; Acharya et al., 2015), the possibility that imaging under isoflurane anesthesia masked the effects of CLP on the BBB was addressed in the present work. Importantly, assessment of BBB integrity with IgG detection on brain sections in animals that had not undergone MRI before sacrifice confirmed that CLP, as it was performed in the present study, did not significantly increase the frequency of perivascular IgG diffusion in the different forebrain regions considered as compared to sham surgery. It is important to keep in mind in this respect that the severity of CLP-induced sepsis depends on the size of the needle used to puncture as well as the number of punctures (Rittirsch, Huber-lang, Flierl, & Ward, 2009) and that the needle size used here was smaller than previous work reporting BBB breakdown after CLP in rodents (Avtan et al., 2011; Comim et al., 2011; Imamura et al., 2011; Jeppsson et al., 1981; Vachharajani et al., 2012; Yokoo et al., 2012). Hence, our experimental model in interesting in that it induces signs of neurological impairment in the absence of BBB breakdown for molecules of high molecular weight.

Glia cell dysfunction has also been suggested to play a role sepsis-associated encephalopathy (SAE) (Papadopoulos et al., 2000). Since isoflurane affects the cytoskeleton of astrocytes *in vitro* (Culley et al., 2013), it was important to determine if brain MRI under isoflurane

anesthesia affected glia cell markers in rats that underwent laparotomy or CLP 24 h earlier. Using the astrocytic cytoskeleton intermediate filament marker GFAP, imaging under anesthesia was found to increase cell width and decrease cell circularity, but not to alter the relative surface of staining in the white matter of the corpus callosum, where we had previously observed changed in water diffusion imaging indicating structural modifications after CLP (Griton et al., in preparation). Although the lack of effect of imaging under anesthesia on the relative surface of GFAP-immunoreactivity may suggest that isoflurane did not affect GFAP expression, it is important to bear in mind that immunohistochemical staining does not vary linearly with the amount of protein. On the other hand, reduced GFAP immunocytochemical staining has been shown to be accompanied with reduced GFAP mRNA expression in cultured astrocytes after exposure to 1.4% isoflurane for four hours (Culley et al., 2013). In the present work, GFAP-immunohistochemistry was however not used to estimate protein expression, but to assess astrocytic cell morphology as a criterion for their activation state. Imaging under anesthesia 24 h after laparotomy increased cell width and decreased circularity of GFAP-stained astrocytes in the corpus callosum. Moreover, at the anatomical level where the third ventricle is traversed by the junction of the white matter anterior commissure, GFAP-positive cells of the corpus callosum showed a higher circularity in CLP animals that had not been subject to imaging under anesthesia than those of CLP rats that were imaged ($p<0.05$). Finally, at this anatomical level and among the animals that were not imaged, GFAP-immunoreactive cells also had a tendency to display higher circularity in the corpus callosum of CLP rats compared to those of sham-operated animals. In the white matter reactive astrocytes show hypertrophy of cell bodies, retraction of processes and a reduction of branching, and loss of their orientation (Sun & Jakobs, 2012), which can be expected to result in increased circularity. Hence, the increased circularity of GFAP-stained cell in the corpus callosum of CLP rats as compared to sham-operated animals that did not undergo imaging can be interpreted to suggest activation of astrocytes. However, this effect seems to be annihilated by imaging as CLP rats that were imaged displayed lower circularity than their septic counterparts that were not.

As isoflurane decreases bacterial LPS-induced pro-inflammatory cytokine expression by microglia both *in vitro* and *in vivo* (Tanaka et al., 2013), it was of interest to study if imaging under isoflurane anesthesia would influence microglial activation after CLP by analyzing the morphology of Iba-1-positive cells. These analyses focused on the corpus callosum where we had previously observed changes in water diffusion imaging indicating structural

modifications in CLP rats (Griton et al., in preparation). Interestingly, these analyses revealed increased circularity of Iba-1-positive cells in the corpus callosum after CLP compared to sham surgery in animals that did not undergo imaging anesthesia and tendencies for increased circularity in sham-operated animals that underwent imaging under anesthesia as compared to sham-operated rats that did not, but decreased circularity in CLP rats that were imaged as compared to CLP animals that were not. Since increased circularity is a hallmark of activation of microglia, our findings indicate that imaging under anesthesia masked CLP-associated microglial activation in the corpus callosum.

Cortical COX-2 plays an important role in neurovascular coupling (Niwa, Araki, Morham, Ross, & Iadecola, 2000; Stefanovic, Bosetti, & Silva, 2006) and prostaglandin has been proposed to play a role in isoflurane-induced hyperemia (Moore et al., 1994). Since our previous worked indicated both lower blood distribution and decreased neuronal COX-2 in the cortex of CLP rats that underwent imaging (Griton et al., in preparation), it was important to consider the possibility that the latter effect was related to isoflurane anesthesia. Here, imaging under anesthesia was found to increase the number of COX-2-positive cells in the cortex in animals that underwent laparotomy 24 h earlier and more COX-2-immunoreactive neurons were counted in the cortex of animals that underwent sham surgery followed by imaging under anesthesia than in that of sham-operated animals not undergoing imaging. Moreover, the decrease in the number of COX-2-positive elements in the cortex of CLP rats as compared to sham-operated animals that subsequently were imaged was not observed in rodents that did not undergo imaging. Interestingly, surgery under isoflurane anesthesia on other body parts than the abdominal cavity also increases COX-2-immunoreactivity in neurons of the spinal cord (Brennan, Harte, Fitzgerald, & McCrory, 2009), suggesting that isoflurane has similar effects on neuronal COX-2 at different levels of the CNS. However, the perivascular induction of COX-2 after CLP did not seem affected by imaging under anesthesia in the present work indicating that its induction previously observed in CLP animals that underwent imaging the latter effect was not an artifact related to isoflurane anesthesia.

In conclusion, this is the first study to show that MRI under isoflurane anesthesia after laparotomy under isoflurane anesthesia reduced BBB breakdown, decreased circularity of white matter astrocytes and increased neuronal COX-2 immunoreactivity in the cortex of rodents. In addition, it annihilated CLP-induced sepsis-associated increased circularity of

white matter glial cells, but without altering perivascular COX-2 induction. These findings indicate that, depending on the measure of interest, MRI under isoflurane anesthesia can modify neurovascular and glial responses and should, therefore, be interpreted with caution.

Acknowledgements

Ibtihel Dhaya was a laureate of a stipend from the Ministère de l'Enseignement Supérieur et de Recherche Scientifique in Tunisia. Administrative help from Adera (Pessac, France) is gratefully acknowledged.

References

Acharya, N. K., Goldwaser, E. L., Forsberg, M. M., Godsey, G. A., Johnson, C. A., Sarkar, A., … Nagele, R. G. (2015). Sevoflurane and Isoflurane induce structural changes in brain vascular endothelial cells and increase blood-brain barrier permeability: Possible link to postoperative delirium and cognitive decline. *Brain Research*, *1620*, 29–41. https://doi.org/10.1016/j.brainres.2015.04.054

Adams, S. D., Radhakrishnan, R. S., Helmer, K. S., & Mercer, D. W. (2008). Effects of anesthesia on lipopolysaccharide-induced changes in serum cytokines. *The Journal of Trauma*. https://doi.org/10.1097/TA.0b013e31805824ca

Aksenov, D., Eassa, J. E., Lakhoo, J., Wyrwicz, A., & Linsenmeier, R. A. (2012). Effect of isoflurane on brain tissue oxygen tension and cerebral autoregulation in rabbits. *Neuroscience Letters*, *524*(2), 116–118. https://doi.org/10.1016/j.neulet.2012.07.019

Avtan, S. M., Kaya, M., Orhan, N., Arslan, A., Arican, N., Toklu, A. S., … Ahishali, B. (2011). The effects of hyperbaric oxygen therapy on blood-brain barrier permeability in septic rats. *Brain Research*, *1412*, 63–72. https://doi.org/10.1016/j.brainres.2011.07.020

Bedirli, N., Bagriacik, E. U., Emmez, H., Yilmaz, G., Unal, Y., & Ozkose, Z. (2012). Sevoflurane and Isoflurane Preconditioning Provides Neuroprotection by Inhibition of Apoptosis-related mRNA Expression in a Rat Model of Focal Cerebral Ischemia. *Journal of Neurosurgical Anesthesiology*, *24*(4), 336–344. https://doi.org/10.1097/ANA.0b013e318266791e

Boost, K. A., Flondor, M., Hofstetter, C., Platacis, I., Stegewerth, K., Hoegl, S., … Zwissler, B. (2007). The beta-adrenoceptor antagonist propranolol counteracts anti-inflammatory effects of isoflurane in rat endotoxemia. *Acta Anaesthesiologica Scandinavica*, *51*(7), 900–908. https://doi.org/10.1111/j.1399-6576.2007.01363.x

Brennan, L. K., Harte, B. H., Fitzgerald, D. J., & McCrory, C. R. (2009). Surgery induces cyclooxygenase-2 expression in the rat cervical spinal cord. *Reg Anesth Pain Med*, *34*(6), 549–552. https://doi.org/10.1097/AAP.0b013e3181b494cb\r00115550-200911000-00004 [pii]

Colon, E., Bittner, E. A., Kussman, B., McCann, M. E., Soriano, S., & Borsook, D. (2017). Anesthesia, brain changes, and behavior: Insights from neural systems biology. *Progress in Neurobiology*, *153*, 121–160. https://doi.org/10.1016/j.pneurobio.2017.01.005

Comim, C., Vilela, M., Constantino, L., Petronilho, F., Vuolo, F., Lacerda-Queiroz, N., … Dal-Pizzol, F. (2011). Traffic of leukocytes and cytokine up-regulation in the central nervous system in sepsis. *Intensive Care Medicine*, *37*, 711–718. https://doi.org/10.1007/s11046-013-9679-3

Culley, D. J., Cotran, E. K., Karlsson, E., Palanisamy, A., Boyd, J. D., Xie, Z., & Crosby, G. (2013). Isoflurane affects the cytoskeleton but not survival, proliferation, or synaptogenic properties of rat astrocytes in vitro. *British Journal of Anaesthesia*, *110*(SUPPL.1), 19–28. https://doi.org/10.1093/bja/aet169

Flondor, M., Hofstetter, C., Boost, K. A., Betz, C., Homann, M., & Zwissler, B. (2008). Isoflurane inhalation after induction of endotoxemia in rats attenuates the systemic cytokine response. *European Surgical Research*, *40*(1), 1–6. https://doi.org/10.1159/000107614

Herrmann, I. K., Castellon, M., Schwartz, D. E., Hasler, M., Urner, M., Hu, G., … Beck-Schimmer, B. (2013). Volatile Anesthetics Improve Survival after Cecal Ligation and Puncture. *Anesthesiology*, *119*(4), 901–906. https://doi.org/10.1002/smll.201500674.Development

Hofstetter, C., Flondor, M., Boost, K. A., Koehler, P., Bosmann, M., Pfeilschifter, J., …

Mühl, H. (2005). A brief exposure to isoflurane (50 s) significantly impacts on plasma cytokine levels in endotoxemic rats. *International Immunopharmacology*, *5*(10), 1519–1522. https://doi.org/10.1016/j.intimp.2005.04.008

Holmström, A., & Åkeson, J. (2005). Desflurane induces more cerebral vasodilation than isoflurane at the same A-line autoregressive index level. *Acta Anaesthesiologica Scandinavica*. https://doi.org/10.1111/j.1399-6576.2005.00697.x

Imamura, Y., Wang, H., Matsumoto, N., Muroya, T., Shimazaki, J., Ogura, H., & Shimazu, T. (2011). Interleukin-1β causes long-term potentiation deficiency in a mouse model of septic encephalopathy. *Neuroscience*, *187*, 63–69. https://doi.org/10.1016/j.neuroscience.2011.04.063

Jeppsson, B., Freund, H. R., Gimmon, Z., James, J. H., von Meyenfeldt, M. F., & Fischer, J. E. (1981). Blood-brain barrier derangement in sepsis: Cause of septic encephalopathy? *The American Journal of Surgery*, *141*(1), 136–142. https://doi.org/10.1016/0002-9610(81)90026-X

Kadoi, Y., & Goto, F. (2004). Selective inducible nitric oxide inhibition can restore hemodynamics, but does not improve neurological dysfunction in experimentally-induced septic shock in rats. *Anesthesia and Analgesia*, *99*(1), 212–20. https://doi.org/10.1213/01.ANE.0000118111.94913.22

Kafa, I. M., Bakirci, S., Uysal, M., & Kurt, M. A. (2010). Alterations in the brain electrical activity in a rat model of sepsis-associated encephalopathy. *Brain Research*, *1354*, 217–226. https://doi.org/10.1016/j.brainres.2010.07.049

Kafa, I. M., Uysal, M., Bakirci, S., & Ayberk Kurt, M. (2010). Sepsis induces apoptotic cell death in different regions of the brain in a rat model of sepsis. *Acta Neurobiologiae Experimentalis*, *70*, 246–260.

Kim, J.-A., Liaoliao, L., & Zhiyi, Z. (2009). Delayed treatment with isoflurane attenuates lipopolysaccharide and interferon γ-induced activation and injury of mouse microglial cells. *Anesthesiology*, *113*(3), 566–573. https://doi.org/10.1038/nrm2621

Kitano, H., Kirsch, J. R., Hurn, P. D., & Murphy, S. J. (2007). Inhalational anesthetics as neuroprotectants or chemical preconditioning agents in ischemic brain. *J Cereb Blood Flow Metab.*, *27*(6), 1108–1128. https://doi.org/10.1007/978-1-62703-673-3

Konsman, J. P., & Blomqvist, A. (2005). Forebrain patterns of c-Fos and FosB induction during cancer-associated anorexia-cachexia in rat. *European Journal of Neuroscience*, *21*(10), 2752–2766. https://doi.org/10.1111/j.1460-9568.2005.04102.x

Konsman, J. P., Veeneman, J., Combe, C., Poole, S., Luheshi, G. N., Dantzer, R., & Se, V. (2008). Central nervous action of interleukin-1 mediates activation of limbic structures and behavioural depression in response to peripheral administration of bacterial lipopolysaccharide. *European Journal of Neuroscience, Vol.*, *28*, 2499–2510. https://doi.org/10.1111/j.1460-9568.2008.06549.x

Konsman, J., Vigues, S., Mackerlova, L., Bristow, A., & Blomqvist, A. (2004). Rat Brain Vascular Distribution of Immunoreactivity : Relationship to Patterns of Inducible Cyclooxygenase Expression by Peripheral Inflammatory Stimuli. *The Journal of Comparative Neurology*, *472*, 113–129. https://doi.org/10.1002/cne.20052

Lee, C., Kwan, W. F., Tsai, S. K., Chen, B. J., & Cheng, M. (1993). A clinical assessment of desflurane anaesthesia and comparison with isoflurane. *Canadian Journal of Anaesthesia*, *40*(6), 487–494. https://doi.org/10.1007/BF03009728

Locatelli, B. G., Ingelmo, P. M., Emre, S., Meroni, V., Minardi, C., Frawley, G., … Sonzogni, V. (2013). Emergence delirium in children: A comparison of sevoflurane and desflurane anesthesia using the Paediatric Anesthesia Emergence Delirium scale. *Paediatric Anaesthesia*, *23*(4), 301–308. https://doi.org/10.1111/pan.12038

Masamoto, K., & Kanno, I. (2012). Anesthesia and the Quantitative Evaluation of Neurovascular Coupling. *Journal of Cerebral Blood Flow & Metabolism*, *32*(7), 1233–1247. https://doi.org/10.1038/jcbfm.2012.50

Meyer, H. S., Egger, R., Guest, J. M., Foerster, R., Reissl, S., & Oberlaender, M. (2013). Cellular organization of cortical barrel columns is whisker-specific. *Proceedings of the National Academy of Sciences*, *110*(47), 19113–19118. https://doi.org/10.1073/pnas.1312691110

Moore, L., Kirsch, J., Helfaer, M., Tobin, J., McPherson, R., & Traystman, R. (1994). Nitric oxide and prostanoids contribute to isoflurane-induced cerebral hyperemia in pigs. *Anesthesiology*, *80*(6), 1328–1337.

Nasu, I., Yokoo, N., Takaoka, S., Takata, K., Hoshikawa, T., Okada, M., & Miura, Y. (2006). The dose-dependent effects of isoflurane on outcome from severe forebrain ischemia in the rat. *Anesthesia and Analgesia*, *103*(2), 413–418. https://doi.org/10.1213/01.ane.0000223686.50202.38

Niwa, K., Araki, E., Morham, S. G., Ross, M. E., & Iadecola, C. (2000). Cyclooxygenase-2 contributes to functional hyperemia in whisker-barrel cortex. *The Journal of Neuroscience*, *20*(2), 763–770.

Papadopoulos, M. C., Davies, D. C., Moss, R. F., Tighe, D., & Bennett, E. D. (2000). Pathophysiology of septic encephalopathy: a review. *Critical Care Medicine*, *28*(8), 3019–3024. https://doi.org/10.1097/00003246-200008000-00057

Peng, J., Drobish, J. K., Liang, G., Wu, Z., Liu, C., Joseph, D. J., … Wei, H. (2014). Anesthetic Preconditioning Inhibits Isoflurane-Mediated Apoptosis in the Developing Rat Brain. *Anesth Analg*, *119*(4), 939–946. https://doi.org/10.1242/jcs.03292.Multiple

Peng, M., Zhang, C., Dong, Y., Zhang, Y., Nakazawa, H., Kaneki, M., … Xie, Z. (2016). Battery of behavioral tests in mice to study postoperative delirium. *Scientific Reports*, *6*(1), 29874. https://doi.org/10.1038/srep29874

Plachinta, R. V, Hayes, J. K., Cerilli, L. a, & Rich, G. F. (2003). Isoflurane pretreatment inhibits lipopolysaccharide-induced inflammation in rats. *Anesthesiology*, *98*(1), 89–95. https://doi.org/10.1097/00000542-200301000-00017

Rittirsch, D., Huber-lang, M. S., Flierl, M. a, & Ward, P. a. (2009). Immunodesign of experimental sepsis by cecal lingation and puncture. *Nat Protoc*, *4*(1), 31–36. https://doi.org/10.1038/nprot.2008.214.Immunodesign

Schaefer, C. F., Biber, B., Brackett, D. J., Schmidt, C. C., Fagraeus, L., & Wilson, M. F. (1987). Choice of anesthetic alters the circulatory shock pattern as gauged by conscious rat endotoxemia. *Acta Anaesthesiologica Scandinavica*. https://doi.org/10.1111/j.1399-6576.1987.tb02619.x

Sicard, K., Shen, Q., Brevard, M. E., Sullivan, R., Ferris, C. F., King, J. A., & Duong, T. Q. (2003). Regional Cerebral Blood Flow and BOLD Responses in Conscious and Anesthetized Rats Under Basal and Hypercapnic Conditions: Implications for Functional MRI Studies. *J Cereb Blood Flow Metab.*, *23*(4), 472–481. https://doi.org/10.1111/j.1747-0285.2012.01428.x.Identification

Stam, R. (2010). Electromagnetic fields and the blood-brain barrier. *Brain Research Reviews*, *65*(1), 80–97. https://doi.org/10.1016/j.brainresrev.2010.06.001

Stefanovic, B., Bosetti, F., & Silva, A. C. (2006). Modulatory role of cyclooxygenase-2 in cerebrovascular coupling. *NeuroImage*, *32*(1), 23–32. https://doi.org/10.1016/j.neuroimage.2006.03.014

Steiger, H. J., & Hänggi, D. (2007). Ischaemic preconditioning of the brain, mechanisms and applications. *Acta Neurochirurgica*, *149*(1), 1–10. https://doi.org/10.1007/s00701-006-1057-1

Sun, D., & Jakobs, T. C. (2012). Structural Remodeling of Astrocytes in the Injured CNS. *Neuroscientist.*, *18*(6), 567–588. https://doi.org/10.1086/498510.Parasitic

Tanaka, T., Kai, S., Matsuyama, T., Adachi, T., Fukuda, K., & Hirota, K. (2013). General anesthetics inhibit LPS-induced IL-1β expression in glial cells. *PLoS ONE*, *8*(12), e82930. https://doi.org/10.1371/journal.pone.0082930

Tétrault, S., Chever, O., Sik, A., & Amzica, F. (2008). Opening of the blood-brain barrier during isoflurane anaesthesia. *European Journal of Neuroscience*, *28*(7), 1330–1341. https://doi.org/10.1111/j.1460-9568.2008.06443.x

Vachharajani, V., Cunningham, C., Yoza, B., Jr, J. C., Vachharajani, T. J., & McCall, C. (2012). Adiponectin-Deficiency Exaggerates Sepsis-Induced Microvascular Dysfunction in the Mouse Brain. *Obesity (Silver Spring)*, *20*(3), 498–504. https://doi.org/10.1038/oby.2011.316.Adiponectin-Deficiency

Wichterman, K., Baue, A. E., & Chaudry, I. H. (1980). Sepsis and Septic Shock -A Review of Laboratory and a Proposal Models. *Journal of Surgical Research*, *29*, 189–201.

Yang, S., Gu, C., Mandeville, E. T., Dong, Y., Esposito, E., Zhang, Y., … Xie, Z. (2017). Anesthesia and surgery impair blood–brain barrier and cognitive function in mice. *Frontiers in Immunology*, *8*(AUG). https://doi.org/10.3389/fimmu.2017.00902

Yang, S., Liu, J., Zhang, X., Tian, J., Zuo, Z., Liu, J., & Yue, X. (2016). Anesthetic isoflurane attenuates activated microglial cytokine-induced VSC4.1 motoneuronal apoptosis. *American Journal of Translational Research*, *8*(3), 1437–1446.

Yokoo, H., Chiba, S., Tomita, K., Takashina, M., Sagara, H., Yagisita, S., … Hattori, Y. (2012). Neurodegenerative Evidence in Mice Brains with Cecal Ligation and Puncture-Induced Sepsis: Preventive Effect of the Free Radical Scavenger Edaravone. *PLoS ONE*, *7*(12), 1–11. https://doi.org/10.1371/journal.pone.0051539

Table and figures

Region	Occurrence / section	ANOVA/ANOVA on Ranks +*Post-hoc*	Occurrence x extent /section	ANOVA/ ANOVA on Ranks +*Post-hoc*
Cortex	Sh.+:0.159 ±0.066	MRI $F_{1,26}$=7.75, p<0.05	Sh.+:0.202 ±0.087	
	Sh.-:0898 ±0.416	Surgery x MRI	Sh.-:1.012 ±0.505	NS
	CLP+:0.201 ±0.068	$F_{1,26}$=3.09, p=0.091	CLP+:0.244 ±0.081	
	CLP-:0.349 ± 0.197	MRI- vs MRI+ p<0.05	CLP-:0.513 ±0.286	
SSs	Sh.+:0.016 ±0.016	H = 14.9	Sh.+:0.023 ±0.023	H = 14.0
	Sh.-:0.162 ±0.057	p<0.01	Sh.-:0.176 ±0.054	p<0.01
	CLP+:0.02 ±0.014	Sh.- vs CLP- p=0.05	CLP+:0.027 ±0.018	Sh.- vs CLP- p=0.06
	CLP-:0	Sh.- vs Sh.+ p=0.095	CLP-:0	
VISC	Sh.+:0	H = 12.7	Sh.+:0	H = 12.2
	Sh.-:0.073 ±0.032	p< 0.01	Sh.-:0.085 ±0.043	p< 0.01
	CLP+:0.004 ±0.004	NS	CLP+:0.004 ±0.004	NS
	CLP-:0.009 ±0.009		CLP-:0.019 ±0.019	
Gu	Sh.+:0.008 ±0.008	H = 6.3	Sh.+:0.017 ±0.017	NS
	Sh.-:0.039 ±0.023	p=0.096	Sh.-:0.039 ±0.023	
	CLP+:0.003 ±0.003		CLP+:0.003 ±0.003	
	CLP-:0		CLP-:0	
AI	Sh.+:0	H = 12.0	Sh.+:0	H = 10.9
	Sh.-:0.057 ±0.037	p<0.01	Sh.-:0.057 ±0.037	p<0.05
	CLP+:0.011 ±0.011		CLP+:0.011 ±0.011	
	CLP-:0.004 ±0.004	NS	CLP-:0.008 ±0.008	NS
Striatum	Sh.+:0.055 ±0.018	Surgery x MRI	Sh.+:0.055 ±0.018	Surgery x MRI
	Sh.-:0.235 ±0.146	$F_{1,26}$=3.64, p=0.068	Sh.-:0.296 ±0.175	$F_{1,26}$=4.71, p<0.05
	CLP+:0.119 ±0.044		CLP+:0.142 ±0.053	
	CLP-:0.043 ±0.043		CLP-:0.043 ±0.043	
GPe	Sh.+:0	H = 6.5	Sh.+:0	H = 6.5
	Sh.-:0.019 ±0.019	p= 0.090	Sh.-:0.019 ±0.019	p= 0.090
	CLP+:0		CLP+:0	
	CLP-:0		CLP-:0	
White matter	Sh.+:0.384 ±0.193	Surgery p=0.073	Sh.+:0.508 ±0.278	MRI p<0.05

	Sh.-:1.031 ±0.435	MRI p<0.05		Sh.-:1.416 ±0.753	Sh.- vs CLP- p<0.05
	CLP+:0.216 ±0.07	MRI- vs MRI+ p<0.05		CLP+:0.245 ±0.083	
	CLP-:0.487 ±0.186			CLP-:0.501 ±0.181	
Score cc-ec	Sh.+:0.080 ±0.063	H = 7.6		Sh.+:0.101 ±0.079	H = 7.3
	Sh.-:0.401 ±0.218	p=0.056		Sh.-:0.471 ±0.234	p= 0.062
	CLP+:0.121 ±0.055			CLP+:0.142 ±0.069	
	CLP-:0.383 ±0.143			CLP-:0.384 ±0.135	
cc	Sh.+:0			Sh.+:0	
	Sh.-:0.059 ±0.059	NS		Sh.-:0.073 ±0.073	NS
	CLP+:0.012 ±0.008			CLP+:0.012 ±0.008	
	CLP-:0.083 ±0.043			CLP-:0.091 ±0.051	
ec	Sh.+:0.022 ±0.011	H = 7.2		Sh.+:0.026 ±0.015	NS
	Sh.-:0.143 ±0.086	p= 0.066		Sh.-:0.147 ±0.086	
	CLP+:0.051 ±0.028			CLP+:0.063 ±0.038	
	CLP-:0.149 ±0.057			CLP-:0.141 ±0.057	
ccg-ec	Sh.+:0	H = 13.5		Sh.+:0	H = 13.5
	Sh.-:0.1 ±0.058	p<0,01		Sh.-:0.1 ±0.058	p<0,01
	CLP+:0	NS		CLP+:0	NS
	CLP-:0			CLP-:0	
fi	Sh.+:0.107 ±0.070			Sh.+:0.116 ±0.078	H = 9.2
	Sh.-:0.059 ±0.028	NS		Sh.-:0.059 ±0.028	p<0.05
	CLP+:0			CLP+:0	NS
	CLP-:0.015 ±0.015			CLP-:0.015 ±0.015	
Score Hippocampus	Sh.+:0.018 ±0.018			Sh.+:0.018 ±0.018	
	Sh.-:0.186 ±0.111	NS		Sh.-:0.186 ±0.111	NS
	CLP+:0.014 ±0.014			CLP+:0.014 ±0.014	
	CLP-:0.046 ±0.03			CLP-:0.046 ±0.03	
CA3	Sh.+:0	H = 7.0		Sh.+:0	H = 7.0
	Sh.-:0.158 ±0.092	p= 0.072		Sh.-:0.158 ±0.092	p= 0.072
	CLP+:0.014 ±0.014			CLP+:0.014 ±0.014	
	CLP-:0.046 ±0.03			CLP-:0.046 ±0.03	

Tableau 1 : Occurrence and extent of perivascular immunoglobulin G diffusion in forebrain sections of animals undergone sham or CLP surgery with or without undergoing imaging under anesthesia. cc: corpus callosum; CP: caudate putamen; ec: external capsule; fi: fimbria; IgG: immunoglobulin G; MO: motor cortex; NS: non-significant; SS: somatosensory cortex; st: stria terminalis; vhc: ventral hippocampal commissure. Group sizes Sham MRI+: n=8; CLP MRI+: n=12.; Sham MRI-: n=4; CLP MRI-: n=6

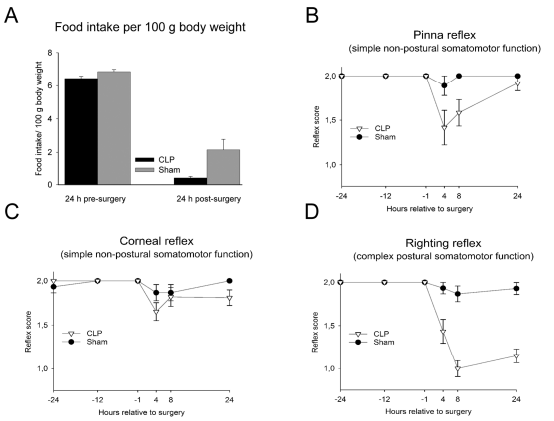

Figure 1:

Food intake relative to body weight (A) during 24h after CLP or sham surgery. Group size Sham: n=13-17; CLP: n=18-25. Reflex scores: Pinna (B), corneal (C) and righting (D) reflexes at 24h, 12h, and 1h prior to surgery then 4h, 8h and 24h later. Group size Sham: n=14-18; CLP: n=19-24.

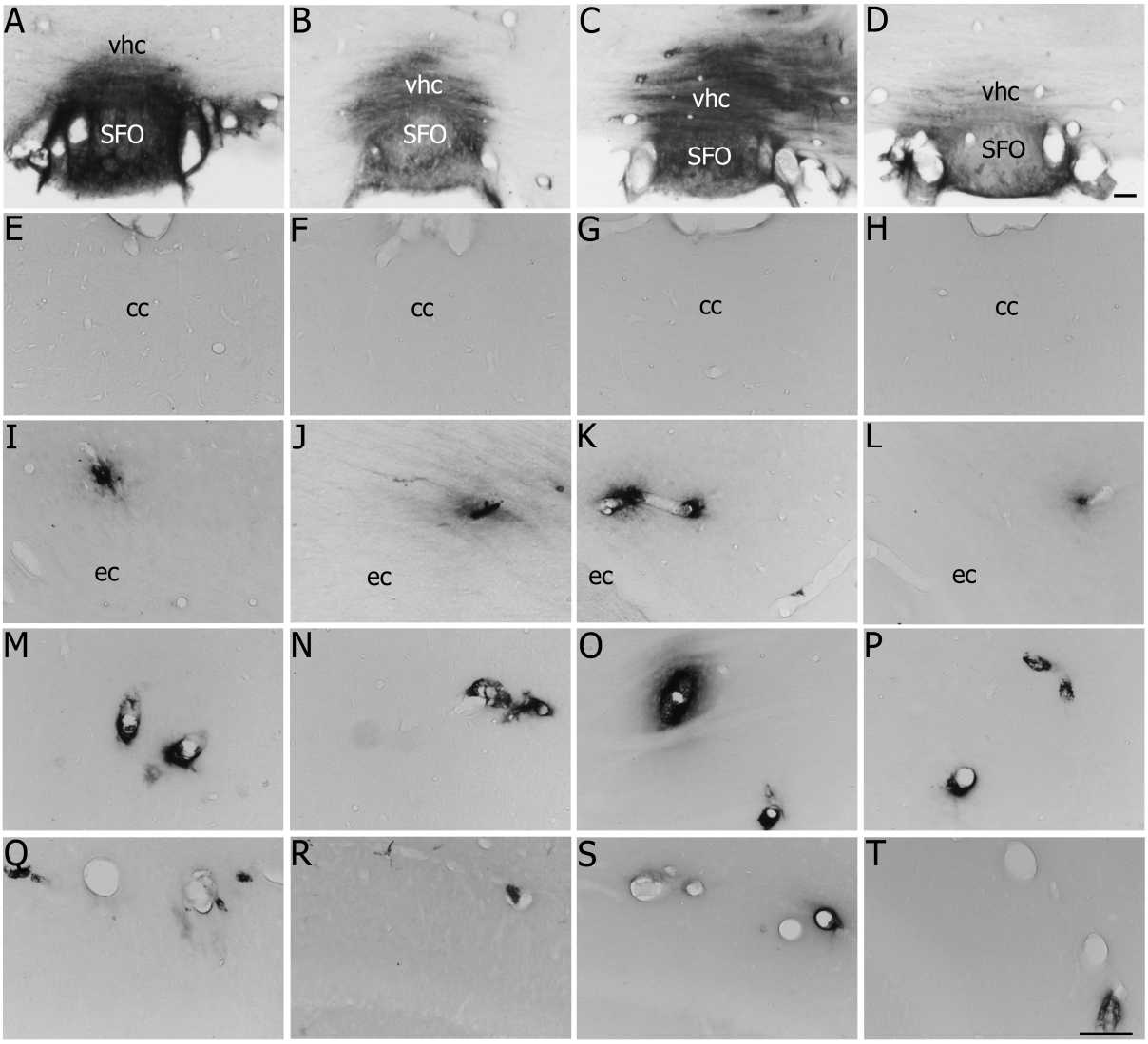

Figure 2 :

Photomicrographs illustrating the distribution of rat IgG-ir in ventral hippocampal comissure (A,B; C,D), the corpus callosum (E,F; G,H), deep layers of the somatosensory cortex (I,J; K,L), dorsolateral striatum (M,N; O,P) and hippocampus (Q,R; S,T), 24 h after laparotomy or cecal ligation and puncture in rats that underwent (A,B to Q,R) or not (C,D to S,T) imaging under isoflurane anesthesia . cc: corpus callosum; ec: external capsule; vhc: ventral hippocampal comissure; SFO: subfornical organ. Scale bar = 100 µm.

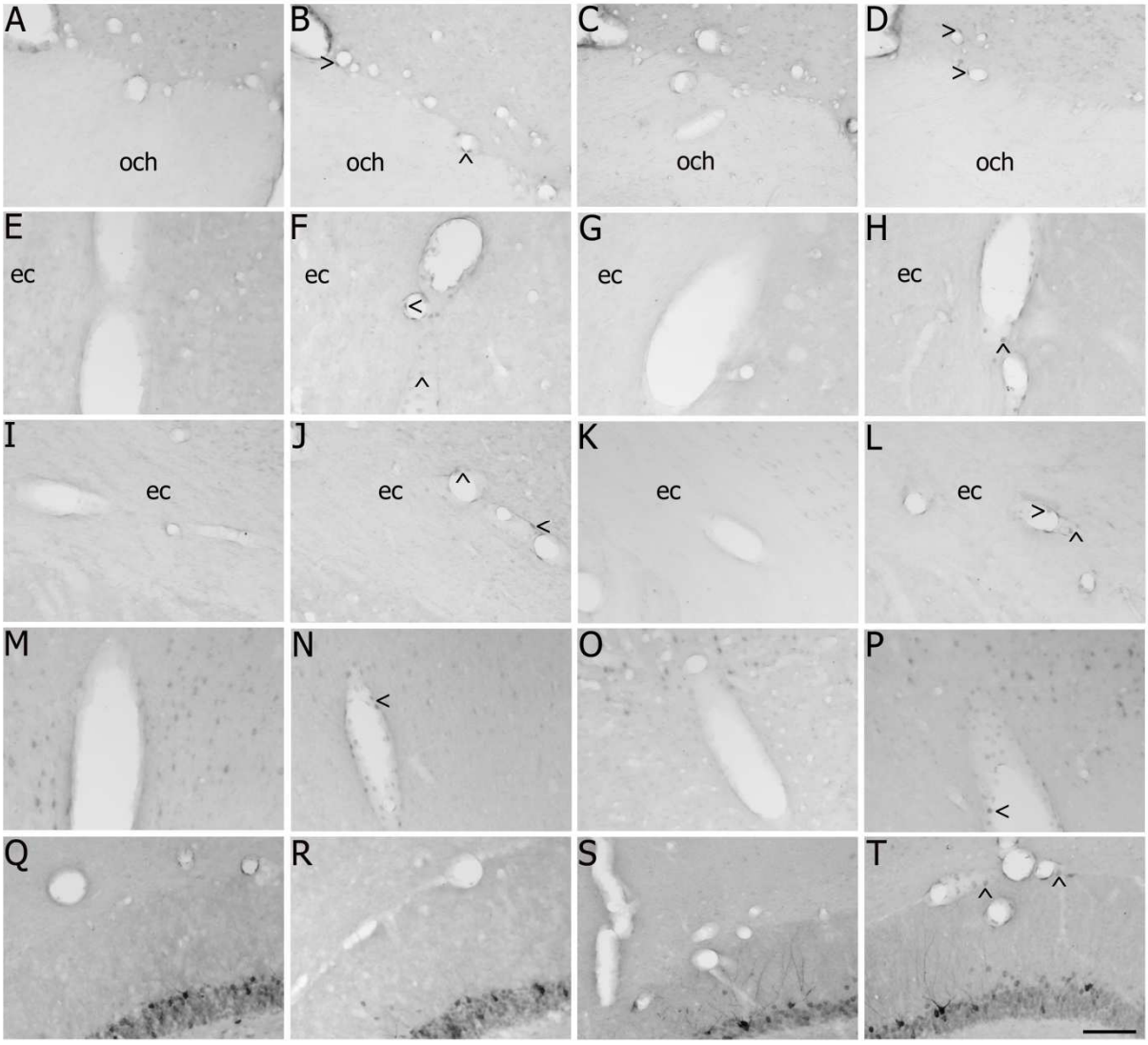

Figure 3 :

Photomicrographs illustrating the distribution of COX-2-ir in para-suprachiasmatic nucleus (A,B; C,D), caudate putamen (E,F; G,H), external capsule (I,J; K,L), the cortical hemispheres (M,N; O,P) and hippocampus (Q,R; S,T) 24h after laparotomy or cecal ligation and puncture in rats that underwent (A,B-Q,R) or not (C,D-S,T) imaging under isoflurane anesthesia.

och: optic chiasm; ec: external capsule. Arrow heads > and < indicate labeling. Scale bar = 100 µm.

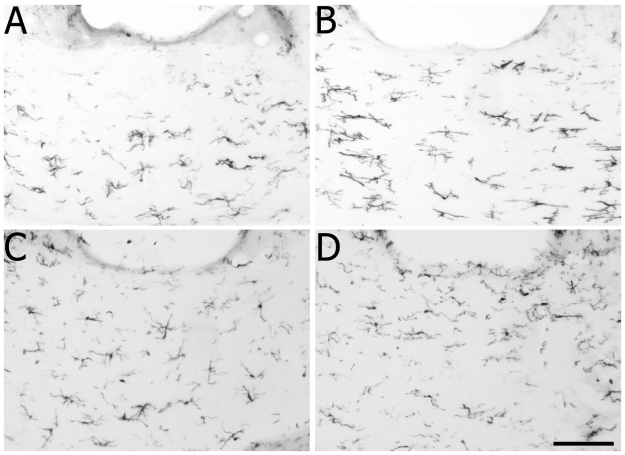

Figure 4 :

Photomicrographs illustrating Iba1-ir microglia in the corpus callosum after laparotomy (A,C) or cecal ligation and puncture (B,D) in rats that underwent (A,C) or not (B,D) imaging under isoflurane anesthesia. Scale bar = 100 μm.

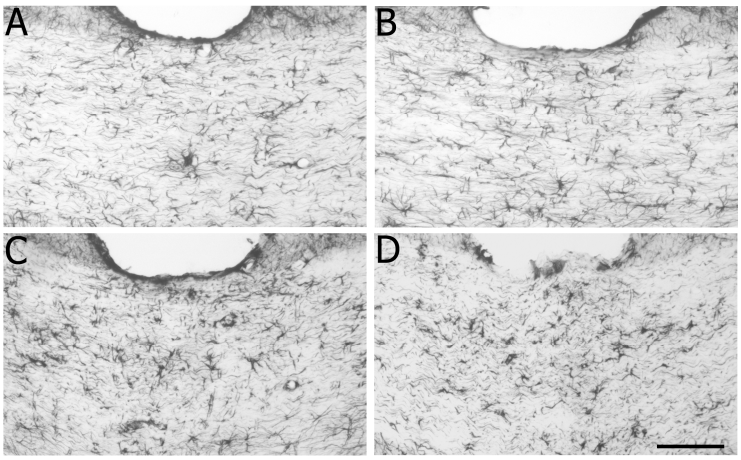

Figure 5 :

Photomicrographs illustrating GFAP-ir astrocytes in the corpus callosum after laparotomy (A,C) or cecal ligation and puncture (B,D) in rats that underwent (A,C) or not (B,D) imaging under isoflurane anesthesia. Scale bar = 100 μm.

Chapter 5

Discussion, conclusions & perspectives

Brief summary

The main objective of this work was to improve our understanding of sepsis-associated brain dysfunction by combining *in vivo* MRI approaches to assess hemodynamical changes and indications of structural modification in the CNS and *post mortem* histological approaches to describe neurochemical and cellular modifications in brains of animals that either underwent intraperitoneal injection of bacterial LPS or CLP. In particular, we studied *in vivo* cerebral blood perfusion with Arterial Spin Labeling (ASL) and brain structure with Diffusion-Weighted Imaging (DWI) in relation to the production of vasoactive inflammatory mediators, altered blood-brain barrier integrity and glial cell morphology on brain sections of the same septic animals

The first chapter presented a review of the literature allowing to introduce the essential concepts and approaches used in this work. In this chapter, we firstly discussed the importance of sickness physiology and behavior for survival after bacterial infection and the pathways via which immune signals reach the brain to induce responses. Next, findings indicating deteriorated neurological status during clinical and experimental sepsis were addressed. This followed by a discussion of the different experimental models of sepsis and imaging approaches after which relevant imaging findings and histological observations on sepsis-associated encephalopathy were resumed. The reviewed findings indicate that fever, anorexia and increased sleep are adaptive responses that can enhance host defenses following a systemic challenge and are brought about by neural and humoral pathways. SAE or brain dysfunction was associated with altered mental status and may be associated with cerebral hypo- or hyperperfusion, autoregulation failure, microcirculatory dysfunction, edema formation, BBB disruption and both gray and white matter damage all indicated by imaging (summarized in Figure 1). In addition, *post mortem* analyses indicated ischemic, hemorrhagic and apoptotic lesions that were often associated with gliosis. At molecular level, the increased production of neuro-inflammatory mediators, such a cytokines, may also contribute to the pathogenesis to brain dysfunction during sepsis.

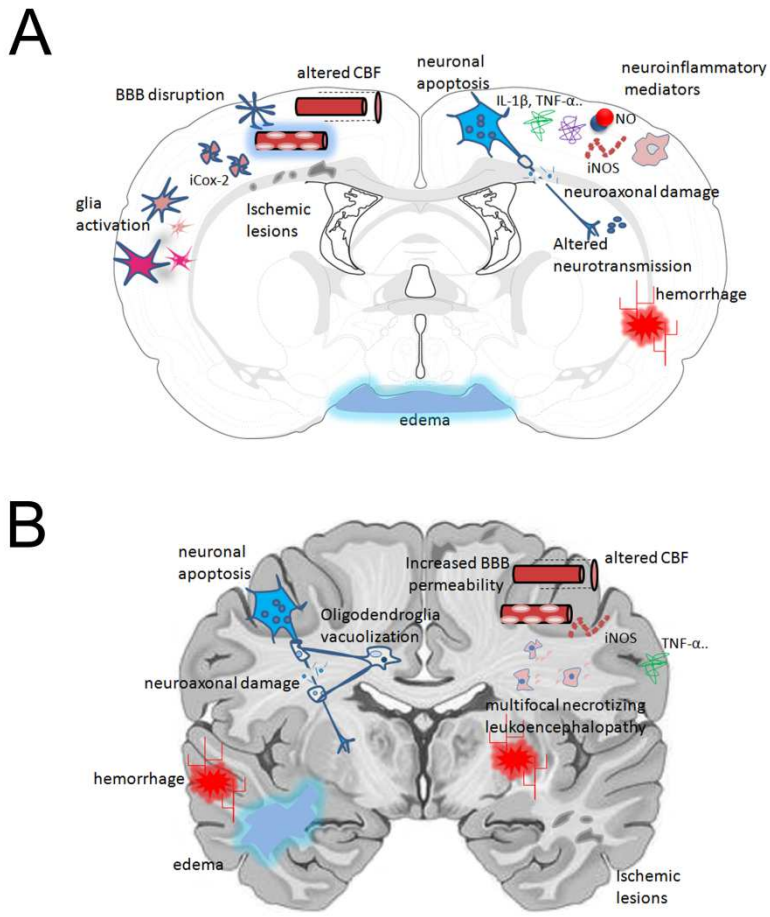

Figure 1: **Pathophysiological mechanisms in SAE as described in the literature. A:** In rats, SAE has been associated with BBB disruption, altered CBF, neuronal apoptosis, increased inflammatory mediator expression, altered neurotransmission, hemorrhage, increased vascular COX-2 expression, glial activation and edema formation in the gray matter. The white matter showed ischemic lesions and neuroaxonal damage. **B:** In humans, SAE has been associated with the same phenomena seen in rats and oligodendroglia vacuolization and multifocal necrotizing leukoencephalopathy in the white matter. BBB: blood-brain barrier, CBF: cerebral blood flow, cCOX-2: constitutive cyclooxygenase-2, iCOX-2: inducible cyclooxygenase-2, NO: nitric oxide.

The second chapter presented our findings using an experimental model that consisted of the intraperitoneal injection of LPS in rats that were subject to hemodynamic (phase contrast and ASL) and structural (DWI) imaging and sacrificed 2.5 h later to detect changes in BBB permeability, the production of pro-inflammatory cytokine IL-1β, the expression of the vasoactive prostaglandin-producing enzyme COX-2, the induction of the cellular activation

marker c-Fos as well as changes in astroglial and microglial cell morphology labeled by GFAP and Iba-1 respectively. We have demonstrated that, compared to ip injection of saline, administration of bacterial LPS in rats increased blood perfusion in the white matter of the corpus callosum without affecting blood flow in the major forebrain-irrigating arteries. In addition, a trend for a distribution of blood perfusion in favor of the external capsule and deep cortical regions was found in LPS-injected animals. Over the duration of the experiment ip LPS injection also resulted in higher water diffusion parallel to the fibers of the corpus callosum as compared to saline. These changes in perfusion and diffusion were not related to global perivascular COX-2 induction or glia cell activation, but linked, in part, to BBB breakdown (Figure 2).

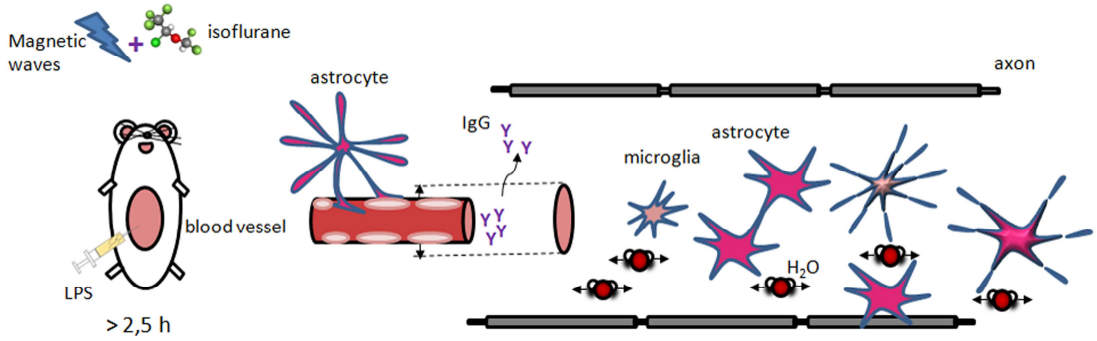

Figure 2: **Changes in the rat corpus callosum white matter 2.5h after ip LPS administration.** Ip LPS injection increased horizontal water diffusion, decreased the height of Iba-1-ir cells at the level of the ventral hippocampal commissure and induced BBB disruption in subcallosal structures. IgG: immunoglobulin G, LPS: lipopolysaccharide

The third chapter contained our findings obtained in the more pathophysiologically-relevant sepsis model consisting of CLP-and in which inflammation-induced changes in food and body weight were used to assess sickness and altered pinna, corneal or righting reflexes as indicators of SAE. After these evaluations hemodynamic (ASL) and structural (DTI and T2) imaging then was performed 24 h after CLP or sham surgery, immediately after which animals were sacrificed for histology. CLP reduced food intake and attenuated the righting reflex and resulted in higher T2-weighted contrast intensities in the cortex, striatum and at base of the brain, decreased blood distribution to the cortex and increased water diffusion in the corpus callosum and ventral striatum compared to sham surgery. These changes were accompanied by decreases in constitutive COX-2 and AQP4 expression in the cortex,

decreases in the number of Iba-1- and GFAP-immunoreactive fragments in the corpus callosum white matter, but not by widespread changes in BBB integrity. The increased maximum value in T2-weighted imaging after CLP can be interpreted to suggest edema formation and may be explained by decreased cortical AQP4 expression, while the lower number of Iba-1 and GFAP fragment may indicate retraction of the most distant glial processes and underlie increased water diffusion (Figure 3).

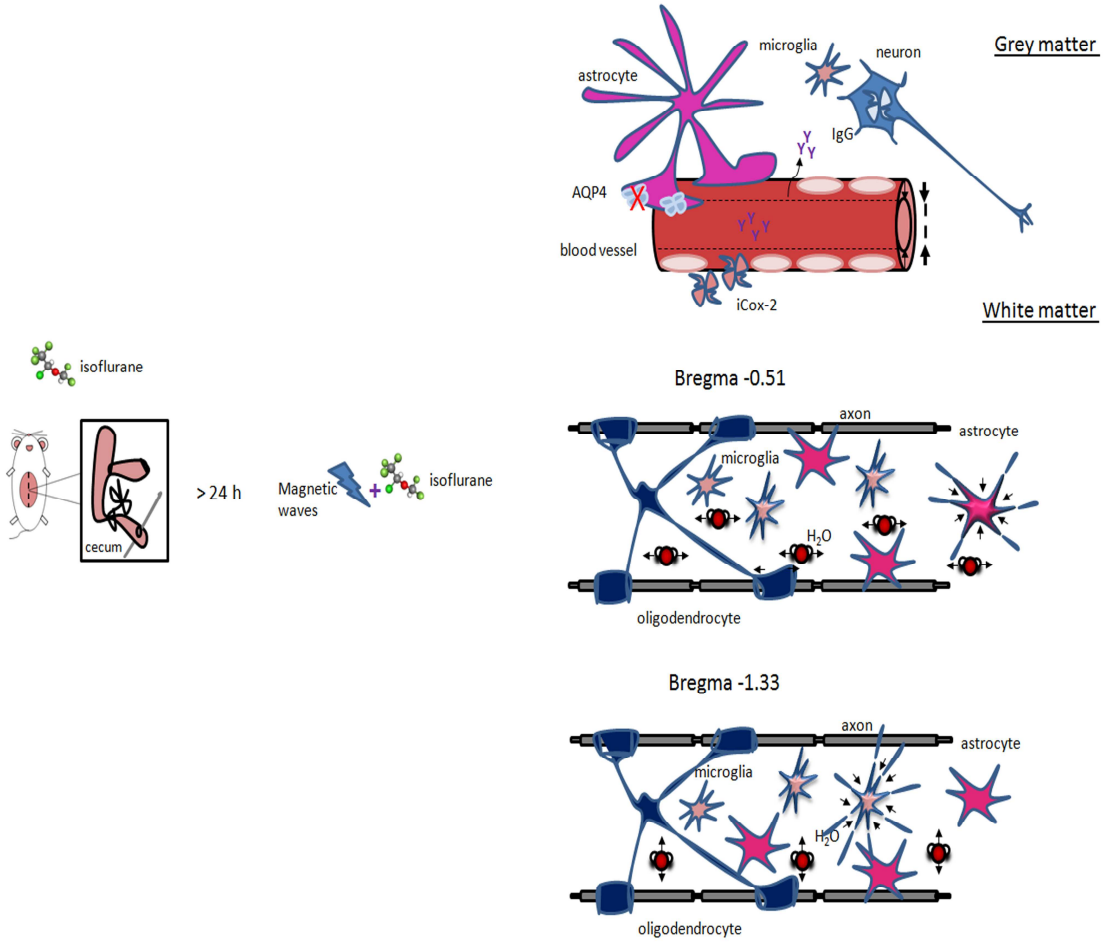

Figure 3: **Cellular and molecular changes linked to altered brain perfusion and white matter structure 24h after CLP-surgery under isoflurane anesthesia.** Decreased CBF distribution to the cortex after CLP surgery and increased T2 intensity were associated with increased vascular COX-2, decreased neuronal COX-2 and decreased AQP4 expression in cortical layers. In the white matter, at bregma -0.51, increased axial water diffusion was associated with decreased GFAP-ir fragments while at bregma-1.33 decreased radial diffusion was associated with decreased Iba-1-ir fragments. IgG: immunoglobulin G, AQP4: aquaporin 4, cCOX-2: constitutive cyclooxygenase-2, iCOX-2: inducible cyclooxygenase-2

The forth chapter described the results of the comparison of histological measures of vasoactive prostaglandin production, BBB integrity and glia cell responses during CLP-induced sepsis between those animals that did undergo additional isoflurane anesthesia after surgery and those that did for imaging to address the possible influence of MRI under anesthesia on brain physiology and CLP-induced pathophysiological mechanisms (Figure 4). Interestingly, BBB integrity was better preserved, white matter astrocytes less round and cortical COX-2-immunoreactivity higher in the rats that underwent MRI under anesthesia as compared to those that did not. In addition, MRI under isoflurane anesthesia annihilated CLP-induced sepsis-associated increased circularity of white matter glial cells, but without altering perivascular COX-2 induction. These findings suggest that the deleterious effects of a single exposure to isoflurane anesthesia may be mitigated by a second exposure in sham-operated rats and that the effects of CLP-induced systemic inflammation on glial cells can be attenuated by imaging under isoflurane anesthesia.

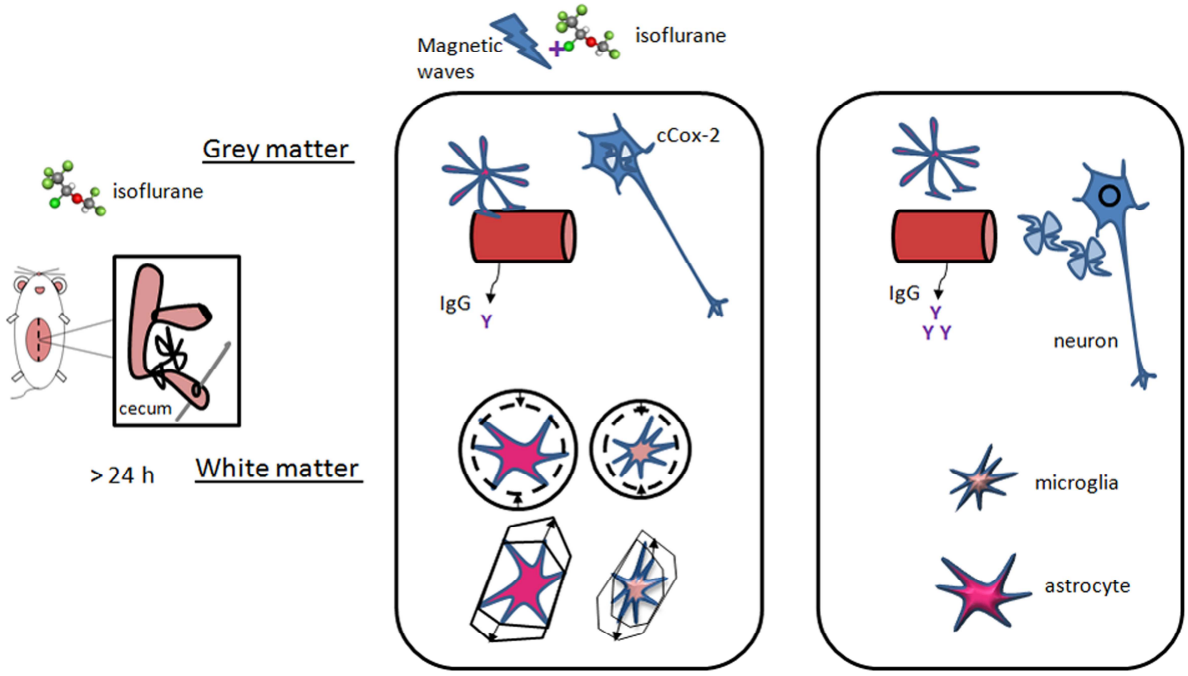

Figure 4: **Cellular and molecular changes linked to altered brain perfusion and white matter structure after CLP-surgery with and without subsequent imaging under anesthesia.** Rats imaged under isoflurane anesthesia after CLP surgery showed decreased BBB disruption, decreased neuronal COX-2 expression in the gray matter and decreased circularity of GFAP and Iba-1-ir cells as well as increased height of Iba-1-ir cells in the white matter in comparison with rats anesthetized only for surgery and that did not undergo imaging.

IgG: immunoglobulin G, cCOX-2: constitutive cyclooxygenase-2, iCOX-2: inducible cyclooxygenase-2

Differences between the two experimental model used: LPS vs CLP

This work confirms that important differences exist between bacterial LPS administration and CLP-surgery as experimental animal models used to study sepsis-associated encephalopathy and histological changes that may explain CNS dysfunction. Indeed, while reductions in gray matter blood perfusion were absent during the first hours after ip LPS administration, a decreased blood distribution to the cortex was observed 24 h after CLP. On the other hand, changes in perfusion of the white matter of the corpus callosum were found only after LPS administration and not after CLP. Interestingly, compatible increases in axial water diffusion were seen in the two models. However, these findings were accompanied by BBB disruption, but no changes in glial cell morphology in the LPS model and by changes in glial morphologies, but no BBB breakdown, after CLP.

In addition, COX-2 expression differed between the two models both in the gray and white matter. Indeed, no differences were observed in constitutive neuronal COX-2 expression in the cortex after LPS challenge, but its expression was markedly decreased after CLP surgery. Since cortical COX-2 plays an important role in neurovascular coupling between neuronal activity and CBF (Niwa, Araki, Morham, Ross, & Iadecola, 2000; Stefanovic, Bosetti, & Silva, 2006) its lower expression may explain the observed decrease in blood distribution towards the cerebral cortex during CLP-induced sepsis. In the gray and white matter, inducible COX-2 was detected around brain blood vessels after CLP but hardly after ip LPS injection.

However, the two experimental animal models may have in common that cerebral responses are attenuated by MRI under isoflurane anesthesia (Figure 7). The small number of animals that did not undergo imaging did not allow statistical analyses after ip injection of LPS. However, a qualitative analysis suggested that perivascular COX-2 induction was reduced after ip LPS administration under anesthesia as compared to the group that did not undergo anesthesia for imaging (Figure 5) while the constitutive expression of COX-2 was higher in the group that underwent imaging. BBB breakdown as shown by IgG diffusion to brain parenchyma in the LPS model showed that it is important in the group that did not undergo imaging and that the effects of LPS on the BBB seemed less important than in awake animals (Figure 6).

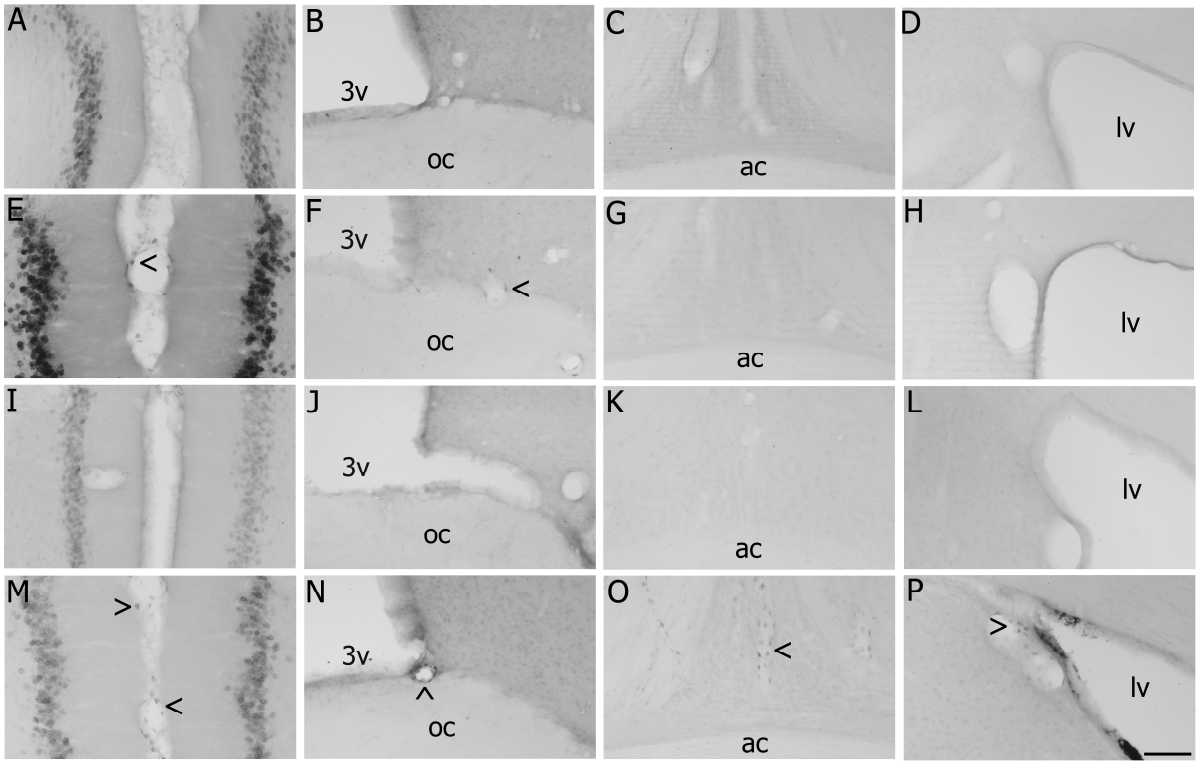

Figure 5: Photomicrographs illustrating the distribution of COX-2-ir in and between the cortical hemispheres (A,E; I,M), in the ventromedial preoptic area (B,F; J,N), the medial preoptic nucleus (C,G; K,O) and in the caudate putamen (D,H; L,P), 2.5 h after intraperitoneal injection of saline (A-D; I-L) or bacterial LPS (E-H; M-P) in isoflurane-anesthetized rats that underwent (A-H) or not (I-P) imaging.

3v: third ventricle; ac: anterior commissure; lv: lateral ventricle; oc: optic chiasm. Arrow heads > or < and ^ indicate labeling. Scale bar = 100 µm.

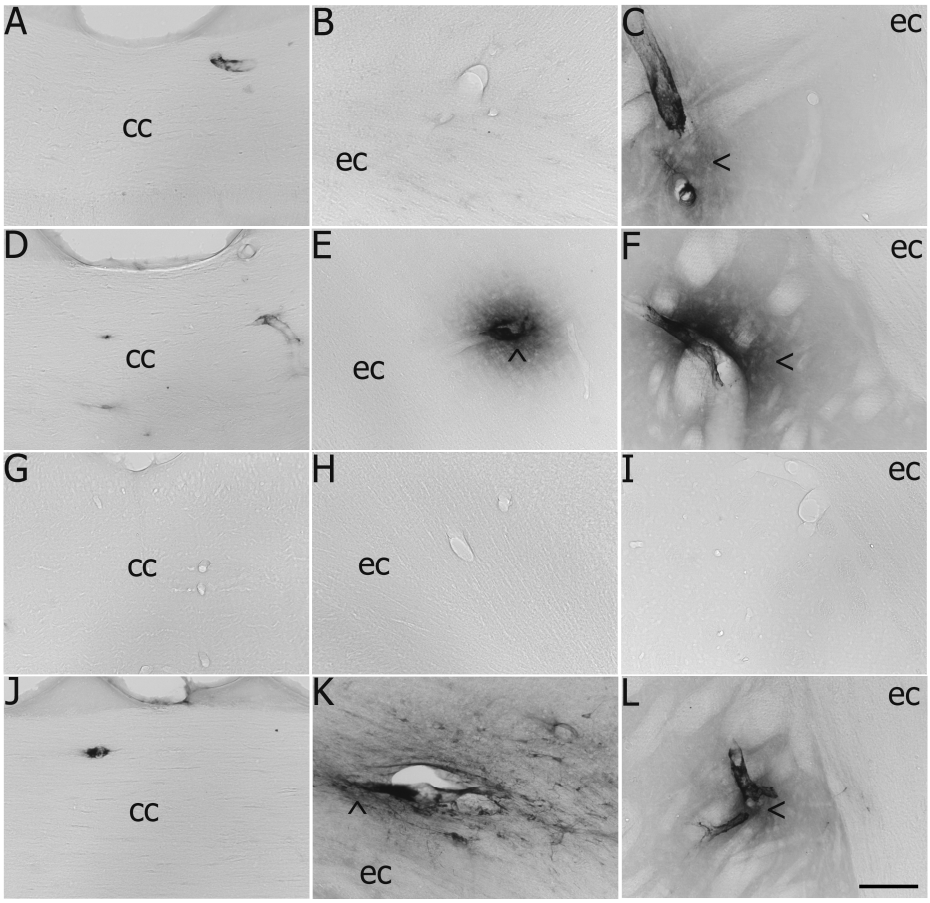

Figure 6 : Photomicrographs illustrating the distribution of rat IgG-ir in the corpus callosum (A,D; G,J), deep layers of the somatosensory cortex (B,E; H,K) and dorsoslateral caudate putamen (C,F; I,L) 2.5 h after intraperitoneal injection of saline (A-C; G-I) or bacterial LPS (D-F; J-L) in isoflurane-anesthetized rats that underwent (A-F) or not (G-L) imaging. cc: corpus callosum; ec: external capsule. Arrow heads < and ^ indicate perivascular diffuse cloud-like labeling. Scale bar = 100 µm.

Although no widespread breakdown of the BBB was observed after CLP as compared to sham surgery in animals that were not imaged, more important perivascular IgG diffusion was seen in sham-operated animals that did not undergo imaging than in sham-operated rats that were imaged.

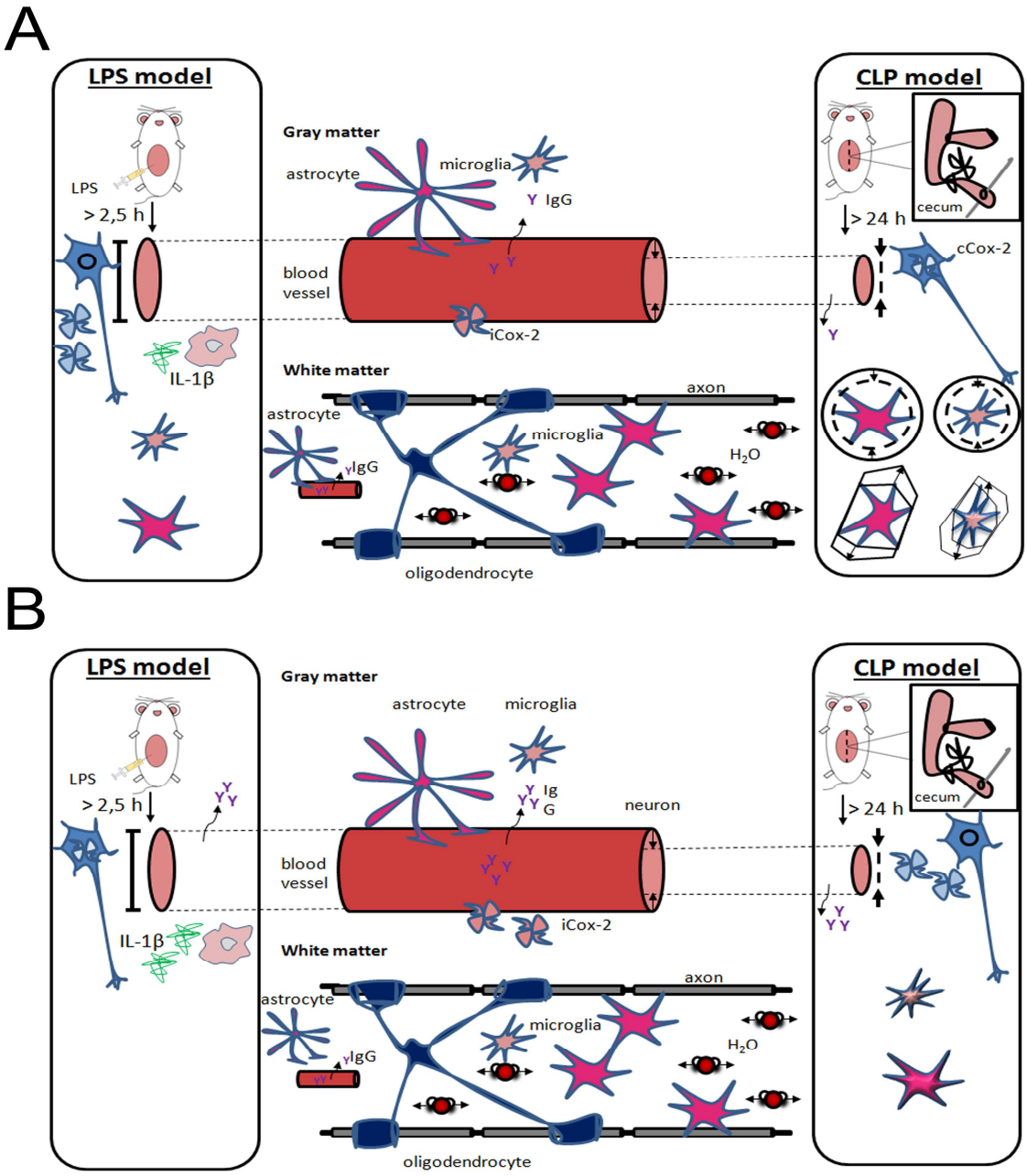

Figure 7:**Cellular and molecular changes linked to altered brain perfusion and white matter structure in two models of systemic inflammation under (A) and without (B) subsequent imaging under anesthesia.** Qualitative analysis showed that imaging under isoflurane anesthesia after ip LPS challenge resulted in higher expression of neuronal COX-2, lower expression of IL-1ß and BBB disruption in comparison with the animals that did not undergo imaging. In CLP rats imaged under isoflurane anesthesia, neuronal COX-2 was lower, BBB integrity was more preserved and GFAP and Iba-1-ir cells were higher and more ramified in comparison with rats that were only imaged for surgery and did not undergo imaging.

These findings suggest that the first exposure to isoflurane anesthesia is deleterious while the second reduced the effect of the first as it was already shown for other phenomena (Peng et al., 2014). Hence, in addition to the differences in host exposure to bacteria and the time of sacrifice, the number of times that rats have been anesthetized may also explain some of the differences between the LPS and CLP models. Indeed, for ip administration, rats were anesthetized once for i.p LPS or saline injection and imaging was performed 30 minutes before and every 30 minutes until 150 minutes after injection, whereas CLP-operated rats were first anesthetized for surgery and a second time 24h later to undergo imaging. In addition, interaction of anesthesia with inflammation may differ in the two models because of the differences in time course of inflammatory responses.

In the clinic, 50% of septic patients do not show imaging abnormalities despite the presence of mental alteration (Polito et al., 2013a; Sharshar et al., 2007). In the CLP model, we observed deteriorated neurological status and increased T2-weighted contrast, but no evidence of BBB disruption. This means that encephalopathy may occur even when BBB is intact and may be caused by hemodynamic or structural changes as proposed by (Morandi et al., 2012; Yokota, Ogawa, Kurokawa, & Yamamoto, 2003). Hence, our CLP model is interesting in that it induces signs of neurological impairment in the absence of BBB breakdown for molecules of high molecular weight.

The present work allowed to combine imaging and *post mortem* analysis in the same animals using MRI approaches that have not been used before to study sepsis-associated CNS dysfunction. It allowed also to compare two widely used sepsis models for this purpose despite the differences in time of sacrifice and anesthesia. Our findings obtained in the CLP model corroborate the idea that CNS dysfunction is consequent to hemodynamic and structural changes that may be related to microscopic changes in prostaglandin synthesis, water transport and changes in glia cell morphology.

The results of this thesis confirm the existence of brain dysfunction in two different experimental models as well as the robustness of the CLP model compared to the bacterial fragment injection model. In addition, they extend the previous results by showing the existence of edematic formation in the striatum, cortex and base of the brain, a redistribution of perfusion to the cortex or corpus callosum differently in both models but comparable structural changes that are in relation to a barrier rupture after 2.5 hours of ip LPS injection and glial cells morphology changes 24 hours following a cecal ligation and puncture (Figure 8). The combination of imaging with the *post mortem* study in the same animals allowed

temporal and spatial relationships to be established between the hemodynamic, metabolic and structural CNS changes indicated by imaging and histological approaches to the brain sections of the same animals and clarify the relationship between these often observed clinical alterations and BBB disruption and glial cell activation.

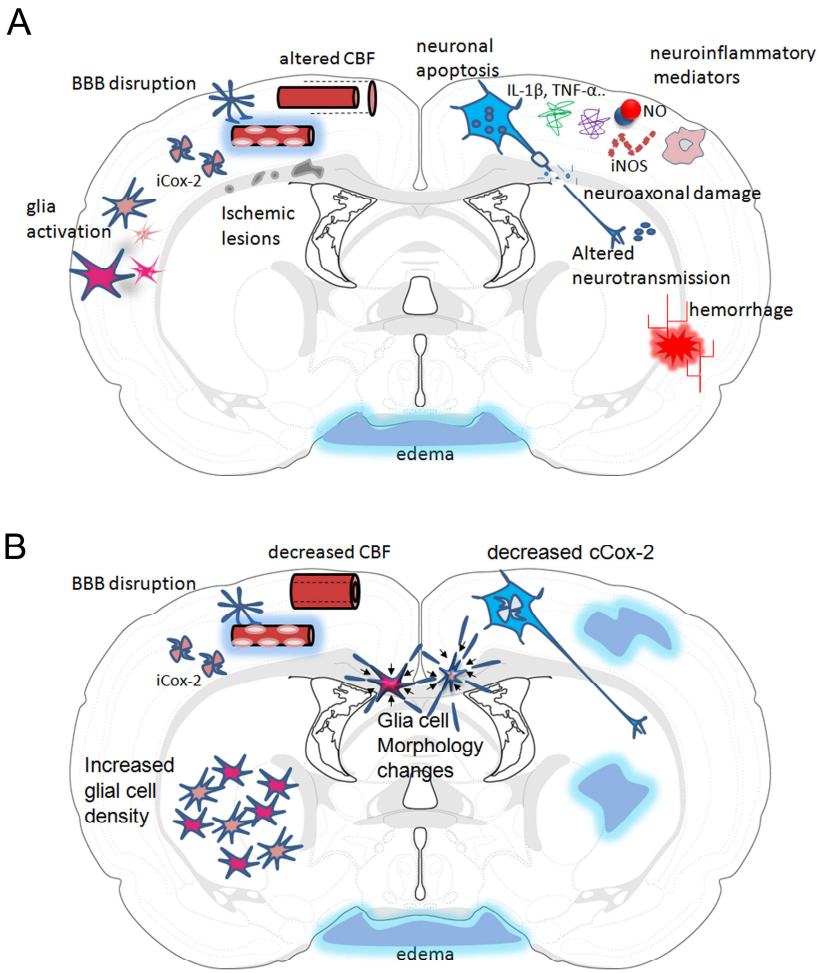

Figure 8: **Findings in the literature vs those obtained in our CLP-model.** In the literature **(A)**, SAE in rats has been associated with BBB disruption, altered CBF, neuronal apoptosis, increased inflammatory mediators expression, altered neurotransmission, hemorrhage, increased vascular COX-2 expression, glial activation and edema formation in the gray matter. The white matter showed ischemic lesions and neuroaxonal damage. In this study **(B)**, SAE in rats after CLP was associated with decreased neuronal COX-2, increased vascular COX-2, decreased blood distribution to the cortex, BBB disruption, changes in white matter glial cell morphology and edema formation. BBB: blood-brain barrier, CBF: cerebral blood flow, cCOX-2: constitutive cyclooxygenase-2, iCOX-2: inducible cyclooxygenase-2.

The originality of this study relates in part to the use of imaging approaches that have not been used clinically or in laboratories to study sepsis-associated encephalopathy such as ASL and phase contrast despite their use in the exploration of other diseases. Another important result of this study is that cognitive impairments may occur in the absence of BBB disruption and that alteration of cerebral blood perfusion may occur without impaired blood flow in the main forebrain-irrigating arteries. This study is also the first to show that MRI under isoflurane anesthesia in rats previously anesthetized for laparotomy reduces BBB disruption, decreases the circularity of white matter astrocytes and increases the immunoreactivity of COX-2 neuronal in the cortex of rodents. These results indicate that, depending on the measure of interest, MRI under isoflurane anesthesia may alter neurovascular and glial responses and should, therefore, be interpreted with caution. However, this does not question the validity of the results of our CLP model, since even though isoflurane masks some effects of inflammation they are not completely absent.

Perspectives

Isoflurane has been recommended as the anesthesia of choice for longitudinal experiments involving the study of neurovascular coupling because it provides robust activity-induced vascular response, easy control and good recovery (Masamoto & Kanno, 2012). However, isoflurane has recently been described to result in BBB breakdown *in vivo* (Acharya et al., 2015; Tétrault, Chever, Sik, & Amzica, 2008) and to induce neuronal cell death (Stary, Sun, & Giffard, 2015). Since anesthesia allowed for surgery and intervention studies while limiting suffering, few are the studies performed in awake animals. In this study, we addressed the possibility that imaging under isoflurane anesthesia masked the effects of CLP on the BBB, COX-2 expression and glia cell responses. Even though we found that the relatively small needle size used for CLP did not induce widespread perivascular IgG diffusion and that perivascular COX-2 induction was not affected by imaging under anesthesia, neuronal COX-2 in the cortex as well white matter glial cell responses were altered by MRI under isoflurane anesthesia.

In order to avoid under- or overestimation of inflammatory responses while studying SAE it would be preferable to perform imaging on awake animals, in particular when one is interested to hemodynamic changes and a few labs have already implemented such approaches (Chwiesko, 2017; Duong, 2007; Sicard et al., 2003). Naturally, *post mortem* MRI cannot be a solution for studying hemodynamics without anesthesia but may be interesting for

studying structural changes. This has already been done on human brains or brain tissue samples (Guilfoyle, Helpern, & Lim, 2003; Miller et al., 2011; Nijeholt et al., 2001; Seehaus et al., 2015) as well as in animal brains (D'Arceuil & de Crespigny, 2007; D'Arceuil, Westmoreland, & de Crespigny, 2007; Dyrby et al., 2007; Guilfoyle et al., 2003; Kroenke, Bretthorst, Inder, & Neil, 2005; Tyszka & Frank, 2009; Wu et al., 2013) and spinal cords (Kim, Trinkaus, Ozcan, Budde, & Song, 2007; Schwartz et al., 2005). This may represent a path worth going down on because *delirium* and cognitive impairment seen in septic patients are, in part, related to structural changes in brain white matter in particular in the corpus callosum (Seehaus et al., 2015). Interestingly, fractional anisotropy (Kim et al., 2007; Wu et al., 2013) and fiber orientation (Kim et al., 2007; Timothy M Shepherd et al., 2009) are not altered a few hours after death subsequent to *in vivo*, *in situ post mortem* or *ex vivo* after tissue fixation. However, water diffusivity significantly decreases after death (Kim et al., 2007; Sun et al., 2005), which result in loss of lesion contrast in fixed brains (Sun et al., 2005). In addition, tissue fixation alters water relaxation and diffusion properties of nervous tissue, even though FA is preserved (T M Shepherd, Thelwall, Stanisz, & Blackband, 2005; Timothy M Shepherd et al., 2009) and results in reduction of ventricular volumes that is accompanied by deformations in its neighboring structures (Wu et al, 2013). Together these findings suggest that *in situ* imaging after death and perfusion fixation can be an alternative to *in vivo* structural imaging under anesthesia.

It is also important to mention that ischemia is present in one third of septic patients (Pereira et al., 2015; Polito et al., 2013b). Moreover, the fact that ischemia affects the subcortical white matter of frontal lobes and temporal regions and is associated with increased mid-term neurological disability and mortality (Fabbian et al., 2010; Jackson & Hopkins, 2009) makes it an important point to discuss given that both white matter damage and hypoperfusion were associated with cognitive impairment and delirium (Girard et al., 2010; Gunther et al., 2012; Jackson & Hopkins, 2009; Marsland et al., 2015; Morandi et al., 2012; Yokota et al., 2003).

During this study we did not use an immunohistochemical marker to detect ischemic lesions because no hyperintensities were seen on DWI, known to detect ischemic brain damage (Minematsu, Li, Sotak, Davis, & Fisher, 1992). However, the observed decreased blood redistribution to cortical layers after CLP may have contribute to formation of ischemic foci and the decrease of the number of neuronal COX-2 may be due to neuronal death. This together with the recent indication of ischemic foyers based on H&E stains of brain sections

of rats following peritonitis (Ehler et al., 2017) makes it important to address ischemic mechanisms that may occur during experimental sepsis.

There is currently no “gold standard” tool or staining to detect ischemic lesions, which makes it important to describe the different mediators and processes involved to understand the mechanisms by which ischemia occurs during sepsis. Indeed, Le & Courter (Le & Courter, 2008), after having compared different techniques for detection of hypoxia, suggest that a combination of biomarkers is more robust than a single marker.

References

Acharya, N. K., Goldwaser, E. L., Forsberg, M. M., Godsey, G. A., Johnson, C. A., Sarkar, A., … Nagele, R. G. (2015). Sevoflurane and Isoflurane induce structural changes in brain vascular endothelial cells and increase blood-brain barrier permeability: Possible link to postoperative delirium and cognitive decline. *Brain Research*, *1620*, 29–41. https://doi.org/10.1016/j.brainres.2015.04.054

Chwiesko, C. (2017). *Bridging human and animal recognition memory: In search of hippocampal fMRI BOLD responses to familiarity and novelty in awake rats*. Ruhr University Bochum.

D'Arceuil, H., & de Crespigny, A. (2007). The effects of brain tissue decomposition on diffusion tensor imaging and tractography. *NeuroImage*, *36*(1), 64–68. https://doi.org/10.1016/j.neuroimage.2007.02.039

D'Arceuil, H. E., Westmoreland, S., & de Crespigny, A. J. (2007). An approach to high resolution diffusion tensor imaging in fixed primate brain. *NeuroImage*, *35*(2), 553–565. https://doi.org/10.1016/j.neuroimage.2006.12.028

Duong, T. (2007). Cerebral blood flow and BOLD fMRI responses to hypoxia in awake and anesthetized rats. *Brain Research*, *1135*(1), 186–194. https://doi.org/10.1016/j.brainres.2006.11.097.Cerebral

Dyrby, T. B., Søgaard, L. V., Parker, G. J., Alexander, D. C., Lind, N. M., Baaré, W. F. C., … Jelsing, J. (2007). Validation of in vitro probabilistic tractography. *NeuroImage*, *37*(4), 1267–1277. https://doi.org/10.1016/j.neuroimage.2007.06.022

Ehler, J., Barrett, L. K., Taylor, V., Groves, M., Scaravilli, F., Wittstock, M., … Petzold, A. (2017). Translational evidence for two distinct patterns of neuroaxonal injury in sepsis: a longitudinal, prospective translational study. *Critical Care*, *21*(1), 262. https://doi.org/10.1186/s13054-017-1850-7

Fabbian, F., Pala, M., Fallica, E., Capone, J., Monetti, V. C., Fratti, D., & Fainardi, E. (2010). Posterior reversible encephalopathy syndrome in an 87-year-old woman with Escherichia coli bloodstream infection. *Clinical and Experimental Nephrology*, *14*(2), 176–179. https://doi.org/10.1007/s10157-009-0234-y

Girard, T., Jackson, J. C., Pandharipande, P. P., Pun, B. T., Thompson, J. L., Shintani, A. K., … Ely, E. W. (2010). Delirium as a Predictor of Long-Term Cognitive Impairment in Survivors of Critical Illness. *Crit Care Med*, *38*(7), 1513–1520. https://doi.org/10.1097/CCM.0b013e3181e47be1.Delirium

Guilfoyle, D. N., Helpern, J. A., & Lim, K. O. (2003). Diffusion tensor imaging in fixed brain tissue at 7.0 T. *NMR in Biomedicine*, *16*(2), 77–81. https://doi.org/10.1002/nbm.814

Gunther, M. L., Morandi, A., Krauskopf, E., Pandharipande, P., Girard, T. D., Jackson, J. C., … Ely, E. W. (2012). Association between Brain Volumes, Delirium Duration and Cognitive Outcomes in Intensive Care Unit Survivors: A Prospective Exploratory Cohort Magnetic. *Critical Care …*, *40*(7), 2022–2032. https://doi.org/10.1097/CCM.0b013e318250acc0.The

Jackson, J., & Hopkins, R. (2009). Acute respiratory distress syndrome, sepsis, and cognitive decline: a review and case study. *Southern Medical …*, *102*(11), 1150–1157. https://doi.org/10.1097/SMJ.0b013e3181b6a592.Acute

Kim, J. H., Trinkaus, K., Ozcan, A., Budde, M. D., & Song, S.-K. (2007). Postmortem delay does not change regional diffusion anisotropy characteristics in mouse spinal cord white matter. *NMR in Biomedicine*, *20*(4), 352–359. https://doi.org/10.1002/nbm

Kroenke, C. D., Bretthorst, G. L., Inder, T. E., & Neil, J. J. (2005). Diffusion MR imaging characteristics of the developing primate brain. *NeuroImage*, *25*(4), 1205–1213.

https://doi.org/10.1016/j.neuroimage.2004.12.045
Le, Q. T., & Courter, D. (2008). Clinical biomarkers for hypoxia targeting. *Cancer and Metastasis Reviews*, *27*(3), 351–362. https://doi.org/10.1007/s10555-008-9144-9
Marsland, A. L., Gianaros, P. J., Kuan, D. C. H., Sheu, L. K., Krajina, K., & Manuck, S. B. (2015). Brain morphology links systemic inflammation to cognitive function in midlife adults. *Brain, Behavior, and Immunity*, *48*, 195–204. https://doi.org/10.1016/j.bbi.2015.03.015
Masamoto, K., & Kanno, I. (2012). Anesthesia and the Quantitative Evaluation of Neurovascular Coupling. *Journal of Cerebral Blood Flow & Metabolism*, *32*(7), 1233–1247. https://doi.org/10.1038/jcbfm.2012.50
Miller, K. L., Stagg, C. J., Douaud, G., Jbabdi, S., Smith, S. M., Behrens, T. E. J., … McNab, J. A. (2011). Diffusion imaging of whole, post-mortem human brains on a clinical MRI scanner. *NeuroImage*, *57*(1), 167–181. https://doi.org/10.1016/j.neuroimage.2011.03.070
Minematsu, K., Li, L., Sotak, C. H., Davis, M. a., & Fisher, M. (1992). Reversible focal ischemic injury demonstrated by diffusion-weighted magnetic resonance imaging in rats. *Stroke*, *23*, 1304–1310. https://doi.org/10.1161/01.STR.23.9.1304
Morandi, A., Rogers, B. P., Gunther, M. L., Merkle, K., Pandharipande, P., Girard, T. D., … Hopkins, R. O. (2012). The Relationship between Delirium Duration, White Matter Integrity, and Cognitive Impairment in Intensive Care Unit Survivors as Determined by Diffusion Tensor Imaging. *Critical Care Medicine*, *40*(7), 2182–2189. https://doi.org/10.1097/CCM.0b013e318250acdc.
Nijeholt, G., Bergers, E., Kamphorst, W., Bot, J., Nicolay, K., Castelijns, J., … Barkhof, F. (2001). Post-mortem high-resolution MRI of the spinal cord in multiple sclerosis: a correlative study with conventional MRI, histopathology and clinical phenotype. *Brain*, *124*(Pt 1), 154–166.
Niwa, K., Araki, E., Morham, S. G., Ross, M. E., & Iadecola, C. (2000). Cyclooxygenase-2 contributes to functional hyperemia in whisker-barrel cortex. *The Journal of Neuroscience*, *20*(2), 763–770.
Peng, J., Drobish, J. K., Liang, G., Wu, Z., Liu, C., Joseph, D. J., … Wei, H. (2014). Anesthetic Preconditioning Inhibits Isoflurane-Mediated Apoptosis in the Developing Rat Brain. *Anesth Analg*, *119*(4), 939–946. https://doi.org/10.1242/jcs.03292.Multiple
Pereira, P. R., Pinho, J., Rodrigues, M., Rocha, J., Sousa, F., Amorim, J., … Ferreira, C. (2015). Clinical, imagiological and etiological spectrum of posterior reversible encephalopathy syndrome. *Arquivos de Neuro-Psiquiatria*, *73*(1), 36–40. https://doi.org/10.1590/0004-282X20140176
Polito, A., Eischwald, F., Maho, A.-L., Polito, A., Azabou, E., Annane, D., … Sharshar, T. (2013a). Pattern of Brain Injury in the Acute Setting of Human Septic Shock. *Critical Care*, *17*(5), R204. https://doi.org/10.1186/cc12899
Polito, A., Eischwald, F., Maho, A.-L. Le, Polito, A., Azabou, E., Annane, D., … Sharshar, T. (2013b). Pattern of Brain Injury in the Acute Setting of Human Septic Shock. *Critical Care (London, England)*, *17*(5), R204. https://doi.org/10.1186/cc12899
Schwartz, E. D., Cooper, E. T., Chin, C.-L., Wehrli, S., Tessler, A., & Hackney, D. B. (2005). Ex vivo evaluation of ADC values within spinal cord white matter tracts. *American Journal of Neuroradiology*, *26*(2), 390–397.
Seehaus, A., Roebroeck, A., Bastiani, M., Fonseca, L., Bratzke, H., Lori, N., … Galuske, R. (2015). Histological validation of high-resolution DTI in human post mortem tissue. *Frontiers in Neuroanatomy*, *9*(July), 1–12. https://doi.org/10.3389/fnana.2015.00098
Sharshar, T., Carlier, R., Bernard, F., Guidoux, C., Brouland, J. P., Nardi, O., … Annane, D. (2007). Brain lesions in septic shock: A magnetic resonance imaging study. *Intensive*

Care Medicine, *33*(5), 798–806. https://doi.org/10.1007/s00134-007-0598-y

Shepherd, T. M., Flint, J. J., Thelwall, P. E., Stanisz, G. J., Mareci, T. H., Yachnis, A. T., & Blackband, S. J. (2009). Postmortem interval alters the water relaxation and diffusion properties of rat nervous tissue--implications for MRI studies of human autopsy samples. *NeuroImage*, *44*(3), 820–6. https://doi.org/10.1016/j.neuroimage.2008.09.054

Shepherd, T. M., Thelwall, P. E., Stanisz, G. J., & Blackband, S. J. (2005). Chemical fixation alters the water microenvironment in rat cortical brain slices - implications for MRI contrast mechanisms. *Proc. Intl. Soc. Mag. Reson. Med.*, *13*, 619.

Sicard, K., Shen, Q., Brevard, M. E., Sullivan, R., Ferris, C. F., King, J. A., & Duong, T. Q. (2003). Regional Cerebral Blood Flow and BOLD Responses in Conscious and Anesthetized Rats Under Basal and Hypercapnic Conditions: Implications for Functional MRI Studies. *J Cereb Blood Flow Metab.*, *23*(4), 472–481. https://doi.org/10.1111/j.1747-0285.2012.01428.x.Identification

Stary, C. M., Sun, X., & Giffard, R. G. (2015). Astrocytes Protect Against Isoflurane Neurotoxicity by Buffering pro Brain-Derived Neurotrophic Factor. *Anesthesiology*, *123*(4), 810–819. https://doi.org/10.1016/S2215-0366(16)30284-X.Epidemiology

Stefanovic, B., Bosetti, F., & Silva, A. C. (2006). Modulatory role of cyclooxygenase-2 in cerebrovascular coupling. *NeuroImage*, *32*(1), 23–32. https://doi.org/10.1016/j.neuroimage.2006.03.014

Sun, S. W., Neil, J. J., Liang, H. F., He, Y. Y., Schmidt, R. E., Hsu, C. Y., & Song, S. K. (2005). Formalin fixation alters water diffusion coefficient magnitude but not anisotropy in infarcted brain. *Magnetic Resonance in Medicine*, *53*(6), 1447–1451. https://doi.org/10.1002/mrm.20488

Tétrault, S., Chever, O., Sik, A., & Amzica, F. (2008). Opening of the blood-brain barrier during isoflurane anaesthesia. *European Journal of Neuroscience*, *28*(7), 1330–1341. https://doi.org/10.1111/j.1460-9568.2008.06443.x

Tyszka, J. M., & Frank, L. R. (2009). High-Field Diffusion MR Histology: Image-Based Correction of Eddy-Current Ghosts in Diffusion-Weighted Rapid Acquisition With Relaxation Enhancement (DW-RARE). *Magn Reson Med.*, *61*(3), 728–733.

Wu, D., Xu, J., McMahon, M. T., van Zijl, P. C. M., Mori, S., Northington, F. J., & Zhang, J. (2013). In vivo high-resolution diffusion tensor imaging of the mouse brain. *NeuroImage*, *83*(410), 18–26. https://doi.org/10.1016/j.neuroimage.2013.06.012

Yokota, H., Ogawa, S., Kurokawa, A., & Yamamoto, Y. (2003). Regional cerebral blood flow in delirium patients. *Psychiatry and Clinical Neurosciences*, *57*(3), 337–339. https://doi.org/10.1046/j.1440-1819.2003.01126.x

Rapport sur la thèse de doctorat en Neurosciences intitulée «Etude de l'interface sang-cerveau au cours d'encéphalopathie associé au sepsis: de l'imagerie à l'histologie»

Présentée par M[lle] Ibtihel DHAYA

La présente thèse en sciences biologiques/neurosciences porte sur l'étude de l'encéphalopathie associée au sepsis (EAS) -définie comme un dysfonctionnement cérébral diffus induit par une réponse systémique à une infection- chez le rongeur en proposant comme hypothèse que l'EAS s'accompagne de changements hémodynamiques et structurelles détectés par imagerie cérébrale en lien avec des modifications morphologiques et biochimiques des cellules endothéliales et gliales .

Ce manuscrit est structuré comme suit :

Le premier chapitre consiste en une revue de la littérature permettant d'introduire les concepts et approches essentiels utilisés dans ce travail. Au cours de ce chapitre, l'importance de la physiologie et du comportement de la maladie pour la survie après une infection bactérienne a été d'abord discutée ainsi que la façon dont le signal inflammatoire gagne le cerveau pour induire des modifications physiologiques et comportementales. Ensuite, les données indiquant une détérioration de l'état neurologique au cours de sepsis décrites dans des études cliniques et expérimentales en plus des résultats d'imagerie et les observations histologiques ont été résumés. Enfin, les différents modèles expérimentaux et approches d'imagerie ont été comparés.

Une analyse de la littérature indique que l'EAS est multifactorielle et peut être associée à une hypo-ou hyperperfusion cérébrale, un échec de l'autorégulation, un dysfonctionnement de la microcirculation, une formation d'œdème, une perturbation de la barrière hématoencéphalique (BHE) et des lésions de la substance grise et blanche. L'imagerie par résonance magnétique (IRM) est un outil de référence pour étudier des changements hémodynamiques et structurels survenant au cours de l'EAS. De plus, des analyses *post mortem* ont indiqué des lésions

ischémiques, hémorragiques et apoptotiques qui étaient souvent associées à des signes de gliose. Ainsi, les cellules endothéliales et gliales peuvent être considérées comme des effecteurs potentiels de changements conduisant à un dysfonctionnement cérébral. Au niveau moléculaire, la production accrue de médiateurs (neuro-)inflammatoires au cours de la réponse inflammatoire systémique pourrait également contribuer à la pathogenèse de la septicémie et au dysfonctionnement cérébral.

Le second chapitre, intitulé «Bacterial lipopolysaccharide-induced systemic inflammation alters perfusion of white matter-rich regions without altering flow in brain-irrigating arteries: relationship to blood-brain-barrier breakdown?», décrit les principales altérations hémodynamiques et structurelles détectées par IRM ainsi que les modifications de la BHE, de l'expression de synthèse de prostaglandines et les changements morphologiques des cellules gliales dans un premier modèle consistant en l'injection des fragments bactériens lipopolysaccharides (LPS) par voie intrapéritonéale. Cette étude montre qu'une injection intrapéritonéale de LPS peut résulter en moins de 2,5 h en une augmentation de perfusion sanguine au niveau du corps calleux, le plus important faisceau de fibres nerveuses liant les deux hémisphères cérébraux ainsi qu'une augmentation de la diffusion horizontale des molécules dans la même structure. Ces changements ont été accompagnés par une rupture de la barrière hémato-encéphalique dans la substance blanche sous-calleuse sans changement morphologique global des cellules gliales.

Dans le chapitre trois, intitulé «Cecal ligature and puncture-induced systemic inflammation increases water diffusion in white matter-rich regions in the absence of blood-brain-barrier breakdown: relationships to changes in glial cell morphology » l'auteure s'intéresse à l'étude de la prise alimentaire et des réflexes de méat auditif, cornéen et de redressement et emploie des approches d'imagerie hémodynamique et structurale suivis par des analyses *post mortem* ciblant des cellules et des molécules pouvant être impliquées dans les changements d'imagerie observés, dans un modèle de septicémie consistant en la ligature et la ponction de ceacum (CLP). Il a ainsi été démontré que la CLP réduisait l'apport alimentaire et diminuait le réflexe de redressement. Ce dysfonctionnement du SNC induit par la septicémie s'accompagnait d'une augmentation du contraste pondéré en T2 dans le cortex, le striatum et à la base du cerveau, ainsi qu'une diminution de la distribution sanguine vers le cortex et une augmentation de la diffusion hydrique dans le corps calleux et le striatum ventral. Ces changements ont été accompagnés par une induction vasculaire de la cyclooxygenase-2, mais

aussi par une diminution de l'expression neuronale constitutive de la cylcooxygenése-2 et de l'expression astrocytaire du canal hydrique l'aquaporine-4 dans le cortex. Enfin, le nombre de fragments ionized calcium-binding adaptor molecule-1 (Iba-1)- et Glial Fibrillary Acidic Protein (GFAP)-immunoréactifs dans la substance blanche du corps calleux était moins important chez les animaux ayant subi la CLP que chez les rats sujets à une laparotomie. L'augmentation de la valeur maximale de l'imagerie pondérée en T2 après CLP suggère la formation d'œdème et peut être mise en lien avec la diminution de l'expression corticale des molécules d'aquaporine-4. La diminution de la distribution sanguine vers le cortex pourrait être due à l'expression amoindrie de la cyclooxygnéase-2 neuronale qui est connue pour jouer un rôle important dans le couplage neurovasculaire. Enfin, l'augmentation de la diffusion des molécules d'eau dans le corps calleux après CLP peut s'expliquer par la diminution du nombre de fragments Iba-1- et GFAP-positifs ce qui peut être interprété comme une rétraction des processus gliaux les plus distants facilitant ainsi la diffusion accrue de l'eau.

Le quatrième chapitre, intitulé « Magnetic resonance imaging under isoflurane anesthesia alters blood-brain barrier permeability and glial cell morphology during sepsis-associated encephalopathy in rats », a consisté en la comparaison de l'expression de l'enzyme la production de prostaglandines vasoactives, de l'intégrité de la BHE et la morphologie des cellules gliales pendant la septicémie expérimentale entre des animaux CLP et ceux dits sham imagés sous anesthésie et des rats CLP et ceux dits sham n'ayant pas subi l'imagerie sous anesthésie. Comme dans le précédent chapitre, la CLP induisait une encéphalopathie telle qu'il a été montré par la détérioration des réflexes ainsi que par l'hypophagie, avec un taux de mortalité de 12,5%. Tous les résultats histologiques indiquaient des modifications plus prononcées dans le groupe qui n'a pas subi l'imagerie sous anesthésie en comparaison avec le groupe qui l'a subi. En effet, l'intégrité de BHE a été d'avantage préservée dans le groupes ayant subi une IRM sous anesthésie par rapport aux animaux qui n'avaient pas été imagés. Ainsi, les microglies et les astrocytes étaient également morphologiquement différentes entre les groupes anesthésiés une seule fois pour la chirurgie abdominal et ceux qui l'ont été deux fois et entre animaux dits sham. En effet, les cellules gliales montraient une forme plus ramifiée chez les animaux ayant subi une CLP et l'imagerie sous anesthésie par rapport aux rats CLP qui n'ont pas été imagés, ce qui peut être interprétée comme une protection contre la gliose. Ces résultats soulignent que l'anesthésie à l'isoflurane, bien n'altérant pas le taux de mortalité, peut atténuer les modifications de la BHE et des cellules gliales au cours de sepsis provoquée par la CLP.

Le cinquième chapitre a pour but de résumer les résultats obtenus dans les différents chapitres et d'en discuter les implications avant de proposer quelques perspectives.

Par ailleurs, les contributions de cette thèse sont importantes:

-Les résultats de cette thèse confirment l'existence d'un dysfonctionnement cérébral dans le modèle expérimental de sepsis provoquée par la CLP. En outre, les résultats obtenus enrichissent aussi l'ensemble des résultats déjà publiés en suggérant que la formation d'œdème dans le striatum, le cortex et à la base du cerveau, la rupture de barrière ainsi que la redistribution de la perfusion sanguine entre substance blanche et grise peuvent différer entre le modèle LPS et le modèle CLP de sepsis malgré l'existence des changements structuraux comparables. La combinaison de l'imagerie *in vivo* et l'étude histologique *post mortem* sur les mêmes animaux a permis d'établir des relations temporelles et spatiales entre les modifications hémodynamiques et structurales du système nerveux central indiquées par des approches d'imagerie et des modifications biochimiques et cellulaires mises en évidence par immunohistochimie sur coupes cérébrales et de proposer que l'augmentation de la perfusion de la substance blanche cérébrale au cours d'une inflammation systémique serait liée à une rupture de la BHE tandis que l'augmentation de la diffusion des molécules d'eau dans la substance blanche interviendrait suite à des modifications morphologiques des cellules gliales.

-L'originalité de cette étude tient aussi en partie à l'utilisation des approches d'imagerie qui n'ont pas encore été utilisés pour étudier l'encéphalopathie associé au sepsis, tels que l'Arterial Spin Labeling (ASL) et l'imagerie par contraste de phase malgré leur usage dans l'exploration des modèles animaux d'autres maladies.

-Un autre résultat important de cette étude est qu'un dysfonctionnement cérébral peut survenir en l'absence de rupture de la barrière hémato-encéphalique et qu'une perturbation de la perfusion cérébrale peut survenir sans altération de la circulation sanguine artérielle en provenance du cercle de Willis.

-Cette étude est aussi la première à montrer que l'IRM sous anesthésie à l'isoflurane chez des rats préalablement anesthésiés pour subir une laparotomie réduit la rupture de BHE, diminue la circularité des astrocytes de la substance blanche et augmente l'immunoréactivité pour la COX-2 neuronale dans le cortex des rongeurs. Ces résultats indiquent que, selon la mesure d'intérêt, l'IRM sous anesthésie à l'isoflurane peut modifier des réponses neurovasculaires et

gliales et devrait, par conséquent, être interprétée avec prudence. Par ailleurs, ceci ne met pas en question la validation des résultats de notre modèle CLP car malgré le fait que l'isoflurane masque quelques effets d'inflammation ces derniers ne sont pas totalement absents.